

**NUMERICAL SIMULATION OF HYDRODYNAMICS IN
PULSED COLUMNS**

By

Nirvik Sen

ENGG01201304030

Bhabha Atomic Research Center

*A thesis submitted to the
Board of Studies in Engineering Sciences*

*In partial fulfillment of requirements
for the Degree of*

DOCTOR OF PHILOSOPHY

of

HOMI BHABHA NATIONAL INSTITUTE

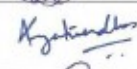
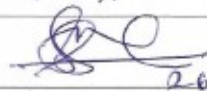
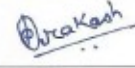


April, 2019

Homi Bhabha National Institute¹

Recommendations of the Viva Voce Committee

As members of the Viva Voce Committee, we certify that we have read the dissertation prepared by Nirvik Sen entitled "Numerical simulation of hydrodynamics in Pulsed Columns" and recommend that it may be accepted as fulfilling the thesis requirement for the award of Degree of Doctor of Philosophy.

Chairman :	Prof. S.B Roy	
Guide / Convener :	Prof. A.W. Patwardhan	
Co-guide : R. H. Subr 4	Prof. S. Mukhopadhyay	 26/4/19
Examiner :	Prof. S.K. Majumder	 26/04/2019
Member 1:	Prof. G. Sugilal	 26/4/19
Member 2:	Prof. R.N. Singh	 26.04.19
Member 3:	Prof. Deep Prakash	 26/04/2019
Technology Advisor :	Dr. K.K. Singh	

Final approval and acceptance of this thesis is contingent upon the candidate's submission of the final copies of the thesis to HBNI.

I/We hereby certify that I/we have read this thesis prepared under my/our direction and recommend that it may be accepted as fulfilling the thesis requirement.

Date: 26/4/2019

Place: Mumbai



Signature

Co-guide (if any)



Signature

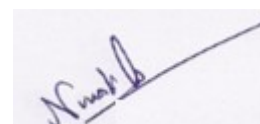
Guide

¹ This page is to be included only for final submission after successful completion of viva voce.

STATEMENT BY AUTHOR

This dissertation has been submitted in partial fulfillment of requirements for an advanced degree at Homi Bhabha National Institute (HBNI) and is deposited in the Library to be made available to borrowers under rules of the HBNI.

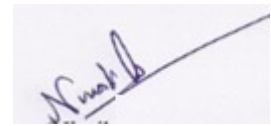
Brief quotations from this dissertation are allowable without special permission, provided that accurate acknowledgement of source is made. Requests for permission for extended quotation from or reproduction of this manuscript in whole or in part may be granted by the Competent Authority of HBNI when in his or her judgment the proposed use of the material is in the interests of scholarship. In all other instances, however, permission must be obtained from the author.



(Nirvik Sen)

DECLARATION

I, hereby declare that the investigation presented in the thesis has been carried out by me. The work is original and has not been submitted earlier as a whole or in part for a degree / diploma at this or any other Institution / University.

A handwritten signature in blue ink, appearing to read 'Nirvik Sen', is written over a horizontal line.

(Nirvik Sen)

List of Publications in Refereed Journal:

Published:

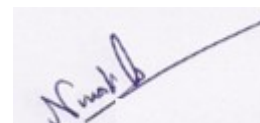
1. Sarkar, S., Sen, N., Singh, K.K., Mukhopadhyay, S., and Shenoy, K.T., 2019. Liquid-liquid Dispersion in Pulsed Disc and Doughnut Column and Pulsed Sieve Plate Column: A Comparative Study. *Progress in Nuclear Energy*, 116, pp. 76-86
2. Sen, N., Singh, K.K., Patwardhan, A.W., Mukhopadhyay, S. and Shenoy, K.T., 2019. CFD-PBM simulations of a pulsed sieve plate column. *Progress in Nuclear Energy*, 111, pp.125-137.
3. Sen, N., Singh, K.K., Patwardhan, A.W., Mukhopadhyay, S. and Shenoy, K.T., 2018. CFD simulations to predict dispersed phase hold up in a pulsed sieve plate column. *Separation Science and Technology*, 53(16), pp. 2587-2600.
4. Sen, N., Sarkar, S., Singh, K.K., Mukhopadhyay, S. and Shenoy, K.T., 2018. Regime Transition and Hold up in Pulsed Sieve-Plate and Pulsed Disc-and-Doughnut Columns: A Comparative Study. *Solvent Extraction and Ion Exchange*, 36(1), pp. 66-83.
5. Goswami, S., Sen, N., Samantray, J.S., Dash, A., Sharma, V.K., Sheony, K.T. and Pant, H.J., 2017. Investigation of flow dynamics of single phase in a pulsed sieve-plate column using radiotracer technique. *Journal of Radioanalytical and Nuclear Chemistry*, 313(3), pp.669-676.
6. Sarkar, S., Sen, N., Singh, K.K., Mukhopadhyay, S. and Shenoy, K.T., 2017. Effect of operating and geometric parameters on dispersed phase hold up in Pulsed Disc and Doughnut and Pulsed Sieve Plate Columns: A comparative study. *Chemical Engineering and Processing: Process Intensification*, 118, pp.131-142.
7. Sen, N., Singh, K.K., Patwardhan, A.W., Mukhopadhyay, S. and Shenoy, K.T., 2016. CFD simulation of two-phase flow in pulsed sieve-plate column– Identification of a suitable drag model to predict dispersed phase hold up. *Separation Science and Technology*, 51(17), pp.2790-2803.
8. Sen, N., Singh, K.K., Patwardhan, A.W., Mukhopadhyay, S., and Shenoy, K.T., 2015. CFD simulations of pulsed sieve plate column: axial dispersion in single-phase flow. *Separation Science and Technology*, 50(16), pp.2485-2495.

Other Publications (Conference):

1. Sen, N., Singh, K.K., Patwardhan, A.W., Mukhopadhyay, S., Shenoy, K.T. CFD modelling to predict mass transfer in pulsed sieve plate extraction columns. *In proceedings, CFD 2017, Trondheim, Norway, May 2017.*
2. Goswami, S., Samantray, J.S., Pant, H.J., Sharma, V.K., Dash, A., Sen, N., Sheony, K.T. Investigation of flow dynamics of aqueous phase in a pulsed sieve plate column using radiotracer technique. *In Proceedings of the thirteenth DAE-BRNS nuclear and radiochemistry symposium, Mumbai, India, February 2017.*

Under preparation:

1. Sen, N., Sarkar, S., Singh, K.K., Shenoy, K.T. Effect of Operating and Geometric Parameters on Axial Dispersion in Pulsed Disc and Doughnut and Pulsed Sieve Plate Columns: A Comparative Study
2. Sen, N., Singh, K.K., Patwardhan, A.W., Mukhopadhyay, S. and Shenoy, K.T. CFD-PBE modelling of continuous phase axial dispersion in Pulsed Sieve Plate Columns.



(Nirvik Sen)

Date: 15/4/2019

ACKNOWLEDGEMENTS

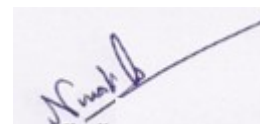
I would like to express my gratitude to Prof. A. W. Patwardhan, my guide, and Dr. Sulekha Mukhopadhyay, my co-guide, for their continuous support, encouragement, patience and for the freedom they provided for free thinking.

I am especially grateful to Dr. K.K. Singh, ChED, BARC, my mentor who is also my technology advisor, for his continuous support, encouragement, and guidance (which ranged from technical/scientific aspects to grooming) without which timely completion of my research work would simply had been impossible.

I am also grateful to Shri K.T. Shenoy, Head ChED for his constant encouragement to pursue my research work.

I would take this opportunity to thank Dr. H.J. Pant, IRAD and my friend cum colleague Shri Sunil Goswami and Shri Sourav Sarkar for their help and support during the experimental work.

Finally mention must be made of my family for their support, understanding and blessings



(Nirvik Sen)

CONTENTS

		Page No.
List of Figures		i
List of Tables		vi
Synopsis		1
Chapter 1	Introduction	13
Chapter 2	Single phase CFD simulation to predict axial dispersion	23
Chapter 3	Monodispersed CFD simulation to predict dispersed phase hold up using experimentally measured drop diameter	42
Chapter 4	Monodispersed CFD simulation to predict dispersed phase hold up using correlated drop diameter	69
Chapter 5	Coupled CFD-PBE simulation to predict dispersed phase hold up and Sauter mean drop diameter	90
Chapter 6	Coupled CFD-PBE simulation to predict continuous phase axial dispersion	128
Chapter 7	Coupled CFD-PBE simulation to predict interphase mass transfer	152
Chapter 8	Conclusion and Future work	158
Nomenclature		169
Reference		172

LIST OF FIGURES

Sl.No.	Figure	Page No
S.1	Comparison of hold up values predicted by CFD simulations and estimated by various correlations reported in literature	4
S.2	Experimental investigation of hydrodynamics in PSPC	7
S.3	Parity plot for a) hold up and b) Sauter mean drop diameter	7
S.4	Contour plot of a) dispersed phase hold up b) dispersed phase drop diameter during positive (left panel) and negative peak of the pulsing cycle (right panel) ($A_f = 2.0$ cm/sec, $V_d = 0.67$ cm/sec, $V_c = 0.56$ cm/sec, 3 inch PSPC)	8
S.5	Parity plot for CFD-PBE predicted and experimentally obtained axial dispersion coefficient	10
S.6	Contour plot of solute mass fraction in continuous and dispersed phase	11
1.1	Schematic diagram of pulsed sieve plate columns (Yadav and Patwardhan, 2008).	15
1.2	Flow regimes in PSPC (Yadav and Patwardhan, 2008).	15
2.1	Computational domains used in the simulations of full column (left) and column consisting of four plates (right)	28
2.2	The computational domain (left) and a section of the computational domain showing one disc and doughnut (right)	29
2.3	Comparison of F-curves obtained for different grid densities ($U = 0.01$ m/sec, $A_f = 0.01$ m/sec)	30
2.4	Comparison of dimensionless F-curves predicted by the CFD simulations carried out for two possible approaches of 2D representation of the actual geometry. ($U = 0.010$ m/sec and $A_f = 0.010$ m/sec)	32
2.5	Comparison of the F-curve obtained from the direct approach and the snapshot approach ($U = 0.01$ m/sec, $A_f = 0.01$ m/sec)	33
2.6	Velocity magnitude contour and velocity vector plots at the four representative points of one pulsing cycle ($U = 0.01$ m/sec, $A_f = 0.01$ m/sec)	34
2.7	Comparison of $F(\theta)$ versus θ curves obtained from the simulations of the column having 4 plates and the column having 20 plates ($U = 0.01$ m/sec, $A_f = 0.01$ m/sec)	35
2.8	Comparison of predicted temporal variation of point velocity with the same observed by using PIV and LDV	36
2.9	Effect of pulsing velocity on axial dispersion coefficient	38
2.10	Effect of superficial velocity on axial dispersion coefficient	38
2.11	Effect of hole diameter on axial dispersion coefficient (percent free area kept at 21 %)	39
2.12	Effect of percent free area on axial dispersion coefficient (hole diameter kept at 3 mm)	40
3.1	Computational domain used for CFD simulations	50
3.2	Variation of hold up with dispersed phase velocity ($V_c = 0.00207$ m/sec, $A_f = 0.02$ m/sec)	53

3.3	Variation of hold up with pulsing velocity ($V_c = 0.00186$ m/sec, $V_d = 0.005$ m/sec)	53
3.4	Profiles of dispersed phase hold up for four different instants of a pulsing cycle ($V_d = 0.004$ m/sec; $V_c = 0.00207$ m/sec; $Af = 0.02$ m/sec)	55
3.5	Velocity profiles for dispersed (top) and continuous (bottom) phase velocity at different instants of the pulsing cycle ($V_d = 0.004$ m/sec; $V_c = 0.00207$ m/sec; $Af = 0.02$ m/sec)	56
3.6	Velocity vector plots for dispersed (top) and continuous (bottom) phase velocity at four different instants of a pulsing cycle ($V_d = 0.004$ m/sec; $V_c = 0.00207$ m/sec; $Af = 0.02$ m/sec)	57
3.7	Velocity vectors of the continuous phase in the bottom disengagement section for positive and negative peak of the pulsing cycle ($V_d = 0.004$ m/sec; $V_c = 0.00207$ m/sec; $Af = 0.02$ m/sec)	58
3.8	Variation of average hold up between the plates with height of the column	58
3.9	Variation of hold up with dispersed phase superficial velocity in reverse phase operation. Comparison of the prediction of CFD model using Kumar-Hartland drag law with experimental values.	60
3.10	Variation of hold up with pulsing velocity for reverse phase operation. Comprison of hold up predicted by CFD model using Kumar Hartland drag law with experimental values.	61
3.11	Sensitivity of hold up on the parameter A_D of the drag model for two different vlaues of pulsing velocities, $V_d = 0.005$ m/sec and $V_c = 0.005$ m/sec	64
3.12	Compariosn of standard Kumar-Hartland drag model and modified Kumar-Hartland drag model	66
3.13	Comaprison of hold up values predicted by CFD simulations and estimated by various correlations reported in literature	67
4.1	Comparison of different correlations to predict drop diameter for TBP - nitric acid system	72
4.2	Effect of dispersed phase superficial velocity on dispersed phase hold up (error bars represnet $\pm 20\%$ of experimental values)	74
4.3	Effect of pulse velocity on dispersed phase hold up (error bars represent $\pm 40\%$ of experimental values)	75
4.4	Profiles of dispersed phase hold up inside the column at different instants of a pulsing cycle ($Af = 0.02$ m/sec; $v_d = 0.006$ m/sec, $v_c = 0.00207$ m/sec)	76
4.5	(A) Dispersed phase velocity magnitude profile for positive (left) and negative (right) peak of the pulsing cycle. (B) Profile of y-component of dispersed phase velocity for positive (left) and negative (right) peak of the pulsing cycle between two plates. ($Af = 0.02$ m/sec; $v_d = 0.004$ m/sec, $v_c = 0.00207$	78

	m/sec)	
4.6	Continuous phase velocity vectors for positive (left) and negative (right) peak of the pulsing cycle ($A_f = 0.02$ m/sec; $v_d = 0.004$ m/sec, $v_c = 0.00207$ m/sec)	79
4.7	Compariosn of experimental values of dispersed phase hold up with the values of dispersed phase hold up predicted by the CFD model embedding the modified Kumar-Hartland drag model.	82
4.8	Profile of dispersed phase hold up (top) and dispersed phase velocity (bottom) for aqueous dispersed mode of operation of column for one of the data sets reported by Din et al., 2010 ($A_f = 0.0112$ m/sec; $v_d = 0.0034$ m/sec; $v_c = 0.0037$ m/sec)	85
4.9	Comaprison of hold up values predicted by CFD simulations and estimated by various correlations reported in literature. The experimental data is from Din et al., 2010 .	87
4.10	Comaprison of hold up values predicted by CFD simulations with experimental values of dispersed phase hold up reported by Sehmel and Babb (Sehmel and Babb, 1963) . ($v_c/v_d = 1$, $A_f = 0.0211$ m/sec, hexane-water system)	87
4.11	Comaprison of dispersed phase hold up values predicted by CFD simulations and experimentally measured hold up values reported by Sehmel and Babb (Sehmel and Babb, 1963) . ($v_c/v_d = 1$, $A_f = 0.01375$ m/sec, benzene-water system)	88
5.1	Schematic drawing of the experimental setup.	95
5.2	A typical computational domain used to model 3 inch PSPC and the mesh in the vicinity of the plates	100
5.3	Effect of pulsing velocity (A_f) on dispersed phase hold up in 2 and 3 inch diameter PSPC	103
5.4	Effect of dispersed phase velocity on column hold up for two different values of interplate spacing.	103
5.5	3D plot of hold up with column throughput and pulsing velocity	104
5.6	Flow regime map for PSPC (MS: mixer-settler regime; D: dispersion regime; QE: quasi-emulsion regime)	105
5.7	Parity plot showing the comparison of dispersed phase hold up values for PSPC predicted by various correlations with experimentally measured hold up values	106
5.8	(a) A representative image of liquid-liquid dispersion in pulsed column used for the evaluation of droplet distribution and (b) corresponding drop size distribution	107
5.9	Effect of pulsing velocity on drop diameter in 3 inch PSPC	108
5.10	Variation of Sauter mean diameter with throughput and pulsing velocity PSPC	108
5.11	Comparision of experimetally measured Sauter mean drop diameter in PSPC with the Sauter mean drop diameter estimated by (a) the correlation of Kumar & Hartland, 1986 (b) the correlation of Gonda & Matsuda, 1986 (c) correlation of	111

	Kagan, et al., 1965 (d) correlation of Sreenivasulu, et al., 1997 and (e) the modified correlation proposed in this chapter	
5.12	Comparison of predicted values of hold up against experimental values for 3 inch PSPC	114
5.13	Comparison of predicted values of Sauter mena drop diameter against experimental values for 3 inch PSPC	115
5.14	CFD-PBE predictions using optimized drag law	116
5.15	Comparison of CFD-PBE predicted hold up against experimental hold up for a) different values of dispersed phase velocity ($A_f = 0.022$ m/sec; $V_c = 0.0042$ m/sec) and b) different values of continuous phase velocity ($A_f = 0.0222$ m/sec; $V_d = 0.0048$ m/sec)	117
5.16	Comparison of CFD-PBE predicted and experimental variation of Sauter mean drop diameter with continuous phase velocity ($A_f = 0.0222$ m/sec; $V_d = 0.0048$ m/sec)	117
5.17	Contour plot of a) dispersed phase hold up b) dispersed phase drop diameter c) Y component of continuous phase velocity and d) turbulence dissipation rates during positive and negative peak of pulsing cycle ($A_f = 0.0222$ m/sec; $V_c = 0.0042$ m/sec; $V_d = 0.0048$ m/sec).	121
5.18	Vector plots of continuous and dispersed phase velocity during positive and negative peak of the pulsing cycle ($A_f = 0.0222$ m/sec; $V_c = 0.0042$ m/sec; $V_d = 0.0048$ m/sec).	122
5.19	Comparison of CFD-PBE predicted hold up against experimental hold up in 2 inch PSPC for a) different values of dispersed phase velocity and b) different values of pulsing velocity	123
5.20	Comparison of CFD-PBE predicted Sauter mean drop diameter against experimental result in 2 inch PSPC	123
5.21	Comparison of CFD-PBE predicted hold up against experimental hold up for 3 inch diameter PSPC having interplate spacing of 10 cm ($V_c = 0.0042$ m/sec; $V_d = 0.0048$ m/sec)	124
5.22	Comparison of CFD-PBE predicted Sauter mean drop diameter against experimental values for a 3 inch diameter PSPC having interplate spacing of 10 cm ($V_c = 0.0042$ m/sec; $V_d = 0.0048$ cm/sec).	124
5.23	Parity plot for a) hold up and b) Sauter mean drop diameter	126
6.1	Schematic diagram of experimental setup	132
6.2	Effect of initial tracer concentration on E-curve (single-phase flow, tracer injection volume = 5 mL)	133
6.3	Effect of injected volume of tracer on resultant E-curve (single-phase flow, tracer concentration = 2.5 M)	133
6.4	Variation of a) mean residence time and b) axial dispersion coefficient with dispersed phase velocity	135
6.5	Variation of a) mean residence time and b) axial dispersion coefficient with continuous phase velocity.	137

6.6	Parity plot for correlations predicting axial dispersion coefficient in PSPC.	141
6.7	Comparison of CFD-PBE predicted axial dispersion coefficient against experimental data for different dispersed phase velocities	142
6.8	Comparison of CFD-PBE predicted axial dispersion coefficient against experimental data for different dispersed phase velocities	142
6.9	Parity plot for CFD-PBE predicted and experimentally obtained axial dispersion coefficient.	143
6.10	Spatial variation of dispersed phase hold up inside the column at different instants of a pulsing cycle ($A_f = 0.0222$ m/sec; $V_d = 0.0062$ m/sec, $V_c = 0.0055$ m/sec)	145
6.11	Spatial variation of Sauter mean drop diameter and turbulent energydissipation rate ($A_f = 0.0222$ m/sec; $V_d = 0.0062$ m/sec, $V_c = 0.0055$ m/sec)	146
6.12	Dispersed phase hold up profiles for two different values of dispersed phase velocity ($V_c = 0.0055$ m/sec; $A_f = 0.0222$ m/sec)	147
6.13	Sauter mean drop diameter profiles for two different values of dispersed phase velocity ($V_c = 0.0055$ m/sec; $A_f = 0.0222$ m/sec)	148
6.14	Continuous phase velocity vector plot for two different values of dispersed phase velocity ($V_c = 0.0055$ m/sec; $A_f = 0.0222$ m/sec)	149
6.15	Dispersed phase velocity vector plot for two different values of dispersed phase velocity ($V_c = 0.0055$ m/sec; $A_f = 0.0222$ m/sec)	150
7.1	Contour plot of dispersed phase hold up (-) (top) and Sauter mean drop diameter (m) (bottom)	157
7.2	Contour plot of turbulence dissipation rate, axial continuous phase velocity, and axial dispersed phase velocity	158
7.3	Contour plot of solute mass fraction in continuous and dispersed phase.	159
7.4	Density of the dispersed phase (kg/m^3)	160

LIST OF TABLES

Sl. No.	Table	Page No.
2.1	Operating conditions for which simulations are carried out	37
3.1	Different reported drag models evaluated in this study	47
3.2	Physical properties of the liquid-liquid system	49
3.3	Conditions and data used for simulations of normal phase operation	52
3.4	Errors in predictions of dispersed phase hold up (expressed as percentage) by different drag models for normal phase operation	54
3.5	Conditions for which simulations are carried out for reverse phase operation	59
4.1	Comparison of the correlations for estimating representative drop diameters in pulsed sieve plate column	73
4.2	Conditions for which simulations are carried out for normal phase operation	74
4.3	Empirical correlations used for predicting dispersed phase hold up in this study	86
5.1	Range of operating and geometrical parameters	101
5.2	Average absolute error in prediction of Sauter mean drop diameter in PSPC by different correlations	112
5.3	Optimized values of parameter C for different levels of pulsing velocity	115
6.1	Correlations to predict axial dispersion in PDDC	139
7.1	Comparison of CFD PBE predicted values against experimental data	156

SYNOPSIS

The research work titled “Numerical simulation of Hydrodynamics in pulsed columns” was carried out to utilize Computational Fluid Dynamic (CFD) based tools to understand the hydrodynamics in pulsed sieve plate extraction columns (PSPC). PSPC represents a class of intensified process contactor of vital importance in solvent extraction processes due to their higher efficiencies and higher throughputs. The absence of any mechanical moving parts makes this class of columns very attractive in the back end of the nuclear fuel cycle. The two phase hydrodynamics in these columns is very complex and is dependent on a large number of operating and geometrical/design parameters. Mass transfer in these columns is, in turn, significantly affected by the prevailing hydrodynamics. Hence, it is important to understand the column hydrodynamics for a proper estimate of the mass transfer efficiency of pulsed columns. Because of limited fundamental understanding of functioning of PSPCs due to intrinsically complex pulsatile, two-phase turbulent flow ridden with continuous coalescence and re dispersion of droplets, design of a PSPC is still based on operational experience and experimental data generated at pilot-scale. Since it is difficult to experimentally investigate local hydrodynamics in a PSPC, especially in large diameter columns, CFD based modeling of PSPCs becomes very important as such models can provide very useful insights into hydrodynamics at a local level. These insights, in turn, reduce the empiricism involved in designing PSPC. Specifically, CFD based approaches can lead to a significant reduction in empiricism typically involved in scale-up of PSPC.

The objective of this research work is to develop a CFD model to predict relevant hydrodynamic parameters in a PSPC, validate the model thoroughly and used the validated model to investigate in detail local as well as global hydrodynamics of the column.

The general work plan of the research work is mentioned as below.

- CFD modeling of single-phase flow in a PSPC, validation of the modeling approach and investigation of effect of column geometries on axial dispersion coefficient (Chapter 1).
- Euler-Euler two-fluid CFD modeling to simulate two-phase flow in PSPC assuming the dispersed phase to be monodispersed with drop diameter available from experiments. The model was validated against reported literature data (Chapter 2).
- Euler-Euler two-fluid CFD modeling to simulate two-phase flow in PSPC assuming dispersed phase to be monodispersed with drop diameter obtained from a suitable empirical correlation. The model was validated against reported literature data (Chapter 3).
- Euler-Euler two-fluid CFD-PB (population balance) coupled model to simultaneously obtain drop size distribution and the two-phase flow variables in the column. The model was validated within-house generated experimental data on hold up and Sauter mean drop diameter. To the best of our knowledge, it is the first reported attempt on CFD-PB modeling of PSPC (Chapter 4).
- CFD-PB coupled two-fluid model was used to predict axial dispersion coefficient in continuous phase in a PSPC. The model was validated against in house generated experimental data on axial dispersion coefficient in continuous phase in PSPC. Prediction of axial dispersion coefficient using CFD-PB simulations of PSPC also, to the best of our knowledge, not reported so far. (Chapter 5).
- CFD-PB coupled model was used to simulate interphase mass transport of a species/solute (form one phase to another). The developed model was validated against reported experimental data. Once again this is the first time, to the best of our knowledge, a CFD-PB model is used to predict interphase

mass transfer of solute in liquid-liquid solvent extraction contactors in general and in pulsed columns in particular.

In chapter 1 CFD simulations of single-phase flow in a pulsed sieve plate column are presented. The computational model was validated against reported experimental data (Kolhe et al., 2011) on axial dispersion coefficient in a 3 inch PSPC. Different possibilities to make computations faster for this computationally challenging equipment are evaluated. The evaluation of these possibilities leads to the following conclusions:

- 2D simulations of pulsed sieve plate column can be carried out to get a reasonably good estimate of axial dispersion in single-phase flow.
- For 2D representation of the actual geometry, hole diameter must be kept same as in the actual geometry. Pitch should be varied to keep the percent free area same.
- A geometry with reduced number of plate can be used to carry out CFD simulations. Four plates are found to be sufficient.
- Instead of the direct approach which involves coupled solution of RANS and the scalar transport equation, a snapshot approach can be used to significantly save the computational time. The snapshot approach involves solution of scalar transport equation alone for four flow fields corresponding to four different points of the sinusoidal pulsing velocity.

The computational approach embedding the above recommendation for quick estimate of axial dispersion coefficient in single-phase flow in a pulsed sieve plate column is validated using the experimental data. A good agreement between the predicted and reported axial dispersion coefficients is observed. The validated computational approach is also found to give physically realistic prediction of effect of hole diameter and percent free area on axial dispersion coefficients.

The study, therefore, provides useful tips to simulate single-phase flow in large scale sieve plate columns so that computational efforts can be reduced significantly while

not sacrificing too much on the accuracy of the predictions. This study paves the way for more complex in two-phase CFD modeling of pulsed sieve plate columns.

In chapter 2 two-phase flow of 30% TBP in dodecane – 3 N nitric acid system in a pulsed sieve plate column has been simulated using a 2D model. Dispersed phase is assumed to be monodispersed. Quantitative accuracy of the model is studied by comparing the predicted hold up with experimentally reported values of hold up in a 3 inch PSPC (Lade et al., 2013). Fig. S.1 shows the comparison of hold up predicted by CFD against those obtained from empirical correlations.

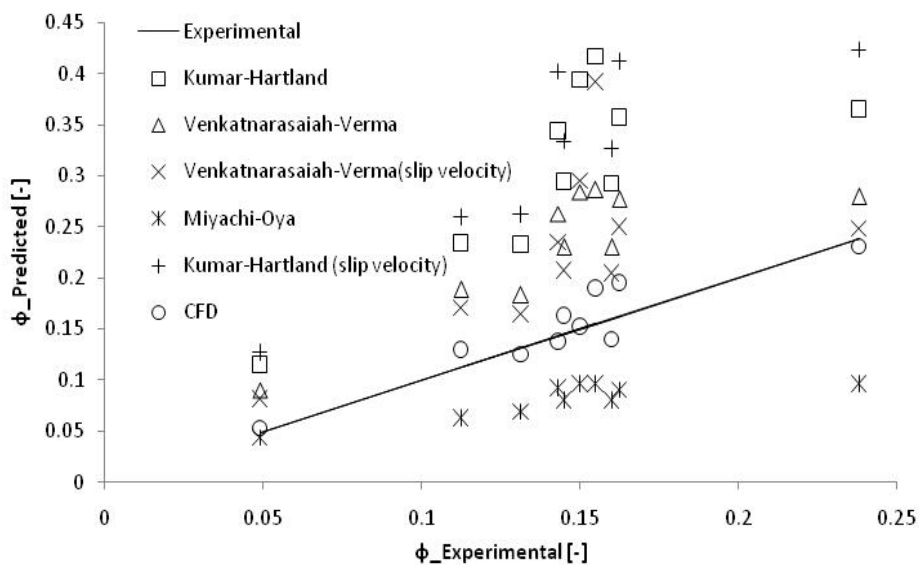


Figure S.1: Comparison of hold up values predicted by CFD simulations and estimated by various correlations reported in literature

Different drag models reported in literature are compared and drag models accounting for the effect of hold up on drag coefficient are found to be better than the drag models which do not account for the effect of hold up on drag coefficient. In particular Kumar-Hartland drag model is found to be the most suitable with the absolute average relative error between the predicted and reported values of hold up being around 15%. In an approach which basically means lumping all uncertainties in two-phase model in the model constant of the drag model, the model of Kumar-Hartland has been modified to reduce the error between the hold up predicted by two-phase CFD model and experimental hold up. It is found that a single drag model cannot represent the

entire range of pulsing velocity. For lower pulsing velocities, a drag model that predicts lower drag coefficient is required. For higher pulsing velocities (≥ 2.5 cm/s), a drag model predicting higher drag coefficient is required. The modified drag model is implemented in the two-phase CFD simulations and the absolute average relative error between predicted and reported hold up is reduced from 15% to about 6%. Hold up values predicted by CFD simulations are compared with the hold up values obtained from the empirical correlations reported in literature. CFD simulations are found to be distinctly better than the empirical correlations in this regard. In this study we have focused on TBP – nitric acid system which is relevant to nuclear fuel reprocessing. Further studies are required to verify if the optimized drag model is able to predict the hold up for other phase systems also.

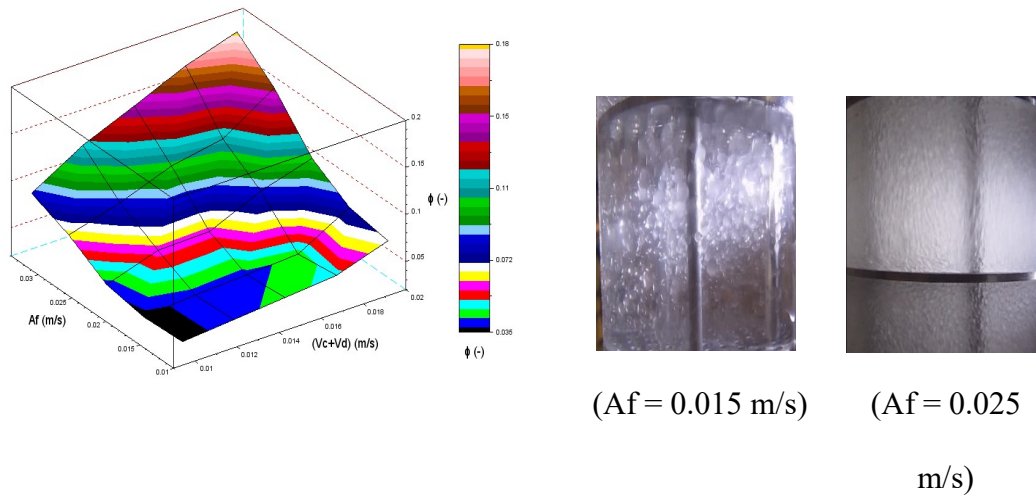
In Chapter 3 two-phase flow of 30% TBP in dodecane – nitric acid system in a pulsed sieve plate column has been simulated using a 2D two-fluid CFD model. Dispersed phase is assumed to be monodispersed. Representative drop diameter used in the two-fluid model is obtained from a suitable correlation which is identified after screening several empirical correlations reported to estimate the drop diameter in pulsed sieve plate columns. This approach thus is a predictive one which doesn't need inputs from experiments with respect to representative drop diameter. Standard Kumar-Hartland drag model is used to model the interphase momentum exchange term. Quantitative accuracy of the computational approach is tested by comparing its predictions of dispersed phase hold up with the reported experimental values of hold up in a 3 inch PSPC ([Lade et al., 2013](#)) and the absolute average relative error in prediction of hold up is found to be about 17%. In an approach which basically means lumping all uncertainties in the computational approach in the model constants of the drag model, the model of Kumar-Hartland has been modified to bring the hold up predicted by two-phase CFD model closer to the experimentally measured values. It is found that a single drag model is not suitable for the entire range of pulse intensity. For lower

pulse intensities, a drag model that predicts lower drag coefficient is required. For higher pulsing intensities (≥ 2.5 cm/s), a drag model predicting higher drag coefficient is required. The modified drag model is implemented in the two-phase CFD model and the absolute average relative error between predicted and reported hold up is found to be about 5.8%. The versatility of the CFD model embedding the modified drag model is tested by comparing its performance against experimental results of dispersed phase hold up in another pulsed column having a different geometry and employing a different phase system. The absolute average relative error between the predicted and experimental results on hold up is about 15%. This result is significantly better than that obtained using standard Kumar-Hartland drag model which tends to severely under-predict dispersed phase hold up. It is also found to be better than the reported empirical correlations to predict dispersed phase hold up in pulsed sieve plate columns reported in literature. The computational approach embedding a modified version of Kumar-Hartland drag model thus offers a simplified way of predicting dispersed phase hold up in a pulsed sieve plate columns and thus can be useful for design and optimization calculations.

In Chapter 4, a predictive 2D coupled CFD-PB model of PSPC is proposed. An optimized drag model based on the drag model of Schiller-Naumann is used to model the inter phase momentum exchange term. The model is extensively validated against experimental data which are obtained by varying both operating (continuous and dispersed phase velocity) and geometrical (different interplate spacing and column diameter) conditions. Two different column diameters (i.e. 2 and 3 inch) are used.

Detailed analysis of experiments have been carried out with respect to variation of column hold up and representative drop diameter with different operating (pulsing, continuous and dispersed phase velocities) and geometrical conditions (column diameter, interplate spacing) and for different phase systems. A sensitivity analysis

was also done. Fig. S.2 shows the variation of hold up and dispersion quality with the operating parameters of a PSPC (3 inch) with a 3N nitric acid-30% TBP/DD system.



Surface plot of hold up (ϕ) with (V_d+V_c) and A_f Effect of A_f dispersion quality
Figure S.2: Experimental investigation of hydrodynamics in PSPC

Absolute average relative errors in prediction (using CFD-PBE) of dispersed hold up and Sauter mean drop diameter are about 12% and 16% respectively. Fig. S.3 below shows the corresponding parity plots. Fig. S.4 below shows the variation of dispersed phase hold up and Sauter mean drop diameter in a typical interplate spacing as obtained from CFD model. The figure shows the profile for both positive and negative

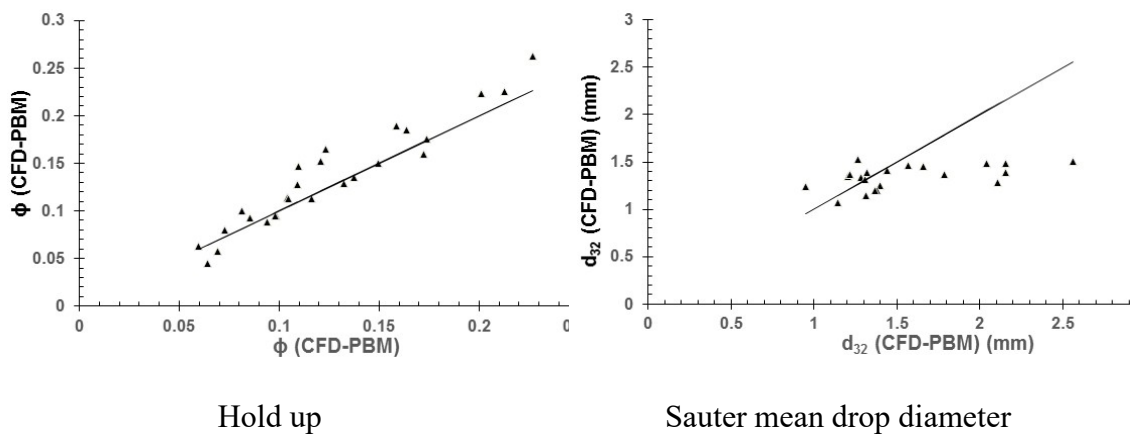
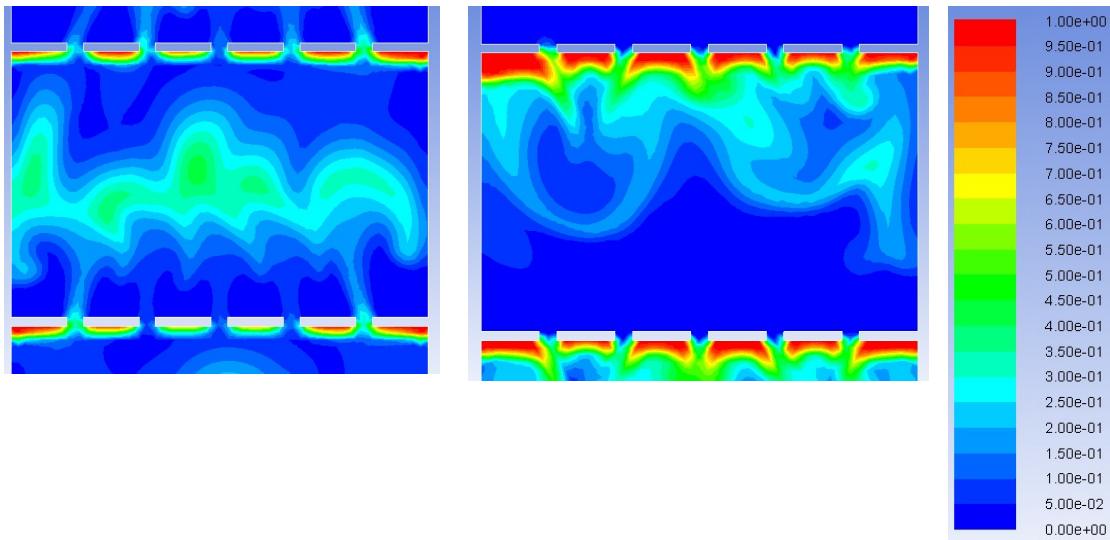


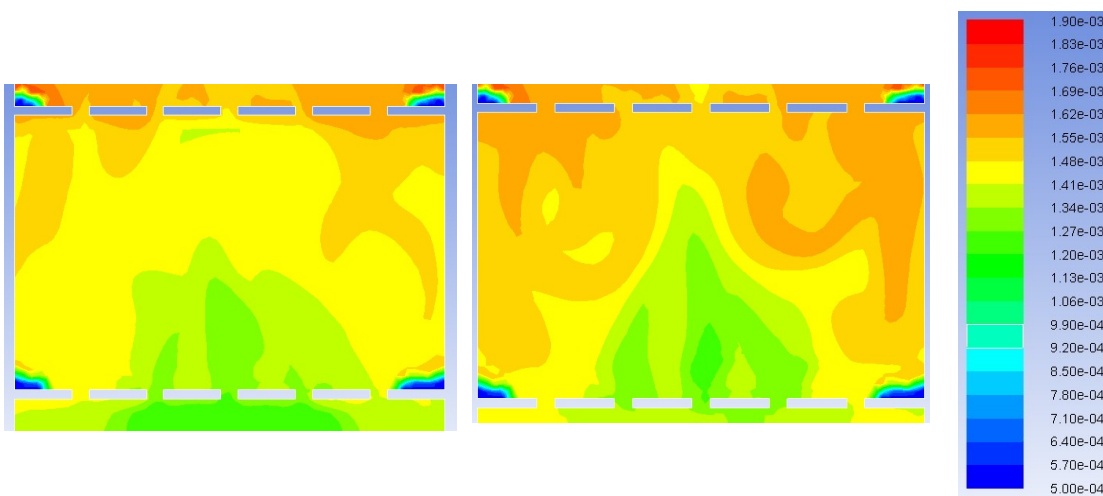
Figure S.3: Parity plot for a) hold up and b) Sauter mean drop diameter

peak of the pulsing cycle. At the positive pulse peak of the pulse the dispersed phase is observed to be ejecting out of the sieve holes while during the negative peak of the

pulse large accumulation of the dispersed phase below the plates is observed. Drops are observed



(Dispersed phase hold up)



(Dispersed phase drop diameter)

Figure S.4: Contour plot of a) dispersed phase hold up b) dispersed phase drop diameter during positive (left panel) and negative peak of the pulsing cycle (right panel) ($A_f = 0.02$ m/sec, $V_d = 0.0067$ m/sec, $V_c = 0.0056$ m/sec, 3 inch PSPC)

to be smaller at the location of sieve holes while their size increases as they approach the next plate above. Turbulence dissipation rates are also observed to be high at the location of the holes. Higher values of turbulence dissipation rates and smaller drops are observed during the positive peak of the pulsing cycle. Re-circulations are observed to be more prominent in the continuous phase than in the dispersed phases. The model can be used as a tool to get useful insights into two-phase hydrodynamics prevalent in a PSPCs. Such insights will be helpful for optimum design of the PSPCs.

In Chapter 5 Continuous phase axial dispersion in two-phase flow of 30% TBP in dodecane – water system in a pulsed sieve plate column has been simulated using a 2D two-fluid CFD-PBE approach. Experiments are also carried out in a 3 inch pulsed sieve plate extraction column to obtain axial dispersion coefficient in continuous phase for different values of continuous and dispersed phase velocity (using KCl as a tracer). The model can simultaneously predict spatial and temporal variations of dispersed phase hold up and Sauter mean drop diameter in the column. The model was there after used to carry out a virtual tracer study to predict axial dispersion coefficient. A drag law of the form proposed by Schiller Naumann is used to model the interphase momentum exchange term. Method of classes is used to solve the PB equations. Standard breakage and coalescence kernels reported in literature are used. Quantitative accuracy of the computational approach to predict axial mixing (in continuous phase) is tested by comparing its predictions of axial dispersion coefficient with the experimentally measured values of the same. The absolute average relative error in prediction of axial dispersion coefficient is found to be 3.83%, respectively.

This is also shown in [Fig. S.5](#) which shows that the parity plot between the experimental and CFD-PBE predicted values of continuous phase axial dispersion coefficient. It is observed that all the points are well within $\pm 10\%$ confidence band marked in the figure as dotted lines. Some preliminary experiments were also

attempted to estimate axial dispersion coefficient using radiotracer technique (^{99m}Te) in large diameter columns (6 inch)

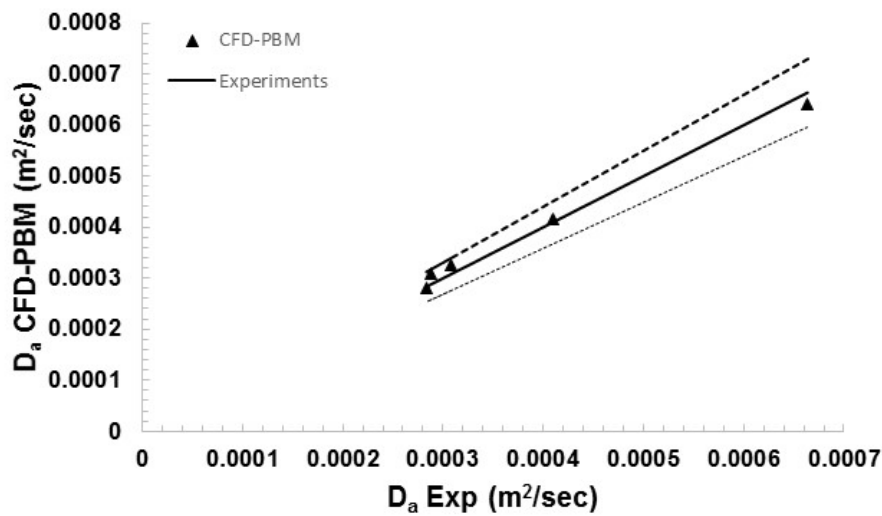


Figure S.5: Parity plot for CFD-PBE predicted and experimentally obtained axial dispersion coefficient.

The validated CFD-PB model was used to gain insights into the flow patterns inside the column. Smaller drops were seen to form in regions near the sieve holes which are characterised by higher values of turbulence dissipation rates. At low dispersed phase velocities sustained re-circulations in the continuous phase were observed while the dispersed phase was seen to preferentially move through the center of the column. However, as the dispersed phase velocity was increased the re-circulations in the continuous phase decreased in span as well as strength and the dispersed phase was also seen to move more uniformly across the column cross section. This observation explained the reason for the decrease in axial dispersion coefficient with increase in dispersed phase velocity as was seen in experimentals as well as in numerical predictions.

In Chapter 6 a 2D CFD-PBE numerical method is developed which can predict space and time varying hydrodynamics and resultant interphase mass transfer characteristics in a pulsed sieve plate extraction column. The developed model is validated against reported experimental data on solute concentration in organic and aqueous phases in a

2 inch PSPC (Gonda et al., 1986). The model prediction is very close to reported results, the absolute average relative error being 2.78%. Fig. S.6 shows the solute concentration (in terms of solute mass fraction) in the organic (dispersed) phase and that in the aqueous (continuous) phase. A gradual decrease in concentration of the solute as the dispersed phase moves up is clearly observed. At the same time whatever solute leaves the dispersed (organic) phase is transferred to the continuous (aqueous) phase and is reflected as an increase in the solute concentration in the continuous phase as it flows downward.

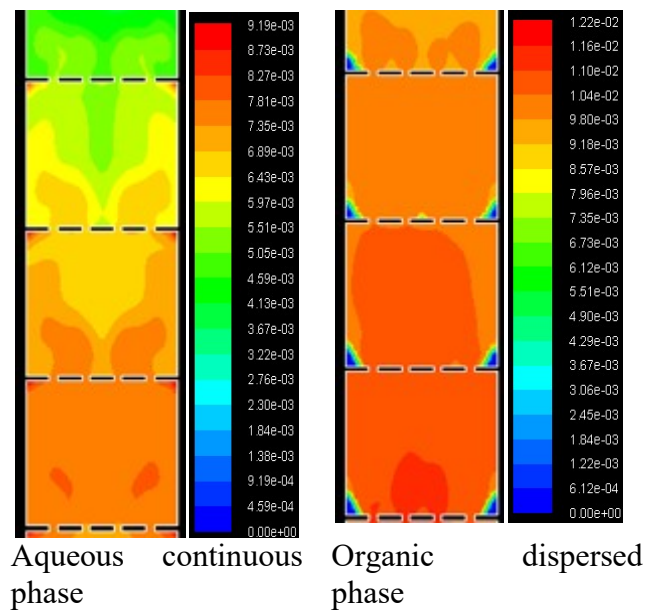


Figure S.6: Contour plot of solute mass fraction in continuous and dispersed phase.

The validated model was then used to understand the local variation of different hydrodynamics parameters like dispersed phase hold up, Sauter mean drop diameter, turbulence dissipation rates and continuous and dispersed phase axial velocity. Transfer of mass from organic phase to aqueous was also clearly revealed along the computational domain. This work provides a way to directly estimate mass transfer performance of a pulsed sieve plate extraction column using CFD model.

Reference:

- Kolhe, N. S.; Mirage, Y. H.; Patwardhan, A. V.; Rathod, V. K.; Pandey, N. K.; Mudali, U. K.; Natarajan, R. (2011) CFD and experimental studies of single phase axial dispersion coefficient in pulsed sieve plate column. *Chemical Engineering Research and Design*, 89(10): 1909-1918.
- Lade, V.; Rathod, V.; Bhattacharyya, S.; Manohar, M.; Wattal, P. (2013) Comparison of normal phase operation and phase reversal studies in a pulsed sieve plate extraction column. *Chem. Eng. Res. Des.*, 91(6): 1133–1144.
- Gonda, K.; Matsuda, T. (1986) Solvent extraction calculation model for PUREX process in pulsed sieve plate column. *J. Nuc. Sci. Tech.*, 23(10): 883-895.

CHAPTER 1

INTRODUCTION

1.1 PULSED COLUMNS

Liquid-liquid extraction is a widely used unit operation in chemical process industry. Examples are waste water purification, metal extraction, recovery of acids, reprocessing of spent nuclear fuel, etc. Numerous designs of liquid-liquid extraction equipment have been developed in order to cover all fields of application. One design which has been known for a long time is the pulsed column. This is a differential contactor with energy input by air pulsing. Compared to other extractors, the pulsed extraction columns are characterized by high throughput and high separation efficiency. These favourable properties have resulted in a widespread application of this equipment in industry (Ferreira et al., 2010; Gameiro et al., 2010; Chaturabul et al., 2012). In general pulsed columns can broadly be classified into two types - pulsed sieve plate columns (PSPC) and pulsed disc and doughnut columns (PDDC). In PSPC the column internal consists of perforated plates while for PDDC the column internal essentially comprises of alternate discs and doughnuts. In the former (PSPC) dispersion is created while the phases are forced to move through small orifices while in the latter (PDDC) the dispersion is created while the phases move in a zig-zag fashion around the disc and in between the doughnuts.

Pulsed sieve plate extraction columns have become the work horse particularly in the back end of the nuclear fuel cycle since long (Ellison, 1952; Liebermann and Jealous, 1953; Schön et al., 1990). In pulsed sieve plate column the mode of providing energy to generate the dispersion and thus enhancing the specific interfacial area and overall volumetric mass transfer coefficient is by air pulsing. The absence of moving mechanical parts obviates frequent repair and servicing. This advantage is of prime importance in nuclear fuel reprocessing.

The two-phase hydrodynamics in these columns is very complex and is dependent on a large number of operating and geometrical/design parameters. Typically pulsed sieve plate column consists of a cylindrical column fitted with perforated plates (Fig. 1.1). It uses mechanical energy in the form of pulsing. Pulsing displaces the layer of heavy liquid resting on each plate and the layer of light liquid collected under the plate. On the upstroke, the displaced volume of light liquid is forced through the holes in the form of jet into the heavy liquid above (Fig. 1.2). On the down stroke, the reverse process takes place, with the heavy liquid jetting downward through the light liquid. For constant phase flow rates there are three stable (mixer-settler, dispersion and emulsion) and one unstable regime of operation (Fig. 1.2) and two flooding types depending on the pulse frequency and amplitude as observed by different investigators. Sege and Woodfield (Sege and Woodfield) defined flooding in pulsed sieve plate columns as the flow condition when the fluid of one phase entering at one end of the column cannot leave at the opposite end and must exit through the outlet line for the second phase. As mentioned before there are two ways a pulsed column can flood. The first way is in the absence or low value of pulsation when the drops (of dispersed phase) coming from the sparger cannot pass through the plate holes of small diameter. As pulsed sieve plate columns do not have any down comer, pulsing is the only source of energy for movement of the phases along the column height. Hence, if pulsing velocity is small, it cannot pass the liquids alternately through the plate holes and flooding occurs. This condition is called as flooding due to insufficient pulsing. The next type of flooding occurs at higher level of pulsing velocity when shear forces on the drops increases significantly and very fine drops are produced. These drops have a terminal rise velocity less than the superficial velocity of the continuous phase. Hence, they start accumulating in the disengaging section of the column at the continuous phase outlet. At higher pulsing velocity drops start going through the continuous phase outlet.

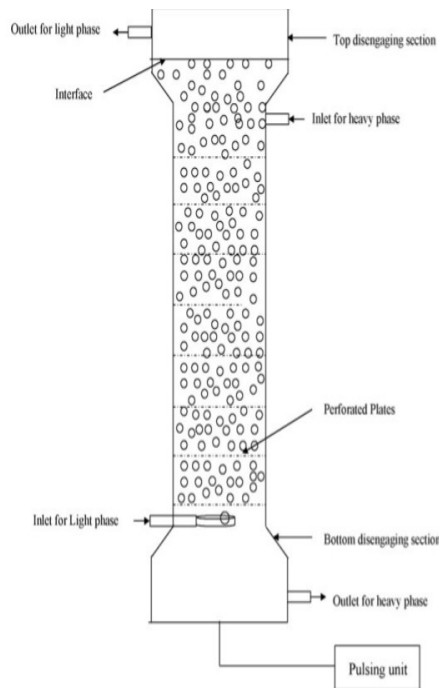


Figure 1.1: Schematic diagram of pulsed sieve plate columns (Yadav and Patwardhan, 2008).

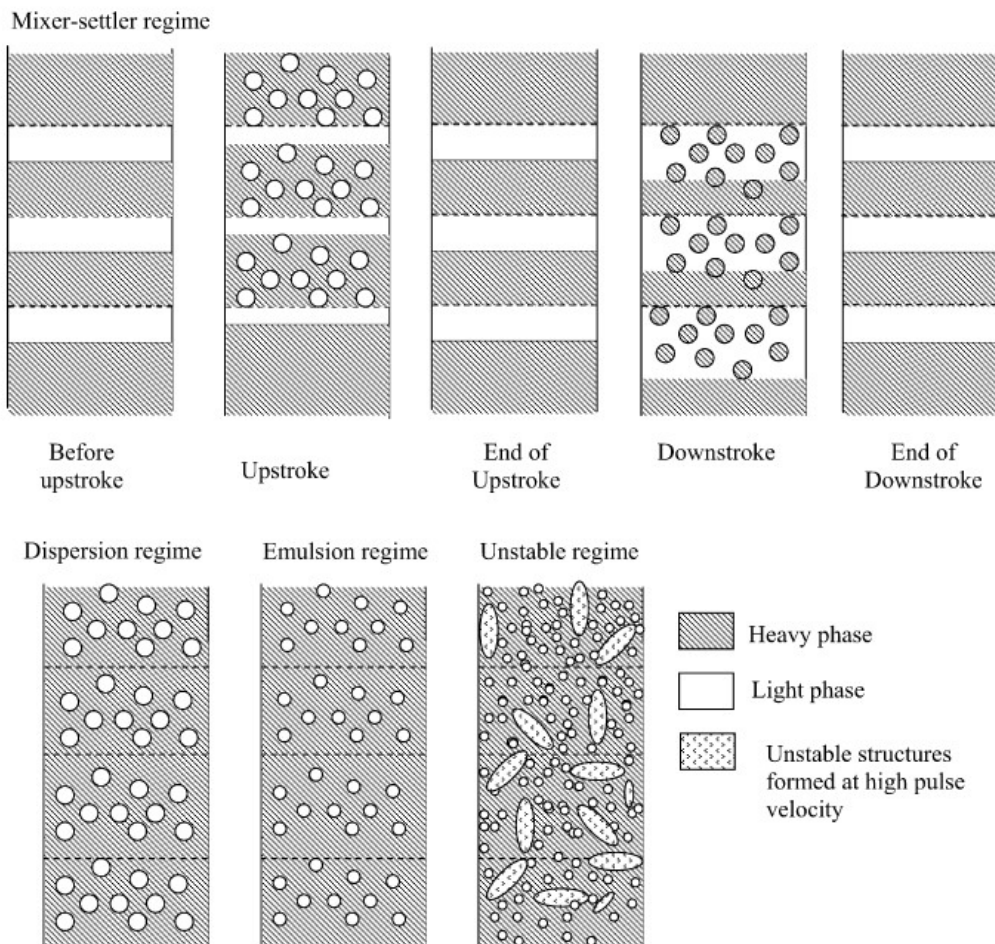


Figure 1.2: Flow regimes in PSPC (Yadav and Patwardhan, 2008).

1.2 LITERATURE SURVEY

Due to compact design, versatility and ease of operation, pulsed columns have been extensively studied as evident by a large number of studies reported in literature. However, most of the reported studies are experimental in nature. Experimental studies on measurement of hold up, drop size distribution and mass transfer rates have also been reported (Thornton et al., 1957; Kumar and Hartland, 1988; Lorenz et al., 1990; Srinivasulu et al., 1997; Kumar and Hartland, 1999; Usman et al., 2009). There have been several experimental studies focused on different regimes of operation in a pulsed column and on phase transition (Sato et al., 1963; Boyadzhiev and Spassov, 1982; Kumar and Hartland, 1983). Experimental studies have been carried out to estimate flooding characteristics also. Some of the studies focus on flooding due to insufficient pulsing (Kagan et al., 1965) while other focus on flooding due to excessive pulsing (Thornton, 1957; Smoot et al., 1959). Extensive experiments have also been carried out to study axial dispersion in two phase flow. Prvcic and co-workers (Kohle et al., 2011) reported back mixing in continuous phase for three different column diameters (72, 152 and 300 mm). Both single-phase (water) and two phase (kerosene-water) systems were reported by the authors. Single-phase axial dispersion was reported to increase with increase in column diameter while it remained independent of column diameter for two phase system. Baird (Baird, 1974) measured axial dispersion coefficients in a 150 mm diameter pulsed column. They used kerosene-water system and reported an increase in axial dispersion coefficient with increase in dispersed phase velocity and pulsing velocity. Yu and Kim (Yu and Kim, 1987) used a 102 mm diameter column to study axial dispersion in continuous phase. The axial dispersion coefficient was reported to increase with both the pulse amplitude and frequency, but it decreased with decrease in plate spacing. Rao and co-workers (Rao et al., 1978) studied continuous phase axial dispersion in a 2 inch PSPC. The phase system used was water and 30% TBP-kerosene. They used a standard plate

cartridge. Axial dispersion coefficient was reported to increase with increase in pulsing velocity (values of dispersed and continuous phase velocities being less than 0.01 m/sec) while for constant pulsing velocity it increased with increase in continuous phase superficial velocity. Axial dispersion coefficient initially increased with an increase in dispersed phase velocity while at still higher values of dispersed phase velocity it did not increase further. One important finding was that axial dispersion coefficient decreased with increase in interplate spacing. Niebuhr and Vogelpohl (Niebuhr and Vogelpohl, 1980) studied axial dispersion in both continuous and dispersed phase in a 80 mm PSPC. Noh and Kim (Noh and Kim, 1980) reported continuous phase axial dispersion in a 108 mm pulsed column. Axial dispersion was seen to increase proportionally with the product of the square of amplitude and frequency.

The end results of most of the experimental studies on pulsed sieve plate columns are empirical correlations. The empirical correlations emanating from these experimental studies on pulsed sieve plate columns are in fact so many that there exists a problem of plenty (Yadav and Patwardhan, 2008). Yadav and Patwardhan (Yadav and Patwardhan, 2008) had given a comprehensive review of previous work reported in PSPC. They also gave a through comparison of different correlations predicting hydrodynamics performance of the column (drop size, hold up, and flooding point) essential for designing a pulsed sieve plate column for a given duty. These hydrodynamic parameters are important in determining the column throughput. The authors also compiled various published literature on mass transfer characteristics in PSPC.

There are several studies on mathematical modeling to predict mass transfer performance of pulsed columns (Gonda and Matsuda, 1986; Torab-Mostaedi and Safdari, 2009). These models, however, embed several empirical correlations for hold up, drop size, mass transfer coefficients and axial dispersion. With each correlation

having its own uncertainty, using several of them in a mathematical model may result in high overall uncertainties in the predictions of such models. Till date the state of art in pulsed sieve plate column design is based on extensive pilot plant data as there is significant risk in designing columns using correlations available in literature. The empiricism associated with these correlations is due to the fact that the most of them are based on studies that focus on global phenomena in a column. There is a dearth of experimental studies that focus on the hydrodynamics at a local level. A comprehensive validated Computational Fluid Dynamics (CFD) model can help one understand the hydrodynamics inside a pulsed sieve plate column from a fundamental level and reduce the uncertainties in design and scale up.

Even though there has been several studies which report CFD simulations of different solvent extraction equipment ([Forney et al., 2002](#); [Wardle et al., 2009](#); [Wardle, 2011](#); [Gandhir and Wardle, 2012](#); [Grafschafter et al., 2017](#)) CFD studies on pulsed column especially pulsed sieve plate columns are very few. Recently, some studies on CFD modeling of pulsed columns have been reported.

CFD studies on single-phase flow are mainly focused on pressure drop and axial dispersion ([Kolhe et al., 2011](#); [Xiaojin et al., 2011](#)). The authors have studied effect of operating parameters like flow velocity and pulsing velocity on axial mixing coefficient. However the effects of different geometric parameters have not been investigated. Yadav and Patwardhan reported two-phase CFD simulations of sieve plate and pulsed sieve plate columns of 0.05m diameter ([Yadav and Patwardhan, 2009](#)). Effects of pulsing on column hydrodynamics, operating regimes and hold up of the dispersed phase were studied. In another study, a 2D two-phase model, based on Euler-Euler two-fluid approach and standard mixture $k-\epsilon$ turbulence model, to simulate pulsed sieve plate column was reported ([Din et al., 2010](#)). But the sieve plates were modeled as a porous medium. Single-phase ([Nabli et al., 1997](#); [Nabli et al., 1998](#)) and two-phase ([Bardin-Monnier et al., 2003a](#); [Bardin-Monnier et al., 2003b](#);

[Retieb et al., 2007](#), [Mate et al., 2000](#)) CFD studies on pulsed disc and doughnut column have also been reported. Majority of the work on two phase CFD simulation of pulsed columns have been carried out using monodispersed assumption - ie a single overall drop size (Sauter mean drop diameter) has been used to describe the quality of dispersion in the whole column. This however is a major limitation as the level of turbulence is not uniform throughout the column but varies both spatially as well as with time. For example in PSPC regions close to the sieve holes are characterised by large values of turbulence intensity and hence drops are expected to be smaller in those regions as compared to other regions in the column. To capture the spatio-temporal variation of Sauter mean drop size as well as dispersed phase hold up (along with other hydrodynamic variable like turbulence and velocity field) all at once CFD based flow and turbulence equations must be solved in conjunction with the population balance equations (PBEs). Recently this approach has been implemented in two reports by Amokrane and coworker ([Amokrane et al., 2014a](#); [Amokrane et al., 2016](#)) for pulsed disc and doughnut columns (PDDC). In the first paper only breakage due to turbulence was implemented while in the second paper both breakage and coalescence were implemented. However limited validation was reported by the authors. To the best of our knowledge there has been no attempt to implement CFD-PBE in PSPC even though PSPC represent a vital contactor in solvent extraction processes, specially nuclear reprocessing. Moreover to the best of our knowledge CFD modeling of axial dispersion coefficient in pulsed sieve plate column till now has been limited to single-phase pulsatile flow ([Kolhe et al., 2011](#); [Xiaojin et al., 2011](#)). To the best of our knowledge there is no work till date on numerical prediction of axial dispersion coefficient in two phase flow in pulsed sieve plate column even though an accurate prediction of axial dispersion/backmixing coefficient (in either phase) is essential to predicting mass transfer performance of the column using one dimensional models. It is these gap areas that this research work aims to address.

1.3 RELEVANCE OF RESEARCH WORK

Mass transfer in pulsed columns is, significantly affected by the prevailing hydrodynamics. Hence, it is important to understand the column hydrodynamics for a proper estimate of the mass transfer efficiency of pulsed columns. Because of limited fundamental understanding of functioning of PSPCs due to intrinsically complex pulsatile, two-phase turbulent flow ridden with continuous coalescence and re dispersion of droplets, design of a PSPC is still based on operational experience and experimental data generated at pilot-scale. Since it is difficult to experimentally investigate local hydrodynamics in a PSPC, especially in large diameter columns, CFD-PBE based modeling of PSPCs becomes very important as such models can provide very useful insights into hydrodynamics at a local level. Such models can be used to estimate dispersed phase hold up, Sauter mean drop diameter, axial dispersion coefficient (in either phase) which can in turn be used to estimate mass transfer performance of the column. As these parameters are estimated from first principles the CFD-PBE model can be said to be scale independent. Thus these insights can reduce the empiricism involved in designing PSPC and predict mass transfer performance of even scaled up (large diameter) columns. Hence, CFD-PBE based approaches can lead to a significant reduction in empiricism typically involved in scale-up of PSPC.

The objective of this research work is to develop a CFD-PBE model to predict relevant hydrodynamic parameters in a PSPC, validate the model thoroughly against reported and in house experimental data and used the validated model to investigate in detail local as well as global hydrodynamics of the column.

1.4 OUTLINE OF RESEARCH WORK

The outline of the research work is mentioned as below.

- CFD modeling of single-phase flow in a PSPC, validation of the modeling approach and investigation of the effect of column geometries on axial dispersion coefficient (Chapter 1).
- Euler-Euler two-fluid CFD modeling to simulate two-phase flow in PSPC assuming the dispersed phase to be monodispersed with drop diameter available from experiments. The model was validated against reported literature data (Chapter 2).
- Euler-Euler two-fluid CFD modeling to simulate two-phase flow in PSPC assuming dispersed phase to be monodispersed with drop diameter obtained from a suitable empirical correlation. The model was validated against reported literature data (Chapter 3).
- Euler-Euler two-fluid CFD-PB (population balance) coupled model to simultaneously obtain drop size distribution and the two-phase flow variables in the column. The model was validated within-house generated experimental data on dispersed phase hold up and Sauter mean drop diameter. To the best of our knowledge, it is the first reported attempt on CFD-PB modeling of PSPC (Chapter 4).
- CFD-PB coupled two-fluid model was used to predict axial dispersion coefficient in continuous phase in a PSPC. The model was validated against in-house generated experimental data on axial dispersion coefficient in continuous phase in PSPC. Prediction of axial dispersion coefficient using CFD-PB simulations of PSPC also, to the best of our knowledge, not reported so far. (Chapter 5).
- CFD-PB coupled model was used to simulate interphase mass transport of a species/solute. The developed model was validated against reported

experimental data. Once again this is the first time, to the best of our knowledge, a CFD-PB model is used to predict interphase mass transfer of solute in a liquid-liquid solvent extraction contactor, in general, and in a pulsed column, in particular.

CHAPTER 2

SINGLE-PHASE CFD SIMULATIONS TO PREDICT AXIAL DISPERSION

2.1 INTRODUCTION

As mentioned above, axial dispersion coefficient is an important parameter that goes as an input to the mathematical models predicting mass transfer performance of the pulsed columns ([Gonda and Matsuda, 1986](#); [Torab-Mostaedi and Safdari, 2009](#)). Presently axial dispersion coefficients are estimated using empirical correlations. Estimation of axial dispersion coefficients using CFD will reduce this empiricism. The problem of predicting the axial dispersion coefficient using CFD is addressed in a phased manner with prediction of axial dispersion in single-phase flow, focus of this study, being the first step. Subsequently, CFD-PBE simulations to predict axial dispersion in two-phase flow in pulsed sieve plate column will be carried out.

In the present chapter single-phase pulsatile flow in PSPC has been modeled using an unsteady state RANS based approach. Suitability of using a RANS based approach has been reported in literature ([Angelov et al., 2007](#)). The challenges involved in modeling the pulsed column are discussed in a review paper ([Grinbaum, 2006](#)). The geometry of a real pulsed sieve plate column is computationally complex. There are a large number of plates with each plate having a large number of small holes. This makes the grid in a 3D geometry of a pulsed sieve plate column too big to handle. Due to pulsing, the flow field inside the column is also time periodic in nature. To capture this time periodic flow, transient simulations with small time step size are required. This makes the simulations computationally intensive. Therefore, to reduce the computational efforts to get results in a reasonable time, some simplifications in the geometry as well as computational approach are required. The simplifications tried in this study are using 2D geometry instead of 3D geometry, using limited

number of plates instead of actual number of plates and to evaluate a new approach called as the snapshot approach to further reduce the computational time. Based on the flow field virtual tracer study was carried out to arrive at axial dispersion coefficient. The model was validated against reported experimental data.

2.2 GOVERNING EQUATIONS AND GEOMETRIES USED IN SIMULATIONS

2.2.1 Governing Equations

In this study 2D CFD simulations have been carried out. Each simulation involves two steps. The two-step method used in this has earlier been reported to predict RTD (Residence Time Distribution) in stirred tanks (Singh et al., 2007; Singh et al., 2008). The first step involves solution of Reynolds Averaged Navier Stokes (RANS) equations along with equations of standard k - ε model of turbulence to predict the transient (time periodic) flow field. The governing equations solved in this step are given by Eqs. (2.1) – (2.9).

$$\frac{\partial \rho}{\partial t} = -(\nabla \cdot \rho \bar{V}) \quad (2.1)$$

$$\frac{\partial(\rho \bar{V})}{\partial t} + \nabla \cdot (\rho \bar{V} \bar{V}) = -\nabla p + \nabla \cdot \bar{\tau} + \rho \bar{F}_b \quad (2.2)$$

$$\bar{\tau} = \bar{\tau}^v + \bar{\tau}^t \quad (2.3)$$

$$\bar{\tau}^v = \mu (\nabla \bar{V} + \nabla \bar{V}^T) \quad (2.4)$$

$$\bar{\tau}^t = \mu^t (\nabla \bar{V} + \nabla \bar{V}^T) \quad (2.5)$$

$$\frac{\partial(\rho k)}{\partial t} + \nabla \cdot (\rho \bar{V} k) = \nabla \cdot \left(\frac{\mu^t}{\sigma_k} \nabla k \right) + G_k - \rho \varepsilon \quad (2.6)$$

$$\frac{\partial(\rho \varepsilon)}{\partial t} + \nabla \cdot (\rho \bar{V} \varepsilon) = \nabla \cdot \left(\frac{\mu^t}{\sigma_\varepsilon} \nabla \varepsilon \right) + \frac{\varepsilon}{k} (C_{1\varepsilon} G_k - C_{2\varepsilon} \rho \varepsilon) \quad (2.7)$$

$$\mu^t = \rho C_\mu \frac{k^2}{\varepsilon} \quad (8)$$

$$G_k = \mu^t (\nabla \bar{V} + \nabla \bar{V}^T) : \nabla \bar{V} \quad (2.9)$$

In the first step, transient simulations are carried out while tracking the evolution of turbulent viscosity for several pulsing cycles. The first step is deemed to be complete after domain averaged turbulent viscosity attains a time periodic constant value. In the second step of simulations, virtual tracer studies are carried out in which a scalar (or tracer) transport equation given by Eq. (2.10) is solved.

$$\frac{\partial \phi}{\partial t} + \bar{V} \cdot \nabla \phi = D \nabla^2 \phi \quad (2.10)$$

Where, D is the effective (tracer) diffusivity. The value of effective (tracer) diffusivity accounts for both the molecular tracer diffusivity and turbulent diffusivity.

Since the flow field in a pulsed sieve plate column is time periodic, ideally tracer transport equation should be solved along with RANS equations. However, this will require solution of a large number of equations for a long period of time (time till the tracer remains inside the column) and is computationally very expensive. To overcome this, an approach called here as the snapshot approach has been used. In this approach, in the second step, flow equations are no longer solved while tracer transport equation is solved for four different flow fields frozen at four points (corresponding to 25%, 50%, 75% and 100% of the time period) of the sinusoidal pulsing velocity. Ensemble averaging is done using the results from all the four simulations. A similar snapshot approach has been used to model baffle impeller interactions in stirred tank in which flow field is time periodic (Ranade et al., 2002). Tracer concentration at the outlet versus time data obtained after ensemble averaging is used to generate the step tracer response i.e. F(t) curves which in turn is processed to calculate the first moment (t_m) and second moment (σ^2) of the RTD (Residence Time Distribution) curve using Eq. (2.11) and (2.12).

$$\sigma^2 = \int_0^{\infty} (t - t_m)^2 dF = \sum_0^{\infty} t^2 \Delta F - t_m^2 \quad (2.11)$$

$$t_m = \int_0^{\infty} t dF = \sum_0^{\infty} t^2 \Delta F \quad (2.12)$$

The values of t_m and σ^2 can be used to obtain the value of Peclet number using the following equation applicable for closed-closed system (Fogler, 1986).

$$\frac{\sigma^2}{t_m^2} = \frac{2}{Pe} - \frac{2}{Pe^2} [1 - e^{-Pe}] \quad (2.13)$$

Peclet number is defined as $Pe = LU/D_a$, where U is the average velocity of the flowing liquid, L is the length between the tracer injection point and tracer monitoring point and D_a is the dispersion coefficient. Typically pulsed columns are quite long with small plate spacing and small holes in plates. This makes the CFD modeling of pulsed sieve plate column computationally quite challenging. Turbulent modeling of a 3D complete pulsed sieve plate column is computationally very expensive. Hence, to keep the computational requirement within modest limits it is necessary to have a 2D model and optimize the computational strategy such that despite this simplification of computational domain the model predicts the hydrodynamic performance of the actual column with reasonable accuracy. The first issue to address is whether to simulate the complete column or a geometry with reduced number of sieve plates. Lorentz et al. suggested that hold up and sauter mean diameter in a pulsed column do not change after first few sieve plates (Lorentz et al., 1990). Hence, it should be possible to represent the column with reduced number of plates. Secondly, in a 2D model of the real 3D sieve plate, percent free area must be kept same. To achieve this, either the pitch or the hole diameter in the 2D model of the sieve plate will be different from the actual sieve plate. The question whether to keep hole diameter same or pitch same in 2D representation of the real 3D sieve plate, must be answered. Thirdly, the flow field in a pulsed column is periodic in time. While carrying out the virtual tracer studies,

ideally one should solve flow equations and scalar transport equation at the same time. However, this approach is computationally expensive. A snapshot approach which solves the scalar transport equation over a finite number of frozen flow fields will significantly reduce the computational load. Suitability of this approach needs to be ascertained.

While solving the RANS equations, the pulsing action is introduced by applying a periodic inlet velocity at an edge in the lower part of the computational domain. The pulsing velocity is defined as

$$U_p = \pi A f \sin(2\pi f t) \quad (2.14)$$

2.2.2 Geometries Used in Simulations

This study uses the geometry and experimental data reported in a recent study on axial dispersion in single-phase flow in a 3 inch diameter pulsed sieve plate column (Kolhe et al., 2011). The column is 1.05 m long. A cartridge having 20 stainless steel sieve plates is fitted inside the column. Diameter of the holes in the plates is 3 mm. Holes are arranged on a 5 mm triangular pitch. Percent free area of plates is 21%. Plate spacing is 50 mm. Two identical disengagement sections of 0.152 m diameter and 0.20 m length are connected to both the ends of the column. A 1 inch diameter pulse leg is connected to the base of the bottom disengagement section. A solenoid valve (3/2 way) operated by an electronic timer and air pressure regulator is provided to get desired magnitude and frequency of the pulse. The concentration of tracer is monitored using a conductivity meter. The conductivity probe is fitted at a distance of 0.08 m below the bottom most plate of the column. The geometry of the column is shown in Fig. 2.1. Fig. 2.1 also shows the computational domain containing four plates which is used in most of the simulations discussed in the coming sections.

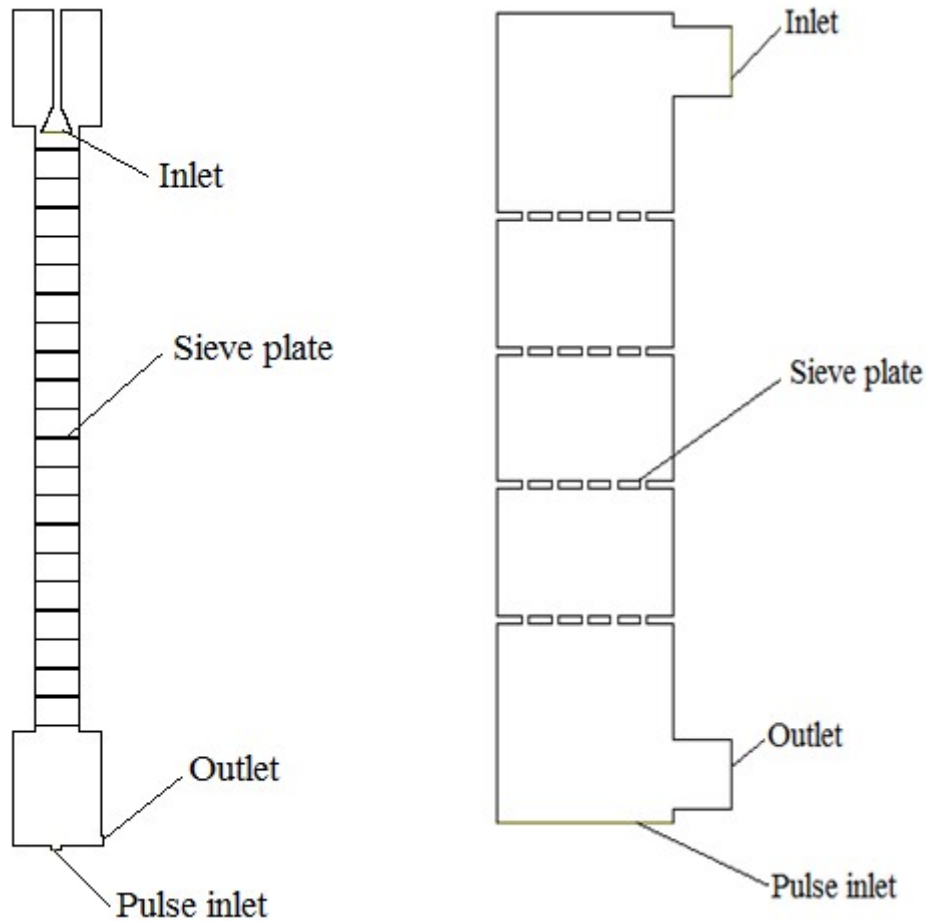


Figure 2.1: Computational domains used in the simulations of full column (left) and column consisting of four plates (right)

An extensive literature survey reveals that there is no experimental study reporting local measurement of velocity field in a pulsed sieve plate column. However, one study on PIV (Particle Image velocimetry) and LDV (Laser Doppler Velocimetry) measurements of local velocity field in a pulsed disc and doughnut column is reported (Bujalski, 2006). In absence of experimental data of local velocity field in a pulsed sieve plate column we have carried out the simulation of pulsed disc and doughnut column to validate the efficacy of the CFD approach adopted in this work to correctly predict the flow field. The pulsed disc and doughnut column for which experimental data on velocity field are reported has 0.1 m internal diameter. The spacing between disc and doughnut is half of the column diameter and the free flow area is 23%. The internal discs are held by a central shaft running throughout the length of the column

while the doughnuts are kept separate from one another and held by spacers. Three metal rods each of 50 mm height, spaced 120° apart radially act as the spacers. Pulsation is provided by a mechanical pulsator. The pulsing amplitude and frequency is controlled by a variable speed motor. The variation of the local velocity at a point (14 mm from the centre line and 7 mm under the doughnut internal) has been experimentally tracked using PIV and LDV. The disc and doughnut column, being truly symmetric in nature, can be represented as an axisymmetric 2D geometry. We have simulated the entire column so as to capture even the entrance and exit effects. A full transient simulation was carried out so as to capture the transient variation of local velocity. The computational domain is shown in Fig. 2.2.

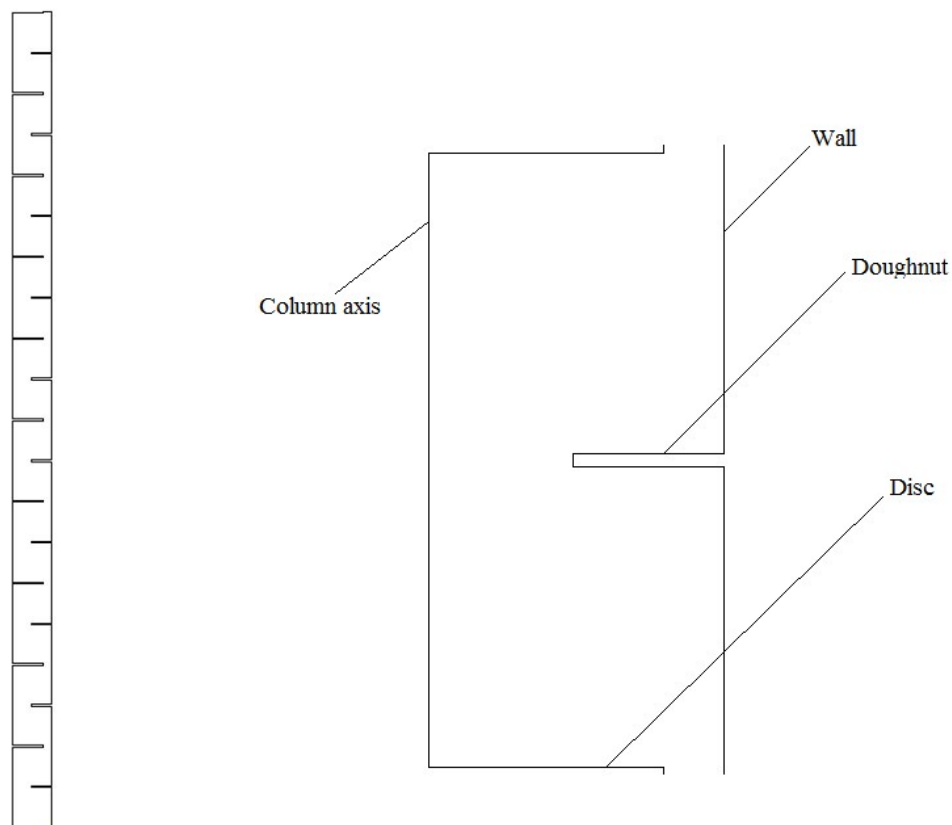


Figure 2.2: The computational domain (left) and a section of the computational domain showing one disc and doughnut (right)

2.3 COMPUTATIONAL APPROACH AND VALIDATION

2.3.1 Identification of an Appropriate Computational Approach

2.3.1.1 Grid Independence Test

Before carrying out final simulations of pulsed sieve plate column grid independence test was performed. For carrying out the grid independence test direct approach (coupled solution of RANS and scalar transport equation) was used. Three grid densities, coarse (2.33×10^5 cells/m²), fine (1.07×10^6 cells/m²) and finer (3.58×10^6 cells/m²) were considered. The total number of cells for the entire computational domain was 25600, 58000, and 84000 for the coarse, fine and finer grid densities, respectively. A reduced computational domain comprising of 4 plates was used. The results of the grid independence test are shown in Fig 2.3. It is found that the dimensionless F-curves for the fine and the finer grid densities are quite close. Hence, the fine grid was concluded to be the optimum grid size. A time step of 0.01 sec was used in the transient simulations. For the fine grid the Courant number is estimated to be 0.7 for a time step of 0.01 sec. The fluctuations in the F-curves of Fig. 2.3 are because of pulsing action which causes the flow to be time periodic.

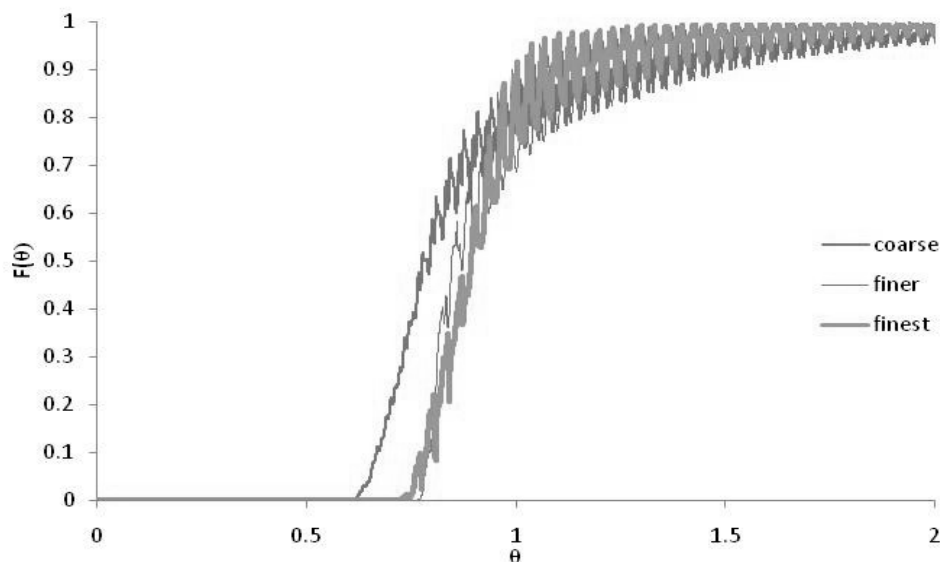


Figure 2.3: Comparison of F-curves obtained for different grid densities ($U = 0.01$ m/sec, $A_f = 0.01$ m/sec)

2.3.1.2 2D Representation of 3D Geometry

In the actual sieve plates the hole diameter is 3 mm, holes are arranged in a triangular pitch and centre-to-center distance between the holes is 5 mm. The fractional opening area is 21%. These 3D values cannot be exactly used in the 2D geometry of the sieve plate. The free opening area in 2D representation must be the same as in the actual geometry. To keep this same in 2D representation, two approaches can be followed – keeping hole diameter same as in the actual geometry, varying the pitch or keeping the pitch same as in the actual geometry, varying the hole diameter. Simulations have been carried out to identify which of the two approaches is more appropriate for 2D representation of 3D geometry. A computational domain comprising of 4 plates has been used in these simulations.

In the CFD simulation carried out using the first approach, the pitch was kept same as in the actual geometry and hole diameter used was 1.23 mm instead of 3 mm. In the CFD simulation carried out using the second approach the hole diameter was kept same as in the actual plate but the pitch was changed such that the fractional free area is constant at 21%. Comparison of the two approaches was carried out by comparing the F-curves predicted by the CFD simulations with the experimental F-curve. [Fig. 2.4](#) shows this comparison. It is seen that the F-curve predicted by the approach in which hole diameter is kept same as in the actual geometry shows a better match with the experimental F-curve. The congruence between the experimental F-curve and the predicted F-curve is good both during the initial rise as well as during the change of slope. Thus the approach in which the hole diameter is kept unchanged in 2D representation of 3D geometry, gives better prediction as compared to the approach in which pitch is kept unchanged. Variances of the dimensionless F-curves were also evaluated for quantitative comparison of the F-curves predicted by the two approaches with the experimental F-curve. The difference between the variances of the predicted and experimental F-curves was about 24.4% for the approach in which the hole diameter was kept the same as in the actual geometry. The difference

between the variances of the predicted and experimental F-curves was about 44% for the approach in which the pitch was kept the same as in the actual geometry. Hence, it is concluded that for 2D representation of the actual sieve plate geometry, the hole diameter must be kept unchanged. In these simulations, the snapshot approach, described latter, is used. Due to use of the snapshot approach, predicted F-curves are free of oscillations.

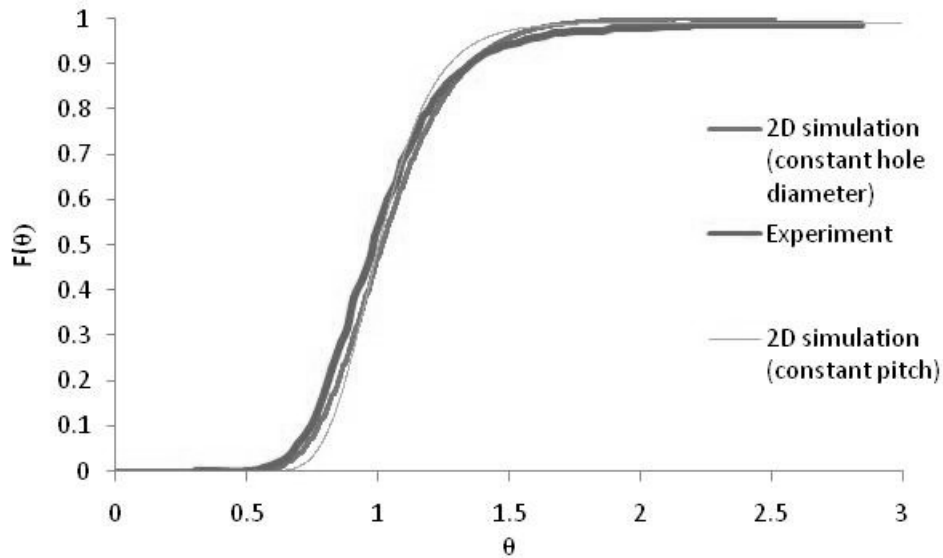


Figure 2.4: Comparison of dimensionless F-curves predicted by the CFD simulations carried out for two possible approaches of 2D representation of the actual geometry. ($U = 0.010$ m/sec and $A_f = 0.010$ m/sec)

2.3.1.3 Snapshot Approach Versus Direct Approach

Since the flow in a pulsed sieve plate column is time periodic, while carrying out the virtual tracer study, flow equations should be solved along with the equation for the scalar transport. This approach can be called the direct approach. However, in this work a snapshot approach has been proposed to reduce the computational time. In the simulations carried out to test suitability of the snapshot approach a column consisting of 4 plates has been considered. In the snapshot approach flow equations are no longer coupled with the tracer transport equation. The tracer transport equation is solved for four different frozen flow fields corresponding to 25%, 50%, 75% and 100% of the time period of the pulse. Ensemble averaging is done using the results

from all the four simulations. Simulations were carried out to compare the F-curves predicted by the direct approach and snapshot approach. Fig. 2.5 shows this comparison. As can be seen difference in F-curves obtained from the direct approach and the snapshot approach is hardly any.

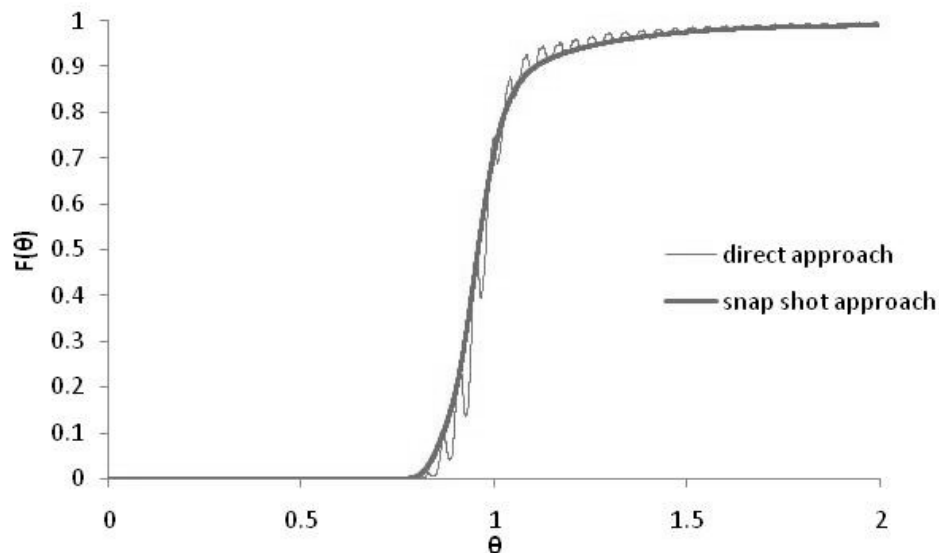


Figure 2.5: Comparison of the F-curve obtained from the direct approach and the snapshot approach ($U = 0.01$ m/sec, $Af = 0.01$ m/sec)

While the F-curve obtained from the direct approach exhibits fluctuations about a mean value, the F-curve obtained from the snapshot approach is smooth. In the direct approach the scalar transport equation is solved along with the momentum, continuity and equations for turbulence model. For a 2D geometry this entails solution of 6 coupled equations at the same time for each time step. On the other hand, in the snapshot approach 4 uncoupled scalar transport equations are solved for each time step. Hence, the computational requirements are significantly reduced in the snapshot approach. Fig. 2.6 shows the velocity contour and the velocity vector plots for the four frozen points which have been used to represent the time periodic velocity field in the computational domain in the snapshot approach. The four representative points of the sinusoidal pulse from left to right are positive peak, mean (while going down), negative peak, and mean (while going up) respectively. It is seen that the velocity is more at the holes. In the regions away from the holes the velocity is more or less

uniform. It is also noted that velocity magnitudes are higher at the inlet and the outlet ports. It is observed that during the positive peak of the pulse (represented by the first image from the left in Fig. 2.6) the velocity vectors are smaller in comparison to those during the negative peak of the pulse (represented by the third image from the left in Fig. 2.6). This is expected because the net flow which is downwards is opposed during the positive peak of the pulse.

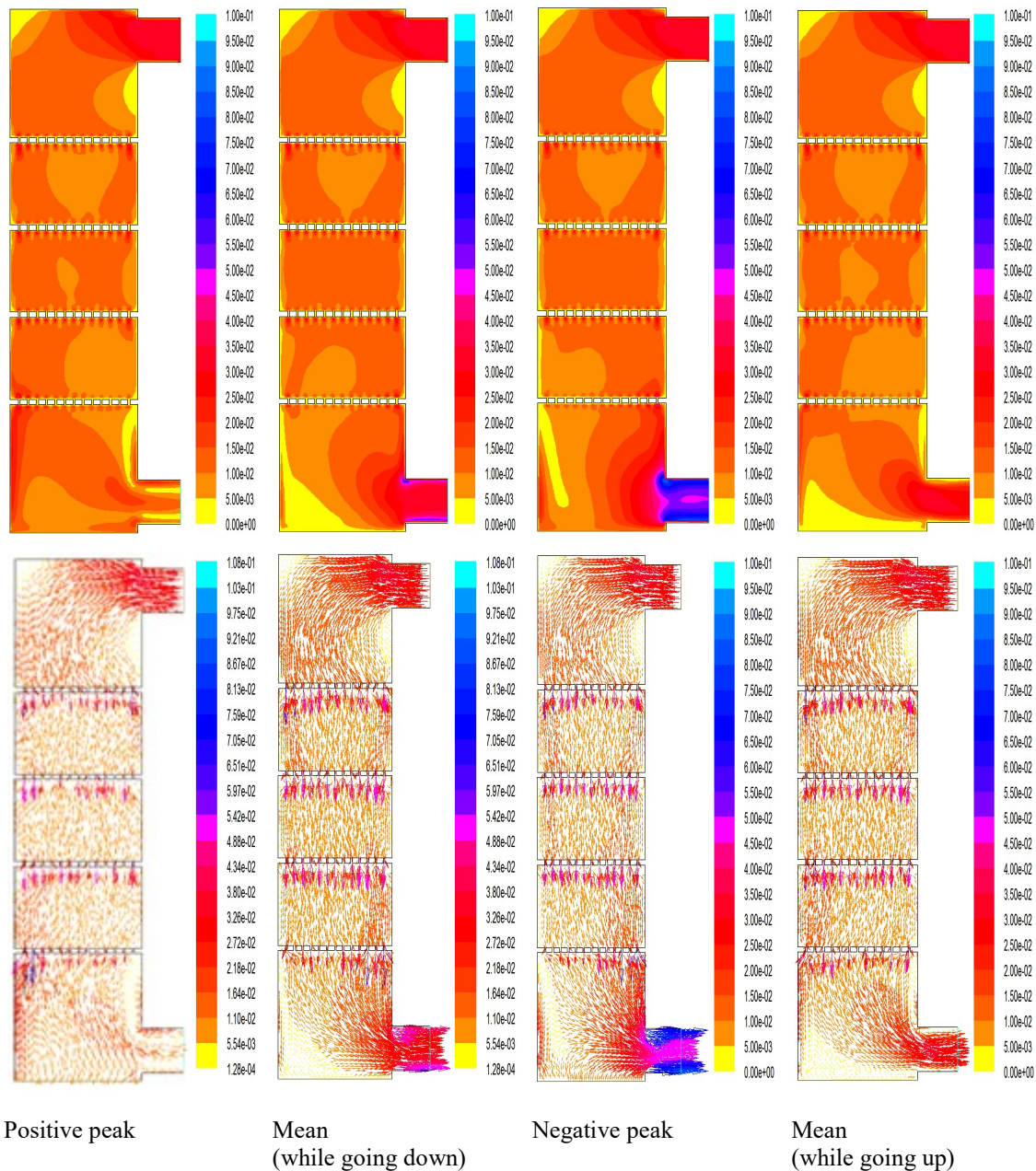


Figure 2.6: Velocity magnitude contour and velocity vector plots at the four representative points of one pulsing cycle ($U = 0.01$ m/sec, $A_f = 0.01$ m/sec)

2.3.1.4 Full Column Versus Simulation of Column with Less Number of Plates

To reduce the computational time only a section of the column consisting of 4 plates has been used in this work. The approach to use a geometry having less number of plates has been reported in earlier studies on CFD simulations of pulsed columns (Kolhe et al., 2011; Yadav and Patwardhan, 2009). However, the suitability of this approach needs to be checked. To check this, simulations were carried out for the full column consisting of 20 plates and the column consisting of 4 plates. The snapshot approach was used in these simulations. The geometries used for the simulations of the full column and the column with 4 plates are already shown in Fig. 2.1. Comparison of $F(\theta)$ versus θ plot obtained from the simulations of the full column and the column containing 4 plates is shown in Fig. 2.7. As can be seen, the F -curves predicted by the simulation of the full column and the column with 4 plates almost overlap. Variances of the two dimensionless F -curves were also evaluated. It was seen that the variance of the predicted dimensionless F -curve for the two cases (0.062 for 20 plates and 0.055 for 4 plates) were quite close. It is, therefore, concluded that the computational approach of considering a column consisting of less than actual number of plates, 4 plates in the present case, is good enough.

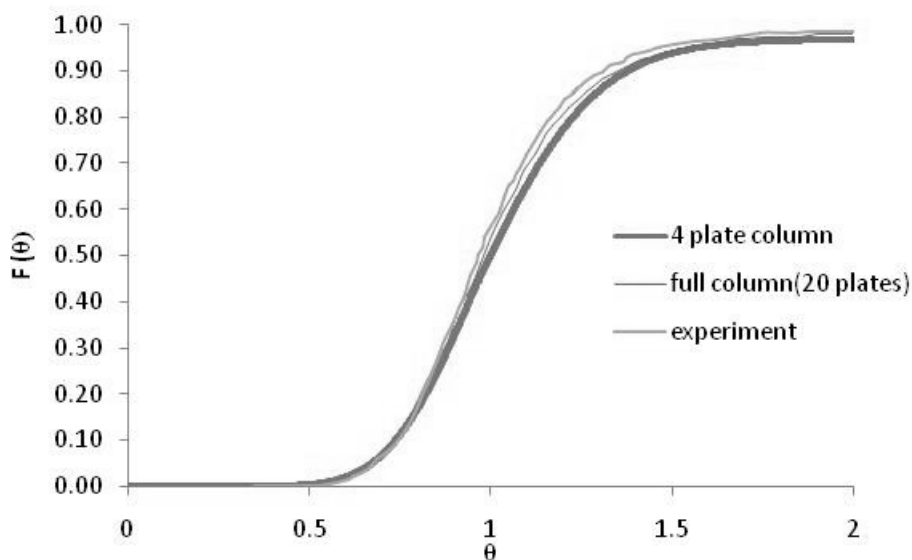


Figure 2.7: Comparison of $F(\theta)$ versus θ curves obtained from the simulations of the column having 4 plates and the column having 20 plates ($U = 0.01$ m/sec, $Af = 0.01$ m/sec)

2.3.2 Validation

2.3.2.1 Validation for Prediction of Velocity Field

In the absence of experimental data on local velocity field in a pulsed sieve plate column, the adequacy of the computational approach proposed in this study for predicting velocity field has been ascertained by carrying out simulation of single-phase flow in a pulsed disc and doughnut column for which experimental data of local velocity field are reported in literature (Bujalski et al., 2006). The details of the geometry are already provided in a previous section. Simulations are carried out for the condition of no net flow and pulsing amplitude of 20 mm and frequency of 1 Hz. This is the condition for which experimental data is reported. The pulse inlet is located at the bottom of the domain, the outlet is defined as the pressure outlet. No slip condition is implemented at the wall. Temporal variation of velocity as predicted by the CFD simulation at a point (14 mm from the centre line and 7 mm under the doughnut internal) is noted and compared with reported LDV and PIV measurements. The predicted velocities are found to be very close to the experimentally measured velocities as is shown in Fig. 2.8. Hence, it is concluded that the computational approach adopted in this work can be used to predict the velocity field with reasonable accuracy.

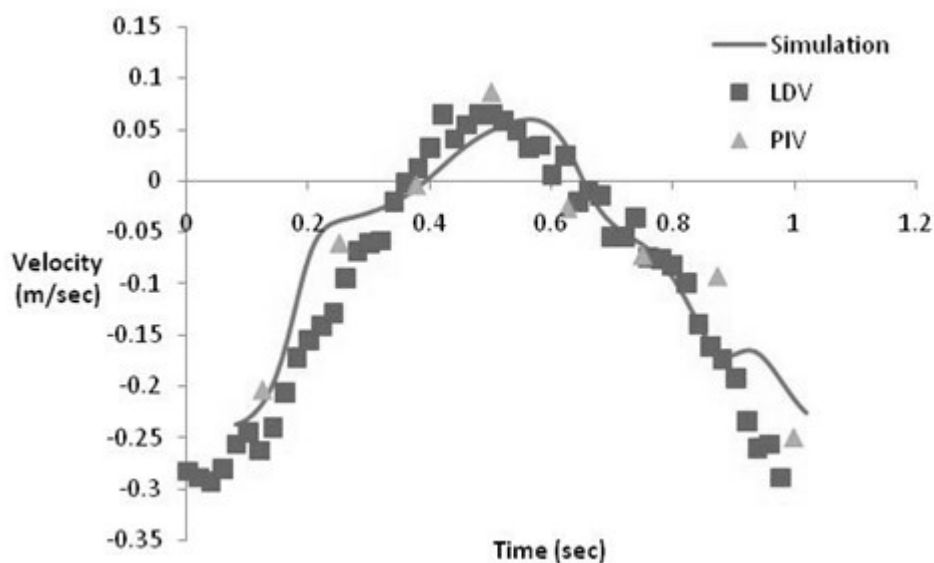


Figure 2.8: Comparison of predicted temporal variation of point velocity with the same observed by using PIV and LDV

2.3.2.2 Validation for Prediction of Axial Dispersion Coefficient

CFD simulations to predict axial dispersion coefficients in pulsed sieve plate column were carried out using the computational strategy finalized in the previous sections. Validation was carried out by comparing the predicted axial dispersion coefficients with the experimentally measured values of axial dispersion coefficients as reported in the literature (Kolhe et al., 2011). The operating conditions for which simulations were carried out are listed in Table 2.1. Three simulations were carried out by varying superficial velocity for a constant pulsing velocity. Three simulations were carried out by varying pulsing velocity for a fixed superficial velocity.

Table 2.1: Operating conditions for which simulations are carried out

Simulation No.	Superficial velocity (U) (m/sec)	Pulsing velocity (Af) (m/sec)
1	0.020	0.020
2	0.025	
3	0.030	
4	0.020	0.015
5		0.020
6		0.025

The comparison of the predicted and measured values of dispersion coefficients is shown in Fig. 2.9 and Fig. 2.10. The figures show that the values of axial dispersion coefficient predicted by the CFD simulations compare reasonably well with the experimentally measured values of dispersion coefficient. The maximum (absolute relative) error between the predicted and the reported values of dispersion coefficient is less than $\pm 15\%$.

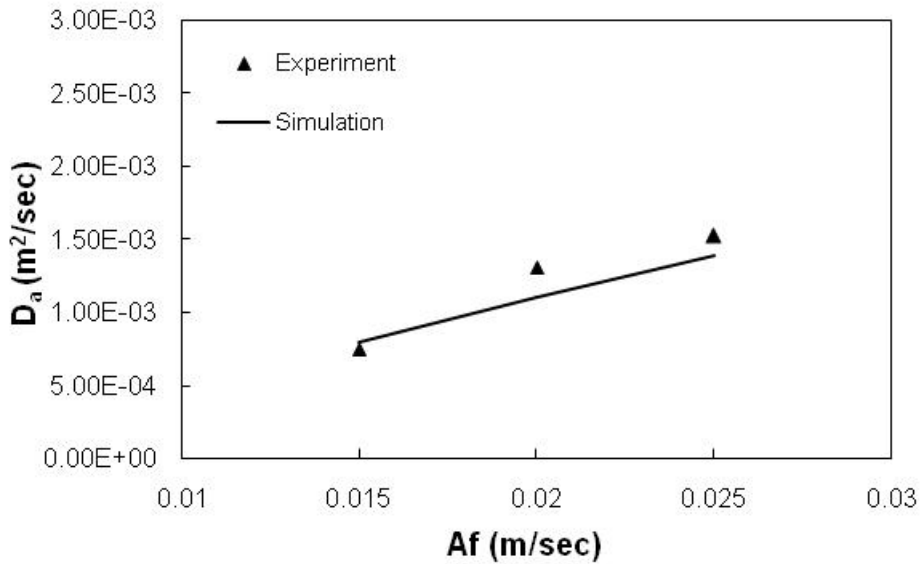


Figure 2.9: Effect of pulsing velocity on axial dispersion coefficient

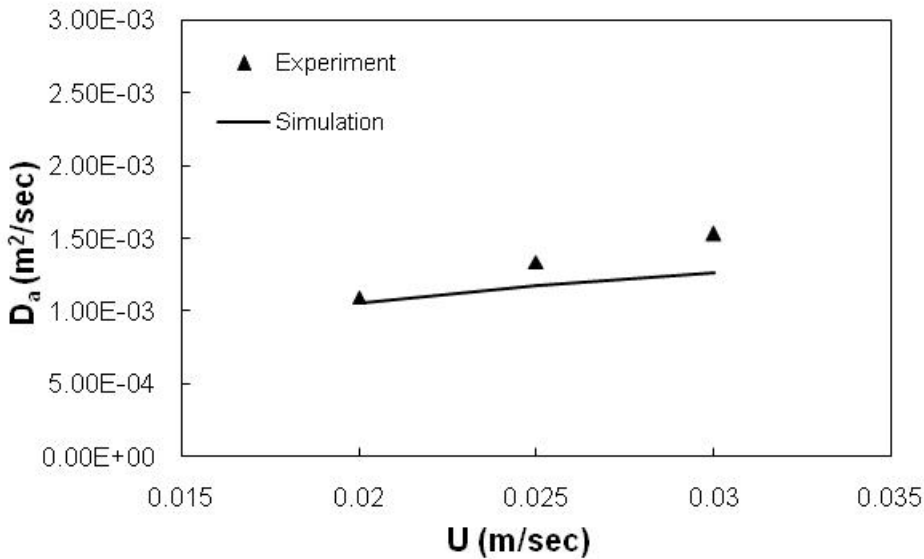


Figure 2.10: Effect of superficial velocity on axial dispersion coefficient

2.3.2.3 Effect of Hole Diameter and Percent Free Area on Axial Dispersion

After validating the computational model it is worth ascertaining that the validated computational approach is giving physically realistic predictions. To ascertain this, the validated computational approach has been used to study how axial dispersion coefficient in single-phase flow in a pulsed sieve plate column is dependent on the geometric parameters (hole diameter and percent free area) of the sieve plates. In the first set of simulations percent free area of 15%, 23% and 27% were used keeping the hole diameter constant at 3 mm. In the second set of simulations, hole diameters of 2

mm, 4 mm, 8 mm and 16 mm were used keeping percent free area 21%. Different hole diameters with the same percentage opening are realized by changing the pitch and number of holes. For hole diameters of 2 mm, 4 mm, 8 mm and 16 mm, number of holes are found out to be 8, 4, 2, 1, respectively. Flow velocity and pulsing velocity were kept constant at 0.025 m/sec and 0.025 m/sec respectively. Fig. 2.11 and Fig. 2.12 show the effects of hole diameter and percent free area on predicted values of axial dispersion coefficient, respectively.

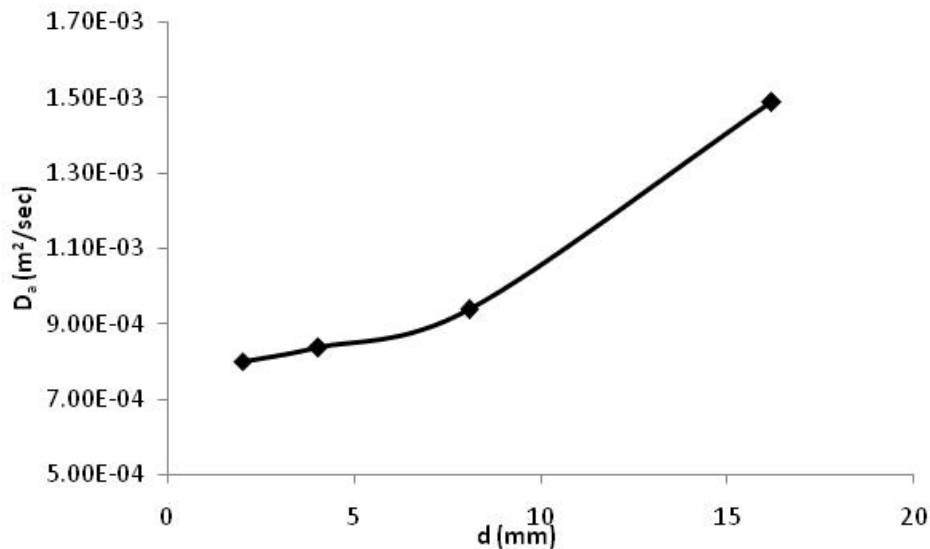


Figure 2.11: Effect of hole diameter on axial dispersion coefficient (percent free area kept at 21 %)

It can be seen that with increase in hole diameter, keeping the percent free area constant, axial dispersion is increasing. As the hole diameter reduces, keeping percent free area the same, the number of holes are reduced. For a less hole diameter, the number of holes are more and hence flow is more uniformly distributed in the column cross-section and tend to approach plug flow leading to reduced value of axial dispersion coefficient. It can also be seen that the axial dispersion coefficient is predicted to be reducing with increasing percent open area. With increase in fractional opening for the same mass flow rate the maximum velocity (which is seen at the holes) will reduce leading to reduced turbulence and reduced back mixing and hence

reduced axial dispersion coefficient. The results from the validated CFD model of the pulsed sieve plate column are thus physically realistic and explainable.

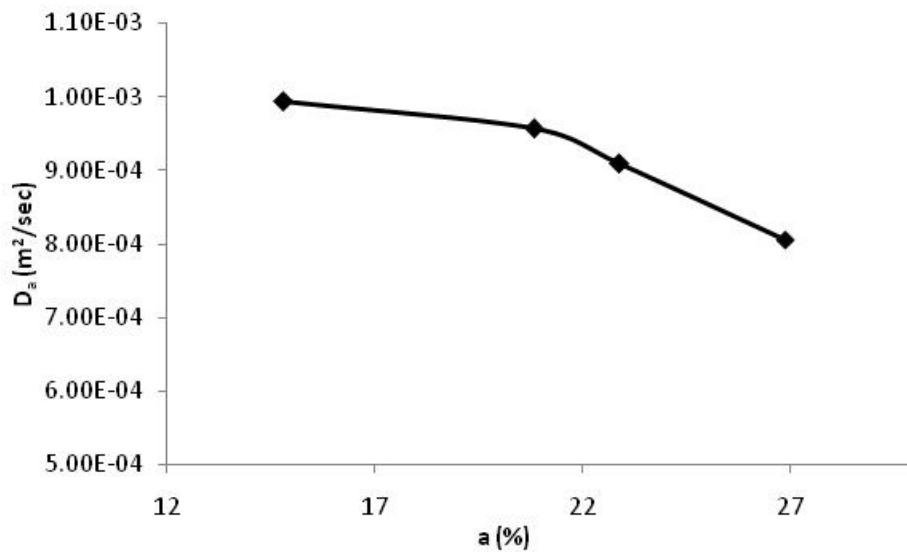


Figure 2.12: Effect of percent free area on axial dispersion coefficient (hole diameter kept at 3 mm)

2.4 CONCLUSION

CFD simulations of single-phase flow in a pulsed sieve plate column are presented. Different possibilities to make computations faster for this computationally challenging equipment are evaluated. The evaluation of these possibilities leads to the following conclusions:

- 2D simulations of pulsed sieve plate column can be carried out to get a reasonably good estimate of axial dispersion in single-phase flow.
- For 2D representation of the actual geometry, hole diameter must be kept same as in the actual geometry. Pitch should be varied to keep the percent free area same.
- A geometry with reduced number of plate can be used to carry out CFD simulations. Four plates are found to be sufficient.
- Instead of the direct approach which involves coupled solution of RANS and the scalar transport equations, a snapshot approach can be used to significantly save the computational time. The snapshot approach involves solution of scalar

transport equation alone for four flow fields corresponding to four different points of the sinusoidal pulsing velocity.

The computational approach embedding the above recommendation for quick estimate of axial dispersion coefficient in single-phase flow in a pulsed sieve plate column is validated using the experimental data. A good agreement between the predicted and reported axial dispersion coefficients is observed. The validated computational approach is also found to give physically realistic prediction of effect of hole diameter and percent free area on axial dispersion coefficients.

CHAPTER 3

MONODISPERSED CFD SIMULATION TO ESTIMATE DISPERSED PHASE HOLD UP USING EXPERIMENTALLY MEASURED DROP DIAMETER

3.1 INTRODUCTION

Having modeled pulsatile single-phase flow in a pulsed sieve plate column with reasonable accuracy in the previous chapter, in the present chapter we report two-dimensional two fluid CFD simulations to capture counter-current two phase flow in a pulsed sieve plate column. Euler-Euler approach has been used to simulate the liquid-liquid two-phase flow. Dispersed phase has been considered as monodispersed. Experimentally measured drop diameter has been used as representative diameter. A geometry with reduced number of plates has been used to reduce the computational domain. Turbulence has been modeled using mixture standard k- ϵ model. The aqueous phase used in simulation is 3M nitric acid. The organic phase used in simulations is 30% tributylphosphate (TBP) in dodecane. For validation, data reported in a recent literature have been used ([Kolhe et al., 2011](#)). Suitability of different drag models reported in literature has been evaluated and the most appropriate drag model is identified. The parameters of this drag model are further modified to improve the prediction of dispersed phase hold up by the two-phase CFD model.

3.2 COMPUTATIONAL APPROACH

A 2D model of the actual pulsed sieve plate column described in a recent paper ([Lade et al., 2013](#)) has been used in this study. The actual column consists of 20 plates but a reduced number of plates has been considered to limit the size of the computational domain and the resulting size of the mesh. Suitability of using 2D model and reduced

number of plates for CFD modeling of pulsed sieve column has been reported earlier (Kolhe et al., 2011; Din et al., 2010). Two-phase flow has been modeled using Euler–Euler model. The model solves the conservation equations for momentum and mass for each phase. This model assumes that both phases can co-exist in each cell in the flow domain. This approach has been used widely for simulating two- phase dispersed flow (Yadav and Patwardhan, 2009; Din et al., 2010; Ranade, 2002; Wang et al., 2014; Retieb et al., 2007). The hold up of each phase in each cell within the flow domain is computed. The momentum exchange between the two phases is modeled through the interphase exchange coefficients (K_{ij}). The continuity equation is given as

$$\frac{\partial}{\partial t}(\alpha_i \rho_i) + \nabla \cdot (\alpha_i \rho_i \overline{U}_i) = 0 \quad (3.1)$$

where α_i is phase fraction of the i^{th} phase and U_i is the velocity of the i^{th} phase. The momentum equation is

$$\frac{\partial}{\partial t}(\alpha_i \rho_i \overline{U}_i) + \nabla \cdot (\alpha_i \rho_i \overline{U}_i \overline{U}_i) = -\alpha_i \nabla p - \alpha_i \nabla \cdot \overline{\tau}_{i,lam} - \alpha_i \nabla \cdot \overline{\tau}_{i,tur} + \alpha_i \rho_i \overline{g} + \sum_{i=1}^n \overline{R}_{ij} + (\overline{F}_i + \overline{F}_{lift,i} + \overline{F}_{vm,i}) \quad (3.2)$$

where $\overline{\tau}_i$ is the stress tensor and composed of two components – viscous stress and turbulent stress. These terms are expressed as:

$$\begin{aligned} \overline{\tau}_{i,lam} &= \mu_i (\nabla \overline{U}_i + \nabla \overline{U}_i^T) \\ \overline{\tau}_{i,tur} &= \mu_{t,m} (\nabla \overline{U}_i + \nabla \overline{U}_i^T) \end{aligned} \quad (3.3)$$

\overline{F}_i is the external body force, $\overline{F}_{lift,i}$ is the lift force, $\overline{F}_{vm,i}$ is the virtual mass force acting on the i^{th} phase. \overline{R}_{ij} is the interaction force between i^{th} and j^{th} phases, whereas p is the pressure shared by all phases. \overline{U}_{ij} is the interphase velocity. μ_i is viscosity of i^{th} phase where as $\mu_{t,m}$ stands for the turbulent mixture viscosity. The turbulent mixture viscosity is evaluated for the mixed phase.

Lift force acting on a particle is mainly due to velocity gradients in the primary phase flow field. In most cases, the lift force is insignificant compared to the drag force and

is often neglected in two-phase CFD simulations of liquid-liquid dispersed flows (Wang and Mao, 2005; Noroozi and Hashemabadi, 2009; Drumm et al., 2009; Din et al., 2010). Virtual mass force becomes significant when the secondary phase accelerates relative to the primary phase. The inertia of the primary phase mass encountered by the accelerating particles exerts a virtual mass force on the particles. However, the virtual mass effect is significant when the density of the secondary phase is much smaller than the density of the primary phase which is not the case for liquid-liquid dispersions. Hence, virtual mass force can also be neglected as has been done in several studies reported in literature on CFD modeling of liquid-liquid dispersions (Din et al., 2010; Noroozi and Hashemabadi, 2009; Sathe et al., 2010).

The momentum equations needs to be closed with appropriate expression for the interphase force $\overline{R_{ij}}$. This force depends on the friction, pressure, cohesion, and other effects, and is subject to the conditions that $\overline{R_{ij}} = -\overline{R_{ji}}$ and $\overline{R_{ii}} = 0$.

The interphase force term is defined in terms of the interphase exchange coefficient (K_{ij}) as

$$\sum \overline{R_{ij}} = \sum K_{ij} (\overline{U_i} - \overline{U_j}) \quad (3.4)$$

where the interphase exchange coefficient is defined in terms of the a drag coefficient (C_D)

$$K_{ij} = \frac{3\alpha_i\alpha_j\rho_j C_D |\overline{U_i} - \overline{U_j}|}{4d_p} \quad (3.5)$$

Turbulence has been modeled using the mixture k - ε model in which the equations for k and ε are solved for the mixture as a whole. The relevant equations are

$$\frac{\partial}{\partial t} (\rho_m k) + \nabla \cdot (\rho_m \overline{U_m} k) = \nabla \cdot \left(\frac{\mu_{t,m}}{\sigma_k} \nabla k \right) + G_{k,m} - \rho_m \varepsilon \quad (3.6)$$

$$\frac{\partial}{\partial t} (\rho_m \varepsilon) + \nabla \cdot (\rho_m \overline{U_m} \varepsilon) = \nabla \cdot \left(\frac{\mu_{t,m}}{\sigma_\varepsilon} \nabla \varepsilon \right) + \frac{\varepsilon}{k} (C_{1\varepsilon} G_{k,m} - C_{2\varepsilon} \rho_m \varepsilon) \quad (3.7)$$

where subscript m refers to the mixture of the two phases. The mixture averaged values for the physical properties and velocity are defined as given in Eqn. (3.8) and (3.9).

$$\rho_m = \sum_{i=1}^n \alpha_i \rho_i \quad (3.8)$$

$$\overline{U}_m = \frac{\sum_{i=1}^n \alpha_i \rho_i \overline{U}_i}{\sum_{i=1}^n \alpha_i \rho_i} \quad (3.9)$$

Turbulent viscosity and turbulent kinetic energy generation terms are also based on the mixture of the two phases and given by Eq. (3.10) and (3.11), respectively.

$$\mu_{t,m} = \rho_m C_\mu \frac{k^2}{\varepsilon} \quad (3.10)$$

$$G_{k,m} = \mu_{t,m} \left(\nabla \overline{U}_m + \nabla \overline{U}_m^T \right) : \nabla \overline{U}_m \quad (3.11)$$

Most of published literature on pulsed column (both pulsed sieve plate and pulsed disc and doughnut column) has reported use of standard k- ε closure law to model turbulence. In fact Amraoke and coworkers ([Amraoke et al., 2014b](#)) had compared k- ε models (standard, RNG and Low Re) with Reynolds Stress Model and reported that the predictions of standard k- ε model is just as good as that of Reynolds Stress Model

There are several factors that affect the accuracy of the prediction of two-phase CFD model of dispersed flows. In reality, there are breakage and coalescence of drops/ bubbles leading to temporal and spatial variation of drop/ bubble size and drop/ bubble size distributions. Hence, assumption of monodispersed droplets/ bubbles which is often invoked to simplify the CFD simulations ([Sathe et al., 2010](#); [Din et al., 2010](#)) itself leads to some inaccuracy. Though CFD modeling of two-phase flow can be made more realistic by coupling the population balance models ([Drumm et al., 2009](#); [Bhole et al., 2008](#)), the choice of breakage and coalescence kernels and values of parameters in the kernels of the population balance model may affect the results. Choice of the two-phase turbulence model may also affect the results ([Aubin et al.,](#)

2004; Amokrane et al., 2014b). Addressing all such computational issues together is practically not feasible. A workable solution can be achieved by lumping all uncertainty in one or two terms of the governing equations and modifying these terms to bring the predicted results closer to the experimental results. This approach has been followed in several studies on two-phase CFD modeling. In Euler-Euler model of dispersed two-phase flow, drag model is the term often modified to bring predictions closer to the measured values (Noroozi and Hashemabadi, 2009; Rusche, 2002). In this study, we also follow a similar approach by focusing on the drag model for two-fluid CFD simulations of pulsed sieve plate column. Different drag models have been reported in literature that can be used for two-fluid CFD simulations of dispersed flows. Table 3.1 lists some of the drag models that have been evaluated in this study. Schiller-Naumann model (Schiller and Naumann, 1935) is one of the widely used drag models for two-fluid CFD simulations of dispersed flows (Kumar et al., 2011; Sathe et al., 2010). However, the basic assumption of this model is that the drop is immersed in an infinite pool of the continuous phase. Presence of nearby drops and their effect on drag is not considered. Hence, the Schiller-Naumann model is basically a drag model that can be applicable for very lean dispersions. The other two drag models for very lean dispersions are model of Morsi-Alexander (Morsi and Alexander, 1972) and Symmetric drag model. Symmetry drag model has the same functional form as the Schiller-Naumann model, the only difference being Reynolds number is defined with respect to the mixture. This is suitable for cases when the dispersed phase, in certain regions of the domain, tends to agglomerate and becomes the continuous phase (Besagni et al., 2014; Cheng and Chen, 2011). Model of Morsi-

Table 3.1: Different reported drag models evaluated in this study**Drag models for lean dispersions**

Schiller
Naumann, 1935

$$C_D = \begin{cases} 24(1 + 0.15\text{Re}^{0.687})/\text{Re} & \text{Re} \leq 1000 \\ 0.44 & \text{Re} > 1000 \end{cases}$$

Morsi
Alexander, 1972

$$C_D = a_1 + \frac{a_2}{\text{Re}} + \frac{a_3}{\text{Re}^2}$$

	a_1	a_2	a_3
$0 < \text{Re} < 0.1$	0	24	0
$0.1 < \text{Re} < 1$	3.690	22.73	0.0903
$1 < \text{Re} < 10$	1.222	29.1667	-3.8889
$10 < \text{Re} < 100$	0.6167	46.50	-116.67
$100 < \text{Re} < 1000$	0.3644	98.33	-2778
$1000 < \text{Re} < 5000$	0.357	148.62	-47500
$5000 < \text{Re} < 10000$	0.46	-490.546	578700
$\text{Re} > 10000$	0.5191	-490.546	5416700

Symmertic

$$K_{12} = \frac{3\alpha_1(\alpha_1\rho_1 + \alpha_2\rho_2)C_D|\vec{U}_1 - \vec{U}_2|}{4d}$$

$$C_D = \begin{cases} 24(1 + 0.15\text{Re}^{0.687}) & \text{Re} \leq 1000 \\ 0.44 & \text{Re} > 1000 \end{cases}$$

$$\text{Re} = \frac{d|\vec{U}_1 - \vec{U}_2|(\alpha_1\rho_1 + \alpha_2\rho_2)}{(\alpha_1\mu_1 + \alpha_2\mu_2)}$$

Drag models for concentrated dispersions

Barnea
Mizrahi, 1975

$$C_D = \left(1 + \phi^{0.333}\right) \left(0.63 + \frac{4.8}{\text{Re}p^{0.5}}\right)$$

$$\text{Re} = \frac{\rho_1 d_2 |\vec{U}_1 - \vec{U}_2|}{\mu_{\text{eff}}} \quad \mu_{\text{eff}} = \frac{\mu_1 K_b \left(0.667 K_b + \frac{\mu_2}{\mu_1}\right)}{K_b + \frac{\mu_2}{\mu_1}}$$

$$K_b = \exp\left\{\frac{5K_a\phi}{3(1-\phi)}\right\} \quad K_a = \frac{\mu_1 + 2.5\mu_2}{2.5(\mu_1 + \mu_2)}$$

Kumar
Hartland, 1985
Augier, 2003

$$C_D = \left(0.53 + \frac{24}{\text{Re}}\right) \left(1 + 4.56\phi^{0.73}\right)$$

$$C_D = C_{\text{DSN}} \{1 - \exp(-5.2\phi)\} \text{ where } C_{\text{DSN}} \text{ is Schiller Naumann drag coefficient}$$

Alexander is based on a solid particle settling in an infinite medium and has a functional form different from the models of Schiller-Naumann. At higher values of hold up the assumption of a single drop in an infinite medium does not hold and presence of surrounding drops increases the effective drag on the drop. Hence, for such conditions drag models which account for the presence of other dispersed phase

drop/bubbles/ particles are indispensable. Three different drag models applicable for concentrated dispersions have been compared in this study. Of these the drag model of Augier ([Augier and Masbernat, 2003](#)) is based on modifying the Schiller-Naumann model to incorporate the effect of hold up on drag coefficient. Model of Kumar-Hatland ([Kumar and Hartland, 1985](#)) is purely empirical but is based on a very wide range of experimental data and is reported to be valid for dispersed phase fraction as high as 76%. Model of Barnea-Mizrahi ([Barnea-Mizrahi, 1975](#)) is based on the concept of the mixture viscosity. In this approach, the resistive effect of the presence of nearby droplets is assumed to increase the effective viscosity of the continuous phase.

In this chapter the developed CFD model has been validated with experimental data reported in a recent study ([Lade et al., 2013](#)). The authors had used TBP-nitric acid system in a 76.2 mm pulsed sieve plate column. The length of the column was 1.0 m. A plate cartridge of SS 316 was used with 20 plates. A standard sieve plate design was used i.e. hole diameter of 3 mm on a 5 mm triangular pitch with 21% free area. The interplate spacing was 50 mm. A pulse leg of 0.0254 m diameter was connected to the base of the bottom disengagement section. The liquid-liquid system used was 30% TBP in dodecane in 3 N Nitric acid solution. Representative drop diameter and hold up were reported as a function of pulsing velocity, dispersed phase velocity and continuous phase velocity. The authors compared results for normal phase operation (aqueous continuous) and reverse phase operation (aqueous dispersed). [Table 3.2](#) shows the physical properties of the liquid-liquid system.

Table 3.2: Physical properties of the liquid-liquid system		
	Density (kg/m ³)	Viscosity (Pa.s)
30% TBP-		
Dodecane	816.69	0.001003
3 NHNO ₃	1128	0.00228

Fig 3.1 shows the computational domain used in this study. It also shows the mesh used in the simulations. 5 plates have been used to keep the computational time within reasonable limits. The other features of the geometry are the same as reported in literature (Lade et al., 2013). A grid density of 1.027×10^6 cells/m² has been used in the present work. This grid density is based on the results of grid independence test carried out for simulation of single-phase flow in the same geometry as mentioned in chapter 2. In the 2D model reported in this work the hole diameter has been kept at 3 mm (same as that in experimental setup) while the pitch has been chosen such that the percent free area is the same as in experimental setup. The inlet of the light phase (organic phase) is at the bottom and the outlet is from the top as is shown in Fig. 3.1. The inlet of the heavier phase (aqueous phase) is at the top and the outlet is at the bottom. The pulse is applied at the bottom, as shown in Fig. 3.1.

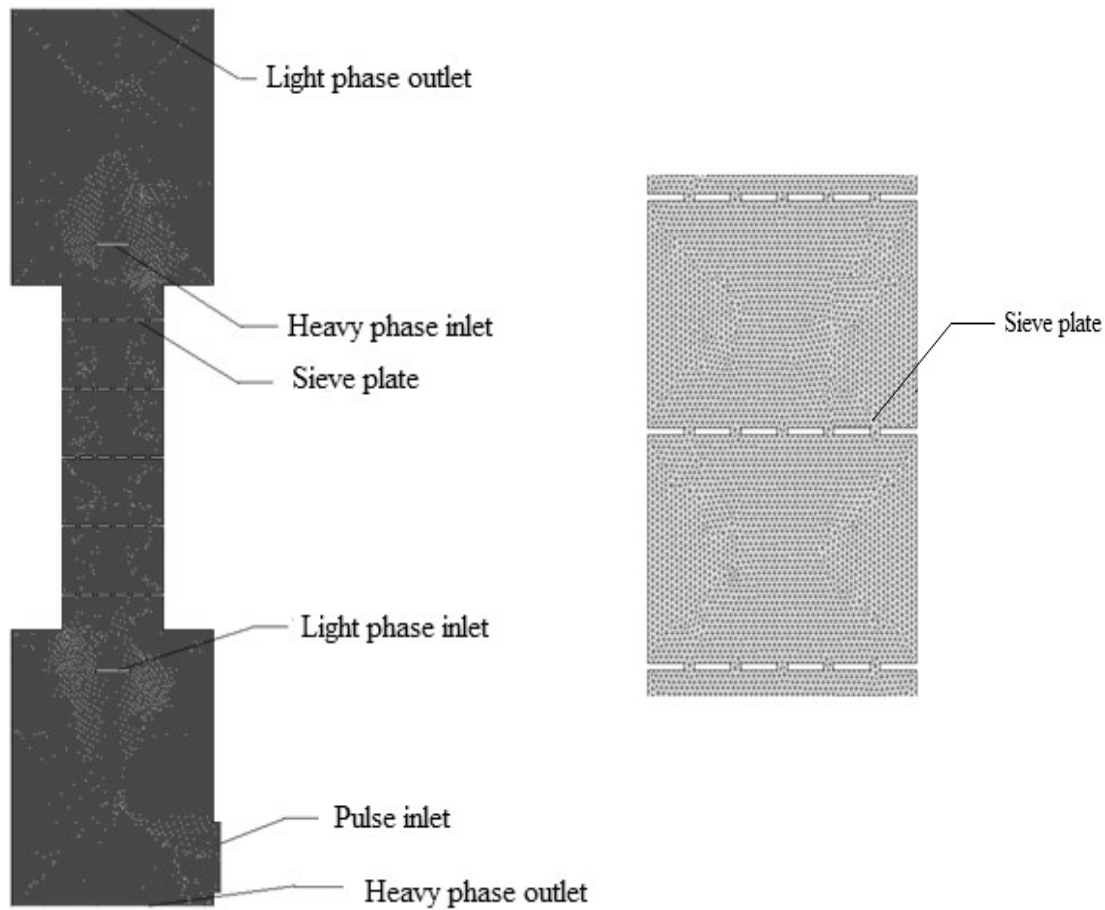


Figure 3.1: Computational domain used for CFD simulations

An outflow boundary condition was defined at the top most boundary (light phase outlet). The light phase and heavy phase have been defined as velocity inlet, where as the light phase outlet (bottom most boundary) have been defined as a negative velocity inlet. A sinusoidal varying velocity was implemented at the pulse inlet using an user defined function as follows.

$$U_p = \pi A f \sin(2\pi f t) \quad (3.12)$$

where U_p is the pulsing velocity, A is the amplitude (maximum displacement) and f is frequency (Hz).

The absolute convergence criterion that was used to terminate the iterations within each time step was 0.0001 for each of the variables solved for. 40-50 iterations were typically needed for the convergence to be attained within each time step (0.01 sec) for the given set of boundary conditions.

3.3 RESULTS AND DISCUSSION

3.3.1 Comprison of Different Drag Models for Normal Operation

The simulations reported in this study are Euler-Euler 2D CFD simulations carried out by assuming monodispersed drops. In reality, the drop diameter varies with space. In the region near the holes drops will be smaller due to higher turbulence. In the regions away from the holes relatively larger drop diameters should be present. Even at a single point there should exist a drop size distribution. However, it has been reported (Usman et al., 2009; Lorenz et al., 1990) that in a pulsed column after first few plates the sauter mean drop diameter becomes constant and does not vary much with the column height. Hence, using a single representative drop diameter to simulate the two-phase flow in the column seems to be a resonable assumption. Still, which diameter should be used as the diameter of the monodispersed phase remains an open question. In most of the studies on two-phase CFD simulations of dispersed flow, Sauter mean diameter which is defined as the ratio of total dispersed phase volume to the total dispersed phase surface area has been used to model the drop size of the monodispersed phase (Yadav and Patwardhan, 2009; Sathe et al., 2010). In this study too we have used the Sauter mean diameter reported in the experimental study for carrying out two-phase CFD simulations. Table 3.3 lists the conditions for which simulation of the normal phase operation are carried out. Pulsing frequency has been kept constant at 1 Hz for all the cases. The maximum pulsing velocity is 2.5 cm/s. Thus the maximum pulse amplitude is 2.5 cm which is half for the plate spacing. Here normal phase operation refers to the operation in which the organic phase is the dispersed phase and the aqueous phase is the continuous phase.

Table 3.3: Conditions and data used for simulations of normal phase operation

Trial	V_d (m/sec)	V_c (m/sec)	Af (m/sec)	ϕ (%)	d_{32} (mm)
1	0.002	0.00207	0.02	4.95	1.275
2	0.004	0.00207	0.02	13.12	1.29
3	0.006	0.00207	0.02	16.25	1.29
4	0.005	0.0018	0.015	11.24	1.65
5	0.005	0.0018	0.02	16.40	1.50
6	0.005	0.0018	0.025	24.00	1.125

Fig. 3.2 and Fig. 3.3 show the variation of the dispersed phase hold up with superficial velocity of the dispersed phase and pulsing velocity, respectively. The superficial velocities mentioned are based on the diameter of the active section of the column. Hold up values predicted by using different drag models in two-phase CFD simulations are also shown. Experimental data in Fig. 3.2 shows that dispersed phase hold up increases with increase in superficial velocity of the dispersed phase. Similar trend has been reported in an earlier study also (Lorenz et al., 1990). This trend is captured by all the drag models. However, the drag models applicable for lean dispersions (Schiller-Naumann, Morsi-Alexander and Symmetric) tend to overpredict the hold up for higher values of dispersed phase superficial velocity. Hold up predicted by the drag models of Barnea-Mizrahi and Kumar-Hartland are close to the experimental hold up values for higher dispersed phase superficial velocity.

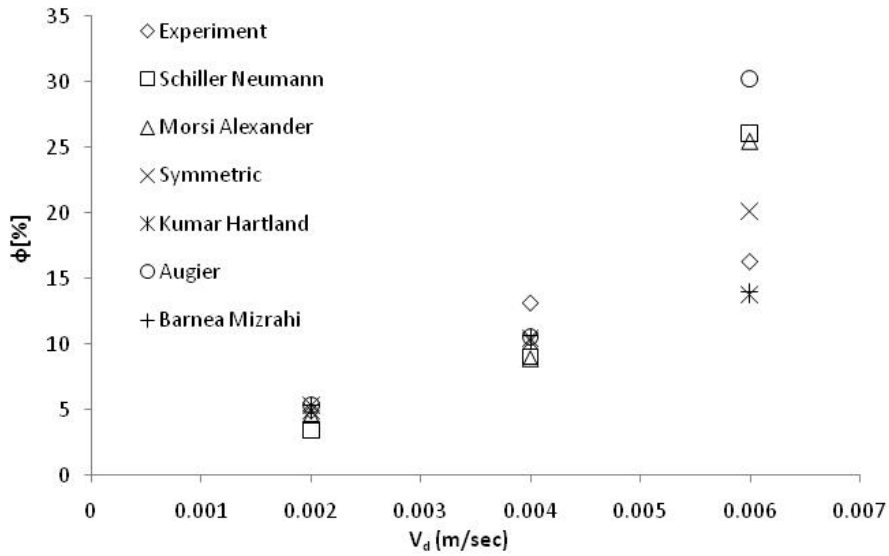


Figure 3.2: Variation of hold up with dispersed phase velocity ($V_c = 0.00207$ m/sec, $Af = 0.02$ m/sec)

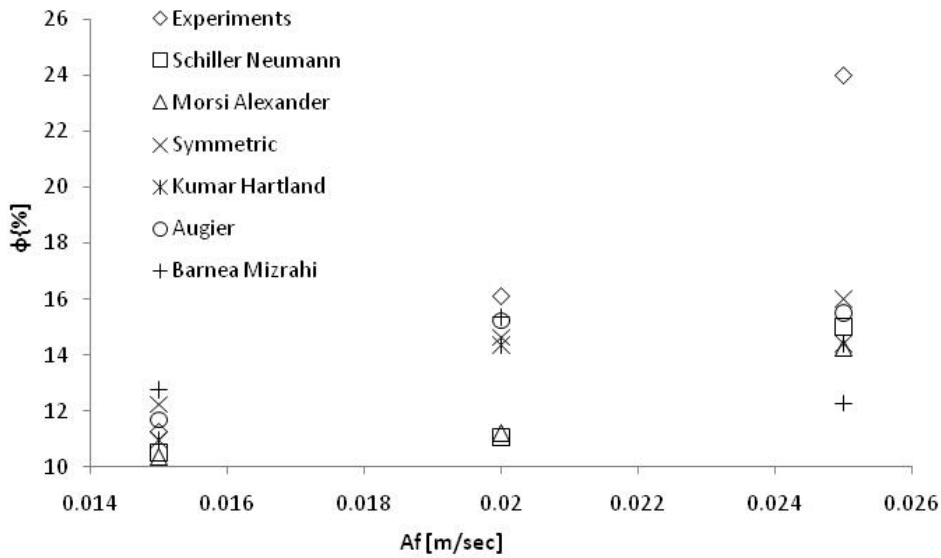


Figure 3.3: Variation of hold up with pulsing velocity ($V_c = 0.00186$ m/sec, $V_d = 0.005$ m/sec)

Drag model of Augier, despite of accounting for effect of hold up on drag coefficient, tends to overpredict the hold up for higher dispersed phase superficial velocity. It is therefore concluded from Fig. 3.2 that Kumar-Hartland and Barnea-Mizrahi drag models are able to capture the variation of hold up with dispersed phase velocity. Experimental data in Fig. 3.3 shows that dispersed phase hold up increases with pulsing velocity. This trend of variation of dispersed phase hold up with pulsing

velocity is also reported in earlier studies (Lorenz et al., 1990). Though the evaluated drag models tend to show a similar trend, at higher values of pulsing velocity, the hold up is underpredicted by all the drag models.

Table 3.4 lists the absolute average relative error between the predicted and the experimentally reported values of hold up obtained using the different drag models. As can be seen the absolute average relative errors in the prediction of the drag models for lean dispersions are higher than the absolute average relative errors in the predictions of drag models for concentrated dispersions. This is expected because drag models for lean dispersions do not account for the effect of hold up on drag coefficient. Among all the drag models, model of Kumar-Hartland is observed to give the least deviation with the experimental data with average deviation of about 15%.

Table 3.4: Absolute average relative errors in predictions of dispersed phase hold up (expressed as percentage) by different drag models for normal phase operation

		Schiller- Nauman n	Morxi- Alexande r	Symme tric	Kumar- Hartland	Augier	Barnea- Mizrahi
	0.002	30.0	7.9	7.9	1.8	8.3	7.9
V_d (m/sec)	0.004	30.9	32.4	20.0	22.2	19.3	19.2
	0.006	60.8	56.9	24.2	15.2	85.8	14.0
	0.015	6.7	7.9	8.7	2.7	3.9	13.4
A_f (m/sec)	0.020	31.4	30.4	9.2	10.9	5.5	4.7
	0.025	37.5	40.6	33.3	39.2	35.4	48.8
Average		32.9	29.4	17.2	15.4	26.4	18.0

Fig 3.4 shows the distribution of the dispersed phase at four different instant of one time cycle as obtained from CFD simulations. The first figure from left is at the instant of the mean position of the pulse while going up. The second figure from left is at the instant of positive peak of the pulse. The third figure from left is at the instant of mean

position of the pulse while going down. The fourth figure from the left is at the instant of the negative peak of the pulse. It is seen that the dispersed phase preferentially moves through the central region of the column. Disengagement of phases in the upper disengagement section can also be seen.

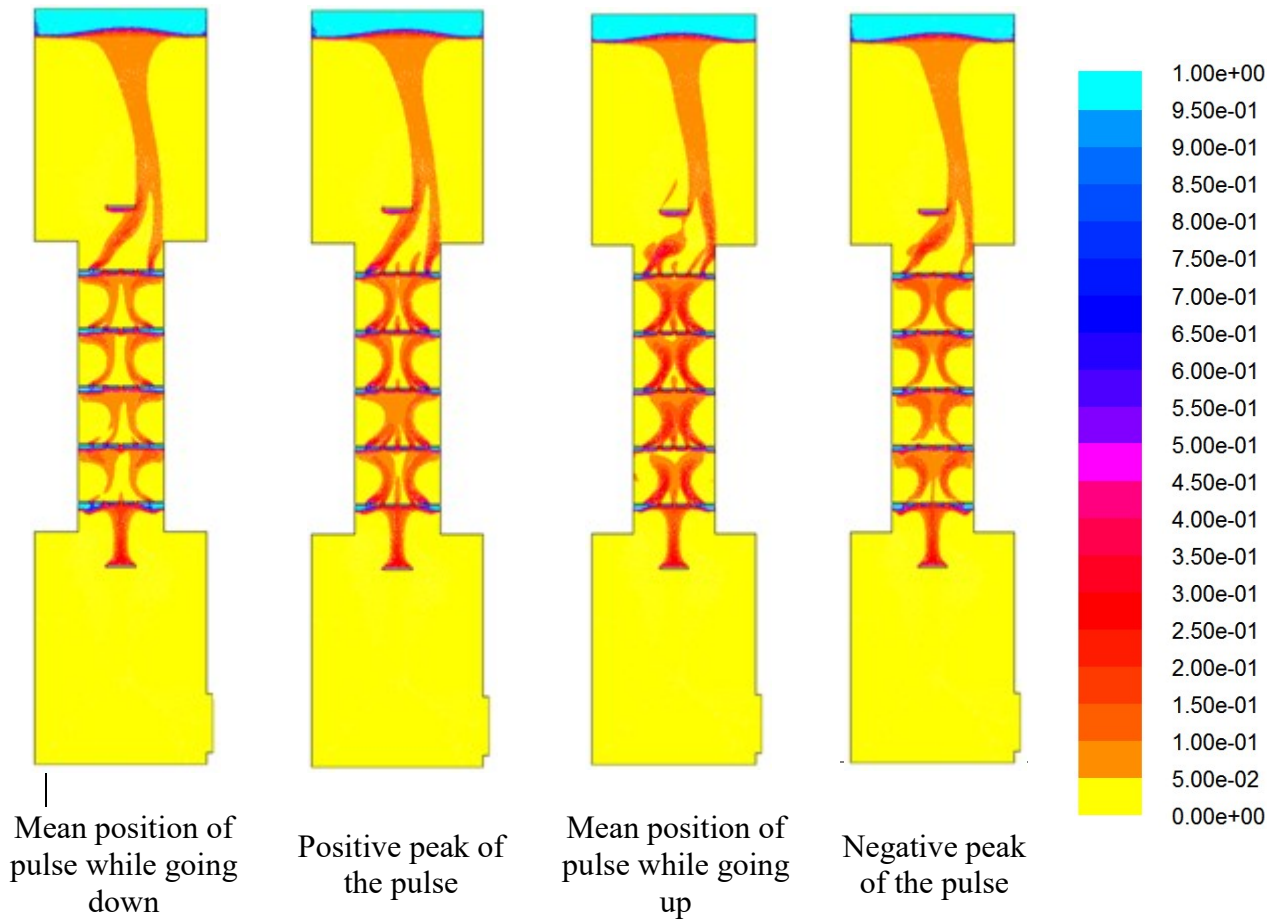


Figure 3.4: Profiles of dispersed phase hold up for four different instants of a pulsing cycle ($V_d = 0.0040$ m/sec; $V_c = 0.00207$ m/sec; $A_f = 0.02$ m/sec)

Fig. 3.5 shows the velocity profile of the continuous phase and dispersed phase in the column. Presence of re-circulation in the continuous phase flow is clearly seen. This is more evident from Fig. 3.6 which shows the velocity vector plots for both the dispersed (top) and the continuous (bottom) phase for a section of the column. Due to the counter-current nature of flow, the net flow of the lighter phase is upward where as the net flow of the heavier phase is downward in a pulsing cycle. The dispersed

phase vector plot shows that across a plate, the majority of velocity vectors of the lighter phase are directed upward.

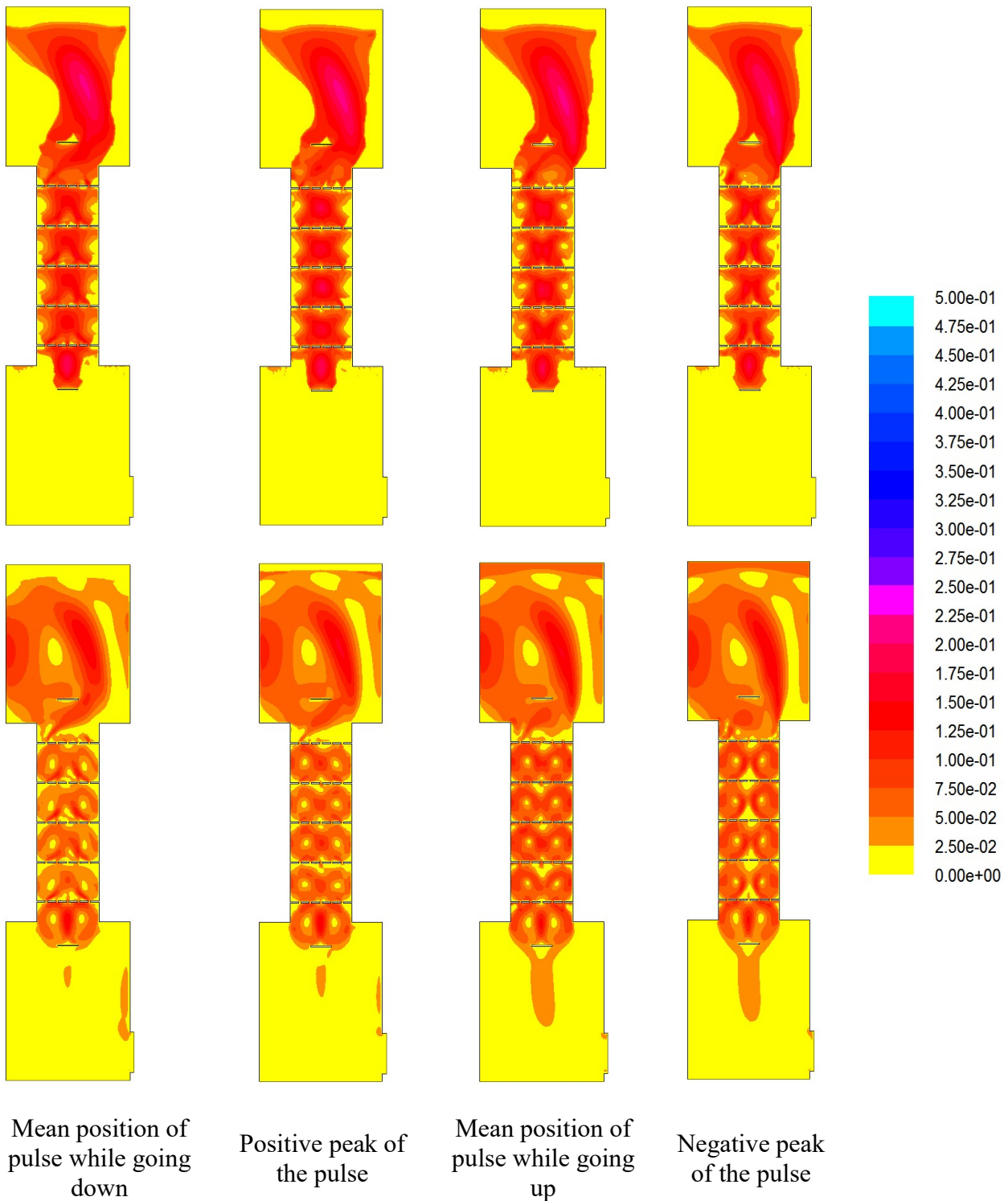


Figure 3.5: Velocity profiles for dispersed (top) and continuous (bottom) phase velocity at different instants of the pulsing cycle ($V_d = 0.004$ m/sec; $V_c = 0.00207$ m/sec; $Af = 0.02$ m/sec)

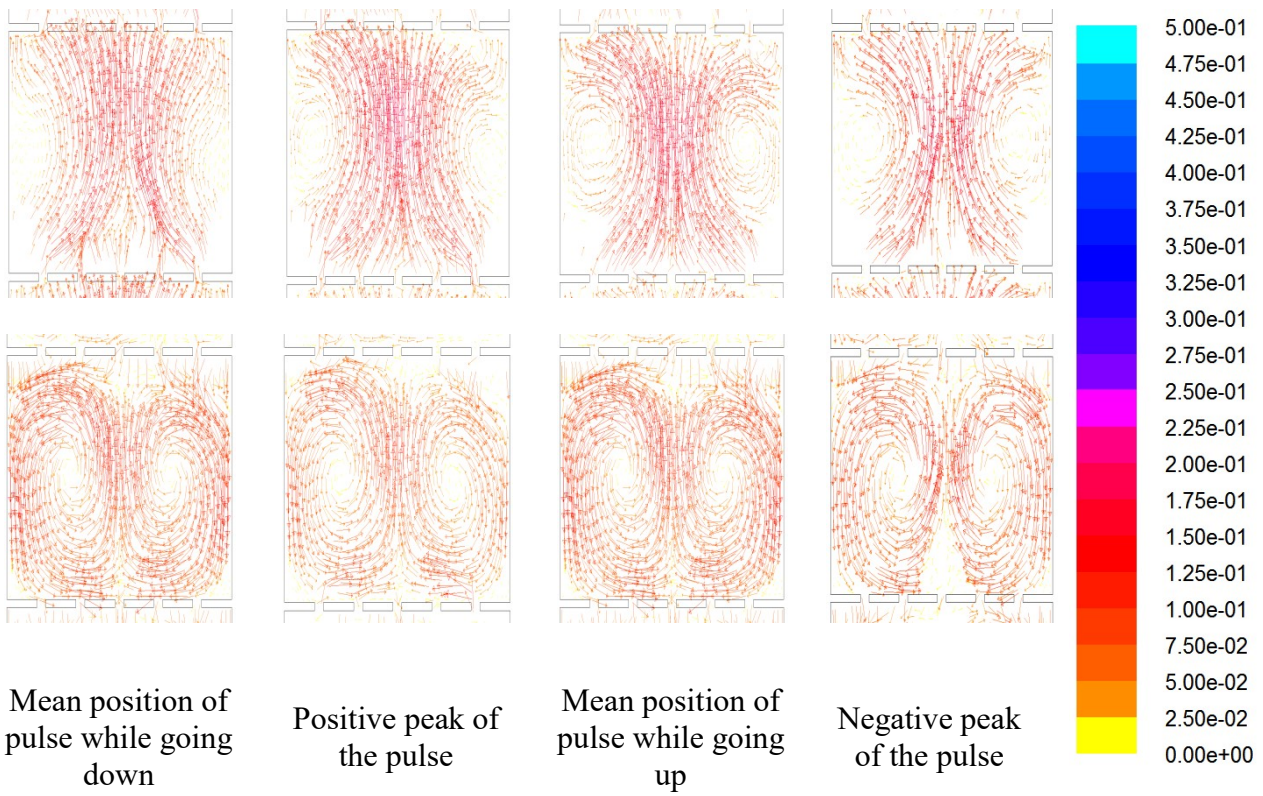


Figure 3.6: Velocity vector plots for dispersed (top) and continuous (bottom) phase velocity at four different instants of a pulsing cycle ($V_d = 0.004$ m/sec; $V_c = 0.00207$ m/sec; $Af = 0.02$ m/sec)

The lighter phase preferentially moves through the central part of the column. It can also be observed that there exists a small re-circulation zone in the lighter phase near the column walls. In this zone velocity vectors of the dispersed phase are directed downward. Similar but stronger re-circulations are also present in the continuous phase as is seen in the continuous phase velocity vector plot. In between the plates there exists two recirculation loops of almost equal size in the continuous phase. Presence of such strong circulation in the continuous phase may lead to axial mixing and reduction in the mass transfer efficiency of the column. The dispersed phase velocity vector plot also reveals that during the positive peak of the pulse the velocity magnitudes are on the higher side. [Fig. 3.7](#) shows the velocity vectors of the continuous phase in the lower disengagement section for two instants of the pulsing cycle (i.e. positive and negative peaks of the pulse). It is clearly seen that during the

positive peak the flow is from the pulse inlet to the column and for the negative peak the flow is from the column to the pulse inlet.

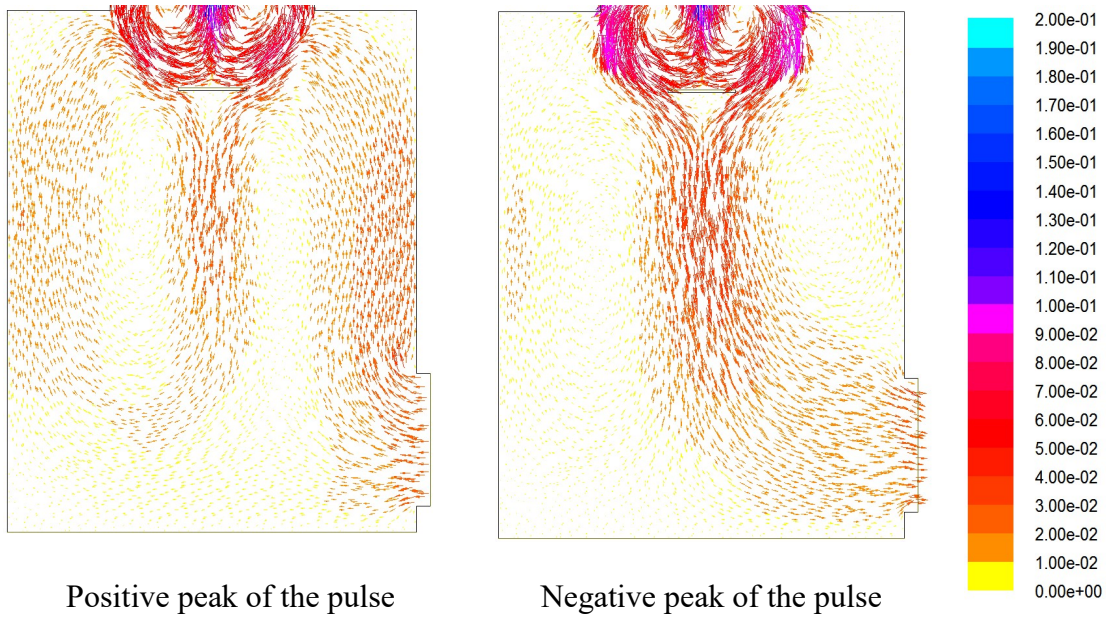


Figure 3.7: Velocity vectors of the continuous phase in the bottom disengagement section for positive and negative peak of the pulsing cycle ($V_d = 0.004$ m/sec; $V_c = 0.00207$ m/sec; $Af = 0.02$ m/sec)

Fig. 3.8 shows the variation of the average hold up between the plates with column height as predicted from CFD simulation. It is observed that average hold up between

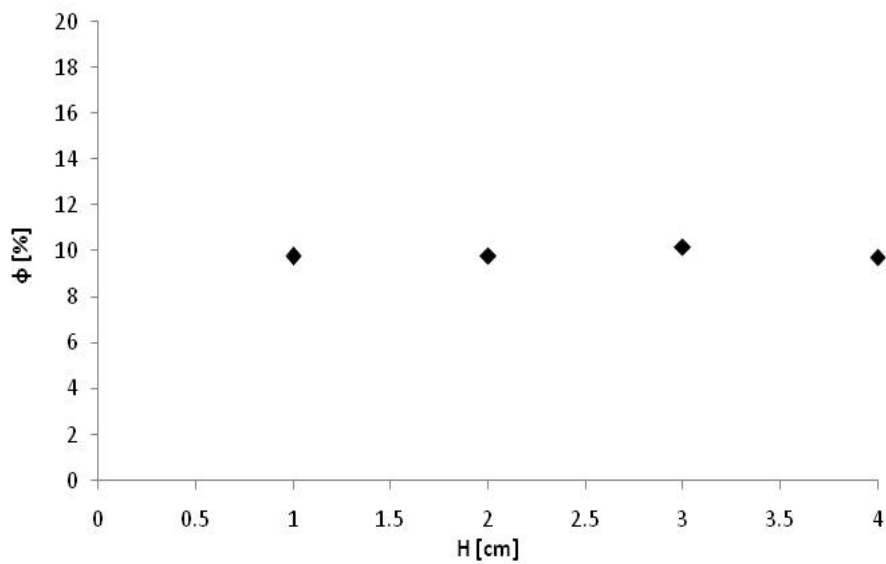


Figure 3.8: Variation of average hold up between the plates with height of the column

the plates does not change much with column height. This shows that the assumption of considering reduced number of plates in the computational model is reasonable.

3.3.2 Evaluation of Kumar-Hartland Model for Reverse Phase Operation

Having observed that Kumar-Hartland model is the best among the reported drag models to predict the dispersed phase holdup in a pulsed sieve plate column for normal phase operation, suitability of the Kumar-Hartland drag model is further tested for the reverse phase operation. In this mode of operation, the heavier phase is the dispersed phase and the lighter phase is the continuous phase. The representative drop diameter used in simulations are the experimentally measured Sauter mean diameters reported for the reverse phase operation (Lade et al., 2013). Table 3.5 lists the conditions for which simulations are carried out.

Table 3.5: Conditions for which simulations are carried out for reverse phase operation

Trial	V_d (m/sec)	V_c (m/sec)	Af (m/sec)	ϕ (%)	d_{32} (mm)
1	0.002	0.00207	0.02	4.33	1.90
2	0.004	0.00207	0.02	7.20	1.90
3	0.006	0.00207	0.02	10.40	1.90
4	0.005	0.0018	0.015	4.50	2.08
5	0.005	0.0018	0.02	6.75	1.80
6	0.005	0.0018	0.025	8.50	1.775

Comparison of the predicted hold up and experimentally reported values is shown in Fig. 3.9 and Fig. 3.10 which show variation of hold up with dispersed phase velocity and pulsing velocity, respectively. Experimental data shown in Fig. 3.9 and Fig. 3.10 suggest that, as seen for the normal phase operation, for reverse phase operation too the hold up increases with increase in superficial velocity of dispersed phase and pulsing velocity. Simulations also predict that hold up increases with increase in

dispersed phase superficial velocity and pulsing velocity. The increase predicted by CFD simulation however is not as marked as seen in the experiments, more so for the increase in hold up with increase in pulsing velocity. If the deviation between the predicted hold up and experimental holdup is quantified, it is noted that simulations incorporating the Kumar-Hartland drag model are able to predict the hold up with absolute average relative error of about 21%. The maximum and minimum absolute relative error with Kumar-Hartland model are about 39% and 10% respectively.

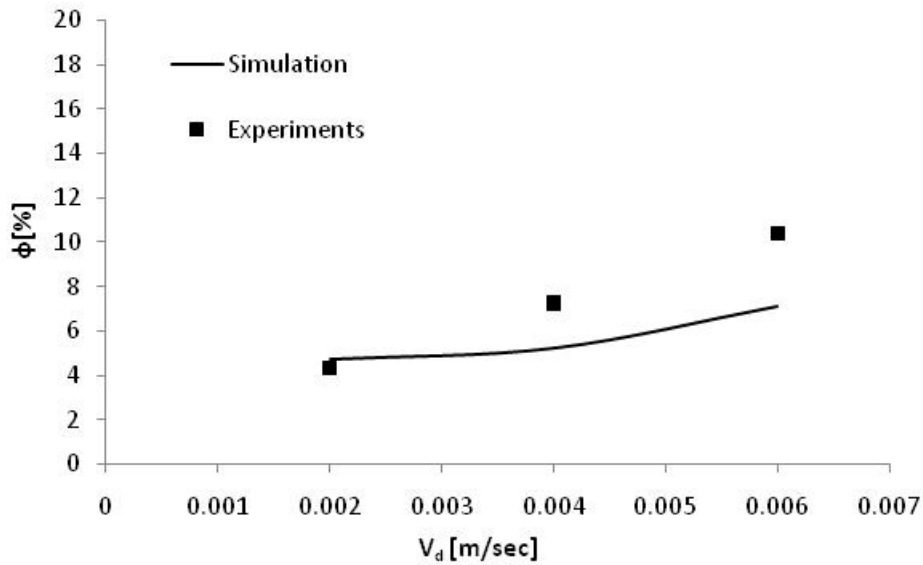


Figure 3.9: Variation of hold up with dispersed phase superficial velocity in reverse phase operation. Comparison of the prediction of CFD model using Kumar-Hartland drag law with experimental values.

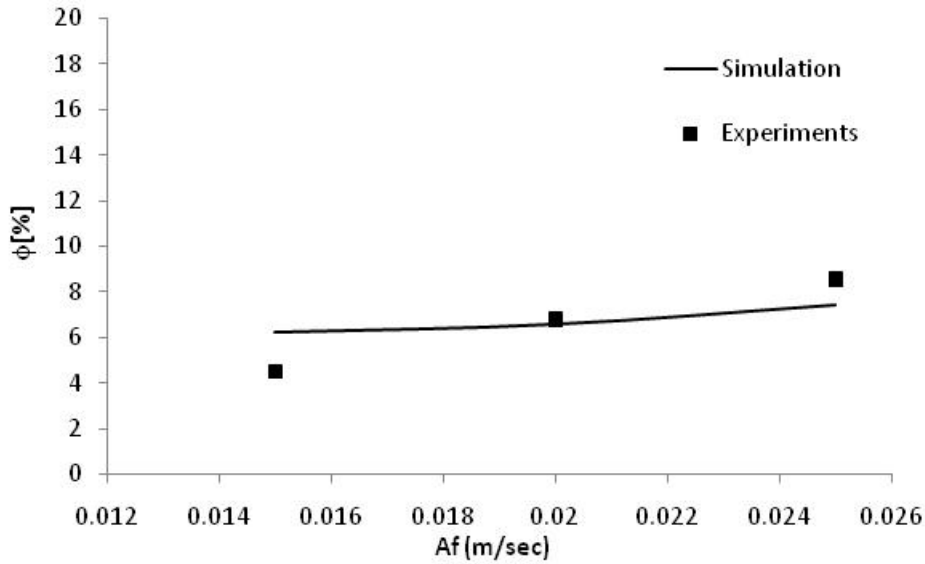


Figure 3.10: Variation of hold up with pulsing velocity for reverse phase operation. Comprison of hold up predicted by CFD model using Kumar Hartland drag law with experimental values.

3.3.3 Optimization of Model Parameters of Kumar Hartland Drag Model

The empirical drag model reported by Kumar-Hartland is based on the analysis of a wide range of experimental data involving several different liquid-liquid system and is indeed reported to be suitable for a general liquid-liquid dispersion (Walvekar et al., 2009). The general form of the equation giving drag coefficient is

$$C_D = \left(0.53 + \frac{24}{\text{Re}} \right) (1 + A_D \phi^B) \quad (3.13)$$

where A_D and B are the empirical constants values of which have been reported by Kumar-Hartland after analyzing the experimental data for several liquid-liquid systems. However, as seen in the previous sections, though this model gives better prediction than other drag models, absolute average relative error in prediction are on the higher side being about 15.4% for the normal phase operation and 21% for the reverse phase operation. In this section possibility of further reducing the absolute average relative error between the predicted and experimentally reported values of hold up is explored. This is done by modifying the values of the constants of Kumar-

Hartland model. It is observed that the hold up predicted by the Kumar-Hartland model in its original form is lower than the experimental hold up for most of the operating conditions studied and specially so for the maximum value of the pulsing velocity reported. Hence, it is reasonable to say that the empirical constant should be modified such that the resultant drag model predicts a larger value of the drag coefficient which will lead to increased resistance to the movement of dispersed phase drops leading to higher hold up.

As explained earlier this essentially means that all the uncertainties associated with the numerical model is lumped into the empirical constants of the drag model. These uncertainties include assumption of a single representative drop diameter, 2D representation of an actual 3D geometry and associated errors in predicting accurately the turbulence properties as well as lack of a drag model tailored for pulsatile flow. Thus lumping all these uncertainties into the drag model seems a practical way forward as explained previously.

As can be seen from Eq. (3.13), with increase in the value of the constant A_D , drag coefficient should increase whereas with increase in the value of constant B the drag coefficient should reduce. Some simulations were carried out to know to what extent the predicted hold up changes with the change in the values of the model parameters or in other words how sensitive the predicted hold up is with respect to the values of A_D and B . The results from these simulations indicates that hold up in the column increases with an increase in A_D where as it is practically independent of B . However, even though insignificant in comparison to A_D , a decrease in B slightly reduces column hold up. An increase in value of A_D by 37.5% increases hold up value by 16% whereas an increase of 58 % in B reduces hold up value by 1.75 %. This shows that it is the value of A_D that has major influence of on the value of the predicted hold up and thus it should be modified to bring the predicted hold up values closer to the experimental values. Since B does not affect the hold up as much as A_D , B was kept

constant at the minimum value of the range of B explored. Thus the recommended value of B is 0.4. The value of A_D was optimised so as to minimize the absolute average relative error between the predicted and the experimental value.

CFD simulations were carried out for different values of A_D keeping B constant at 0.4 for the conditions given in [Table 3.3](#). It was observed that the absolute average relative error between the experimental and predicted hold up values was minimum when A_D was 6.2. The corresponding absolute average relative error is 13.1%.

The absolute average relative error obtained with Kumar-Hartland model in its original form was 15.35% Hence, the improvement in the accuracy of prediction is not that significant. It is observed that the Kumar Hartland model both in its original form and with optimised empirical constant underpredicts the hold up at the highest pulsing velocity. If the experimental data point for the highest pulsing intensity is not included in the analysis to estimate the error, the absolute average relative error between the experimental and simulated data points is as low as 8.6%.

With a view to reduce the error further another approach was used in which the value of the constant A_D is chosen based on the operating condition. The existing experimental data set was split into two parts. All the data points pertaining to pulsing velocity less than 0.025 m/sec is considered as one set and that pertaining to the pulsing velocity of 0.025 m/sec is considered as the second set. It is observed from [Fig. 3.11](#) that when pulsing velocity is 0.020 m/sec (less than 0.025 m/sec) value of hold up tends to saturate with respect to values of A_D beyond 5 and does not increase with further increase in A_D . However for higher values for pulsing velocity (i.e. $A_f = 0.025$ m/sec) hold up values keeps on increasing with an increase in value of A_D . Thus the sensitivity of hold up on drag coefficient is different for low and high value of pulsing intensity. This might be attributed to the non linear dependence of drag force on the level of turbulence present inside the column which is directly related to

pulsing velocity. Thus Fig. 3.11 does justify use of a piece-wise definition of drag model for different levels of turbulence which is represented by pulsing velocity.

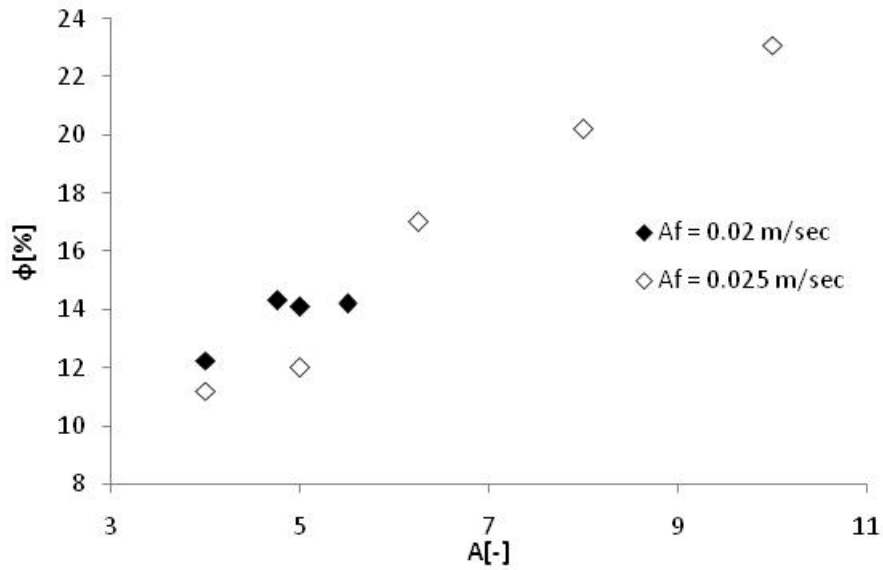


Figure 3.11: Sensitivity of hold up on the parameter A_D of the drag model for two different values of pulsing velocities, $V_d = 0.005$ m/sec and $V_c = 0.005$ m/sec

Optimum value of A_D was found out separately for the two sets. For pulsing velocity less than 2.5 cm/s, optimum value of A_D is 6.1 (corresponding absolute average relative error is 7.44%) whereas for pulsing velocity of more than or equal to 2.5 cm/s, optimum value of A_D is 10.0 (corresponding error is 3.75%). The final form of the modified drag law is expressed below

$$C_D = \begin{cases} \left(0.53 + \frac{24}{Re}\right)(1 + 6.2\phi^{0.4}) & \forall Af < 0.025 \text{ m/sec} \\ \left(0.53 + \frac{24}{Re}\right)(1 + 10.0\phi^{0.4}) & \forall Af \geq 0.025 \text{ m/sec} \end{cases} \quad (3.14)$$

It is observed that a single drag model is not suitable to represent the entire range of pulsing velocity and the predictions are improved by having a piece-wise definition of the drag model. At higher pulsing velocities the extent of turbulence in the column will be higher which should lead to higher values of drag. Drag is known to increase with intensity of turbulence (Khopkar et al., 2006a; Khopkar et al., 2006b). It is expected that as pulsing velocity increases drag coefficient should also increase.

Hence, a piece-wise model which predicts higher drag at higher pulsing velocities is physically realistic. The need to have a piece-wise drag model may also be attributed to the possibility of change of flow regime with change in pulsing velocity. Using the piece-wise definition of drag model (Eqn. 3.14) the absolute average relative error is reduced from 15.35 % to 5.56 % which represents a significant improvement over the original drag model. It may be noted here that the entire data set corresponds to normal phase operation.

Validity of the modified Kumar-Hartland model was checked by implementing it in the two-phase CFD model. The data used for simulations were the data given in [Table 3.3](#) as well as unseen additional experimental data points for dependence of hold up on continuous phase velocity. All these data corresponds to normal phase operation of the column. The comparison of the hold up predicted by the standard and modified Kumar Hartland drag model is shown in [Fig. 3.12](#). As can be seen the predictions of the modified drag model are better than the standard drag model. The absolute average relative error of the modified drag model is 10.8% whereas the same using the standard drag model is 15.35%. It is seen that modified Kumar Hartland drag model fares better than the standard Kumar Hartland drag law.

3.3.4 Comparison with Empirical Correlations

Pulsed sieve plate extraction column has been extensively studied by different researchers. Thus there exists a wide pool of experimental data. This has resulted in many correlations to predict column performance

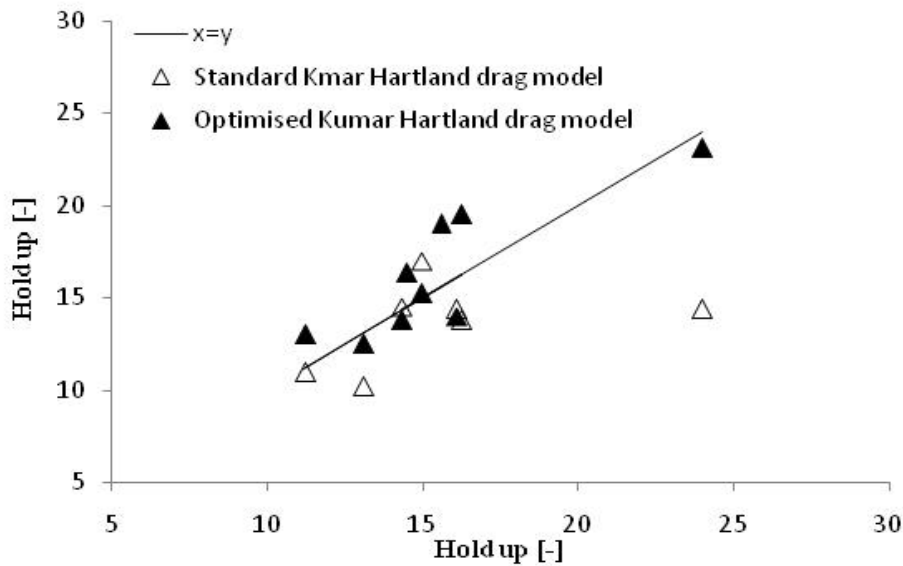


Figure 3.12: Comparison of standard Kumar-Hartland drag model and modified Kumar-Hartland drag model

parameters of the column. In this context an attempt has been made to compare the predictions of hold up obtained from CFD model (using the piece-wise optimised Kumar Hartland drag model) with the hold up estimated from different correlations. Correlations of Kumar and Hartland (Kumar and Hartland, 1988), Miyachi and Oya (Miyachi and Oya, 1965), and Venkatnarsaiah and Verma (Venkatnarsaiah et al., 1998) are compared. Venkatnarsaiah and Verma had given correlations both for direct estimation of hold up in the column as well as for estimation of slip velocity. Slip velocity can be used to back calculate column hold up. Hold up from yet another correlation for slip velocity due to Kumar and Hartland (Kumar and Hartland, 1994) has also been compared. The correlations can be found elsewhere (Yadav and Patwardhan, 2008). Fig. 3.13 shows the comparison between column hold predicted using CFD and those obtained from empirical correlations for normal phase operation. It is observed that while most of the correlations overpredict hold up, the correlation of Miyachi and Oya underpredicts hold up. Most importantly it is observed that predictions of hold up obtained from CFD simulations with the modified drag model reported in this study are distinctly better than the estimates obtained from empirical

correlations. It may be mentioned that amongst the reported empirical correlations the one due to Venkatnarsaiah and Verma (slip velocity based) outperforms others.

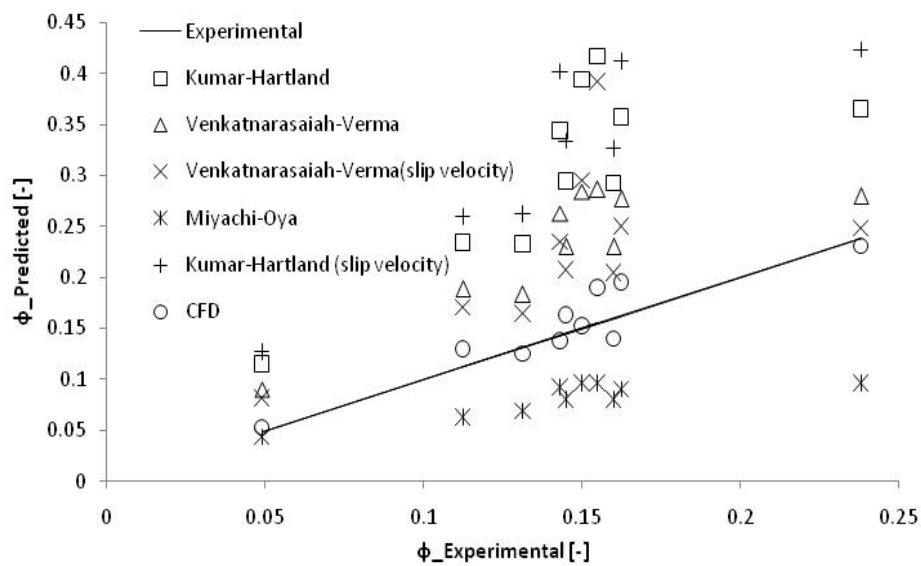


Figure 3.13: Comparison of hold up values predicted by CFD simulations and estimated by various correlations reported in literature

3.4 CONCLUSION

Two-phase flow of 30% TBP in dodecane – 3 N nitric acid system in a pulsed sieve plate column has been simulated using a 2D model. Dispersed phase is assumed to be monodispersed. Quantitative accuracy of the model is studied by comparing the predicted hold up with experimentally reported values of hold up. Different drag models reported in literature are compared and drag models accounting for the effect of hold up on drag coefficient are found to be better than the drag models which do not account for the effect of hold up on drag coefficient. In particular Kumar-Hartland drag law is found to be the most suitable with the absolute average relative error between the predicted and reported values of hold up being around 15%. In an approach which basically means lumping all uncertainties in two-phase model in the model constant of the drag model, the model of Kumar-Hartland has been modified to reduce the absolute average relative error between the hold up predicted by two-phase CFD model and experimental hold up. It is found that a single drag model cannot represent the entire range of pulsing velocity. For lower pulsing velocities, a drag

model that predicts lower drag coefficient is required. For higher pulsing velocities (≥ 2.5 cm/s), a drag model predicting higher drag coefficient is required. The modified drag model is implemented in the two-phase CFD simulations and the absolute average relative error between predicted and reported hold up is found to be about 10%. Hold up values predicted by CFD simulations are compared with the hold up values obtained from the empirical correlations reported in literature. CFD simulations are found to be distinctly better than the empirical correlations. In this study we have focused on TBP – nitric acid system which is relevant to nuclear fuel reprocessing. Further studies are required to verify if the optimized drag model is able to predict the hold up for other phase systems also.

CHAPTER 4

MONODISPERSED CFD SIMULATION TO ESTIMATE DISPERSED PHASE HOLD UP USING CORRELATED DROP DIAMETER

4.1 INTRODUCTION

In the previous chapter we had developed a CFD based model to capture counter-current two phase flow in PSPC. An assumption of monodispersed drops was made but the major disadvantage was that the user needs to provide the value of the representative drop diameter. This requires experimental measurement which reduces the utility of CFD based approach. In the present chapter, we remove this limitation. Here we report 2D two-phase CFD simulations of a PSPC where in the representative drop size is obtained from a suitable correlation based on the geometry of the column and the operating conditions. Two fluid Euler-Euler (monodispersed) approach has been used to model the dispersed liquid-liquid flow. The main objective of the study is to screen the reported correlations to predict drop diameter in a PSPC and use the best among them along with a suitable drag model to predict the dispersed phase hold up with reasonable accuracy. Thus the study aims at suggesting a predictive CFD model that can be implemented directly without a-priori knowledge of drop diameter so as to predict dispersed phase hold up in the column. Moreover, the phase system considered in this work is 3 N nitric acid and 30% TBP in dodecane which is relevant to nuclear fuel cycle.

4.2 COMPUTATIONAL APPROACH AND THE COMPUTATIONAL DOMAIN

4.2.1 Computational approach

The computational approach in this chapter is essentially the same as that used in chapter 3 with the exception that the representative drop diameter is estimated from a suitable correlation rather than being measured experimentally. In brief two-fluid Euler–Euler monodispersed approach has been used to model counter-current two phase flow in pulsed sieve plate column. Mass, and momentum equations are solved for either phase with a suitable closure expression for interphase momentum exchange term. Turbulence is modeled using a mixture k- ϵ model. The relevant equations (along with description) can be found in section 3.2.1 in chapter 3 and have been omitted here for brevity.

Based on the findings of our previous study drag model due to Kumar and Hartland has been used. The diameter used in CFD simulations is obtained using a reported correlation for the drop diameter in pulsed sieve plate columns. The use of a correlation to predict drop diameter instead of using experimental drop diameter makes the model predictive (no requirement for any experimental input) though the uncertainty associated with the correlation of drop diameter also adds to the uncertainty of the computational model. The absolute average relative error between predicted hold up and reported hold up is analysed. As has been done previously in chapter 3 the constants of the drag model are subsequently modified to reduce the absolute average relative error between the experimental and predicted values of dispersed phase hold up. Performance of the modified drag law is then verified by carrying out simulations of a PSPC of different geometry and employing a different phase system.

4.2.2 Computational domain

The computational domains used in the simulations in this chapter are essentially the same as used in chapter 3 except for column diameter. The details of the geometry, boundary conditions and the grid density used are discussed in detail in section 3.2.2 in chapter 3 and hence have been omitted here for brevity. For validation, the

experimental data on hold up reported in three studies are used (Lade et al., 2013, Din et al., 2010, Sehmel and Babb, 1963). Lade and coworkers. had used a 3 inch column while and coworkers and Sehmel and Babb had used a 2 inch column. The column diameter in the corresponding computational models are chosen accordingly.

4.3. RESULTS AND DISCUSSION

4.3.1 Screening of correlations to predict representative drop size

A prior knowledge of the representative drop diameter to be used in two-phase simulations is required. Representative drop diameter can be obtained experimentally or can be estimated from one of the reported correlations. The second approach to estimate the drop diameter (from a suitable correlation) has been followed in this chapter as this makes the computational approach free from any experimental input and, in a sense, the computational approach becomes predictive requiring no experimental input. In literature, there are several studies on measurement of drop sizes and drop size distribution in PSPCs (Usman et al., 2006; Miyauchi and Oya, 1965; Kagan et al., 1965; Pilhofer and Mewes, 1979; Misek, 1964; Kumar and Hartland, 1996; Kumar and Hartland, 1986; Srinivasulu et al., 1997). A comprehensive review of different correlations proposed for estimation of representative drop diameters in a PSPC has been reported in a previous study (Yadav and Patwardhan, 2008). In this study we too have done the screening of the correlations for estimating the drop diameter by using the experimentally measured Sauter mean diameters for TBP – nitric acid system as reported by Lade and coworkers (Lade et al., 2013). The comparison of different correlations for estimating drop diameter reported by Lade and coworkers (Lade et al., 2013) is shown in Fig. 4.1.

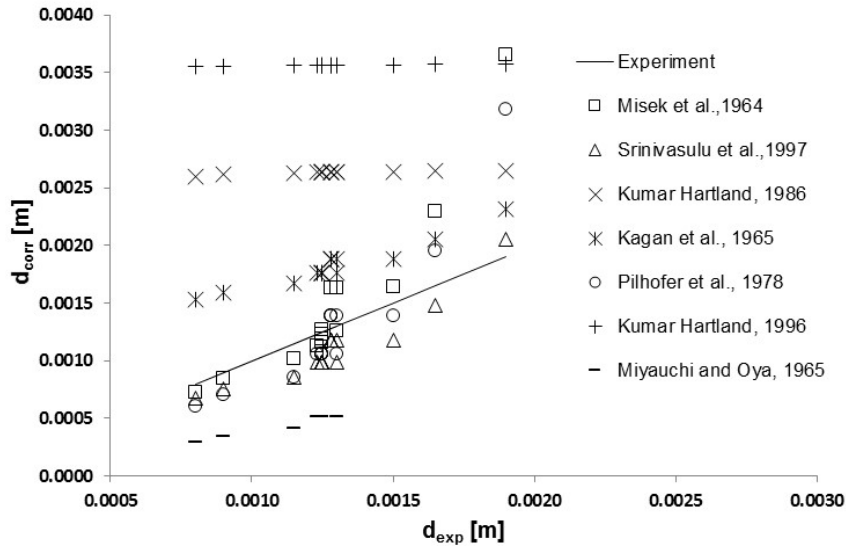


Figure 4.1: Comparison of different correlations to predict drop diameter for TBP - nitric acid system

Table 4.1 summarizes the different correlations screened and the absolute average relative error in estimation of drop diameters for each correlation. It can be observed that the predictions of different correlations vary widely from each other and from the experimental drop diameter. This could be attributed to typical uncertainties inherent in such empirical correlations which are based on experiments for a specific range of operating and geometric parameters and with a specific phase system. It is observed that both the correlations of Kumar and Hartland (Kumar and Hartland, 1996; Kumar and Hartland, 1986) over-predict drop diameters to a significant extent. The same is true for the correlation of Kagan and coworkers (Kagan et al., 1965). The correlation of Miyauchi and Oya (Miyauchi and Oya, 1965) under-predicts the drop diameter. Correlation proposed by Srinivasulu and coworkers (Srinivasulu et al., 1997) shows the best match with the experimental data. Yadav and Patwardhan (Yadav and Patwardhan, 2008) also have recommended the correlation proposed by Srinivasulu and coworkers for scale-up of pulsed sieve plate column. Hence, we have used the correlation of Srinivasulu and coworkers (Srinivasulu et al., 1997) to estimate the drop size required for two-phase flow simulations.

4.3.2 Prediction of hold up using standard Kumar-Hartland drag model

In the simulations, carried out by using standard Kumar-Hartland drag model, we have used the Sauter mean diameter obtained by the correlation of Srinivasulu and coworkers. Table 4.2 lists the conditions for which simulations were carried out. Table 4.2 also lists the experimentally reported Sauter mean drop diameter as well as the Sauter mean drop diameter obtained from the correlation of Srinivasulu and coworkers.

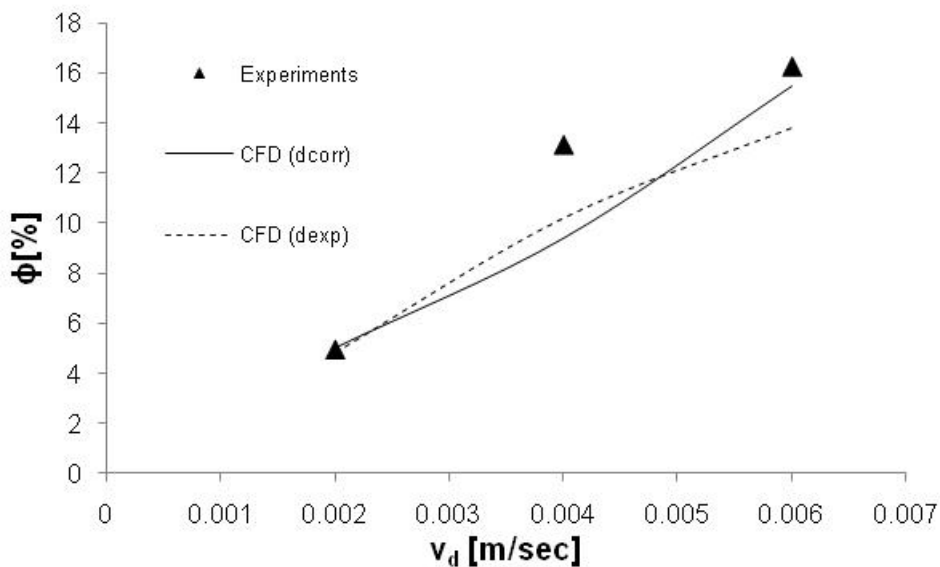
Table 4.1: Comparison of the correlations for estimating representative drop diameters in pulsed sieve plate column

Reference	Correlations	Absolute average relative error (%)
Miyauchi and Oya, 1965	$d_{32} = 2.03 \times 10^{-5} \left(\frac{Af}{h^{-0.33}} \right)^{-1.2} \quad \text{for } \frac{Af}{h^{-0.33}} > 5.57 \times 10^{-2}$	60
Kagan et al., 1965	$d_{32} = 0.92 \frac{(Af)^{-0.3} \alpha^{0.5} \mu_c^{0.1}}{\rho_c^{0.6} g^{0.4}}$	45
Pilhofer and Mewes, 1979	$d_{32} = 0.18 \left(\frac{\sigma}{\rho_c} \right)^{0.6} \left(\frac{\pi^2 (1 - \alpha^2) (Af)^3}{0.72 \alpha^2 h} \right)^{-0.4}$	18
Misek, 1964	$d_{32} = 0.439 d \left[\frac{\sigma \alpha^{0.5}}{d (\pi Af + V_c)^2 \rho_c} \right]^{0.6}$	19
Kumar and Hartland, 1996	$\frac{d_{32}}{\sqrt{\sigma / \Delta \rho g}} = 1.35 \alpha^{0.4} \left(\frac{h}{\sqrt{0.072 / 998} g} \right)^{0.18} \left(\frac{\mu_d g^{1/4}}{0.78} \right)^{0.14} \left(\frac{\sigma}{0.072} \right)^{0.06} \left[0.23 + e^{\left(\frac{-29.66 Af^2}{g \alpha} \right)} \right]$	188
Kumar and Hartland, 1986	$\frac{d_{32}}{h} = \frac{\alpha^{0.32}}{\left(0.645 \left(\frac{\sigma}{\Delta \rho g h^2} \right)^{-0.5} \right) + 2.38 \left[\frac{\left(\frac{\pi^2 (1 - \alpha^2) (Af)^3}{0.72 \alpha^2 h} \right)}{g} \left(\frac{\Delta \rho}{g \sigma} \right)^{0.25} \right] \left(h \left(\frac{\Delta \rho g}{\sigma} \right)^{0.5} \right)^{-1.15}}$	113
Srinivasulu et al., 1997	$d_{32} = 0.08 \left(\frac{\sigma}{\rho_c} \right)^{0.4} (Af)^{-0.8} \alpha^{0.48} d^{0.26} h^{0.34}$	16

Table 4.2: Conditions for which simulations are carried out

Trial	v_d (m/sec)	v_c (m/sec)	Af (m/sec)	ϕ_{exp} (%)	d_{32} (Experimental) (mm)	d_{32} (Correlation) (mm)
1	0.002	0.00207	0.02	5.60	1.28	1.18
2	0.004	0.00207	0.02	13.12	1.28	1.18
3	0.006	0.00207	0.02	16.25	1.30	1.18
4	0.005	0.0018	0.015	11.24	1.65	1.48
5	0.005	0.0018	0.02	16.40	1.50	1.18
6	0.005	0.0018	0.025	24.00	1.25	0.98

Fig. 4.2 shows comparison of the predicted and experimental results of variation of hold up with dispersed phase velocity. Fig. 4.3 shows the predicted and experimental results on variation of hold up with pulsing velocity. Hold up is calculated in the active section of the column (i.e. the section housing the sieve plates). Due to the inherent time periodic nature of the flow field, an arithmetic average of dispersed phase hold up for one complete cycle (100 counts) is considered to calculate the dispersed phase hold up reported in Figs. 4.2-4.3.

**Figure 4.2:** Effect of dispersed phase superficial velocity on dispersed phase hold up.

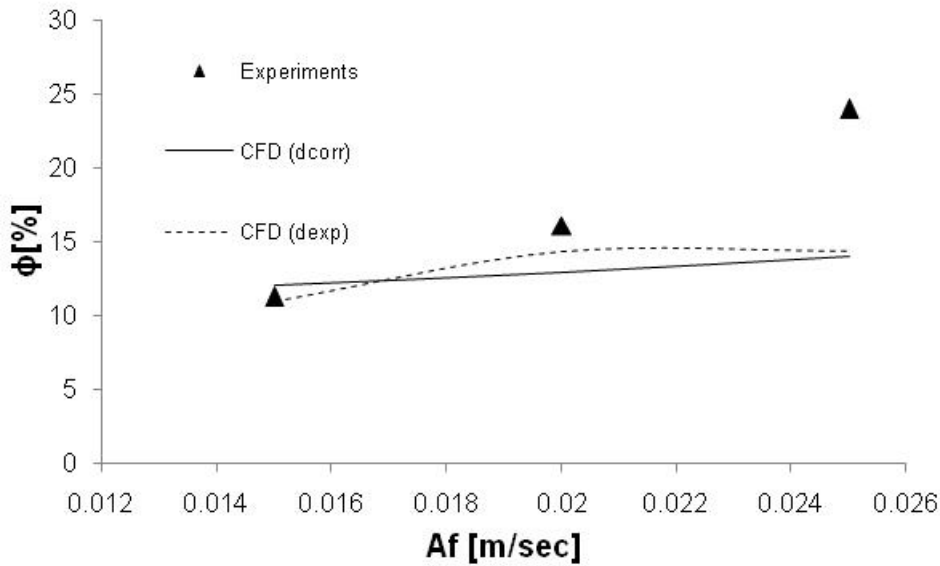
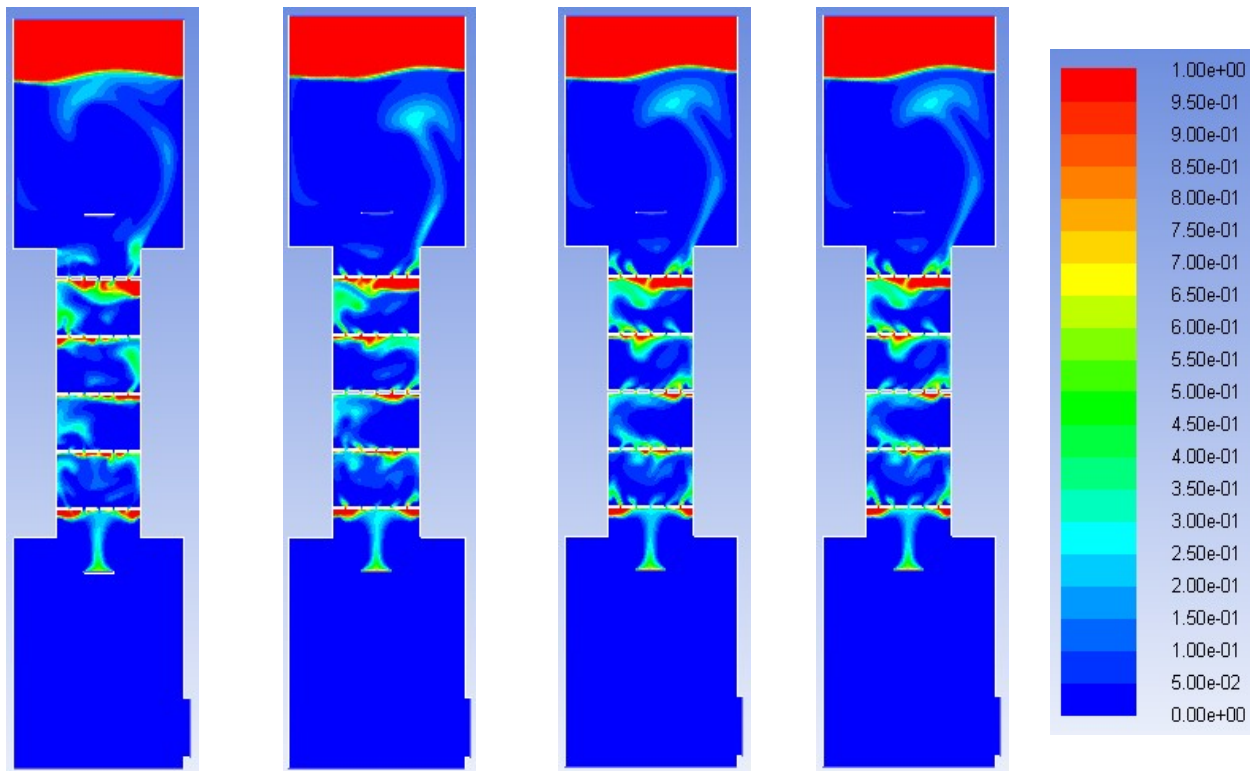


Figure 4.3: Effect of pulsing velocity on dispersed phase hold up.

Fig. 4.2 and Fig. 4.3 contain the results of the simulations carried out with the drop diameter obtained from the correlation as well as the results of the simulations carried out with the experimentally measured drop diameter. Results from CFD simulations using experimental drop diameter are from our work reported in Chapter 2. When the drop diameter obtained from the correlation is used, the absolute average relative error between the predicted and experimental hold up considering all the six data points is about 17%. This deviation is attributed to the combined effect of the limitations and assumptions in the used two-fluid model as well as the correlation used to estimate the drop diameter. It is also observed that when experimental drop diameter is used in the two-fluid model the predicted results are slightly better with the absolute average relative error between the predicted and experimental hold up being about 15%. This difference of about 2% can be attributed to the error incurred in prediction of the drop diameter using correlation.

Fig 4.4 shows the distribution of the dispersed phase at four different instants of one pulsing cycle as obtained from CFD simulations. The first figure from left is at the instant of the mean position of the pulse while going up. The second figure from left

is at the instant of positive peak of the pulse. The third figure from left is at the instant of mean position of the pulse while going down.



Mean position of pulse while going up

Positive peak of the pulse

Mean position of pulse while going down

Negative peak of the pulse

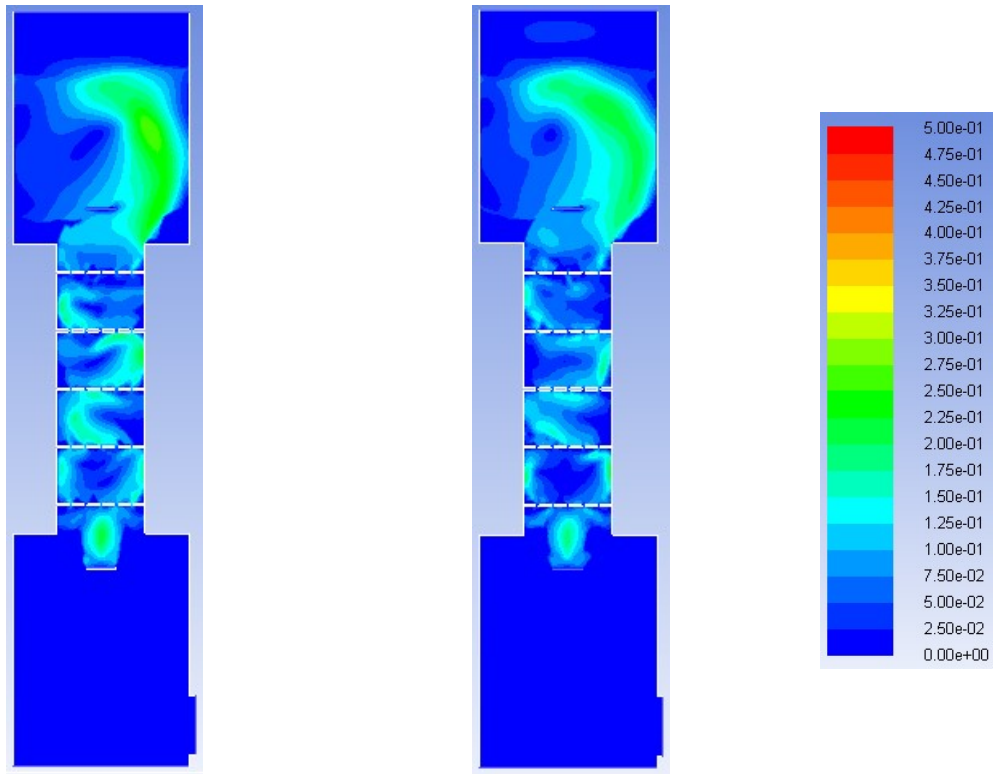
Figure 4.4: Profiles of dispersed phase hold up inside the column at different instants of a pulsing cycle ($A_f = 0.02$ m/sec; $v_d = 0.006$ m/sec, $v_c = 0.00207$ m/sec)

The fourth figure from the left is at the instant of the negative peak of the pulse. It is interesting to note that even though overall profile of the dispersed phase hold up inside the column does not change much during a pulsing cycle, local distribution of the dispersed phase does change. The dispersed phase is seen to rise up like a plume. The dispersed phase moves alternately along the walls of the column. On close observation it can be seen that the dispersed phase oozes out of the holes during the positive part of the pulsing cycle as evident by higher values of hold up above the holes and spreading above the plates in the first two figures from the left. During the downward stroke of the pulse this ejection of the dispersed phase through the holes is not evident. A slight accumulation of the dispersed phase (in form of a thin layer)

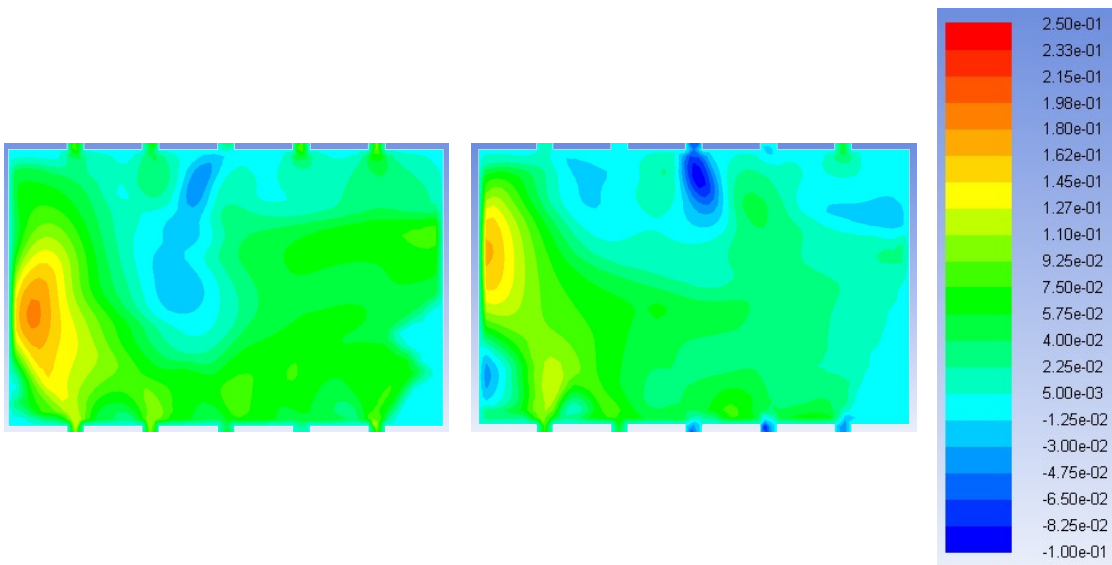
below the plates is also visible. One important observation is that accumulation of dispersed phase below the bottom most plate is more than below other plates. This is because the bottom most plate is the first to intercept the upward flow of the dispersed phase. Thereafter, the accumulation underneath each plate is similar. This also shows that the entrance effect is predominantly limited to the bottom most plate which justifies using reduced number of plates in the computational domain. Disengagement of phases in the upper disengagement section can also be seen. Another important observation from [Fig. 4.4](#) is that except for a thin film accumulating at the base of each plate the lighter phase is mostly dispersed for the entire pulsing cycle. Similar flow pattern (of the lighter phase) were observed for other values of dispersed phase velocities and pulse intensities. Thus it can be said that the column operated under dispersion regime in the range of operating conditions considered in this work. The fact that dispersed phase hold up increased with increase in pulsing velocity also suggests the same. Had the column operated in mixer- settler regime dispersed phase hold up should have first reduced then increased with increase in pulsing velocity.

[Fig. 4.5](#) shows the profile of dispersed phase velocity magnitude in the column. It also shows variation of y-component of dispersed phase velocity between two plates. The contours are shown at positive and negative peaks of the pulsing cycle for pulsing velocity of 0.02 m/sec. During the positive peak of the pulse, y-component of dispersed phase velocity assumes positive values to a greater extent than during negative peak. This signifies that the dispersed phase is forced upwards to a greater extent during the positive peak of the pulse. Additionally, it is observed that the velocity is higher alternately along one of the walls of the column. This signifies that the dispersed phase moves up alternately along one of the walls of the column in the form of a plume.

Continuous phase velocity vectors at positive (right) and negative (left) peak of the pulsing cycle for pulsing intensity of 0.02 m/sec are shown in [Fig. 4.6](#). Presence of



(A)



(B)

Figure 4.5: (A) Dispersed phase velocity magnitude profile for positive (left) and negative (right) peak of the pulsing cycle. (B) Profile of y-component of dispersed phase velocity for positive (left) and negative (right) peak of the pulsing cycle between two plates. ($Af = 0.02$ m/sec; $v_d = 0.006$ m/sec, $v_c = 0.00207$ m/sec)

re-circulations in the continuous phase is clearly visible. A single re-circulation loop is observed in the space between two consecutive plates and it is large enough to sweep the entire interplate space. In fact, it is the presence of such re-circulations that increase the backmixing in these columns. These continuous phase re-circulations trap the dispersed phase droplets moving up the column. The fact the continuous phase re-circulation pattern closely follow the way the dispersed phase moves up inside the column also lends support to this argument.

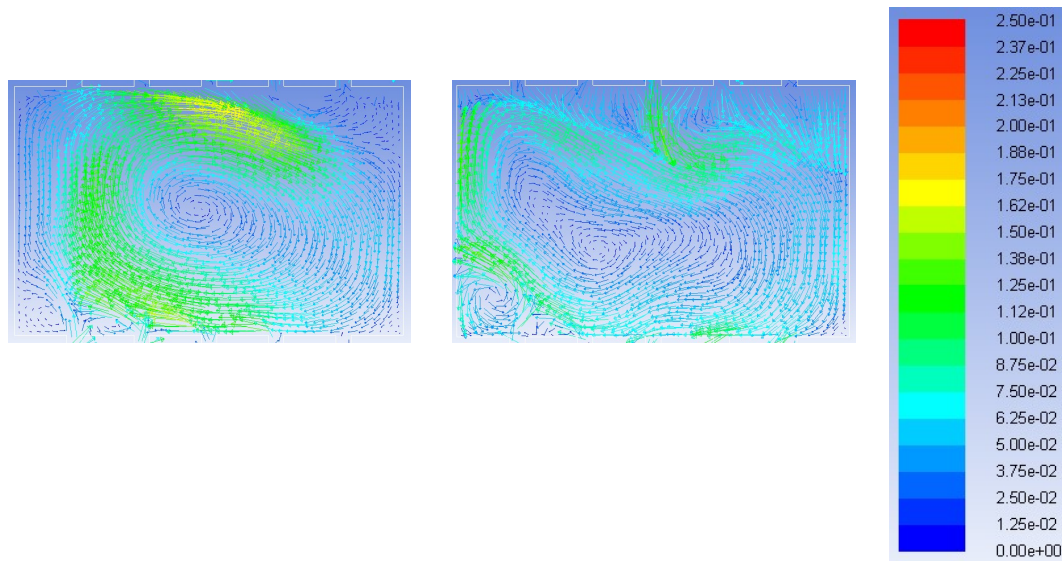


Figure 4.6:Continuous phase velocity vectors for positive (left) and negative (right) peak of the pulsing cycle ($A_f = 0.02$ m/sec; $v_d = 0.006$ m/sec, $v_c = 0.00207$ m/sec).

4.3.3 Optimization of Constants of Kumar-Hartland Drag Model

In chapter 3 we had followed an approach where in all uncertainties in the CFD model were lumped in the empirical constants of the drag model. This was a practical way forward to reduce the errors in prediction. We also follow a similar approach in this chapter. In the previous sub-section it was seen that absolute average relative error in prediction of dispersed phase hold up using standard drag model of Kumar-Hartland (Table 3.1) along with the drop diameter predicted by the correlation of [Srinivasulu et al., 1997](#) is 17.2 %. In this section we attempt to further reduce this error between

predicted and reported values of dispersed phase hold up. This is done by varying the values of the constants of Kumar-Hartland model.

As seen from Figs. 4.3 and 4.4, dispersed phase hold up predicted by the Kumar-Hartland model in its standard form is lower than the experimental values of hold up for most of the operating conditions studied. Hence, it is reasonable to say that the empirical constant should be modified such that the modified drag model predicts a larger value of the drag coefficient which will lead to increased resistance to the movement of dispersed phase leading to its increased retention in the column causing dispersed phase hold up to increase.

In chapter 3, we have used the similar approach of modifying the constants of the standard Kumar-Hartland model to reduce the deviation between the hold up predicted from CFD simulations and hold up obtained in experiments. However, in the previous work representative drop diameters used in the simulations were experimentally measured drop diameters. In the present work, the drop diameters used in simulations are obtained from a correlation. Thus the values of the optimum values of the constants of Kumar-Hartland model are expected to be different from the previously reported optimum values and need to be worked out again. In chapter 3, it was shown that amongst the two empirical constants A_D and B , the effect of A_D on dispersed phase hold up is more pronounced than that of B . It was shown that an increase in value of A_D by 37.5% increased dispersed phase hold up value by 16% whereas an increase of 58% in B reduced dispersed hold up only by 1.75%. Since B does not affect the hold up much, B was kept constant at the minimum value of the range of B explored, the recommended value of B being 0.4. The value of A_D was optimized so as to minimize the absolute average relative error between the predicted and the experimental value. The same approach has been considered in this chapter.

Total 21 simulations were carried out. The results from these simulations were regressed to have a correlation which relates hold up with the pulsing velocity,

dispersed phase velocity, Sauter mean diameter used in the simulations and value of the empirical constant A_D . The independent variables (value of empirical constant A_D , pulse intensity, dispersed phase velocity and drop diameter) and dependent variable (hold up) were arranged in relevant dimensionless groups and the best fit equation was obtained by non-linear regression using LAB Fit. This correlation was used to identify the optimum value of A_D for which the error between the predicted hold up and the experimental hold up is minimum. A single value of A_D was not found to be good for the entire range of the experimental data hence the optimum value of A_D was found out separately for the two sets. For pulsing intensity less than 0.025 m/s, optimum value of A_D was found to be 7.8 whereas for pulsing intensity of more than or equal to 0.025 m/s, optimum value of A_D was found to be 10.0. The final form of the modified drag model is given by Eq. (4.1).

$$C_D = \begin{cases} \left(0.53 + \frac{24}{Re}\right)(1 + 7.8\phi^{0.4}) & \forall Af < 0.025 \text{ m/s} \\ \left(0.53 + \frac{24}{Re}\right)(1 + 10.0\phi^{0.4}) & \forall Af \geq 0.025 \text{ m/s} \end{cases} \quad (4.1)$$

A final round of simulations was carried out with the modified drag model given in Eqn. (4.14). The data used for this round of simulations included a set of data reported by Lade and coworkers (Lade et al. 2013) for variation of dispersed phase hold up with continuous phase velocity (not included in Table 4.2) which was kept aside exclusively to test the modified drag model. The absolute average relative error between the predicted and reported values of dispersed phase hold up could be reduced to 5.8% using the modified drag model. Fig. 4.7 shows the parity plot which clearly shows the close match between the predicted and experimentally reported values of dispersed phase hold up. The data considered are variation of dispersed phase hold up with pulsing velocity (in Table 4.1) and with continuous phase velocity (fresh data).

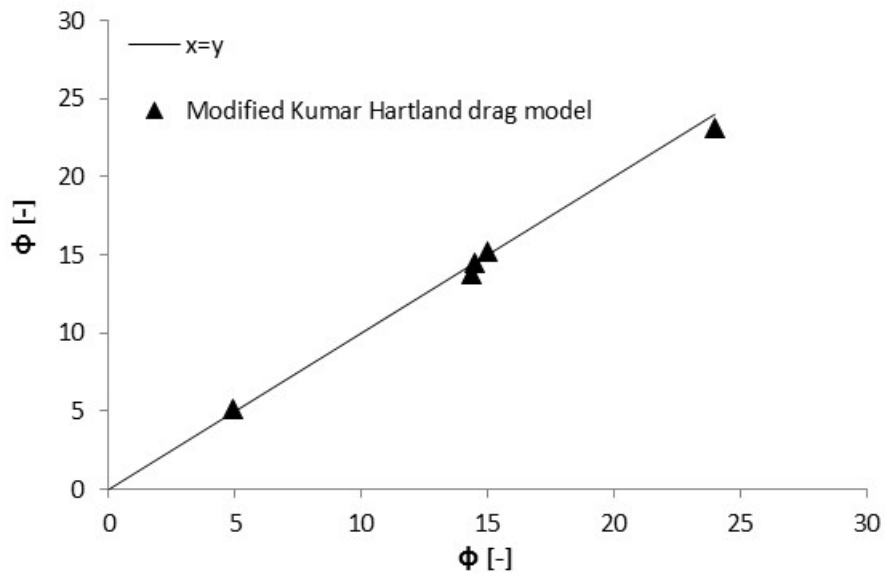


Figure 4.7: Comparison of experimental values of dispersed phase hold up with the values of dispersed phase hold up predicted by the CFD model embedding the modified Kumar-Hartland drag model.

4.3.5 Validity of the modified Kumar-Hartland drag model for a different column

The validity of the modified drag model proposed in this chapter is put to test by using experimental results on hold up reported in a pulsed column of a different geometry (Din et al., 2010). The experimental study reports hold up and dispersed phase axial dispersion in counter-current two-phase flow of water (dispersed phase) and kerosene (continuous phase) in a pulsed sieve plate columns of 0.05 m diameter. The sieve hole diameter is 0.002 m. Open area of the sieve plates used is 25%. The data used is for reverse phase operation in which the heavier phase is the dispersed phase. The methodology developed in the previous section is used for the simulations of the new geometry. Drop diameter used in simulations is obtained from the correlation due to Srinivasulu and coworkers (Srinivasulu et al., 1997) using the geometrical details of the column and physical properties of the phase system considered.

Fig. 4.8 shows the dispersed phase hold up and dispersed phase velocity contour for the pulsing velocity of 0.0112 m/sec. It is observed that the dispersed phase moves downward alternately along one of walls of the column in the form of a plume. This is also evident from the profile of dispersed phase velocity. Infact, similar features were observed in Fig. 4.4 which also showed that the dispersed phase moved up in the form of a plume. Significant accumulation of the dispersed phase (i.e. heavier phase in this case) is clearly observed just above the sieve plates. Values of dispersed phase velocities are observed to be higher during the negative peak and at the instant defined as mean position of pulse while doing down. This is attributed to the fact that during the positive peak of the pulse the downward flow of the dispersed phase is reduced as the pulse is directed upwards. Thereafter during the negative peak the heavier (dispersed) phase is pulled down leading to higher velocities.

Fig. 4.9 shows the comparison of the predicted and experimental values of dispersed phase hold up. In the same figure the performance of CFD model embedding standard Kumar-Hartland drag model is also shown. Even though both the models could capture an increase in dispersed phase hold up with increase in pulse intensity (Af) standard Kumar-Hartland model underpredicts the dispersed phase hold up. The performance of the optimized Kumar-Hartland drag model is found to be reasonably good. The average absolute relative error between the predicted and reported experimental values of hold up is about 15%. Even though this error in prediction of dispersed phase hold up is relatively higher than the same for the data of Lade and coworker (Lade et al., 2013) it can be considered to be resonably good. The relatively worse results for the data of Din and coworkers (Din et al., 2010) can be sttributed to different plate geometry because hydrodynamics in the column, specially the prevailing turbulence inside the column depends significantly on the plate geometry.

Fig. 4.9 also compares the performance of the CFD model developed in this work vis-à-vis different correlations reported in literature for prediction of hold up. Table 4.3

lists the correlations tested. The comparison is on the basis of the experimental data reported by Din and coworkers. Venkatnarsaiah and Verma have given correlations for direct estimation of dispersed phase hold up in the column as well as for estimation of slip velocity. Slip velocity can be used to back calculate dispersed phase hold up. It can be observed from [Fig. 4.9](#) that the predictions of the CFD model are distinctly better than the predictions of the empirical correlations reported in literature. All the empirical correlations significantly under-predict the dispersed phase hold up. The minimum absolute average relative error in dispersed phase hold up prediction with the best empirical correlation is about 48% where as that of CFD is around 15%. Thus it can be conclude that the 2D CFD model embedding a modified drag model is able to predict hold up better than the CFD model embedding the standard drag model and the correlations reported in literature. Thus the proposed computational approach is a reasonably good approach to predict the hold up in a pulsed sieve plate column.

The modified drag model is also tested for normal phase (i.e. aqueous continuous) operation in a pulsed column with the data reported by Sehmel and Babb ([Sehmel and Babb, 1963](#)). The authors used a 2 inch diameter column containing 43 plates. The plate spacing, hole diameter and percent open area were 2 inch, 1/8 inch and 23%, respectively. They had used three different phase systems (hexane-water, benzene-water and methyl isobutyl ketone-water) and reported dispersed phase hold up for different values of phase velocity and pulse intensity.

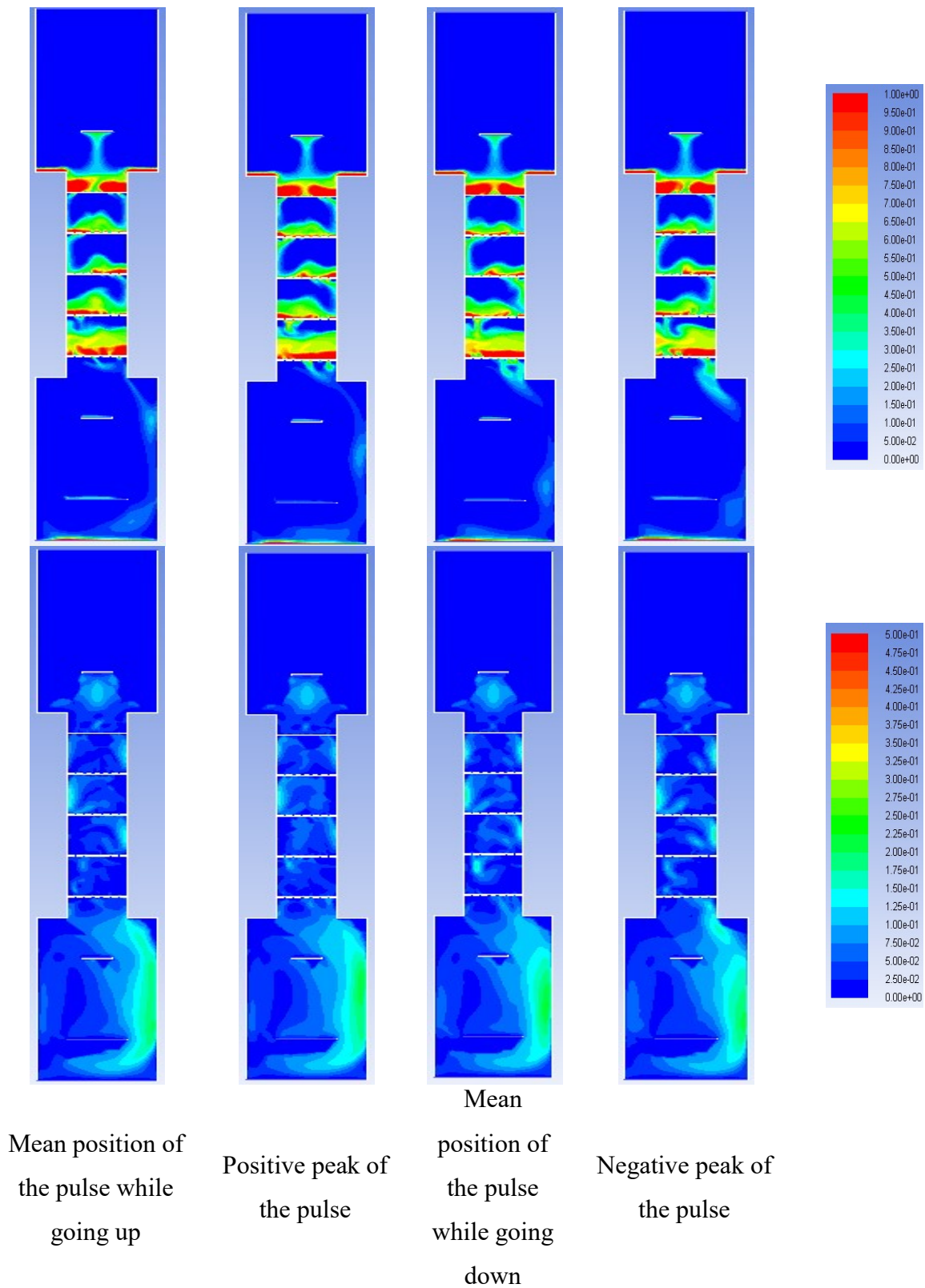


Figure 4.8: Profile of dispersed phase hold up (top) and dispersed phase velocity (bottom) for aqueous dispersed mode of operation of column for one of the data sets reported by [Din et al., 2010](#) ($A_f = 0.0112$ m/sec; $v_d = 0.0034$ m/sec; $v_c = 0.0037$ m/sec)

Table 4.3: Empirical correlations used for predicting dispersed phase hold up in this study

Reference	Expression
Kumar and Hartland, 1988	$\phi = K_1 \exp(K_2 Af - (Af)_m) V_d^{0.86} (V_c + V_d)^{0.28} \Delta\rho^{-0.30} \rho_d^{-0.93} \mu_d^{0.77} \alpha^{-0.56} h^{-0.56}$ $(Af)_m = 9.69 \times 10^{-3} \left(\frac{\sigma \Delta\rho^{0.25} \alpha}{\mu_d^{0.75}} \right)^{0.33} \quad K_1 = 2.10 \times 10^6 \quad K_2 = 44.53$
Miyauchi and Oya, 1965	$\phi = 4.93 \times 10^2 \psi^{0.84} V_d^{2/3} \quad \text{for } \psi < 0.0031 \text{m}^{11/12} \text{s}^{-1}$ $\phi = 3.42 \times 10^6 \psi^{0.24} V_d^{2/3} \quad \text{for } \psi > 0.0031 \text{m}^{11/12} \text{s}^{-1}$ $\psi = \frac{Af}{(\beta h)^{1/3}} \left(\frac{\mu_d^2}{\sigma \Delta\rho} \right)^{1/4} \quad \beta = \frac{\alpha^2}{(1-\alpha)(1-\alpha^2)}$
Venkatnarsaiah and Verma, 1998 (direct hold up estimation)	$\phi = K_1 \exp(K_2 Af - (Af)_m) V_d^{1.02} V_c^{0.02} \Delta\rho^{-0.23} \mu_d^{0.52} \alpha^{-0.4} h^{-0.4} d^{-0.3}$ $(Af)_m = 9.69 \times 10^{-3} \left(\frac{\sigma \Delta\rho^{0.25} \alpha}{\mu_d^{0.75}} \right)^{0.33} \quad K_1 = 116.5 \quad K_2 = 39.35$
Venkatnarsaiah and Verma, 1998 (hold up estimation using slip velocity)	$V_{\text{slip}} = K_1 \exp(K_2 Af - (Af)_m) \Delta\rho^{0.22} \mu_d^{-0.38} \alpha^{0.32} h^{0.31} d^{0.22}$ $(Af)_m = 9.69 \times 10^{-3} \left(\frac{\sigma \Delta\rho^{0.25} \alpha}{\mu_d^{0.75}} \right)^{0.33} \quad K_1 = 1.35 \times 10^{-2} \quad K_2 = -33.3$

Figs. 4.10 and 4.11 shows the comparison between the predicted and reported values of dispersed phase hold up for two different phases systems i.e. hexane-water system and benzene-water system. As is observed from Figs. 4.10 and 4.11 the dispersed phase hold up predicted by CFD is reasonably close to the reported values of dispersed phase hold up. The average absolute relative error is prediction is about 14%. This shows the efficacy of the CFD model embedding the modified Kumar-Hartland drag model for predicting dispersed phase hold up in PSPCs having different geometries and operating with different phase systems.

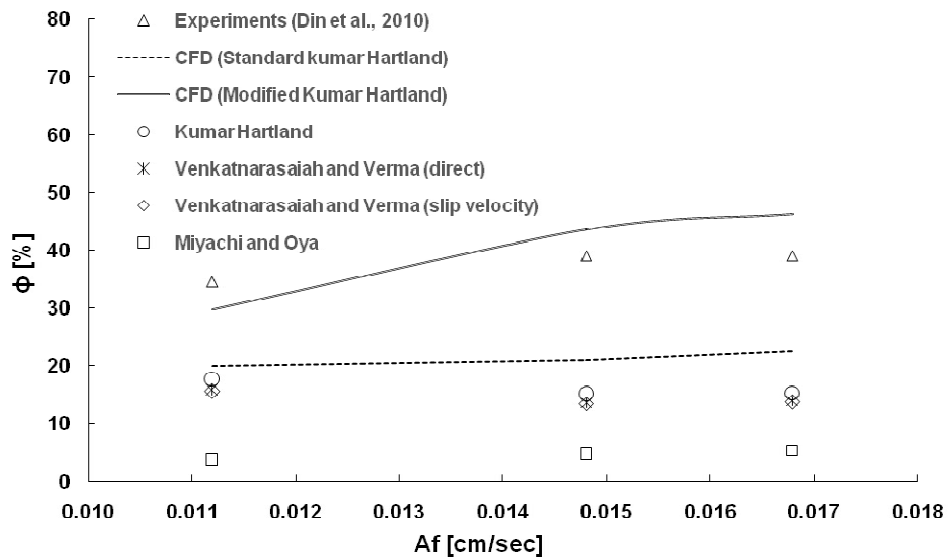


Figure 4.9: Comparison of hold up values predicted by CFD simulations and estimated by various correlations reported in literature. The experimental data is from [Din et al., 2010](#).

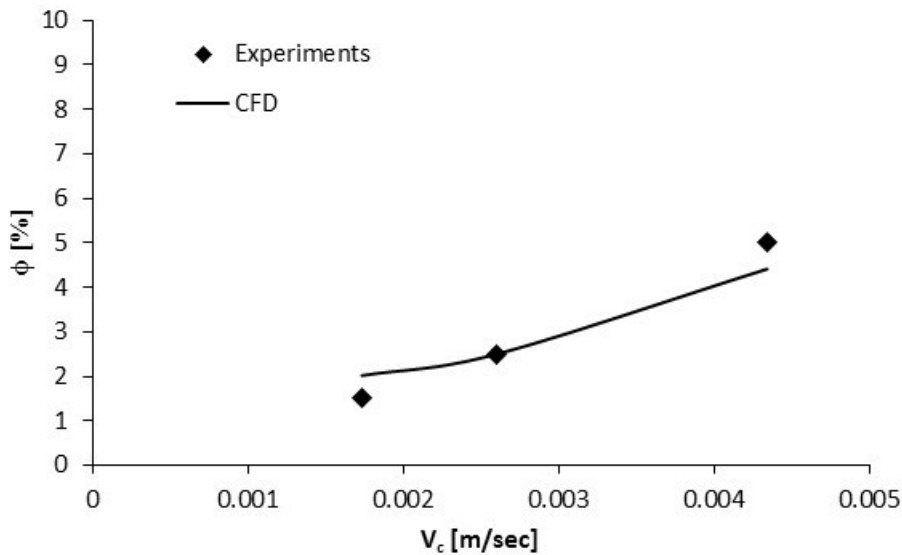


Figure 4.10: Comparison of hold up values predicted by CFD simulations with experimental values of dispersed phase hold up reported by Sehmel and Babb ([Sehmel and Babb, 1963](#)). ($v_c/v_d = 1$, $A_f = 0.0211$ m/sec, hexane-water system)

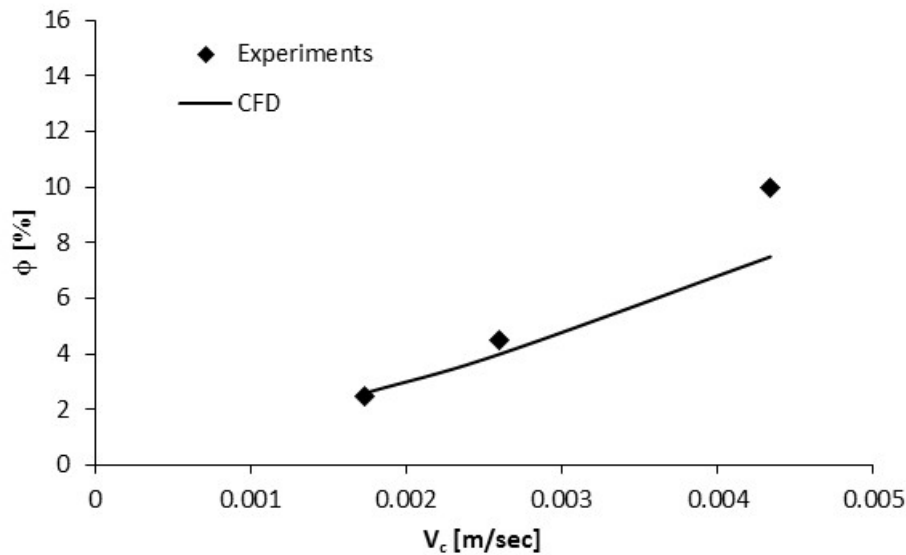


Figure 4.11: Comparison of dispersed phase hold up values predicted by CFD simulations and experimentally measured hold up values reported by Sehmel and Babb (Sehmel and Babb, 1963). ($v_c/v_d = 1$, $Af = 0.01375$ m/sec, benzene-water system)

4.4 CONCLUSION

Two-phase flow of 30% TBP in dodecane –nitric acid system in a pulsed sieve plate column has been simulated using a 2D two-fluid CFD model. Dispersed phase is assumed to be monodispersed. Representative drop diameter used in the two-fluid model is obtained from a suitable correlation which is identified after screening several empirical correlations reported to estimate the drop diameter in pulsed sieve plate columns. Standard Kumar-Hartland drag model is used to model the interphase momentum exchange term. Quantitative accuracy of the computational approach is tested by comparing its predictions of dispersed phase hold up with the reported experimental values of hold up and the average absolute error in prediction of hold up is found to be about 17%. In an approach which basically means lumping all uncertainties in the computational approach in the model constants of the drag model, the model of Kumar-Hartland has been modified to bring the hold up predicted by two-phase CFD model closer to the experimentally measured values. It is found that a

single drag model is not suitable for the entire range of pulse intensity. For lower pulse intensities, a drag model that predicts lower drag coefficient is required. For higher pulsing intensities (≥ 2.5 cm/s), a drag model predicting higher drag coefficient is required. The modified drag model is implemented in the two-phase CFD model and the error between predicted and reported hold up is found to be about 5.8%. The versatility of the CFD model embedding the modified drag model is tested by comparing its performance against experimental results of dispersed phase hold up in another pulsed column having a different geometry and employing a different phase system. The absolute average relative error between the predicted and experimental results on hold up is about 15%. This result is significantly better than that obtained using standard Kumar-Hartland drag model which tends to severely under-predict dispersed phase hold up. It is also found to be better than the reported empirical correlations to predict dispersed phase hold up in pulsed sieve plate columns reported in literature. The computational approach embedding a modified version of Kumar-Hartland drag model thus offers a simplified way of predicting dispersed phase hold up in a pulsed sieve plate columns and thus can be useful for design and optimization calculations.

CHAPTER 5

COUPLED CFD-PBE SIMULATION TO PREDICT DISPERSED PHASE HOLD UP AND SAUTER MEAN DROP DIAMETER

5.1 INTRODUCTION

In our previous chapters (Chapter 3-4) we have captured counter-current two phase in PSPC and validated the model against reported data in literature. The major limitation however in these studies was the assumption of monodispersed drops. In reality the drop size distribution as well as the Sauter mean drop diameter varies with time and space. For example the drops would be smaller in the regions close to the sieve holes and larger in places away from the holes. The drop size may also vary within the pulsing cycle itself. These variations in drop size may effect the velocity field as well the dispersed phase hold up. Thus it is imperative to capture the spatio-temporal variation of drop size (and drop size distribution) by coupling population balance equations with the Navier-Stokes equations (along with appropriate closure models for turbulence). CFD and CFD coupled with population balance models (PBM) have been used to model dispersed liquid-liquid two-phase flow in various types of equipments ([Wang and Mao, 2005](#); [Gimbun et al., 2009](#); [Kerdouss et al., 2008](#); [Modes and Bart, 2001](#); [Alopaeus et al., 1999](#); [Alopaeus et al., 2002](#); [Drumm et al., 2009](#); [Drumm and Bart, 2006](#); [Vikhansky and Markus, 2004](#); [Wardle, 2011](#); [Sathe et al., 2009](#); [Wardle et al., 2008](#); [Gandhir and Wardle, 2012](#)). Even though some CFD studies have been carried out for pulsed columns, most of them cater to pulsed disc and doughnut columns. Only a few are dedicated towards pulsed sieve plate columns. However as far as CFD-PBE based modeling of pulsed columns is concerned only a couple of recent reports exist for PDDC. Amokrane and coworker ([Amokrane et al.,](#)

2014a) reported a CFD-PBE based approach to model pulsed disc and doughnut column (PDDC). The single-phase CFD model was first validated against experimental PIV data then coupled CFD-PBE model was presented for two-phase flow simulations. However, validation of the CFD-PBE model was not reported. Only drop breakage was considered in PBE. Recently, the same group (Amokrane et al., 2016) reported a CFD-PBE model considering both drop breakage and coalescence. The authors measured drop size distribution in a 1 inch column and optimized the breakage and coalescence kernels of the PB model. To the best of our knowledge CFD-PBE based modeling has not been reported for PSPC so far.

In the present work, we report 2D two-phase CFD-PBE simulations of a PSPC for the first time. This research work thus closes one essential gap area with respect to numerical modeling of pulsed sieve plate columns. Euler-Euler approach is used to model the two phase liquid-liquid flow. Experiments are performed in PSPCs of different geometries and for a wide range of operating conditions. The 2D CFD-PBE model is validated extensively against experimental data of dispersed phase hold up and drop size. Thus in this work we report a comprehensively validated and tested CFD-PBE model of PSPC for the first time.

5.2 EXPERIMENTAL SETUP AND COMPUTATIONAL APPROACH

5.2.1 Experimental setup

The schematic diagram of PSPC is shown in Fig. 5.1. Two different columns having 2 and 3 inch diameter are used. Height of the active section of the columns (cylindrical part between two disengagement sections) is 0.5 m. The columns were made of glass so as to allow optical access to the liquid-liquid dispersed flow in the column. The flow in the column was counter current. The light phase is fed to the bottom of the column through a centrifugal pump and rotameter. After passing through the column,

the light phase separates out from the two-phase mixture in the upper disengagement section and overflows back to its feed tank. Similarly, the heavy phase from another feed tank is fed to the top of the column through another centrifugal pump and rotameter. The heavy phase flows downwards through the column and separates out from the light phase in the lower disengagement section. The top and bottom disengagement sections were made of SS 316 L with a glass window. The heavy phase then rises through the balance leg (Fig. 5.1) and is recycled back to the heavy phase feed tank. The balance leg is used to ensure the column is filled with heavy phase and maintain the liquid-liquid interface in the top disengagement section during aqueous continuous operation in which the aqueous phase is the continuous phase while the organic phase is made dispersed. A standard sieve plate cartridge (3 mm hole diameter in triangular pitch of 5 mm, 23% open area) has been used to study effect of operating parameters. Cartridges with two different interplate spacing (50 mm and 100 mm) have been used to study the effect of variation of column geometry on hold up and drop diameter. The sieve plates help to increase the interfacial area between the two immiscible liquids by breaking the droplets of dispersed phase. An air pulsing unit located at the base of lower disengagement section is used to provide pulse to the process fluids to facilitate counter-current flow. The pulsing system essentially comprised of a three way solenoid valve (Make: AirMax) along with a pneumatic loop. The loop comprised of a reciprocating compressor (Make: Crompton) and a surge tank where in the pressure could be maintained constant at a desired value using a pressure transmitter (located on top of the tank, a PID controller and a control valve controlling the flow to the tank from the compressor). Experiments to vary pulsing velocity are carried out by varying pulsation amplitude keeping pulsation frequency constant at 1 Hz. This was achieved by varying the set pressure in the surge tank. Duty cycle of pulsation is kept 30%. In present study, two different phase systems have been used - water, 30% TBP/dodecane system and 3N

nitric acid, 30% TBP/dodecane system. This method of operation (normal phase operation) forms a liquid–liquid interface in the upper disengagement section. A sampling port is located at the center of the active section of the column. This port is used to withdraw the dispersion to measure dispersed phase hold up following the method reported recently (Liu et al., 2015). At first pulsing and continuous phase flow (at their respective values) are established in the column. Thereafter, the dispersed phase flow is started at the desired flow rate. The dispersed phase moves up the column in the form of drops and at the top disengagement section they coalesce and forms a separate layer and finally goes out though the top of the column. The column is operated like this till a steady state is reached. Thereafter the valve in the port is opened quickly and the dispersion is collected in a measuring cylinder for a short duration of time (around 5 seconds). The two phases thereafter settle in the measuring cylinder and the measurement of dispersed phase hold up is carried as the fraction of the total volume occupied by the lighter (dispersed phase).

A high speed video camera (Make: Mikrotron, Model: MotionBLITZ EoSens 1MC 1370) was installed at the center of the column section to obtain image of the dispersion generated in the column. The images were captured at a rate of 200 frames per second. The images were analyzed to obtain Sauter mean drop diameter for a specified set of operating conditions. Further details of experiments are reported elsewhere (Sarkar et al., 2017).

5.2.2 Computational approach

Two-fluid Euler-Euler model is used to model liquid-liquid two-phase flow in PSPCs. in the present chapter. The model solves the conservation equations for momentum and mass for both phases and assumes the phases as interpenetrating continua. The phase fraction (or hold up) of the dispersed phase in each computational cell is computed by solving a convection diffusion transport equation for the phase fraction itself. The momentum exchange between the two phases is modeled through the

interphase exchange coefficients which in turn is defined in terms of a drag coefficient (C_D). Turbulence has been modeled using the mixture k- ϵ model in which the turbulence equations are solved for the mixture as a whole. This approach reduces the number of equations to be solved as turbulence equations are not solved for each phase. The relevant governing equations can be in chapter 3 and 4 and are omitted here for brevity.

The exchange of momentum between the phases is only through the drag force which is quantified using the drag model of Schiller and Naumann as expressed by Eq. (5.1). The above drag law has been extensively used in dispersed liquid-liquid flow.

It can be mentioned here that Kumar Hartland drag law (which is a drag model for concentrated dispersion) had been used in previous chapters. However implementing this drag law coupled with PBE led to numerical instabilities. Moreover it is worth noting that even though Kumar Hartland drag law is expected to hold for concentrated dispersions it has an entirely empirical basis. However the conditions for which the law was obtained did not include pulsatile flows. In fact this is one of the possible reasons while it was necessary to fine tune the original form of the law so as to reduce the error to acceptable limits. However even though formulated for lean dispersions Schiller-Naumann law has a theoretical basis. Hence, this law (which was eventually fine tuned as well to account for pulsatile flow) was used in the rest of work due to its fundamental as well as simple form.

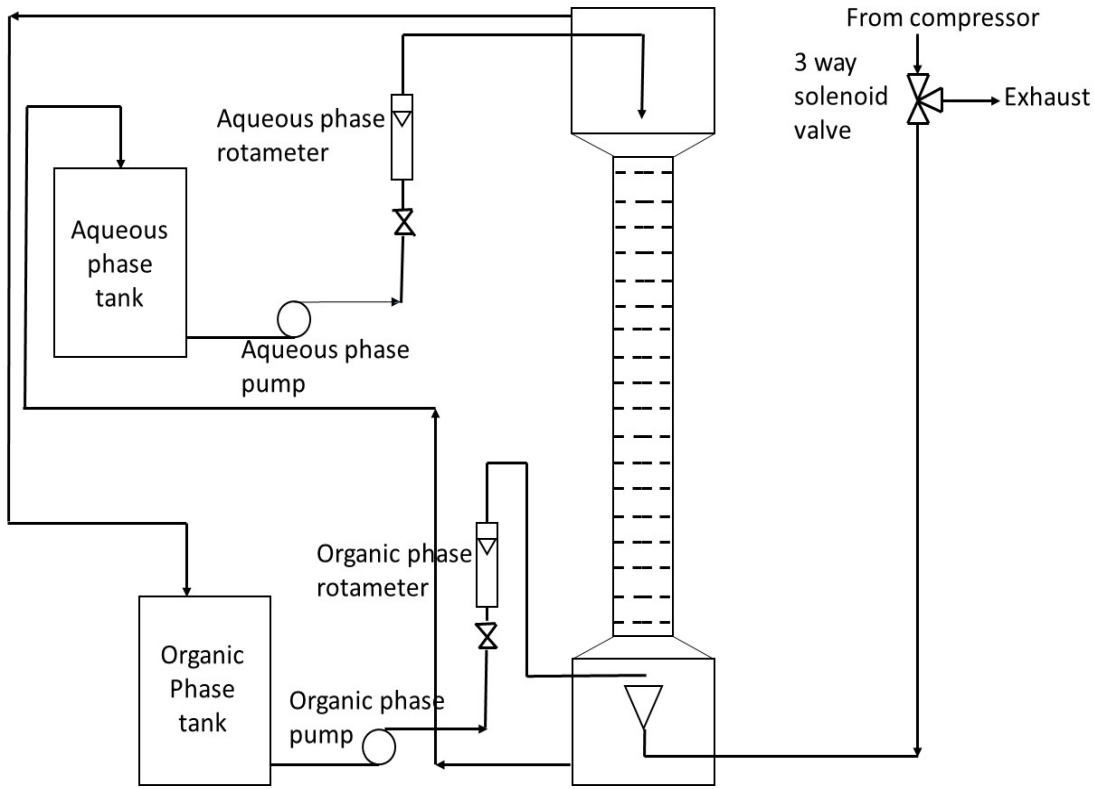


Figure 5.1: Schematic drawing of the experimental setup.

$$C_D = \frac{24}{\text{Re}} (1 + 0.15 \phi^{0.67}) \quad (5.1)$$

One major limitation of the previously reported two-phase CFD simulations of PSPCs is the assumption of monodispersed drops. With this assumption the coalescence and redispersion of droplets which is continuously happening inside the column is not accounted for. Thus the local drop dynamics is not captured with the assumption of monodispersed droplets. In this work we have incorporated population balance equations (PBE) along with flow and turbulence equations to do away with this assumption.

Local drop size distribution of a liquid-liquid dispersion depends on local velocity, breakage and coalescence rates of droplets in each computational cell. Breakage and coalescence rates in turn depends on physical properties of the phase system considered, local turbulent energy dissipation rates and dispersed phase hold up. This physics is captured by the population balance equations, one for each characteristic

length (or diameter) of drop (L) in a computational cell. The population balance equation is given by Eq. (5.2) (Marchisio et al., 2003; Singh et al., 2009).

$$\frac{\partial}{\partial t}\{n(L, t)\} + \nabla \cdot (\bar{U} \cdot n(L, t)) = B^a(L; t) - D^a(L; t) + B^b(L; t) - D^b(L; t) \quad (5.2)$$

Here B^a and B^b are birth rates of a droplet of size L at any time t due to aggregation and breakage, respectively. D^a and D^b are the death rates of a droplet of size L at any time t due to aggregation and breakage, respectively. $n(L; t)$ is the number of droplet having characteristic length L at any time per unit volume per unit characteristic size.

The expressions for the birth and deaths rate are given by the following equations

$$B^a(L; t) = \frac{L^2}{2} \int_0^L \frac{\beta\{(L^3 - \lambda^3)^{1/3}, \lambda\}}{(L^3 - \lambda^3)^{2/3}} n\{(L^3 - \lambda^3)^{1/3}; t\} n(\lambda; t) d\lambda \quad (5.3)$$

$$D^a(L; t) = n(L; t) \int_0^\infty \beta(L, \lambda) n(\lambda; t) d\lambda \quad (5.4)$$

$$B^b(L; t) = \int_L^\infty a(\lambda) b(L|\lambda) n(\lambda; t) d\lambda \quad (5.5)$$

$$D^b(L; t) = a(L) n(L; t) \quad (5.6)$$

Where, β is the aggregation (coalescence) kernel, a is the breakage kernel and b is the daughter droplet distribution. In their pioneering work, Coualoglou and Tavlarides (Coualoglou and Tavlarides, 1976) have proposed models for drop breakage and coalescence rates in a stirred vessel. Binary breakage was assumed and daughter droplet distribution was assumed to be a normal distribution. Coalescence rate was considered as a product of collision efficiency and drop collision rates. Hsia and Tavlarides (Hsia and Tavlarides, 1980) predicted the drop size distributions of liquid-liquid dispersions in continuous-flow stirred tank using Monte Carlo method. Once again binary breakage was assumed. Model predictions were compared with experimental data of Coualoglou and Tavlarides and good agreement was observed. Sovova (Sovova, 1981) solved the population balance model for batch agitated liquid-liquid dispersions. They evaluated three different models for collision efficiency, the first model being the one proposed by Coualoglou and Tavlarides, the second model being the one premised on the work of Howarth (Howarth, 1964) (which postulated

that chances of coalescence of colliding drops depends on the impact of the collision itself rather than on the intervening film drainage while The third model was a combination of the two. Laso and co-workers ([Laso et al., 1987](#)) presented a simplified way of solving the population balance models by discretizing the equations in such a way that the characteristic volume of drops in any given class was twice the characteristic volume of the previous drop class. They further assumed that breakage was a first order process, coalescence a second order process, breakage resulted into two equally sized drops and coalescence was possible among equally sized drops. Alopaeous and co-workers ([Alopaeous et al., 2002](#)) reported that spatial variation of turbulent energy dissipation rates in a stirred tank should lead to a spatial variation in the drop size distribution which should be predicted by a computational model. For this, a multi block model comprising 11 compartments was proposed by the authors. These compartments differed in average values of energy dissipation rate and exchanged flow. The information of the average energy dissipation rates and exchange flow rates was obtained from single-phase CFD simulations with suitably averaged physical properties. The same group ([Alopaeous et al., 1999](#)) applied the multi block model to carryout parametric fitting for Exxsol in water dispersions in a 50 L batch stirred tank. Measurement of drop size distributions were carried out at three different locations in the tank. This model was based on the breakage model of Narsimhan and co-workers ([Narsimhan et al., 1979](#)) modified to account for viscous forces within the drop phase as quantified by Calabrese and co-workers ([Calabrese et al., 1986](#)). A recent study ([Gabler et al., 2006](#)) attempted to model drop-size distributions for the dispersion of toluene in water in a batch stirred tank. Combinations of breakage rate, coalescence rate, and daughter droplet distributions, as used by Coualoglou and Tavlarides and Alopaeus and co-workers ([Alopaeous et al., 1999](#)) were tried. .As can be seen that that quite a few of the above mentioned works have used the kernels originally proposed by Hsia and Tavlarides [Hsia and](#)

Tavlarides, 1980). Hence, in this work breakage, daughter droplet distribution and aggregation kernels proposed by Hsia and Tavlarides have been used directly. As mentioned above these constants have been arrived at using liquid-liquid dispersed turbulent flow in stirred tanks. Pulsed column also involves turbulent flow of liquid-liquid dispersion. Thus we expect that the kernels should hold good for PSPCs also. A detailed comparison of the different kernels proposed by different researcher is beyond the scope of this work.

Breakage kernel, coalescence kernel and daughter droplet distribution are given in Eqs. 5.7-5.9. These kernels have been chosen as they are widely used in modeling drop/bubble size distribution as explained earlier.

$$a(L) = C_1 \frac{\varepsilon^{1/3}}{(1+\phi)L^{2/3}} \exp \left\{ -C_2 \frac{\sigma(1+\phi)^2}{\rho_d \varepsilon^{2/3} L^{5/3}} \right\} \quad (5.7)$$

$$\beta(L, \lambda) = h(L, \lambda) \eta(L, \lambda) = \left[C_3 \frac{\varepsilon^{1/3}}{(1+\phi)} (L + \lambda)^2 \left(L^{2/3} + \lambda^{2/3} \right)^{1/2} \right] \exp \left\{ -C_4 \frac{\mu_c \rho_c \varepsilon}{\sigma^2 (1+\phi)^3} \left(\frac{L\lambda}{L+\lambda} \right)^4 \right\} \quad (5.8)$$

$$b(L, \lambda) = 30 \left(\frac{L^3}{\lambda^3} \right) \left(1 - \frac{L^3}{\lambda^3} \right) \quad (5.9)$$

Where, $h(L, \lambda)$ and $\eta(L, \lambda)$ are collision frequency and collision efficiency, respectively.

The population balance equations are solved using the method of classes. 10 bins are used to represent the range of droplet diameter. The smaller drops are sufficiently captured due to non-linear bin size used (there were four bins in the range of 0.0005 to 0.001 m while the remaining 6 bins were used to span over a range of 0.001-0.004 m). The range of drop sizes is considered to be from 0.5 mm to 4 mm. This choice of drop diameter range is based on the values of drop sizes typically observed in a pulsed column (Lorentz et al., 1990, Usman et al., 2009). As mentioned before, standard breakage and coalescence kernels with their respective constants are used.

Choice of two-phase turbulence model is of vital importance as turbulence not only affects the momentum conservation equations but also population balance equations.

Thus it has a significant effect on the results (Aubin et al., 2004; Amokrane et al., 2014b) of a two-phase CFD simulation. Thus capturing the turbulence variables is very important in prediction of two phase flow. Turbulence has been modeled using the mixture k- ϵ model. However, inherently a 2D model will not be able to predict the true scales of turbulence-inherently a 3D phenomenon-with a high degree of accuracy. A complete 3D model will be definitely better in this regard. However, using a 3D CFD model incorporating PBM is prohibitively expensive. A workable solution is achieved by lumping all the probable uncertainties of 2D model in one or two terms of the governing equations and optimising these terms to reduce the errors in its. This approach has been followed in several studies on two-phase CFD modeling and the drag model is the most often modified to bring predictions closer to the measured values (Rusche, 2002). A similar approach approach has been followed in this work.

The absolute average relative error between predicted hold up and reported hold up is analysed. The model constants in the drag model are subsequently modified to reduce the error between the experimental and predicted values of dispersed phase hold up. This approach essentially means that all the uncertainties due to the modeling turbulence using a 2D computational model are lumped into the values of the model constants of the drag model. Performance of the modified drag model is then verified by carrying out additional simulations.

5.2.3 Computational domain

The computational domain used in the present work is the same as was used in the experiments with the exception of number of plates considered in the computational domain. A reduced number of plates (5 plates) has been considered to limit the size of the computational domain and thus the computational time. Suitability of using 2D model and reduced number of plates for CFD modeling of PSPCs has been reported earlier in chapter 2,3 and 4. The computational domain in this chapter is slightly different from those reported in earlier chapters in that the pulse leg is located

centrally, and not from one side as is the case in earlier chapters, as per the experimental setup mentioned earlier. Unsteady state simulations are carried out. Time step is sufficiently small to ensure Courant number around 0.5. A typical computational domain is shown in Fig. 5.2. A grid density of 1.027×10^6 cells/m² is used. This grid density is found to be sufficient as reported in earlier chapter. The cell size used was sufficient to ensure a maximum Courant number around 0.5 for a time step of 0.01 sec (in transient simulations). The appropriateness of the grid density used is also reflected in the fact that the average value of wall Y^+ is 0.08 and 0.015 for continuous and dispersed phase respectively. The outlet of the light phase (organic phase) is at the top while the inlet is from the bottom. Outlet of the heavier phase (aqueous phase) is from the bottom and its inlet is at the top. The pulse is applied at the bottom as shown in Fig. 5.2.

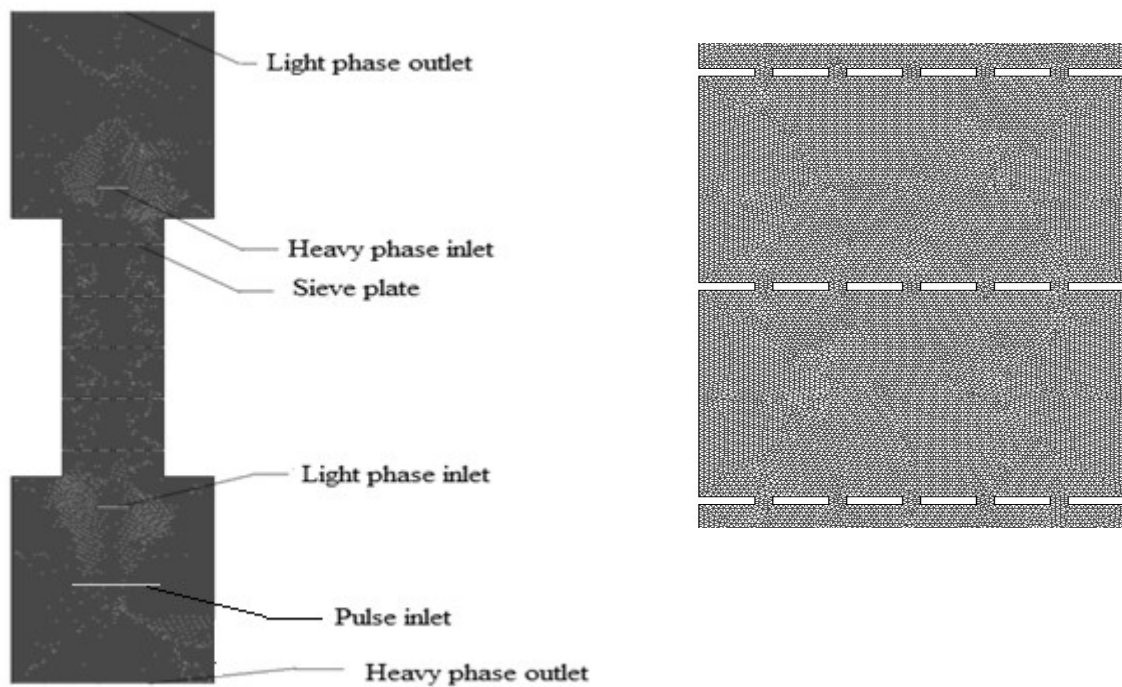


Figure 5.2: A typical computational domain used to model 3 inch PSC and the mesh in the vicinity of the plates

A sinusoidal pulsing velocity is implemented at the pulse inlet using an user defined function as per Eqn. 3.12.

5.3 RESULTS AND DISCUSSION

5.3.1 Experimental results

Extensive experiments are conducted to study the effects of different operating and geometrical parameters on hold up and Sauter mean drop diameter. [Table 5.1](#) lists the range of different operating and geometrical parameters used in the present work along with phases systems used.

Table 5.1: Range of operating and geometrical parameters

Parameter	Range
Pulsing velocity (A_f)	0.0167-0.0389 (m/sec)
Dispersed phase velocity (V_d)	0.0034-0.0122 (m/sec)
Continuous phase velocity (V_c)	0.003-0.0055 (m/sec)
Column diameter (D)	2 and 3 (inch)
Inter plate spacing (h)	0.05 and 0.10 (m)
Phase systems	Water, 30% TBP/dodecane and 3 N nitric acid, 30% TBP/dodecane

[Fig. 5.3](#) shows the effect of pulsing velocity on hold up for columns of different diameters (water, 30%TBP/Dodecane system). It is clearly seen that hold up increases with an increase in pulsing velocity. This is attributed to increased level of turbulence inside the column with an increase in pulsing velocity which in turn increases the rate of drop breakage leading to smaller drops. These smaller drops have more retention in the column causing hold up to increase with increase in pulsing velocity. Furthermore, an increase in pulsing velocity also increases the level of re-circulation in the

continuous phase between the plates. This also enhances the tendency of the dispersed phase drops to be retained in the column leading to higher hold up. Another interesting point is that hold up (for the same pulsing velocity is more in the smaller diameter column. This may be attributed to enhanced wall effect in smaller diameter column. In other words in a small diameter column the presence of wall restricts the free movement of the dispersed phase there by increasing the hold up slightly.

Fig. 5.4 shows effect of dispersed phase velocity on dispersed phase hold up for two different values of interplate spacing (water, 30%TBP/Dodecane system). It is seen that hold up increases with increase in dispersed phase velocity for both values of plate spacing. This is attributed to the fact that an increase in dispersed phase velocity leads to a larger relative presence of the dispersed phase causing higher hold up. Additionally it is observed that for all values of dispersed phase velocity hold up is more for interplate spacing of 50 mm. If interplate spacing is increased from 50 mm to 100 mm the level of turbulence in the column decreases which decreases hold up. As and when a pulse strikes the plates, flow is squeezed through the holes causing large shear gradients at the holes leading to extensive boundary layer separation and generation of eddies which in turn result in enhanced turbulence levels. Thus for a given height of the column lower the plate spacing more will be the instances of such boundary layer separation leading to higher number density of eddies which in turn increase the level of turbulence in the column thereby increasing hold up. In other words smaller plate spacing can be interpreted as enhanced resistance in the flow path of the dispersed phase. This causes enhanced retention of dispersed phase inside the column leading to enhancement in hold up.

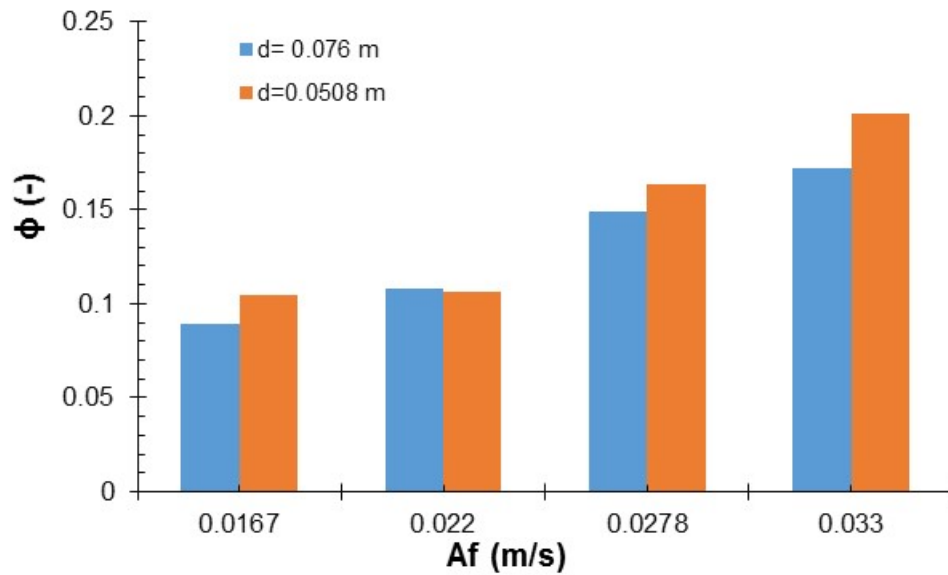


Figure 5.3: Effect of pulsing velocity on dispersed phase hold up in 2 and 3 inch diameter PSPC

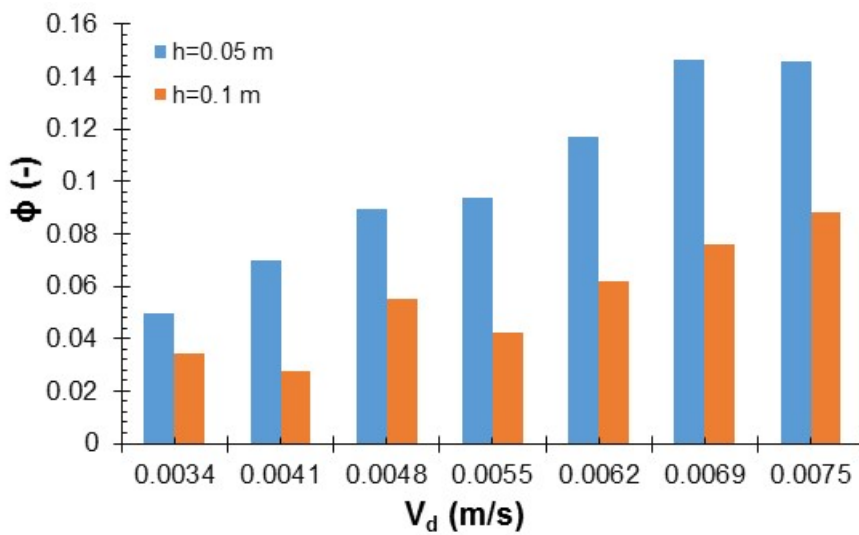


Figure 5.4: Effect of dispersed phase velocity on column hold up for two different values of interplate spacing.

Fig. 5.5 shows 3D plots illustrating the dependence of hold up on pulsing velocity and dispersed phase velocity for PSPC (3N nitric acid, 30%TBP/Dodecane system). Experiments are carried out in a 3 inch column with standard cartridge. These surface plots allow better visual interpretation of the nature of variation of hold up with the

operating parameters of the column. Hold up is clearly seen to increase with increase in A_f as well as column throughput (V_c+V_d).

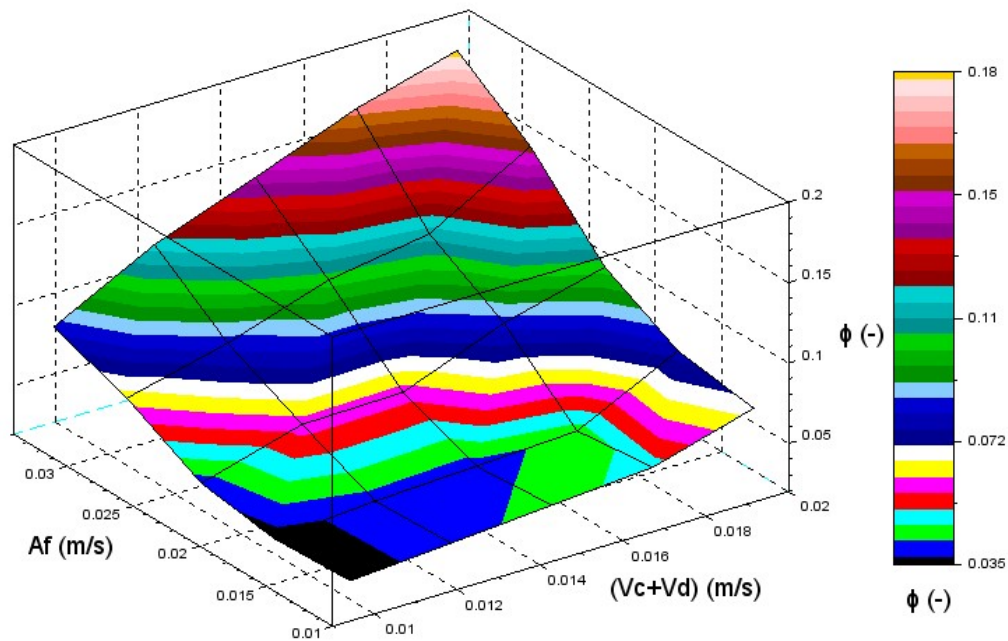


Figure 5.5: 3D plot of hold up with column throughput and pulsing velocity.

Fig. 5.6 shows the regime maps for PSPC. The demarcation of mixer-settler, dispersion and quasi emulsion regime has been shown in the regime maps. The transition lines have also been marked. The typical trend that emerges from the above plots is that the mixer-settler regime is dominant at lower values of pulsing velocity and higher values of (V_c+V_d) . The transition to quasi emulsion regime typically occurs at higher values of pulsing velocity. As seen from Fig. 5.6, in PSPC the span of the dispersion regime reduces as total throughput increases. These findings are also similar to earlier findings which reported a gradual transition from mixer settler to dispersion regime on increase of pulsing velocity which eventually changed to quasi emulsion/emulsion state on further increase in pulsing velocity.

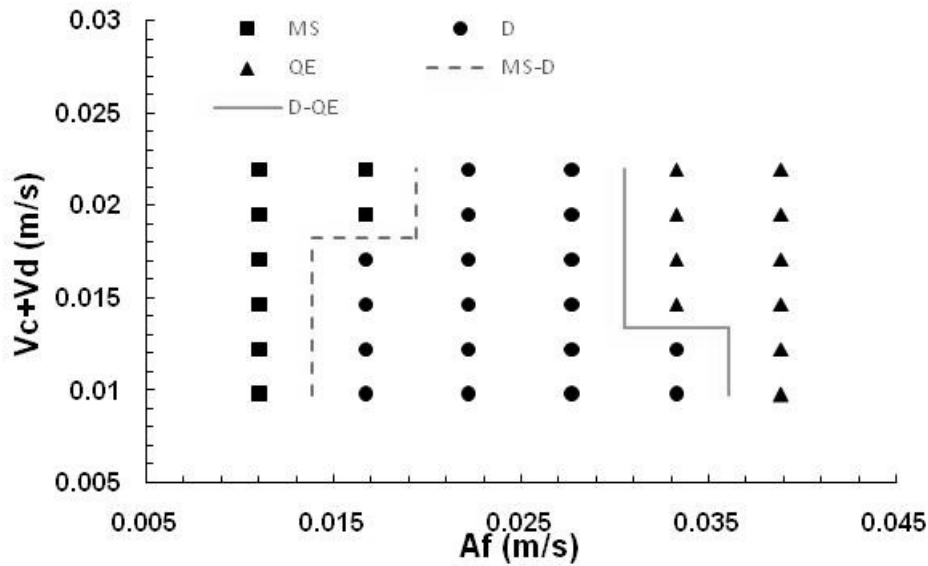


Figure 5.6: Flow regime map for PSPC (MS: mixer-settler regime; D: dispersion regime; QE: quasi-emulsion regime)

Several correlations have been proposed to predict dispersed phase hold up in PSPC. Kumar and Hartland (Kumar and Hartland, 1994) proposed empirical correlations for hold up with the physical properties of the liquid–liquid systems, column geometry and operating conditions as the independent variables. Venkatnarsaiah and Verma (Venkatnarsaiah et al., 1998) measured dispersed phase hold up for water–kerosene system with n-butyric acid and benzoic acid as solute. The data showed a profound influence of the hole diameter and free area of the plates and plate spacing on the dispersed phase hold up. They formulated a correlation for evaluation of column hold up. Tung and co-workers (Tung and Luecke, 1986) and Miyauchi and Oya (Miyauchi and Oya, 1965) also proposed correlations for estimating dispersed phase hold up in PSPCs. The above-mentioned correlations for predicting dispersed phase hold up were evaluated with our experimental data of hold up in PSPC for the entire range of different parameters studied.

Fig. 5.7 shows the comparison of hold up measured in our experiments with the hold up obtained from various reported correlations. It is seen that out of four correlations for predicting hold up in PSPC evaluated in this work, correlation due to Miyauchi

and Oya (Miyachi and Oya, 1965) is found to be the most effective. Absolute average relative error in prediction of the correlation is 18.8%. The correlation due to Kumar and Hartland is observed to give significant deviation as it over-predicts hold up.

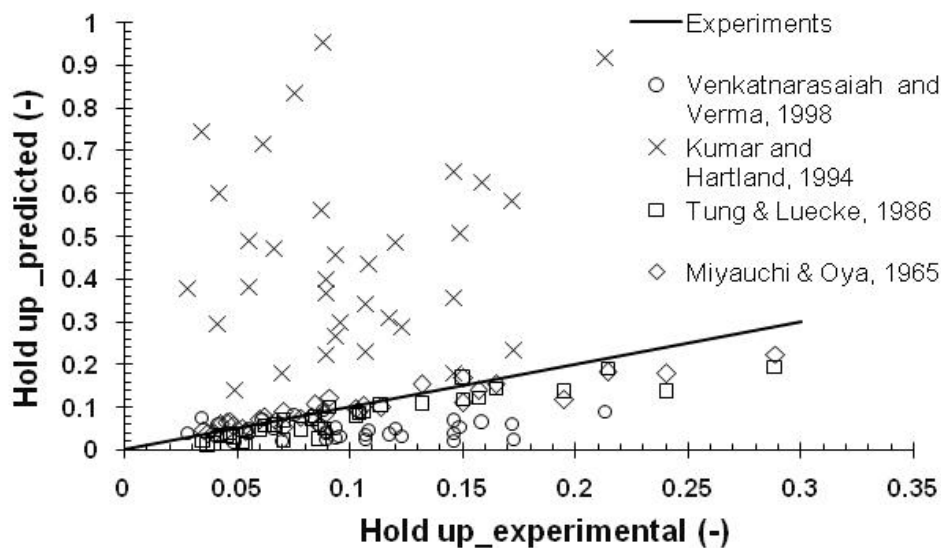


Figure 5.7: Parity plot showing the comparison of dispersed phase hold up values for PSPC predicted by various correlations with experimentally measured hold up values

Similar to the data generated for column hold up extensive data was generated for Sauter mean drop diameter in PSPC. Effect of different geometrical parameters (interplate spacing and column diameter) has also been studied. A liquid-liquid dispersion comprises of droplets of different sizes. The drop size distribution in a liquid-liquid dispersion varies with space as well as time. Drop size distribution in a pulsed column may depend on the operating conditions like dispersed phase, continuous phase and pulsing velocities as well as the geometrical parameters and phase system involved. A representative image of the dispersion and corresponding drop size distribution is given in Fig. 5.8.

Fig. 5.9 shows the effect of pulsing velocity on drop diameter. A reduction in Sauter mean drop diameter with increase in pulsing velocity is clearly observed. Increase in

As Af increases the turbulence dissipation rates inside the column which enhances the rate of drop breakage leading to smaller drops.

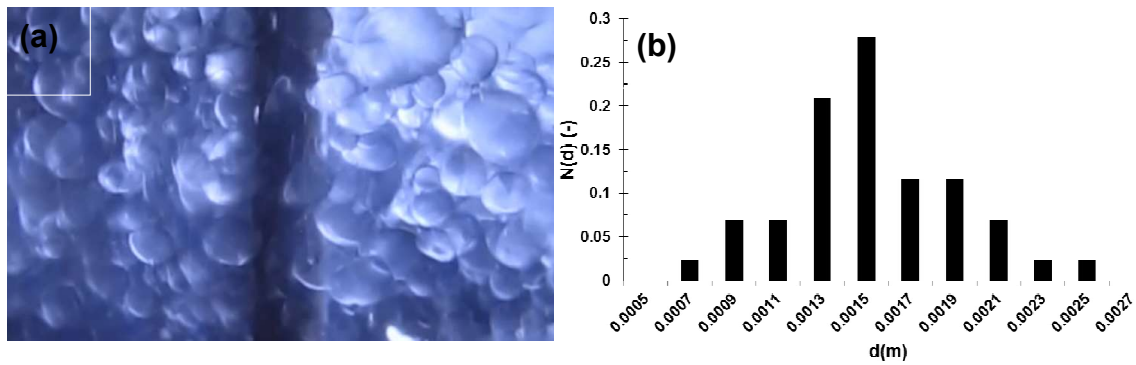


Figure 5.8: (a) A representative image of liquid-liquid dispersion in pulsed column used for the evaluation of droplet distribution and (b) corresponding drop size distribution

Three dimensional plots showing the effects of pulsing velocity and total throughput on Sauter mean drop diameter is given in Fig. 5.10. It is noted that Sauter mean drop diameter increases marginally with an increase in throughput and reduces significantly with an increase in pulsing velocity. Increase in Sauter mean diameter with an increase in throughput can be attributed to increase in dispersed phase hold up which leads to more coalescence and larger drops.

Several correlations for estimating Sauter mean drop diameter in PSPC have been reported. These correlations are based on regression analysis of the experimental data. These correlations are evaluated for their efficacy to predict the Sauter mean drop diameter for our experimental data. Kumar and Hartland (Kumar and Hartland, 1986) proposed a correlation to predict Sauter mean drop diameter based on the regression of various reported experimental data using dimensional analysis. The correlation is given by Eq. (5.10)

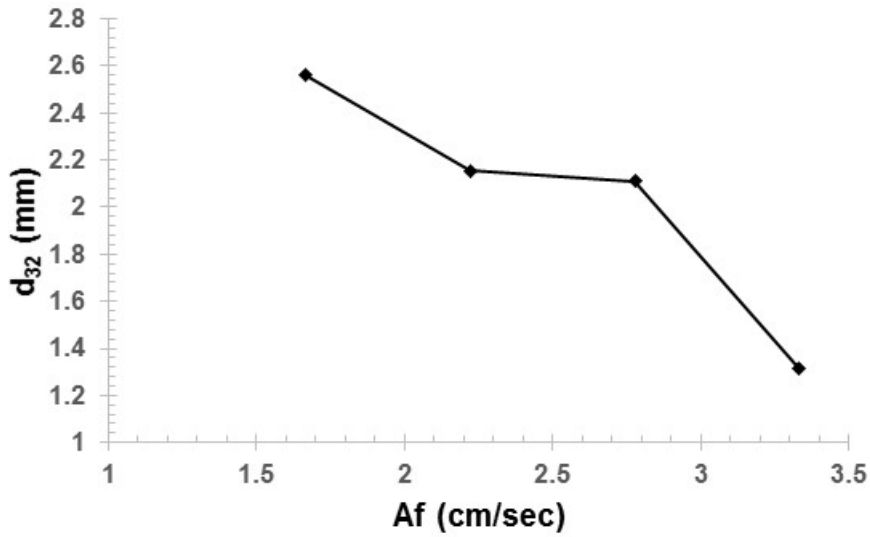


Figure 5.9: Effect of pulsing velocity on drop diameter in 3 inch PSPC.

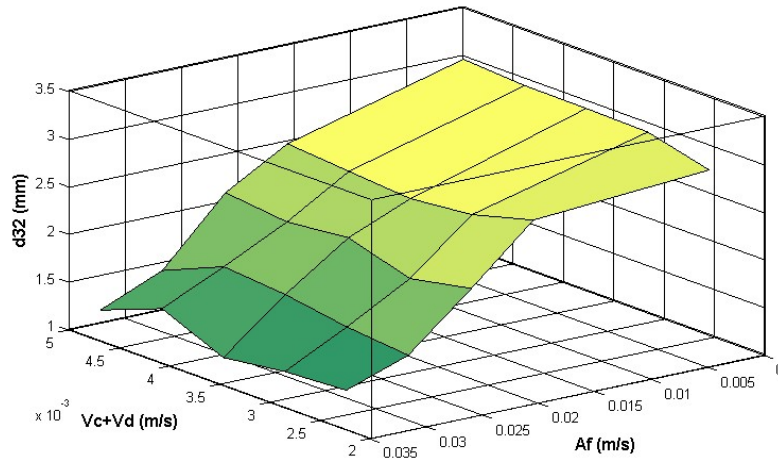


Figure 5.10: Variation of Sauter mean diameter with throughput and pulsing velocity in PSPC

$$\frac{d_{32}}{\sqrt{\frac{\sigma}{\Delta\rho g}}} = 1.35e^{0.4} \left(\frac{h_p}{\sqrt{\frac{\sigma_*}{g\rho_*}}} \right)^{0.18} \left(\frac{\mu_d g^{0.25}}{\rho_*^{0.25} \sigma_*^{0.75}} \right)^{0.14} \left(\frac{\sigma}{\sigma_*} \right)^{0.06} \left[0.23 + \exp \left(-29.66 \frac{Af^2}{ge} \right) \right] \quad (5.10)$$

This correlation takes into account the effects of physical properties like dispersed phase viscosity, interfacial tension and density difference between continuous and dispersed phase. It also accounts for the effects of geometric parameter like plate spacing, fractional open area. Among the operating parameters effects of pulsing amplitude and pulsing frequency are taken into account. This correlation, however,

does not consider the effects of dispersed and continuous phase velocities, column diameter and sieve plate hole diameter. Fig. 5.11a shows comparison of experimentally obtained Sauter mean drop diameter with the Sauter mean diameter estimated by Eq. 5.10. It is observed that the correlation proposed by Kumar and Hartland given by Eq. 5.10 under predicts drop size. Predictions are found to deviate from experimental values significantly for low pulsing velocities. Absolute average relative error of the prediction is about 33%. Another correlation is proposed (Gonda and Matsuda, 1986) for aqueous continuous phase for PUREX process. The correlation is given by Eq. (5.11).

$$d_{32} = (0.055 + 4.4 \times 10^7 v_a^{3.33}) d_n^{0.7} h_p^{0.4} (Af)^{-0.313} \quad (5.11)$$

This correlation takes into account the effects of dispersed phase velocity, hole diameter, plate spacing and pulsing velocity. This correlation does not account for the effect of physical properties. This correlation also does not account for the effect of fractional open area, column diameter and continuous phase velocity. Fig. 5.11b shows comparison of our experimentally obtained Sauter mean drop diameter with Sauter mean drop diameters evaluated by Eq. (5.11). It is observed that the correlation given by Eq. (5.11) over predicts the drop diameter. The predictions of the correlation are found to be good for high pulsing velocity i.e. in quasi-emulsion region. Absolute average relative error in the prediction of this correlation is found to be about 47%. Another correlation reported by Kagan and co-workers (Kagan et al., 1965) for the prediction Sauter mean drop diameter in pulsed sieve plate column is given by Eq. (5.12).

$$d_{32} = 0.92 \frac{(Af)^{-0.3} \sigma^{0.5} \mu_c^{0.1}}{\rho_c^{0.6} g^{0.4}} \quad (5.12)$$

This correlation considers various physical properties like interfacial tension, continuous phase density and viscosity. Among the operating parameters the correlation only takes into account pulsing velocity. Other geometrical parameters like hole diameter, plate spacing are not accounted for. Absolute average relative error

in the prediction of Sauter mean drop diameter from this correlation is found to be about 50%. Fig. 5.11c shows comparison of experimental Sauter mean drop diameter with Sauter mean diameters predicted by the correlation of Eq. (5.12). Sreenivasulu and co-worker (Sreenivasulu et al., 1997) have given yet another correlation for the prediction of Sauter mean drop diameter in PSPCs (Eq. 5.13).

$$d_{32} = C \left(\frac{\sigma}{\rho_c} \right) e^{0.48} d_n^{0.26} h_p^{0.34} (Af)^{-0.8} \quad (5.13)$$

This correlation accounts for the effect of physical properties like interfacial tension, continuous phase density on Sauter mean diameter. Geometrical parameters like plate spacing, fractional open area and hole diameter are input parameters in this correlation. Among the operating parameters this correlation takes account of pulsing velocity only. C is a constant which is 0.08 for the case of no mass transfer and 0.1 for the case of mass transfer from dispersed to continuous. Absolute average relative error in prediction of drop size by this correlation is found to be about 64%. Fig. 5.11d shows comparison of experimentally measured Sauter mean drop diameter with the drop diameter predicted by the correlation of Eq. (5.13).

Thus none of the correlations is found to be satisfactory in predicting Sauter mean drop diameter measured in our experiments. Since correlation of Eq. (5.13) accounts for all geometric parameters and the most important operating parameter i.e. pulsing velocity, it is modified to suit to our experimental data. The optimum value of C for our experimental data is found to be 0.11. Absolute average relative error in prediction of Sauter mean drop diameter by the modified correlation is 8.9%. Fig. 5.11e shows comparison of experimentally measured Sauter mean drop diameter with Sauter mean diameter estimated by the modified correlation. Absolute average relative error in prediction of Sauter mean drop diameter by the modified correlation and the previously reported correlations are summarized in Table 5.2.

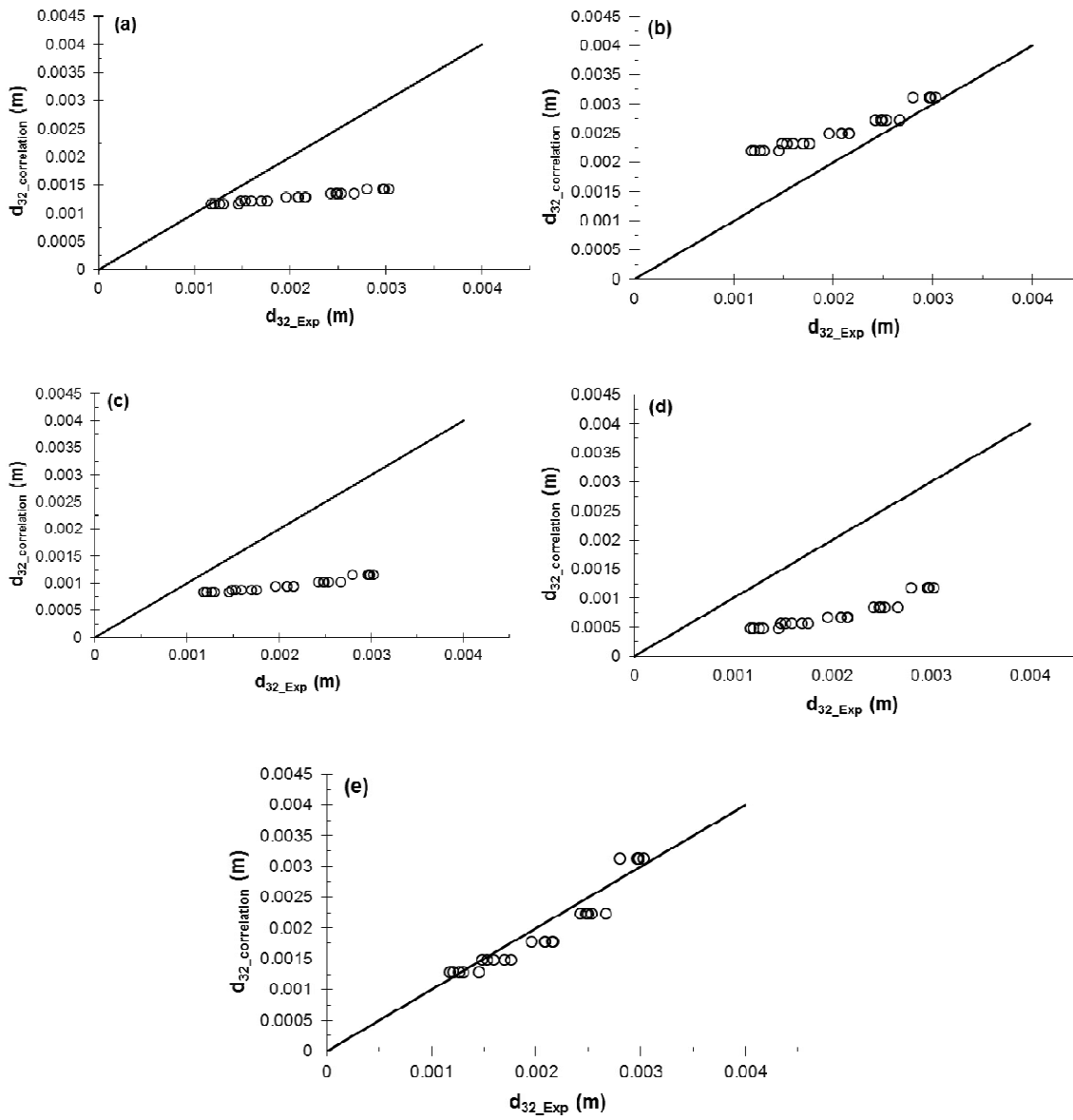


Figure 5.11: Comparison of experimentally measured Sauter mean drop diameter in PSPC with the Sauter mean drop diameter estimated by (a) the correlation of [Kumar & Hartland, 1986](#) (b) the correlation of [Gonda & Matsuda, 1986](#) (c) correlation of [Kagan, et al., 1965](#) (d) correlation of [Sreenivasulu, et al., 1997](#) and (e) the modified correlation proposed in this study

Table 5.2: Absolute average relative error in prediction of Sauter mean drop diameter in PSPC by different correlations

Reference	Absolute average relative error (%)
Kumar & Hartland, 1986	33.29
Gonda & Matsuda, 1986	47.3
Kagan, et al., 1965	50.58
Sreenivasulu, et al., 1997	63.8
Present work	8.9

5.3.2 Development of CFD-PBE numerical model of PSPC

The 2D CFD-PBE model using standard Schiller-Naumann drag model and standard breakage and coalescence kernels is successfully implemented.

One important factor that can affect the final drop size distribution in the active section of the column is the initial drop size distribution. In this regard preliminary simulations were carried out with various combinations of initial drop size distribution (in the range of 0.0005-0.004 m). However the Sauter mean drop diameter obtained from these simulations did not vary to any significant extent. The variation (between the maximum and minimum value of Sauter mean drop diameter obtained) was 4.22%. It is also important to note here that there was no effect (of initial drop size distribution) on column hold up at all. The weak influence of initial drop size distribution can be related to the high level of turbulence inside the column.

Some preliminary simulations were carried out to study effect of number of bins (5, 10 and 15) on the results (predicted dispersed phase hold up and Sauter mean drop diameter). Results indicate that as we keep on increasing the number of bins, there is a slight reduction in dispersed phase hold up where as the Sauter mean drop diameter increases. Sauter mean drop diameter increased by 27% as number of bins was increased from 5 to 10 where as it increased by 14.8% as number of bins was

increased further from 10 to 15. Corresponding effect on dispersed phase hold up was about 0.5%. However, computational time increases significantly as the number of bins is increased. Hence, keeping in view the large increase in computational time for number of bins more than 10 as well as the fact the corresponding change in hold up is less than 1%, the number of bins was fixed at 10. An increase in Sauter mean drop size with bin size may be attributed to the fact that with increase in bin size even a very small number of drop belonging to bin sizes representing large drop diameters will have a significant effect on the overall volume as volume scale to the third power of size. This may lead to a situation where the overall Sauter mean drop size increases with increase in bin size.

Fig. 5.12 shows comparison of the predicted and experimental results of variation of hold up with pulsing velocity for a 3 inch PSPC. Values of dispersed and continuous phase velocities are 0.0048 m/sec and 0.0042 m/sec respectively. Hold up (as well as Sauter mean drop diameter) has been evaluated in the section of the column between the 4th and the 5th plates. Due to the inherent time periodic nature of the flow, an arithmetic average of hold up for one complete cycle is done to evaluate reported hold up. Fig.5.12 shows that the model is able to predict the trend of variation of hold up with pulsing velocity i.e. the hold up increases with increase in pulsing velocity. Fig. 5.13 shows the comparison of predicted variation of Sauter mean drop diameter with pulsing velocity against experimental values. It is seen that the CFD-PBE model is able to predict the general trend of Sauter mean drop diameter with pulsing velocity i.e. drop size reduces with increase in pulsing velocity. However, absolute average relative error in prediction of Sauter mean drop diameter is about 33%

It is observed that even though the general trend is being captured by the numerical model, error between the hold up predicted by the numerical model and those obtained experimentally is significant. Absolute average relative error in prediction of

hold up was 18.4 %. The error is more at higher values of pulsing velocities. In the present work a 2D computational domain is used to keep computational time within reasonable limits. However turbulence being inherently a 3D phenomena cannot be captured using a 2D approach with a very high degree of accuracy. The fact that the predictions are worse at high values of pulsing velocity and thus at higher levels of turbulence also supports this view. A 3D CFD-PBE model embedding Schiller-Naumann drag model is expected to give better predictions. However, 3D model would be computationally very expensive. Another important factor is that the drag law (due to Schiller-Naumann) considered in this work is based on the assumption of a drop settling in an infinite media. The theoretical formulation does not consider a pulsatile flow. Infact non one of drag laws listed earlier in chapter 3 (theoretical as well as purely empirical) has been proposed for pulsatile flow. Thus using Eqn, (5.1) in its original form to predict hydrodynamics in a pulsed column itself may lead to some uncertainties. Thus we adopted a method where in all such uncertainties (associated with the prediction of turbulence as well as use of a drag law derived for non pulsatile flow) is clubbed in the constant of the drag model.

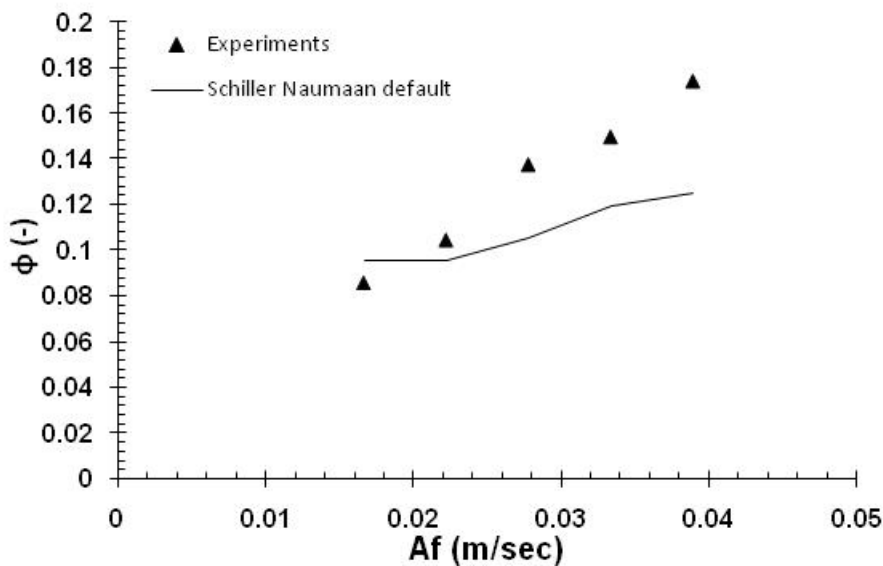


Figure 5.12: Comparison of predicted values of hold up against experimental values for 3 inch PSPC

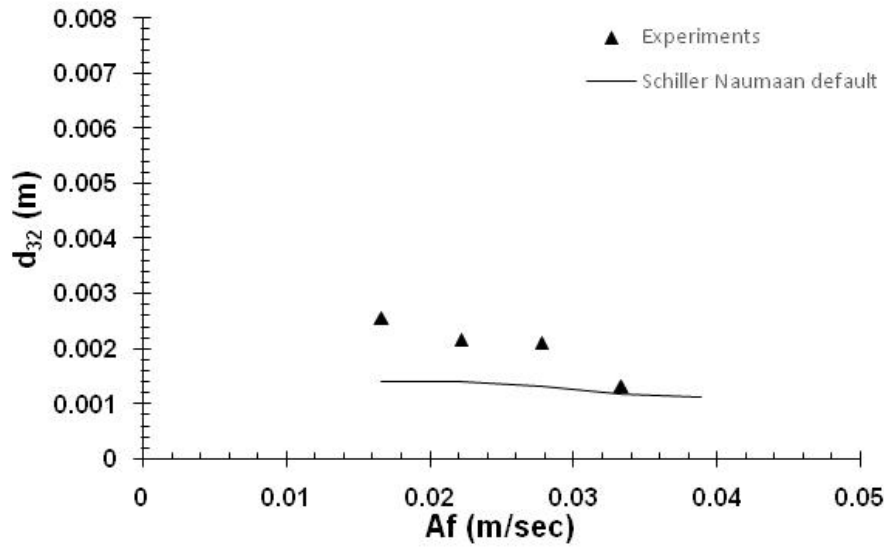


Figure 5.13: Comparison of predicted values of Sauter mena drop diameter against experimental values for 3 inch PSPC

The drag law due to Schiller and Naumann has the following general form

$$C_D = \frac{24}{\text{Re}} (1 + K \phi^{0.67}) \quad (5.14)$$

The value of K as reported by Schiller and Naumann is 0.15. However as seen in the previous section, the CFD-PBE model under predicts hold up at high levels of pulsing velocity. Thus the parameter K is modified to reduce the absolute average relative error in prediction of hold up. [Table 5.3](#) below lists the optimum values of K for different values of pulsing velocity.

Table 5.3: Optimized values of parameter K for different levels of pulsing velocity

Af (m/sec)	K
0.0167	0.05
0.0222	0.05
0.0278	0.125
0.0333	0.15
0.0389	0.2

For values of A_f other than listed in Table 5.3, optimum value of K is obtained by linear interpolation. Fig. 5.14 shows the CFD-PBE prediction of column hold up with pulsing velocity incorporating the optimized drag model. The predicted values are seen to be reasonably close to the experimental values across the entire range of pulsing velocities studied. The predictions with the optimized drag model are better than those obtained with standard Schiller-Naumann drag model.

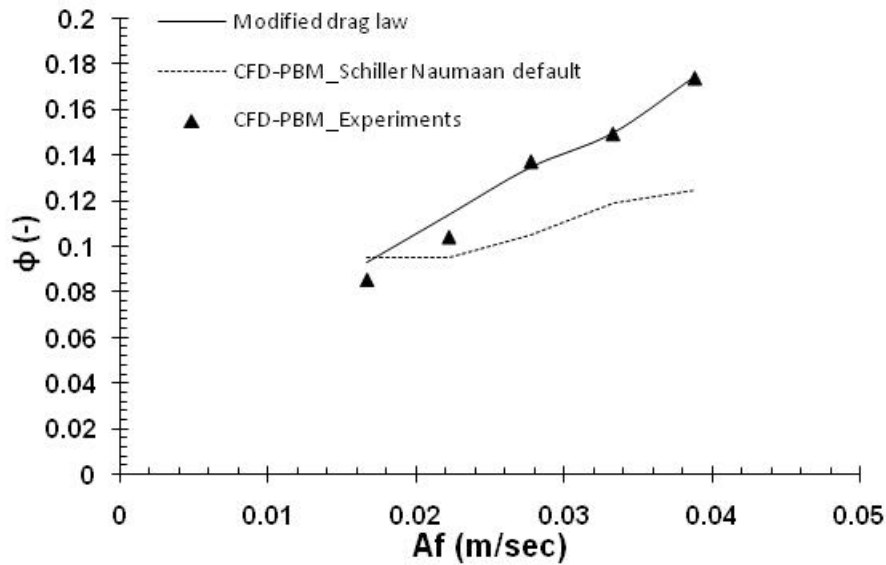


Figure 5.14: CFD-PBE predictions using optimized drag law.

The absolute average relative error was reduced from 18.4 % to 4.2 % by incorporating the modified drag model. The model embedding the modified drag model was tested against a set of fresh data representing variation of hold up with dispersed phase velocity. Fig. 5.15 shows the CFD-PBE predictions against experimental value of hold up for a 3 inch column for different values of dispersed phase velocity and continuous phase velocity. A good match between the experimental data and those predicted from the CFD-PBE model is observed. The absolute average relative error in prediction of hold up is 10.9 %.

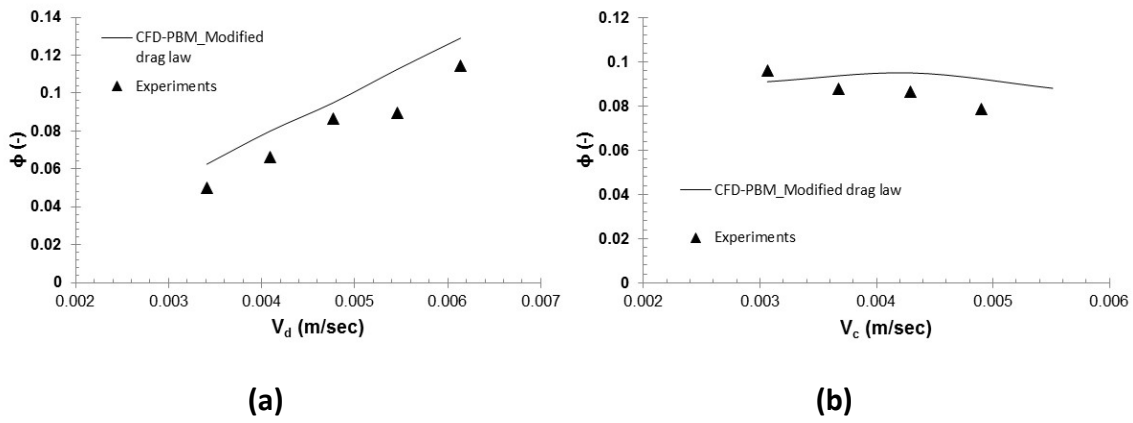


Figure 5.15: Comparison of CFD-PBE predicted hold up against experimental hold up for a) different values of dispersed phase velocity ($A_f = 0.022$ m/sec; $V_c = 0.0042$ m/sec) and b) different values of continuous phase velocity ($A_f = 0.0222$ m/sec; $V_d = 0.0048$ m/sec).

Similarly absolute average relative error in prediction of Sauter mean drop diameter using CFD-PBE code incorporating modified drag model is 20.4%. Fig. 5.16 below shows the predicted variation of Sauter mean drop diameter with continuous phase velocity and its comparison with the experimental data.

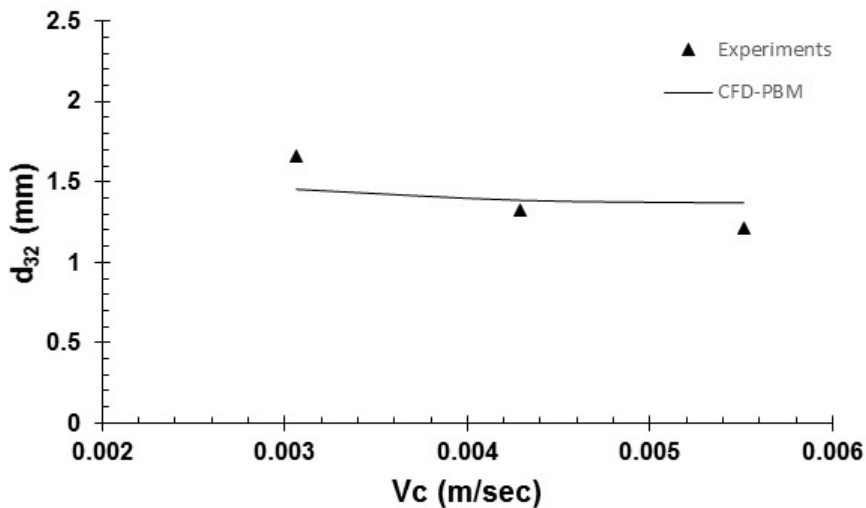


Figure 5.16: Comparison of CFD-PBE predicted and experimental variation of Sauter mean drop diameter with continuous phase velocity ($A_f = 0.0222$ m/sec; $V_d = 0.0048$ m/sec)

The validated model incorporating the modified form of drag model was then used to understand the local hydrodynamics in the column. Fig. 5.17 below shows spatial variations of dispersed phase hold up, dispersed phase drop diameter, Y component of continuous phase velocity, turbulence dissipation rates, breakage, and coalescence rates in a typical interplate section in the 3 inch column. As pulsatile flow is inherently unsteady results at the positive and negative peak of the pulse are compared.

During the positive peak of the pulse the dispersed phase is clearly seen to be ejected through the holes. Accumulation of the dispersed phase below the plate at the peak of the pulse is also minimum as most of the dispersed phase is being ejected out. Accumulation of dispersed phase below the plates, however, is significant during the negative peak of the pulse. Additionally, no dispersed phase is seen to move upward through the holes during the negative peak of the pulse.

Spatial variation of dispersed phase drop diameter shows drop diameter to be smaller close to the sieve holes of the lower plate while the drop diameter increases as the dispersion reaches bottom of the next plate due to high coalescence rates just below the plate. During the positive peak of the pulse size of the drops just below the top plate are smaller than during the negative peak of the pulse. This is attributed to higher breakage rates during the positive peak of the pulse as the columns contents are forcibly pushed through the holes at this instant.

Spatial variation of Y component of continuous phase velocity clearly reveals upward direction of flow of the continuous phase during the positive peak of the pulse and downward flow of the continuous phase during negative peak of the pulse. The downward velocity is also seen to be more near the sieve holes signifying that the continuous phase is issuing out downwards from the holes during negative pulse peak.

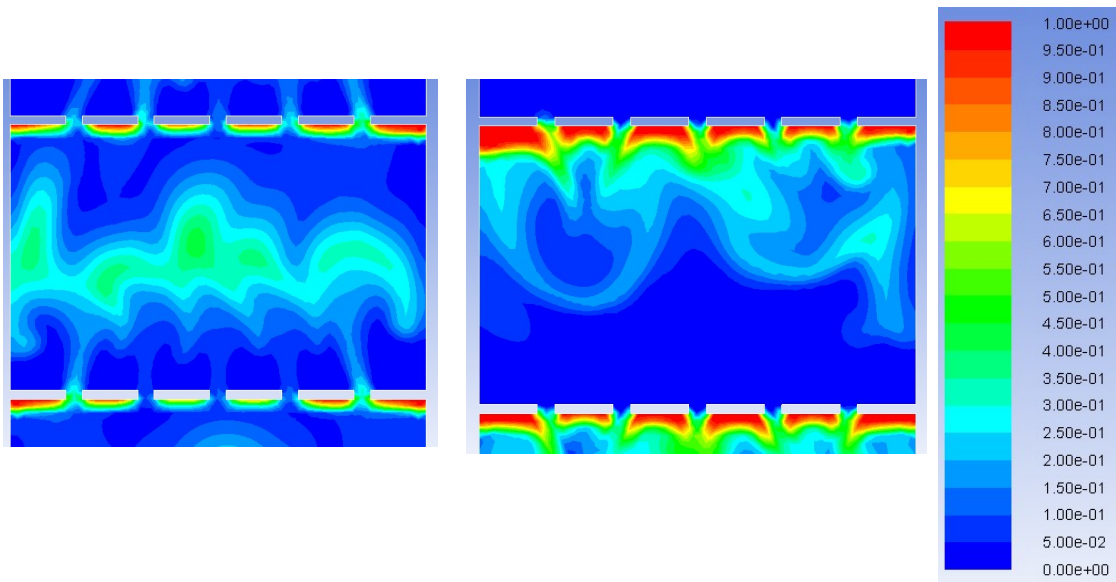
Spatial variation of turbulence dissipation rate shows maximum dissipation of turbulence at the location of the sieve holes which is expected as shear rates are

expected to be higher at the holes through which the flow issues out. On comparing the snapshots at positive and negative peak of pulse, it can be seen that dissipation rates are higher during the positive peak. Spatial variation of dissipation rates also indicate upward flow issuing out of the holes during positive peak and downward flow during negative peak.

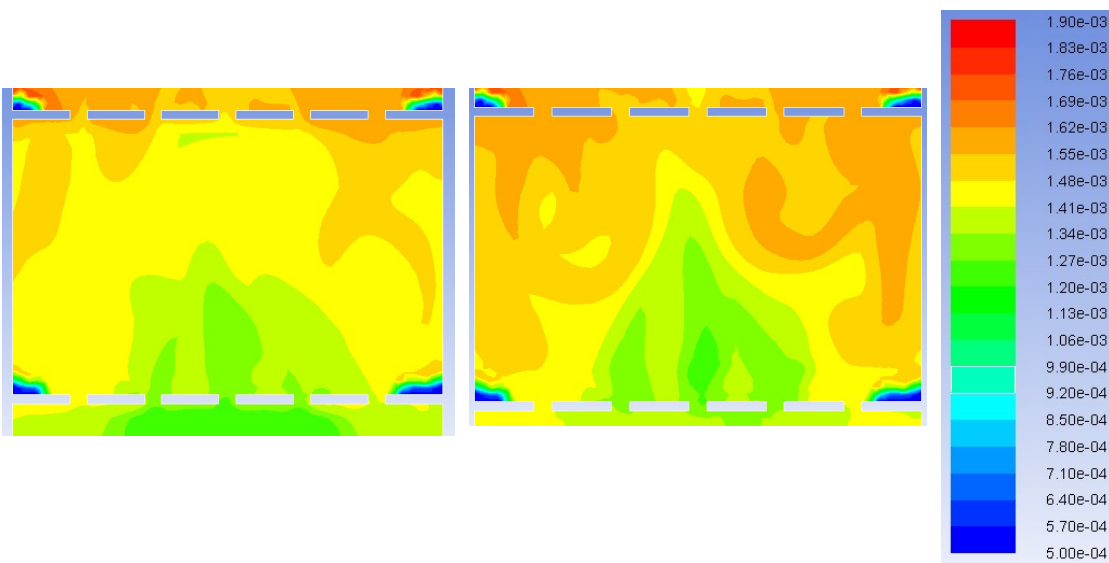
Fig. 5.18 shows the velocity vectors of dispersed and continuous phase both at positive and negative peak of the pulse. The velocity vectors through the holes indicate that the continuous phase is pushed up during positive peak of the pulse while it is pulled down during the negative peak. However the downward movement of the continuous phase is more prominent. Similarly dispersed phase is pushed up through the sieve holes during the positive pulse peak. Significant re-circulation (multiple interacting re-circulation loops) are observed in both phase. One interesting observation is that re-circulations are more prominent in the continuous phase than in the dispersed phase.

5.3.3 Extensive validation of the developed CFD-PBE model.

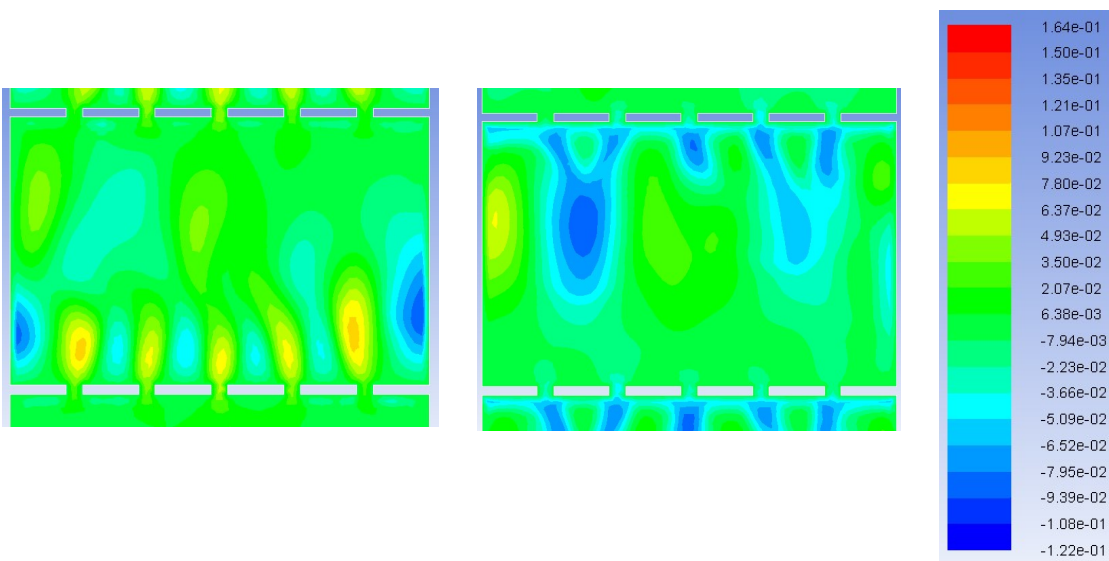
The CFD-PBE model described in the previous sections was tested for its efficacy to predict hold up and drop diameter in a PSPC incorporating different geometrical parameters. The model was validated against experimental data of hold up and Sauter mean drop diameter for two different column diameters and two different interplate spacing. Fig. 5.19 shows comparison of predicted and experimental variation of hold up with dispersed phase velocity and pulsing velocity for a 2 inch column. Absolute average relative error between prediction and experimental results is found to be about 16%.



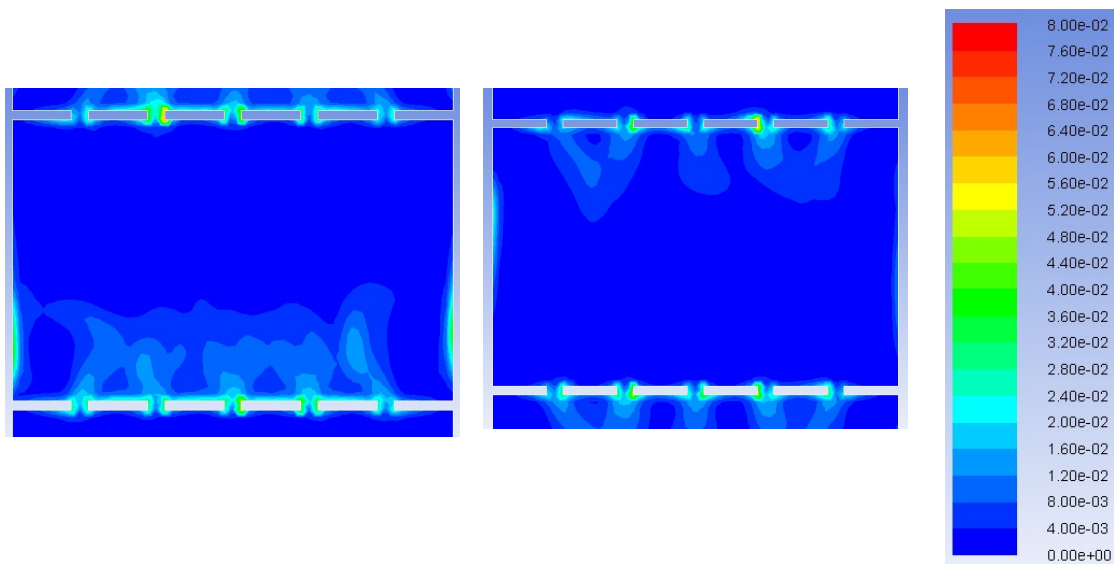
(Dispersed phase hold up)



(Dispersed phase drop diameter, m)



(Y component of continuous phase velocity, m/sec)



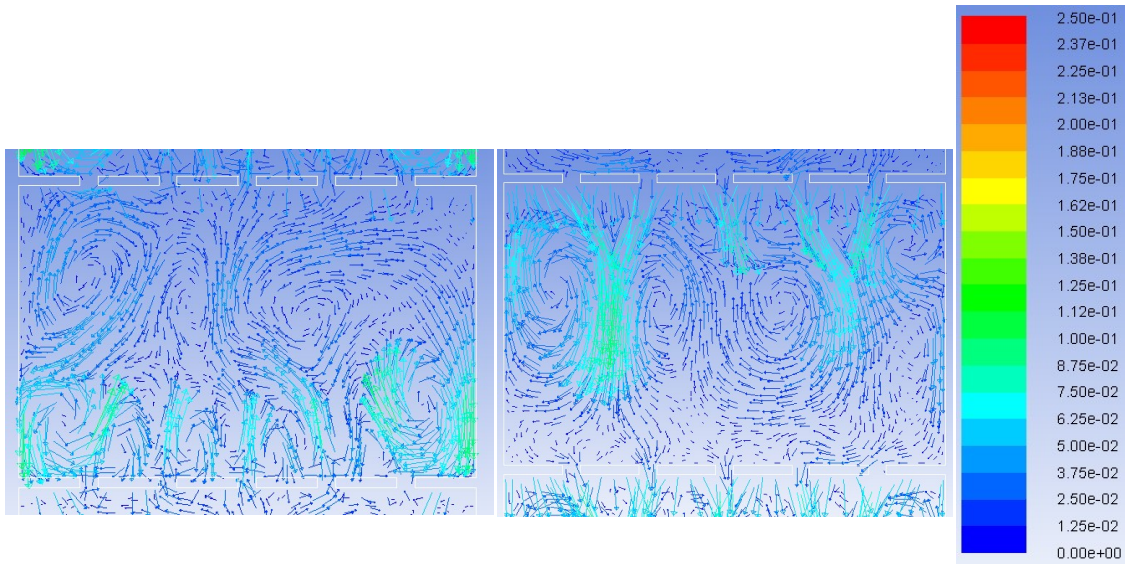
(Turbulence dissipation rates, m^2/sec^3)

Positive peak

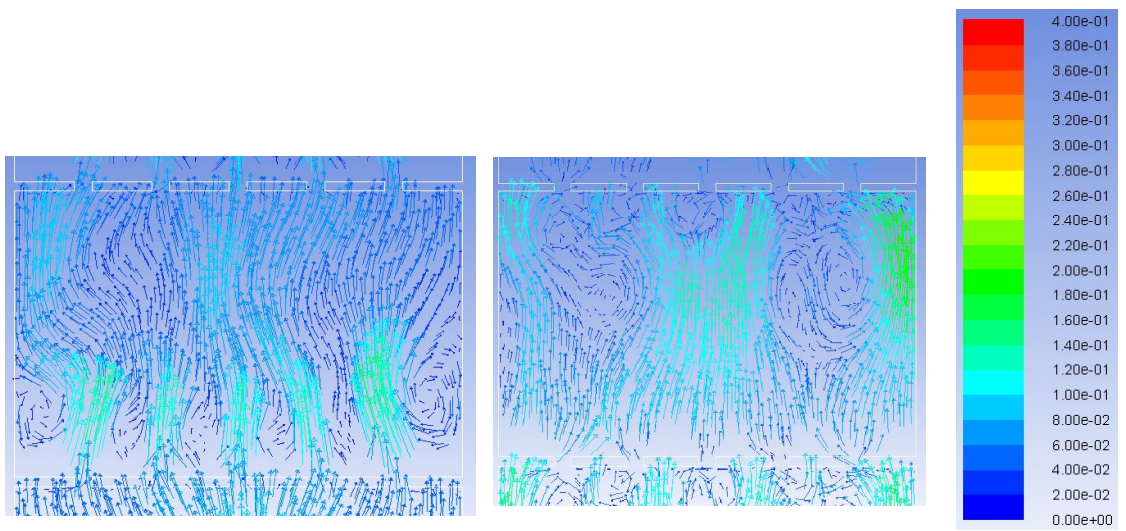
Negative peak

Figure 5.17: Contour plot of a) dispersed phase hold up b) dispersed phase drop diameter c) Y component of continuous phase velocity and d) turbulence dissipation rates during positive and negative peak of pulsing cycle ($A_f = 0.0222$ m/sec; $V_c = 0.0042$ m/sec; $V_d = 0.0048$ m/sec).

Fig. 5.20 shows comparison of predicted and experimentally observed variation of Sauter mean drop diameter with dispersed phase velocity for a 2 inch column. Absolute average relative error between prediction and experimental results was found to be about 13%. CFD-PBE simulations are further carried in a 3 inch PSPC with an interplate spacing of 10 mm and the predicted results on column hold up and Sauter mean drop diameter were compared against experimental data. Fig. 5.21 shows of the comparison of predicted and measured hold up with variation of pulsing velocity.



(Continuous phase velocity vector plot, m/sec)



(Dispersed phase velocity vector plot, m/sec)

Positive peak

Negative peak

Figure 5.18: Vector plots of continuous and dispersed phase velocity during positive and negative peak of the pulsing cycle ($Af = 0.0222$ m/sec; $V_c = 0.0042$ m/sec; $V_d = 0.0048$ m/sec).

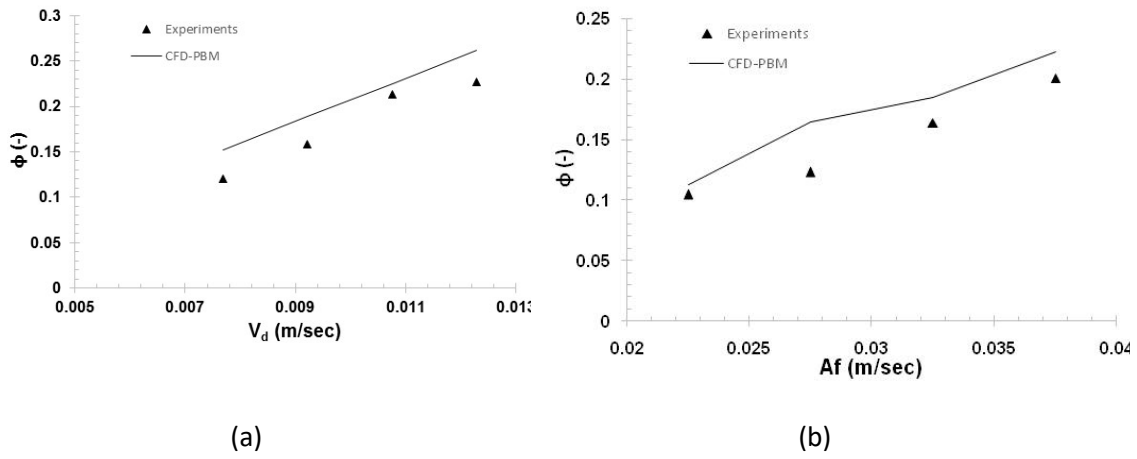


Figure 5.19: Comparison of CFD-PBE predicted hold up against experimental hold up in 2 inch PSPC for a) different values of dispersed phase velocity and b) different values of pulsing velocity.

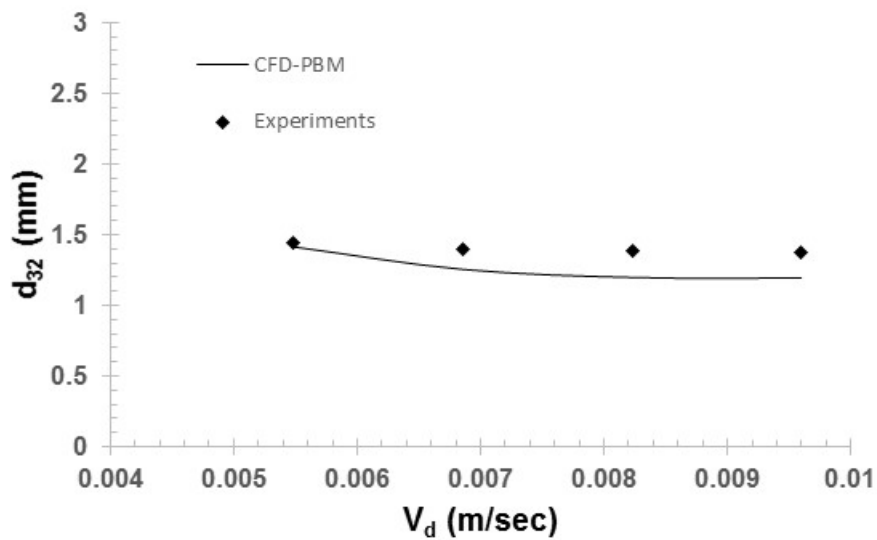


Figure 5.20: Comparison of CFD-PBE predicted Sauter mean drop diameter against experimental result in 2 inch PSPC

The predicted values are observed to be reasonably close to the experimental values. The model is also able to capture the experimental trend. The absolute average relative error between predicted and experimental hold up is about 22%.

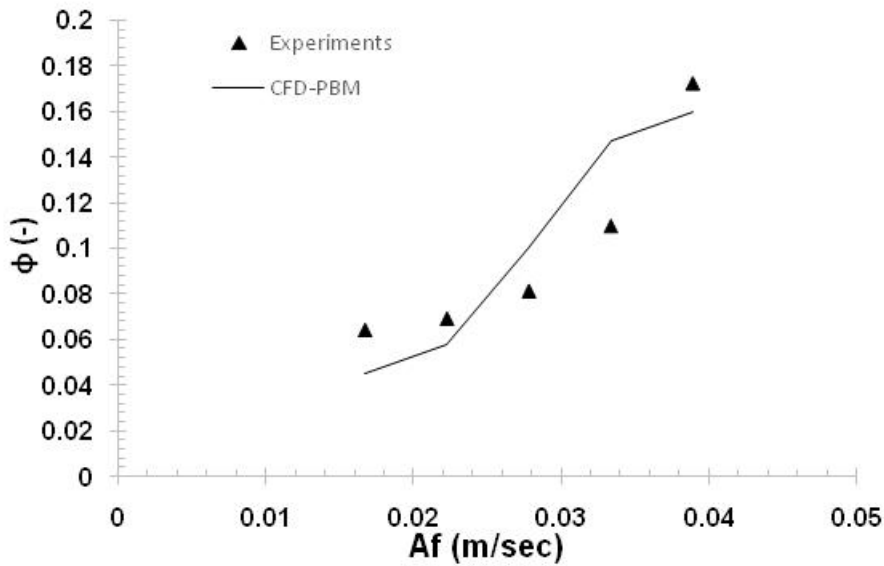


Figure 5.21: Comparison of CFD-PBE predicted hold up against experimental hold up for 3 inch diameter PSPC having interplate spacing of 10 cm ($V_c = 0.0042$ m/sec; $V_d = 0.0048$ m/sec).

Fig. 5.22 shows variation of Sauter mean drop diameter with pulsing velocity for PSPC with interplate spacing of 10 cm. Once again the drop diameters predicted by the CFD-PBE model are found to be in good agreement with experimental value with absolute average relative error being about 11.23%.

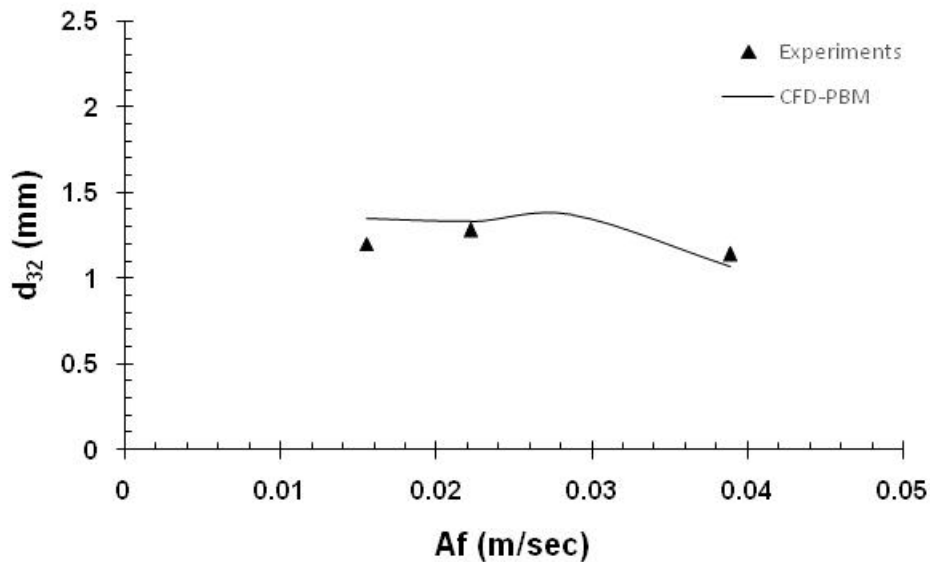


Figure 5.22: Comparison of CFD-PBE predicted Sauter mean drop diameter against experimental values for a 3 inch diameter PSPC having interplate spacing of 10 cm ($V_c = 0.0042$ m/sec; $V_d = 0.0048$ m/sec).

Thus the CFD-PBE model reported in this work is validated extensively against experimental data on hold up and drop diameter for a wide range of operating and geometrical parameters. Fig. 5.23 shows the overall parity plot for column hold up and Sauter mean drop diameter across the entire set of experimental data used in this work. The entire data set includes effect of column design (diameter, interplate spacing), operating parameters (continuous, dispersed and pulsing velocity) and phase systems (30% TBP/DD-water and 30%TBP/DD and water). Even though the results for different phase systems have not been shown separately the relevant data have been included in Fig. 5.23. Absolute average relative error across the entire range of experimental data used in this work in prediction of hold up and Sauter mean drop diameter with respect to experimental data are about 12% and 16%, respectively. One important observation is that the match between predicted and experimental Sauter mean drop diameter is not that good as the drop diameter exceeds 2 mm. One reason for this is that the breakage and coalescence that were used in the present work have been developed for liquid-liquid dispersion in a stirred tank where the maximum drop diameter is not large as 2 mm. The points corresponding to drop diameter larger than 2 mm corresponds to those in the mixer settler regime of operation of the column which is typically characterized by larger drops. Hence, it is reasonable to expect that closure models used in the PB equations incorporated in this work would not be able to capture the dynamics of large drops. Having said so in industry pulsed columns are typically operated in dispersion or quasi emulsion regime which are characterized by smaller drops. Hence, even though the PB model closure kernels are not general enough to consider all operating regimes in a pulsed column they are tailored for dispersion/quasi emulsion regime.

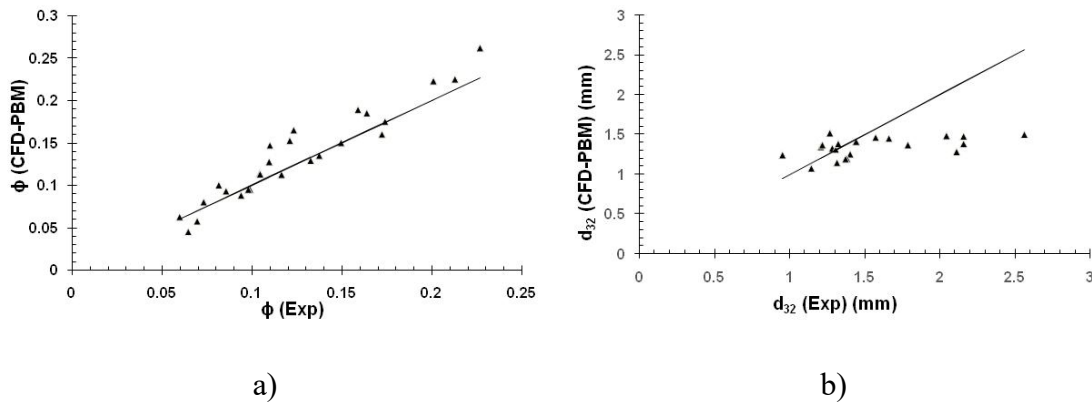


Figure 5.23: Parity plot for a) hold up and b) Sauter mean drop diameter

5.4 CONCLUSION

A predictive 2D coupled CFD-PBE of PSPCs is proposed. An optimized drag model based on the drag model of Schiller-Naumann is used to model the inter-phases momentum exchange term. The model is extensively validated against experimental data which are obtained by varying both operating (continuous and dispersed phase velocity) and geometrical (different interplate spacing and column diameter) conditions. Absolute average relative errors in prediction of dispersed hold up and Sauter mean drop diameter are about 12% and 16 % respectively. The validated model is used to understand the spatial and temporal variation of the local hydrodynamics parameters. Spatial variations of various hydrodynamic variables in an inter-plate zone are analyzed at the positive and negative peaks of the pulse. At the positive pulse peak of the pulse the dispersed phase is observed to be ejecting out of the sieve holes while during the negative peak of the pulse large accumulation of the dispersed phase below the plates is observed. Drops are observed to be smaller at the location of sieve holes while their size increases as they approach the next plate above. Turbulence dissipation rates are also observed to be high at the location of the holes. Higher values of turbulence dissipation rates and smaller drops are observed during the positive peak of the pulsing cycle. Re-circulations are observed to be more prominent in the continuous phase than in the dispersed phases. The model can be

used as a tool to get useful insights into two-phase hydrodynamics prevalent in a PSPCs. Such insights will be helpful for optimum design of the PSPCs.

CHAPTER 6

COUPLED CFD-PBE SIMULATION TO PREDICT CONTINUOUS PHASE AXIAL DISPERSION

6.1 INTRODUCTION

As mentioned before for an accurate estimation of mass transfer performance of PSPC (using a 1D dispersed plug flow model) it is essential to estimate axial dispersion coefficient in either phase with reasonable accuracy. The state of art with respect to estimation of axial dispersion coefficient in PSPC till date are essentially empirical correlations reported by a host of researchers over the years. A generalized correlation for axial dispersion coefficient in continuous phase was reported by Tung and Luecke (Tung and Luecke, 1986) with published data for PSPC, which takes into account the effect of column geometries. A similar correlation was proposed by Srinikethan and co-workers (Srinikethan et al., 1987) taking into account the effect of pulse amplitude, pulse frequency, continuous phase velocity and plate details (hole diameter, interplate spacing) on axial dispersion coefficient. The authors provided correlations for both mixer settler and emulsion regime of column operation. Kumar and Hartland (Kumar and Hartland, 1989) collected 992 data points with and without mass transfer for 28 liquid–liquid systems from 13 different sources and proposed an unified correlation for continuous phase axial dispersion in PSPC. The correlation could be used with a wide range of systems and over a range of operating conditions.

Numerical modeling of axial dispersion coefficient in pulsed sieve plate column till date has been limited to single-phase pulsatile flow (Kolhe et al., 2011; Xiaojin et al., 2011). To the best of our knowledge there is no work till date on numerical prediction of axial dispersion coefficient in two phase flow in pulsed sieve plate column.

In this chapter, we report for the first time a 2D two-phase CFD-PBE based numerical model to predict continuous phase axial dispersion coefficient. Euler-Euler approach is used to model the two phase liquid-liquid flow. A method of classes is used to model the population balance equations. Mixture k- ϵ model is used to model the turbulence inside the column. A virtual tracer study is carried out to arrive at the residence time distribution in the continuous phase. Experiments are carried out in a 3 inch PSPC to obtain axial dispersion coefficient in the continuous phase. Model predictions are validated against experimental results on axial dispersion coefficient in the continuous phase. To the best of our knowledge this is the first time a CFD-PBE model is being used to predict axial dispersion in either phase. Thus the model reported in this work can be used to predict all relevant hydrodynamic parameters (i.e hold up, Sauter mean drop diameter, axial dispersion coefficient) required for a first hand estimation of mass transfer performance of a PSPC using a dispersed plug flow model.

6.2 EXPERIMENTS

6.2.1 Experimental Setup

The schematic of the experimental setup used in this work is shown in [Fig. 6.1](#). It consists of a glass column of 0.076m diameter. The aqueous and organic phases are fed to the column (from feed tanks) by means of two centrifugal pumps. Volumetric flow rates of either phase could be varied using rotameter. A 3 way valve (Make: AirMax) and compressed air are used to provide air pulsation in the pulsed leg. The active section of the column is 0.5 m long. There are two disengagement sections, one each at the top and the bottom so as to allow the phases to separate. Water is used as the continuous phase and 30% TBP in dodecane is used as the dispersed phase. Physical properties of the materials are given in the [Table 6.1](#). A typical experiment consists of initially filling the column with continuous phase and starting the pulsation

at the desired pulsing velocity (pulsing frequency maintained at 1 Hz). There after dispersed phase is introduced in to the column. The required flow rates of the continuous and dispersed phases are set using rotameters. Suitability of KCl as a tracer has been widely reported earlier (Kolhe et al., 2011). A syringe is used to inject the tracer into the column from one side. Care is taken to ensure that the entire tracer volume is injected quickly (with in 1 sec). The tracer is injected at a point located 50 mm form the top of the column. An online conductivity meter (range of 0-2 mS/cm, Make: ATI's Q45C4) is located at the bottom of the active column section (50 mm above the base of the active column section) to continuously monitor the conductivity of the continuous phase. The increase in conductivity (over and above the background value) is entirely due to the presence of the tracer. A 16 channel data acquisition system (Make: Ambetronics) stores the data from the meter at a sampling frequency of 1 Hz. Amplitude of the pulsation is measured by measuring top and bottom positions of the liquid in the pulse leg. Experiments are carried out for different continuous and dispersed phase flow rate as well as for different pulsation amplitude keeping pulsation frequency constant at 1 Hz. Duty cycle of pulsation is kept 30%. Physical properties of the phase system are reported elsewhere (Sarkar et al., 2017).

6.2.2 Computational approach

The CFD-PBE based approach developed and validated in the previous chapter was further used to estimate axial dispersion coefficient in pulsed sieve plate columns. As mentioned before till date there has been no report on numerical estimation of axial dispersion coefficient in two phase flow in PSPC.

Estimation of axial dispersion using the CFD-PBE model essentially involved solving a species transport equation in the continuous phase as shown by Eqn. (6.1) below.

$$\frac{\partial C}{\partial t} \phi_c + \phi_c U \cdot \nabla C = \phi_c D \nabla^2 C \quad (6.1)$$

where

C is the tracer concentration, U is the velocity field, ϕ_c is the continuous phase volume fraction and D is the effective diffusion coefficient in continuous phase. Effective diffusion coefficient essentially comprises of molecular diffusion and eddy (turbulent) diffusion.

Initially for the given operating conditions the two phase flow field was established. The hydrodynamic simulations were continued till steady state value (periodic) of column hold up and Sauter mean drop diameter were obtained. There after a certain region (above the top plate) was patched with a value of the tracer and fully coupled unsteady simulations (flow, PBE and species transport equations solved simultaneously) were carried out to arrive at a time varying profile of tracer concentration at a location below the bottom most plate in the column. This essentially yielded the concentration curve which was thereafter normalised to obtain the E curve.

The pulsing action was introduced into the computational model using an user defined function as per Eqn. (3.12).

6.2.3 Computational domain

In the present 2D computational model a reduced number of plates (5 plates) has been considered to limit the size of the computational domain and the resulting computational time. Unsteady state simulations are carried out with a time step of 0.01 sec corresponding to Courant numbers around 0.5 in all cases. The computational domains used in the present work is the same as reported in chapter 5. Details of the geometry are omitted here for brevity.

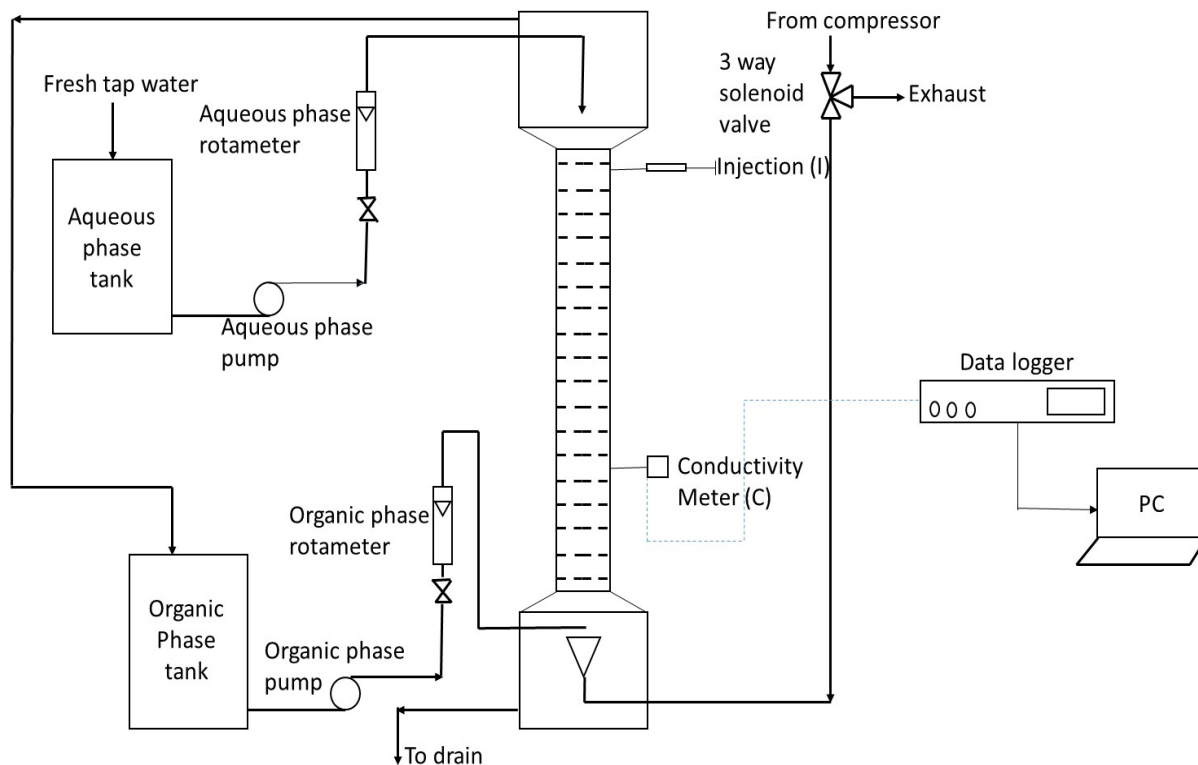


Figure 6.1: Schematic diagram of experimental setup

6.3 RESULTS AND DISCUSSION

6.3.1 Experimental investigation of continuous phase axial dispersion

In this work axial dispersion in the continuous phase is studied in PDDC and PSPC. The concentration of the tracer (KCl) at the outlet is monitored as a function of time which gives the C-curve. This is converted into the corresponding E-curve by normalizing the concentration data by the total quantity of the tracer injected. Details of normalization procedure are given elsewhere (Fogler et al., 2002) and are omitted here for brevity. A few preliminary experiments were carried out to understand effect of tracer concentration and injected tracer volume on the resultant E-curve. These preliminary experiments were conducted with single-phase flow of the heavier phase (water) under pulsing. Fig. 6.2 shows the effect of initial concentrations of the tracer on E-curve for a constant volume of tracer i.e. 5 mL. It is observed that E-curve becomes independent on the tracer concentration as tracer concentration is raised

above 1.5 M. Even though a concentration of 1.5 M was sufficient we used a KCl concentration of 2.5 M so as to increase the sensitivity of the conductivity data.

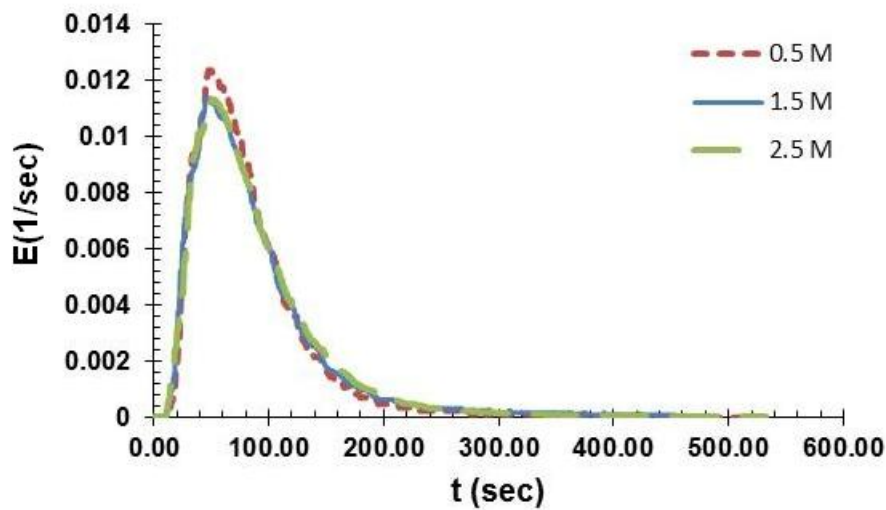


Figure 6.2: Effect of initial tracer concentration on E-curve (single-phase flow, tracer injection volume = 5 mL)

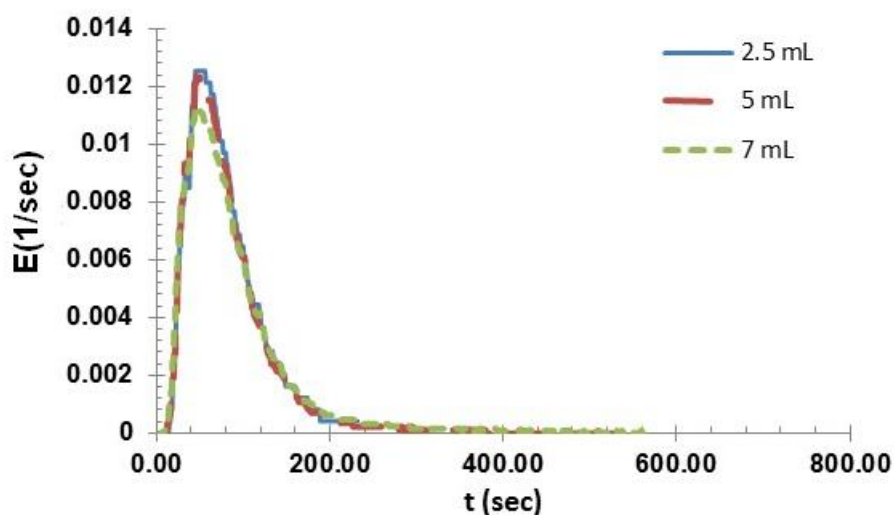


Figure 6.3: Effect of injected volume of tracer on resultant E-curve (single-phase flow, tracer concentration = 2.5 M).

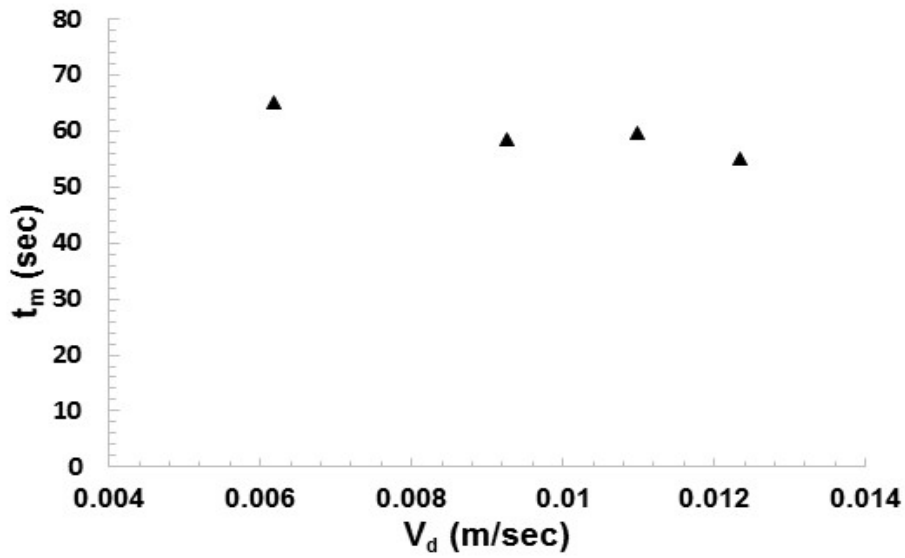
Similarly Fig. 6.3 shows the effect of quantity of tracer (of a given concentration) injected on the E curve. In these experiments concentration of tracer was maintained at 2.5 M. It is observed from Fig. 6.3 that E-curves obtained for injected volume of 5 mL and 2.5 mL are the same. However there is a slight

deviation if volume of tracer injected is 7 mL. As mentioned earlier a syringe was used to inject the tracer into the column. Even though utmost care was taken to ensure that the tracer sample could be injected very quickly it still involves some finite time. A larger tracer volume will thus involve a longer injection time which will have a broader E-curve. Based on above findings a tracer volume of 2.5 mL and a tracer concentration of 2.5 m have been chosen in this work. The E-curve obtained from the experiments is analyzed to obtain first and second moments of the E-curve which are then used to calculate Peclet number. The details of the associated analysis is reported elsewhere (Fogler, 2002) and are omitted here for brevity.

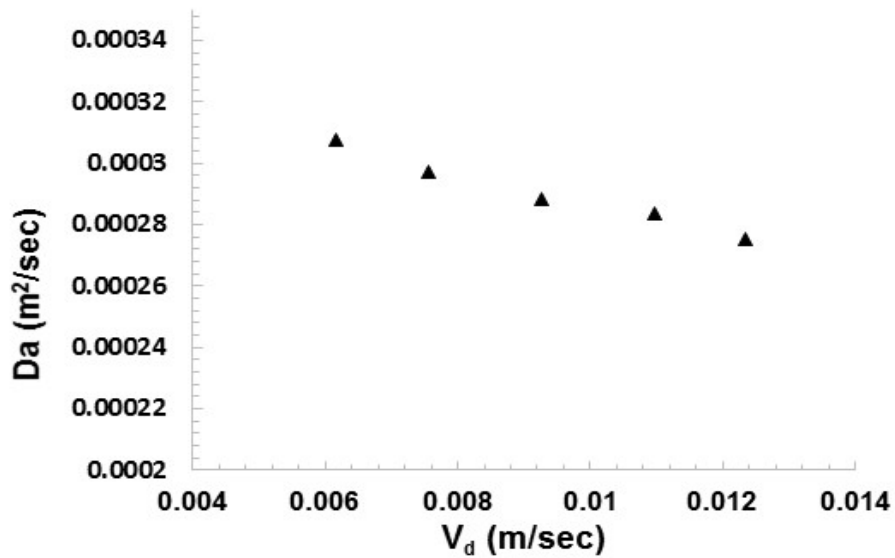
Experiments are carried for different values of dispersed phase velocity (0.0062-0.012 m/sec) and continuous phase velocity (0.005-0.001 m/sec). The pulsing amplitude and frequency are maintained fixed at 2.2 cm and 1 Hz respectively as typically used in industrial scale units. Thus the pulsing velocity is maintained at 0.022 m/sec.

Fig. 6.4 shows the variation of mean residence time and axial dispersion coefficient with different dispersed phase velocity. Continuous phase velocity and pulsing velocity are maintained at 0.0055 m/sec and 0.022 m/sec respectively.

An increase in dispersed phase velocity is seen to in general reduce the mean residence time of the continuous phase (Fig. 6.4 a). This is attributed to the fact that with increase in dispersed phase velocity the relative presence of the dispersed phase in the column will increase which will reduce the space available



(a)



(b)

Figure 6.4: Variation of a) mean residence time and b) axial dispersion coefficient with dispersed phase velocity.

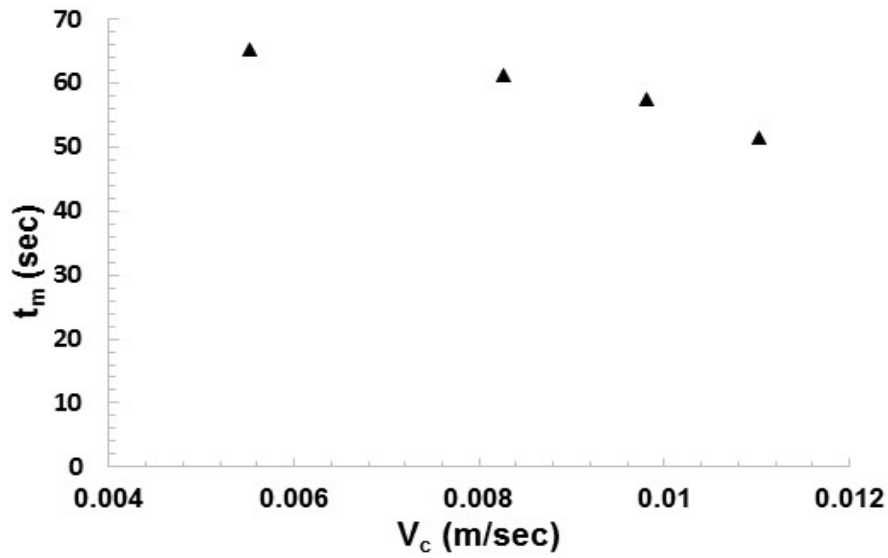
for the continuous phase thereby leading to faster exit of the continuous phase from the column leading to smaller mean residence times.

It is seen that axial dispersion coefficient decreases slightly with increase in dispersed phase velocity for PSPC (Fig. 6.4 b). An increase in dispersed phase velocity will decrease the space available for the continuous phase to move down

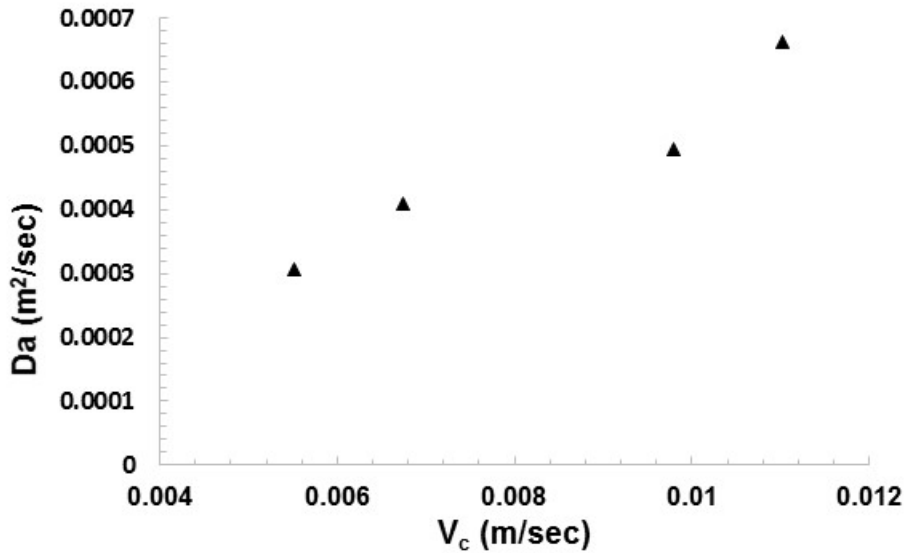
thereby increasing local velocities and hence strength of re-circulations in the continuous phase. This will tend to increase axial mixing in the column. Another point is presence of dispersed phase drops in an existent re-circulation (in continuous phase) will tend to break a large re-circulation into smaller (multiple) ones. This effect tends to reduce axial dispersion/mixing. A combination of these factor will govern the nature of dependence of axial mixing on dispersed phase velocity. In PSPC presence of sieve holes inject drops of dispersed into established re-circulations there by breaking such re-circulations into smaller ones. Due to this effect axial dispersion does not increase with dispersed phase velocity. On the contrary it reduces.

[Fig. 6.5](#) shows the variation of mean residence time and axial dispersion coefficient with different continuous phase velocity. Dispersed phase velocity and pulsing velocity were maintained at 0.0062 m/sec and 0.022 m/sec respectively.

It is observed that mean residence time reduces with an increase in continuous phase velocity ([Fig. 6.5 a](#)). As the continuous phase velocity is raised the time spent by continuous phase in the column reduces for PSPC. It is also seen that axial dispersion coefficient keeps on increasing with increase in continuous phase velocity for PSPC ([Fig. 6.5 b](#)). This is because of the fact that as continuous phase velocity is increased the re-circulations in the continuous phase gains strength and becomes stronger thus increasing the axial mixing.



(a)



(b)

Figure 6.5: Variation of a) mean residence time and b) axial dispersion coefficient with continuous phase velocity.

At this junction it may be mentioned that using KCl as tracer it is not possible to measure axial dispersion coefficient in the organic dispersed phase. However using radio tracer technique it is possible to measure axial dispersion coefficient in both the phases. Some preliminary single phase experiments in this regard were carried out. A radiotracer $Te\ 99m$ was used to estimate axial dispersion coefficient in a 6 inch PSPC (1 m high equipped with standard cartridge) under single phase flow of water. Effect

of pulsing velocity and superficial flow velocity on the axial dispersion coefficient was seen. Axial dispersion coefficient was seen to increase with increase in pulsing velocity while it decreased with increase in superficial phase velocity.

Several correlations for estimating continuous phase axial dispersion in PSPC have been reported. In some of these studies, the correlations were regressed based on limited experimental data and hence are applicable only to the range of operating and geometrical conditions for which the correlation was developed. An example is the correlation developed by Kagan and co-worker (Kagan et al., 1973) for two-phase operation of a pulsed sieve plate column. Later on Tung and Luecke (Tung and Luecke, 1986) developed a more generalized correlation for continuous phase axial dispersion taking into account the effect of column geometries. A similar correlation was also proposed by Srinikethan and co-worker (Srinikethan et al., 1987) which took into account the effect of pulsation velocity and continuous phase velocity on continuous phase axial dispersion separately via different number groups. Later on, Kumar and Hartland (Kumar and Hartland, 1989) collected 992 data points with and without mass transfer for 28 liquid–liquid systems from 13 different sources and presented a unified correlation for continuous phase axial dispersion in pulsed sieve plate columns. The data on continuous phase axial mixing generated in this work across a range of operating and geometrical parameters were compared against prediction from the above set of empirical correlation in the present work. Fig. 6.6 shows the parity plot of the experimental and correlation predicted data on axial dispersion coefficient. Table 6.1 below shows the correlations compared in this work along with the absolute average relative error in prediction. It is observed that prediction of the correlation due to Kagan and Kumar and Hartland tends to over predict the axial dispersion coefficient. The performance of the correlation due to Tung and Luecke was better while that due to Srinikethan was the best. Absolute average relative error in prediction using correlation provided by Srinikethan and co-

workers was around 16%. The superior performance can be attributed to the fact that Srinikethan and co-workers considered effect of sieve-hole diameter, inter plate spacing as well as percent opening area in their correlation. Correlation due to Tung and Luecke and Kagan used an estimate of dispersed phase hold up to ascertain axial dispersion. This parameter needed to be estimated from a suitable correlation for hold up thereby increasing the inaccuracies. In the present work hold up was estimated from correlation due to Venkatnarsaiah and Verma (Venkatnarsaiah et al., 1989) as it was found the most appropriate (chapter 3). Surprisingly correlation due to Kumar and Hartland was seen to over predict axial dispersion. One possible reason is that the authors considered a wide range of geometrical parameters and included data for columns ranging in diameter from 50 mm to 300 mm. Even though this made their correlation valid even for large diameter column the correlation did not perform well for small diameter columns as used in this work (50-75 mm).

Table 6.1: Correlations to predict axial dispersion in PDDC

Sl. No.	Reference	Equation	Absolute average relative error
1	Kagan et al., 1973	$D_a(1-\phi) = 1.26 \times 10^{-4} \frac{A^{1.2} f^{1.35}}{(V_c + V_d)^{1.4}}$	165.68 %
2	Tung and Luecke, 1986	$\frac{D_a(1-\phi)}{hV_c} = 0.250\phi^{-1.30} \left(\frac{d_o}{h}\right)^{0.565} \left(\frac{Af}{V_c}\right)^{0.606}$	41.10 %
3	Srinikethan et al., 1987	$\frac{D_a}{hV_c} = 3.25 \left(\frac{\mu_c}{V_c d_o \rho_c}\right)^{0.2} \left(\frac{d_o}{h}\right)^{0.8} \left(\frac{Af}{V_c}\right)^{0.3} \varepsilon^{-0.8}$	16.12 %

Kumar

and

Hartland

, 1989

$$\frac{D_a \Delta \rho}{\mu_c} = 46.15 e^{(k_2 \psi)} \left(\frac{V_d \mu_c}{\sigma} \right)^{0.11} \left(\frac{\mu_c}{\mu_d} \right)^{-0.37} \left(\frac{d_o}{h} \right)^{0.36} \left(\frac{\mu_c}{(\sigma \Delta \rho h)^{0.5}} \right) \left(\frac{\Delta \rho h}{\rho^* h^*} \right)^{1.06}$$

where

$$k_2 = 0.80 \quad \text{for } Af < 2Af_m$$

$$0.37 \quad \text{for } Af > 2Af_m$$

$$\psi = \begin{cases} \left(\frac{Af - Af_m}{Af_m} \right)^3 - \left(\frac{Af - Af_m}{Af_m} \right)^2 & \text{for } Af < 2Af_m \\ \frac{Af - 2Af_m}{Af_m} & \text{for } Af > 2Af_m \end{cases} \quad 52.40 \%$$

$$Af_m = 9.69 \times 10^{-3} \left(\frac{\sigma \Delta \rho^{0.25} \phi}{\mu_d^{0.75}} \right)^{0.33}$$

$$\rho^* = 998 \text{ kg/m}^3$$

$$h^* = 0.05 \text{ m}$$

Correlation for

hold up (ϕ)

due to

Venkatnarsaia

h et al., 1998

$$\phi = 116.5 e^{(39.35|Af - Af_m|)} V_d^{1.02} V_c^{0.02} \Delta \rho^{-0.23} \mu_d^{0.52} d_o^{-0.3} \varepsilon^{-0.4} h^{-0.4}$$

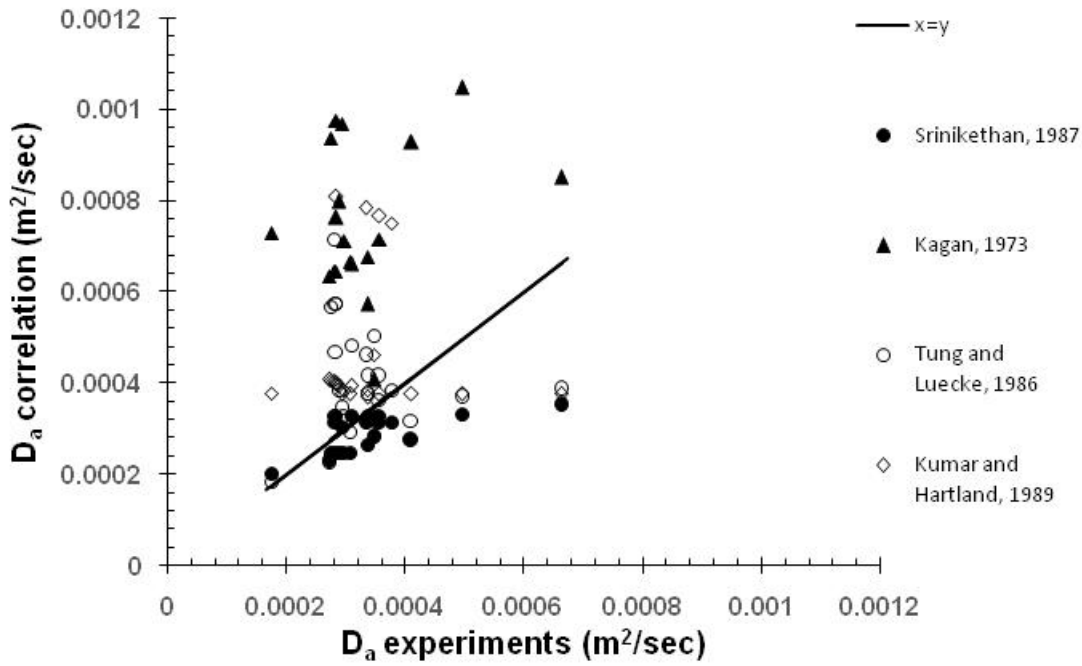


Figure 6.6: Parity plot for correlations predicting axial dispersion coefficient in PSPC.

6.3.2 Validation of CFD-PBE predictions

The developed 2D CFD-PBE model is used to arrive at a periodic steady state value of column hold up and Sauter mean drop diameter for a given set of operating parameters. Hence, the two phase flow field is established before virtual tracer study is initiated. This methodology is similar to what is adopted in experiments where the tracer was injected once the two phase flow is properly established. The E curve obtained from the virtual tracer study is there after used to arrive at the first and second moment of the curve. This is there after used to calculate the axial dispersion coefficient.

Fig. 6.7 shows the comparison of axial dispersion coefficient predicted from CFD-PBE model against experimental results for different values of dispersed phase velocity. Values of continuous phase velocity and pulsing velocity were fixed at 0.0055 m/sec and 0.022 m/sec respectively.

Similarly Fig. 6.8 shows the comparison of axial dispersion coefficient predicted from CFD-PBE model against experimental results for different values of continuous phase

velocity. Values of dispersed phase velocity and pulsing velocity were fixed at 0.0062 m/sec and 0.022 m/sec respectively.

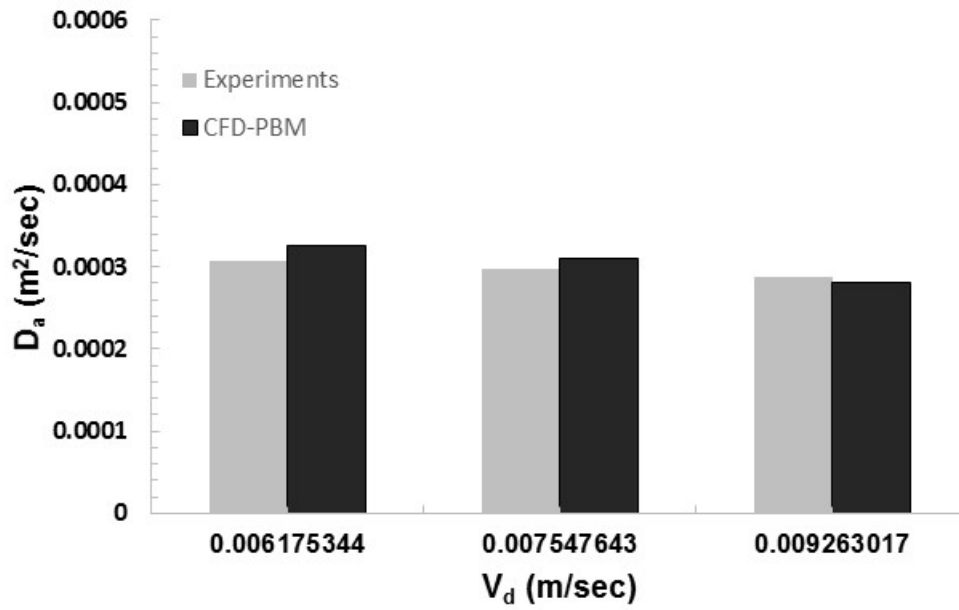


Figure 6.7: Comparison of CFD-PBE predicted axial dispersion coefficient against experimental data for different dispersed phase velocities

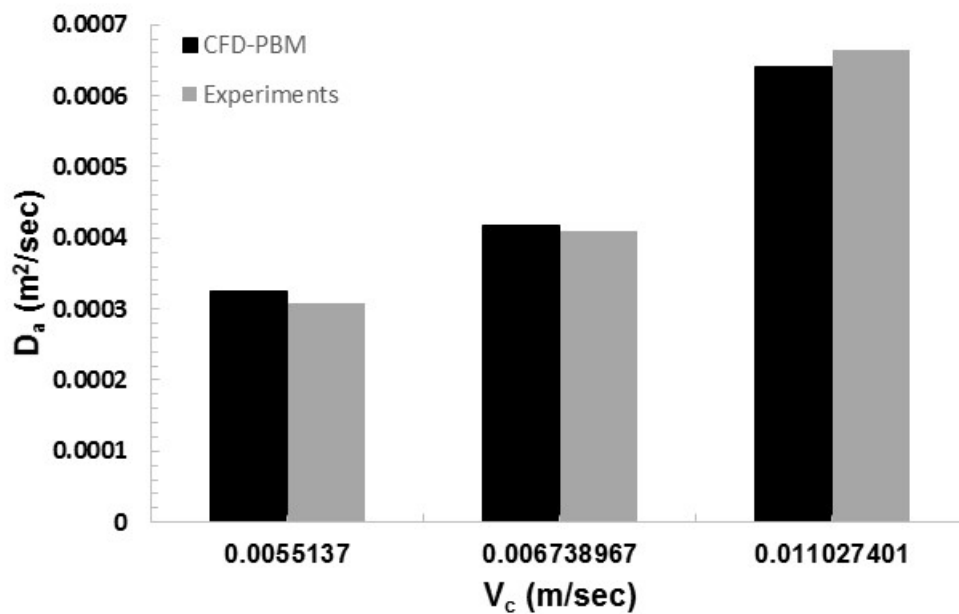


Figure 6.8: Comparison of CFD-PBE predicted axial dispersion coefficient against experimental data for different continuous phase velocities

As evident from Fig. 6.7 and Fig. 6.8 the prediction obtained from CFD-PBE model are seen to be very close to the experimental values of axial dispersion coefficient. Quantitatively it is seen that absolute average relative error in prediction is 3.83 %. This is also shown in Fig. 6.9 which shows that the parity plot between the experimental and CFD-PBE predicted values of continuous phase axial dispersion coefficient. It is seen that all the points are well within $\pm 10\%$ confidence band marked in the figure as dotted lines.

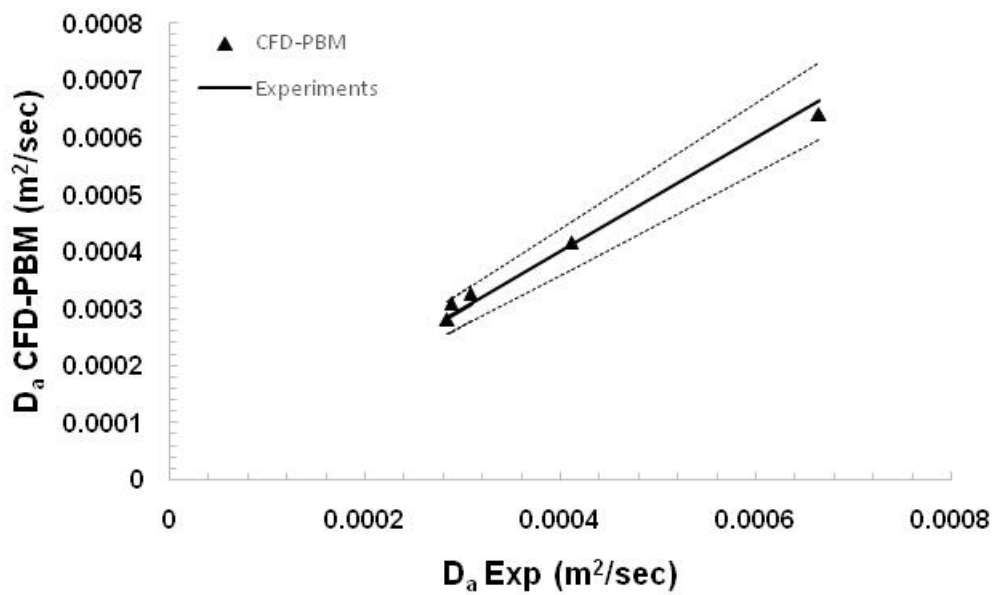


Figure 6.9: Parity plot for CFD-PBE predicted and experimentally obtained axial dispersion coefficient.

6.3.3 Local two phase flow hydrodynamics

Thus in this chapter we report a 2D CFD-PBE model which can predict continuous phase axial dispersion coefficient in a PSPC with a good accuracy. In the present section we use the model to obtain insights into the local hydrodynamics inside the column.

Fig. 6.10 shows the contour of dispersed phase hold up and Sauter mean drop diameter at two different instants of time during a pulsing cycle. The first figure from left is at the instant of positive peak of the pulse while the second figure from left is at

the instant of the negative peak of the pulse. It is interesting to note that within a pulsing cycle local distribution of the dispersed phase changes significantly during the pulsing cycle. It can be clearly seen that during the positive peak of the pulsing cycle the dispersed phase is forced upwards through the sieve holes while during the negative peak an accumulation of the dispersed phase is clearly observed below the plate. This is attributed to the fact that during the positive peak the dispersed phase (moving up) is being pushed forcibly through the holes thus distributing it across the column. On the other hand during the negative stroke the dispersed phase accumulates below the plate due to lack of any upward force pushing the dispersed phase upwards. Fig. 6.10 also shows the contour plot of Sauter mean drop diameter in an interplate space. It can be observed that there is not much of a difference in the contour of Sauter mean drop diameter between the positive and negative pulse peak. In both cases drops are seen to be smaller near the sieve holes while they grow in size as they move upwards.

Fig. 6.11 shows the spatial variation of Sauter mean drop diameter, and turbulent energy dissipation rate in an interplate space (between 4th and 5th plate from bottom). The instant of time corresponds to the positive peak of the pulsing cycle. The drop diameter is smaller in and around the holes which are also characterized by high local values of turbulent energy dissipation rate. High values of turbulent energy dissipation rate leads to higher rate of drop breakage leading to generation of smaller drops in regions around the sieve holes. As the drops move up and away from the holes they

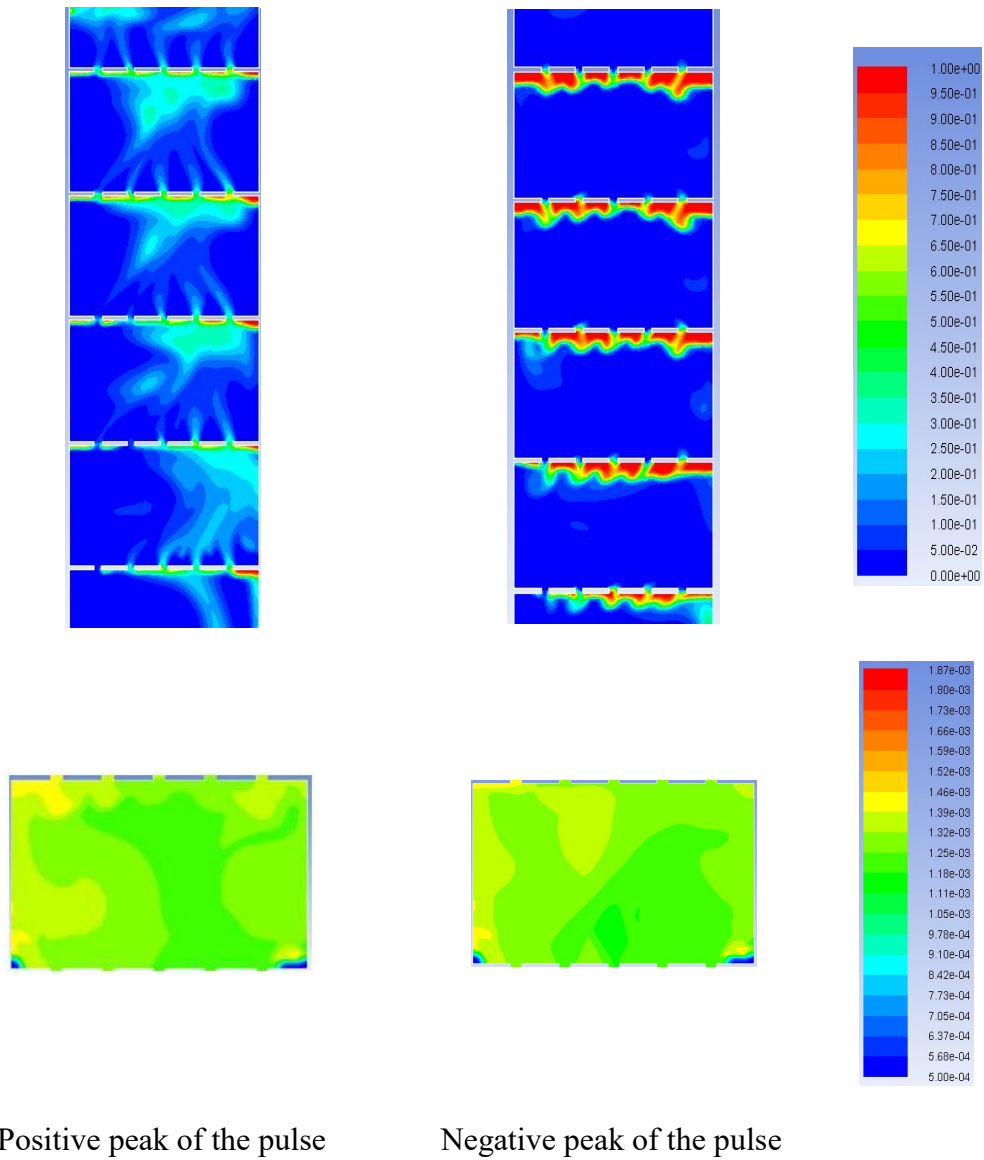


Figure 6.10: Spatial variation of dispersed phase hold up inside the column at different instants of a pulsing cycle ($Af = 0.0222$ m/sec; $V_d = 0.0062$ m/sec, $V_c = 0.0055$ m/sec)

tend to coalesce in absence of any significant local turbulent energy dissipation rate leading to formation of larger drops. Infact presence of significant coalescence eventually leads to formation of a thin layer of dispersed phase just below the next plate as is observed in [Fig. 6.10](#).

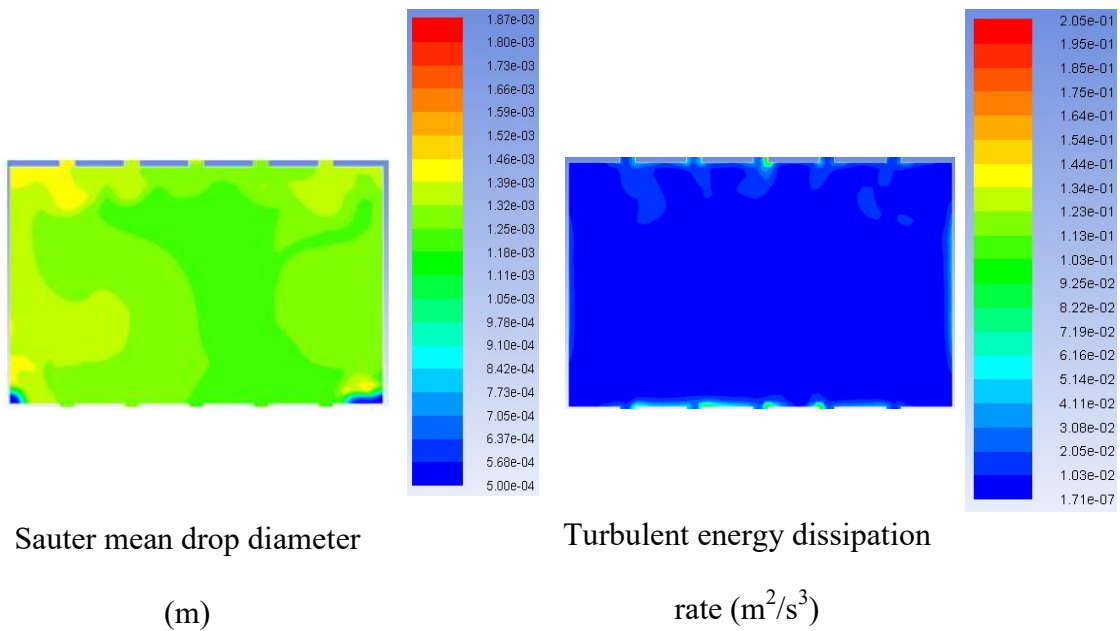


Figure 6.11: Spatial variation of Sauter mean drop diameter and turbulent energydissipation rate ($A_f=0.0222$ m/sec; $V_d= 0.0062$ m/sec, $V_c = 0.0055$ m/sec)

Fig. 6.12 shows the comparison of dispersed phase hold up inside the column for two different values of dispersed phase velocity. The hold up profiles are at the positive peak of the pulsing cycle. An increase in dispersed phase hold up is clearly observed for higher dispersed phase velocity. Infact for a dispersed phase flow velocity of 0.0075 m/sec a thin layer of dispersed phase is clearly seen to accumulate below the plates. The dispersed phase is seen to eject out of the sieve holes - a characteristic of the positive peak of the pulsing cycle.

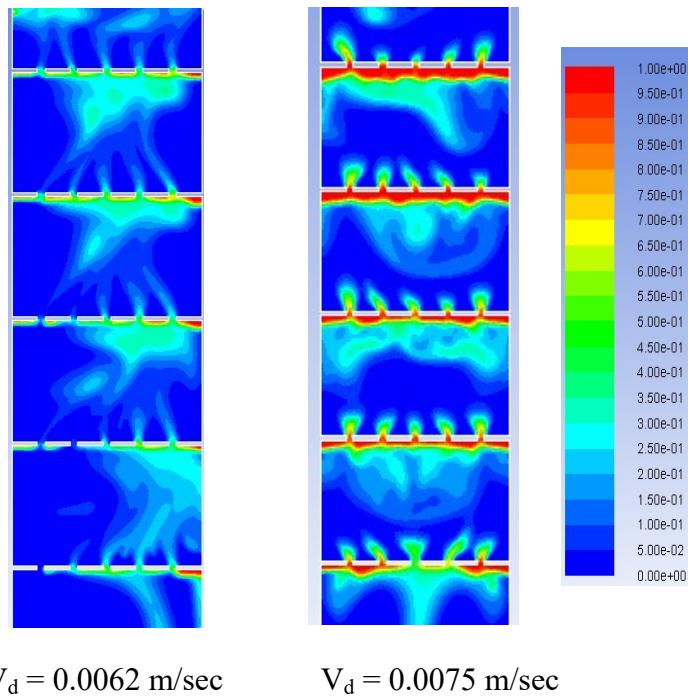


Figure 6.12: Dispersed phase hold up profiles for two different values of dispersed phase velocity ($V_c = 0.0055$ m/sec; $A_f = 0.0222$ m/sec)

Fig. 6.13 shows the comparison of the contour plot of Sauter mean diameter at two different values of dispersed phase velocity (i.e 0.0062 m/sec and 0.0075 m/sec). The comparison is made at the positive peak of the pulsing cycle. A clear increase in Sauter mean drop diameter is observed as the dispersed phase velocity is raised. As dispersed phase velocity is increased more and more number of drops are packed below the sieve plate which leads to a higher rate of collision between them leading to the higher coalescence rate leading to larger drops. Furthermore the increase in Sauter mean drop size as the drops move away from the holes in the sieve plate is clearly revealed in both the cases though the difference becomes more and more prominent as the dispersed flow velocity is raised.

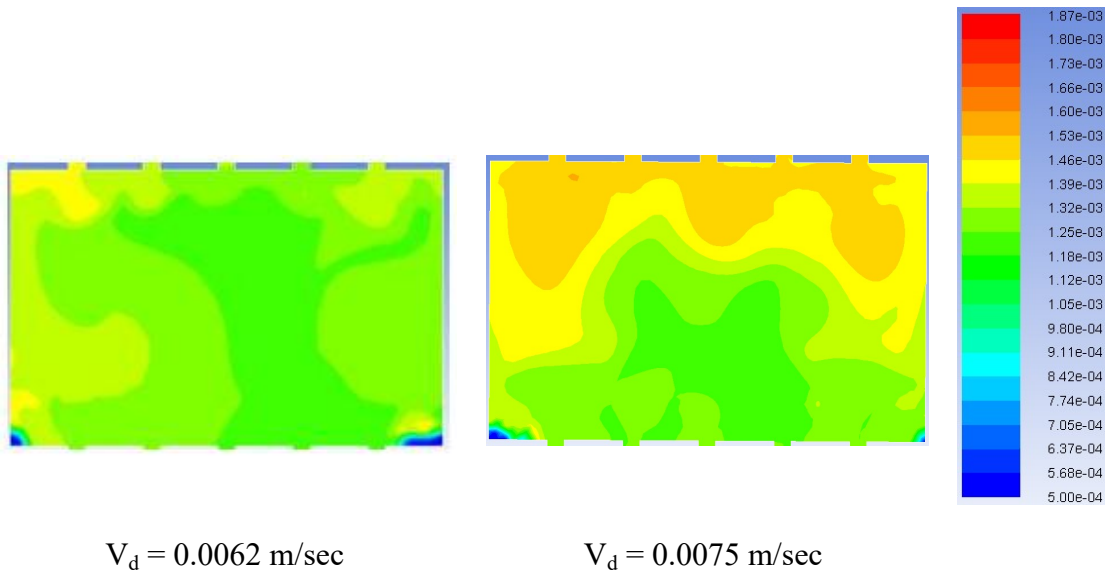
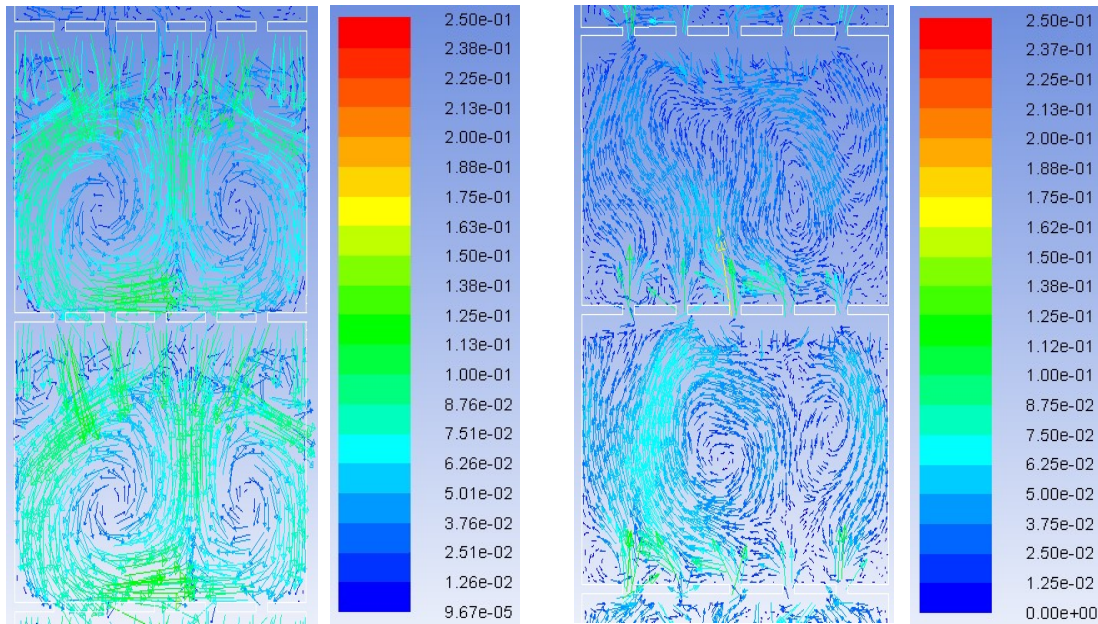


Figure 6.13: Sauter mean drop diameter profiles for two different values of dispersed phase velocity ($V_c = 0.0055$ m/sec; $A_f = 0.0222$ m/sec)

Fig. 6.14 shows the velocity vector plot of continuous phase at two different dispersed phase velocities. (i.e 0.0062 m/sec and 0.0075 m/sec). The comparison is made at the positive peak of the pulsing cycle. Values of continuous phase velocity and pulsing velocity was maintained constant at 0.0055 m/sec and 0.0222 m/sec respectively. At low values of dispersed phase velocity two well defined counter rotating circulatory loops are formed in the continuous phase. However as dispersed phase velocity is raised these loops are no longer well defined and are essentially broken down into many smaller circulations. For the same continuous phase velocity and pulsing velocity the strength of the circulations is also reduced as evident qualitatively by lower local velocity in the circulatory loops. Such a difference can be attributed to the fact that at high values of dispersed phase velocity a larger quantity of dispersed phase will be pushed in to the continuous phase streams thereby breaking up the continuous phase circulations. Hence, a large sustained circulation in the continuous phase is effectively broken down into smaller and weaker circulations. This is also evident from Fig. 6.15 below which compares the dispersed phase velocity vector plot for two

different velocities. It is clearly seen that at low dispersed phase velocity the dispersed phase



$V_d = 0.0062$ m/sec

$V_d = 0.0075$ m/sec

Figure 6.14: Continuous phase velocity vector plot for two different values of dispersed phase velocity ($V_c = 0.0055$ m/sec; $A_f = 0.0222$ m/sec)

preferentially moves up through the centre of the column. Thus the flow pattern of the dispersed phase is not uniform across the cross section. Hence, at low values of V_d the dispersed phase moves up through the centre while significant re-circulations are set up in continuous phase. As the dispersed phase velocity is increased from 0.0062 m/sec to 0.0075 m/sec the non uniform flow pattern of the dispersed phase is disrupted and the dispersed phase starts moving much more uniformly across the cross section of the column. Hence, as the dispersed phase is now being pushed out more uniformly across the column they tend to break up the sustained re-circulations in the continuous phase as is seen in the previous figure.

This decrease in size and strength of re-circulations in continuous phase essentially leads to somewhat reduced axial mixing in the column and can be interpreted as the

reason why axial dispersion coefficient reduced as dispersed phase velocity was increase.

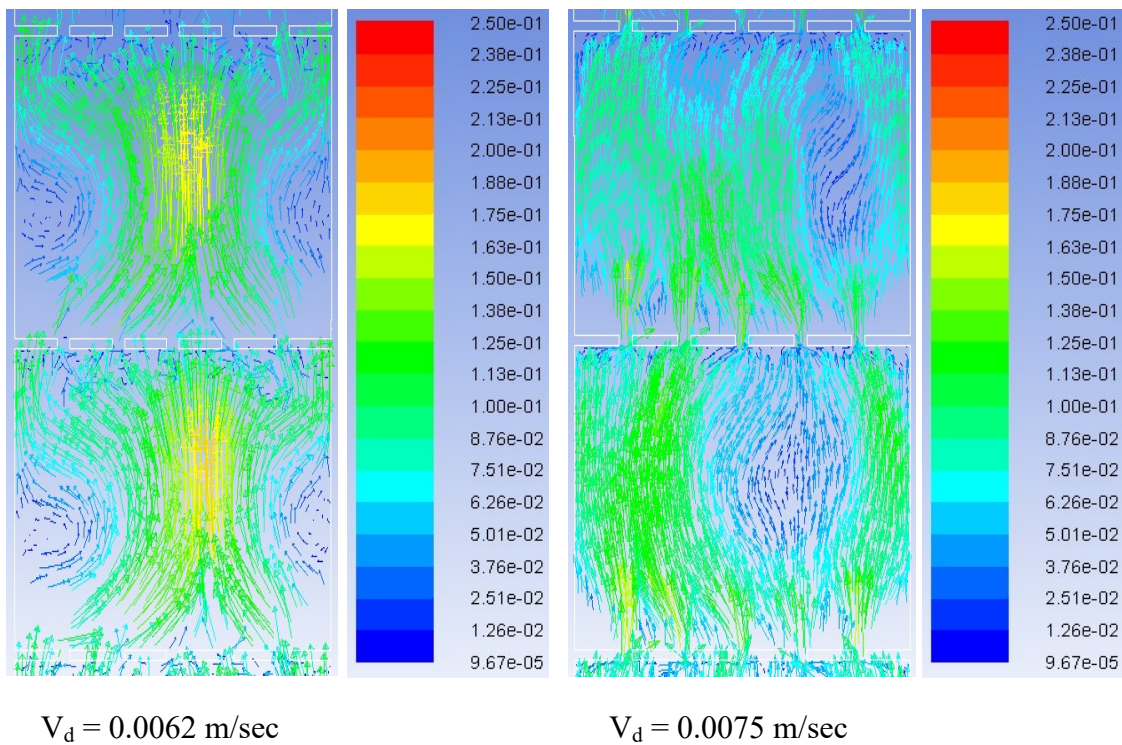


Figure 6.15: Dispersed phase velocity vector plot for two different values of dispersed phase velocity ($V_c = 0.0055 \text{ m/sec}$; $A_f = 0.0222 \text{ m/sec}$)

6.4 CONCLUSION

Continuous phase axial dispersion in two-phase flow of 30% TBP in dodecane – water system in a pulsed sieve plate column has been simulated using a 2D two-fluid CFD-PBE approach. Experiments are also carried out in a 3 inch pulsed sieve plate extraction column to obtain axial dispersion coefficient in continuous phase for different values of continuous and dispersed phase velocity. The model can simultaneously predict spatial and temporal variations of dispersed phase hold up and Sauter mean drop diameter in the column. The model was there after used to carry out a virtual tracer study to predict axial dispersion coefficient. A drag law of the form proposed by Schiller Naumann is used to model the interphase momentum exchange term. Method of classes is used to solve the PB equations. Standard breakage and

coalescence kernels reported in literature are used. Quantitative accuracy of the computational approach to predict axial mixing (in continuous phase) is tested by comparing its predictions of axial dispersion coefficient with the experimentally measured values of the same. The absolute average relative error in prediction of axial dispersion coefficient is found to be 3.83%, respectively..

The validated CFD-PBE model was used to gain insights into the fundamental flow patterns inside the column. Smaller drops were seen to form in regions near the sieve holes which are characterised by higher values of turbulence dissipation rates. At low dispersed phase velocities sustained re-circulations in the continuous phase were observed while the dispersed phase was seen to preferentially move through the center of the column. However as the dispersed phase velocity was raised the re-circulations in the continuous phase decreased in span as well as strength and the dispersed phase was also seen to move more uniformly across the column cross section. This observation explained the reason for the decrease in axial dispersion coefficient with increase in dispersed phase velocity as was seen in experimentals as well as in numerical predictions.

CHAPTER 7

COUPLED CFD-PBE SIMULATION TO PREDICT INTERPHASE MASS TRANSFER

7.1 INTRODUCTION

1D mathematical models (dispersed plug flow models) to predict mass transfer in PSPCs have been reported ([Gonda and Matsuda, 1986](#); [Torab-Mostaedi, 2009](#)). In fact in nuclear fuel cycle dedicated codes based on 1 D modeling are available (SOLVEX, SEPHIS-MOD4, Revised MIXSET, PULCO). However these mathematical models embed several empirical correlations. With each correlation having its own uncertainty, using several of them in a mathematical model may result in significant overall uncertainty in the predictions of the model. This research work sought to develop CFD-PBE based numerical models (based on first principles) that can predict relevant hydrodynamic parameters (Sauter mean drop diameter, dispersed phase hold up, continuous and dispersed phase axial dispersion coefficient) that goes an input to the 1D code. As these parameters are predicted from first principles they are fairly independent of scale of operation or the phase systems involved. Thus we believe our work goes a long work to reduce the uncertainties or empiricism in the hydrodynamic input parameters to the 1D code. This in turn makes the 1D code rather robust.

In this chapter we go ahead one step ahead and report, for the first time, 2D two-phase CFD-PBE based simulations to directly predict interphase mass transfer of a species/solute from organic to aqueous phase. CFD based studies to predict interphase mass transport are in general rare ([Kashid et al., 2007](#); [Szafran et al., 2004](#)). Studies that couple a CFD-PBE approach with interphase mass transport are still rarer. Only recently Attarakih and coworkers ([Attarakih et al., 2015](#)) reported an approach where in they coupled a reduced bivariate population balance model with CFD (2D) and

predicted mass transfer in a rotating disc contactor. However to the best of our knowledge there has been no such attempt for liquid-liquid solvent extraction in pulsed columns.

In this research work a CFD-PBE based model (with interphase mass transport) is developed and validated against reported experimental data of a 2 inch diameter PSPC. The model revealed spatial and temporal variation of hydrodynamic parameters of the column under pulsing conditions and resultant effect on mass transfer in a 2D computational domain.

7.2 MODEL DESCRIPTION

7.2.1 Computational approach

The CFD PBE model used in this chapter is the same as reported in chapter 5. The equations are omitted here for brevity. However in addition to solving flow, turbulence and population balance equations two more species transport equations (one for either phase) are solved. Mass transfer of k^{th} solute (x_k) from one phase (phase i) to the other phase (phase j) was modeled by solving species transport equation in either phase with mass exchange (source) term as shown in Eqn. (7.1-7.2). Concentration of solute, k in the second phase (phase j) is denoted by y_k .

$$\frac{\partial x_k}{\partial t} \phi_i + \phi_i \mathbf{U} \cdot \nabla x_k = \phi_i D \nabla^2 x_k - K_L a \left(x_k - \frac{y_k}{K_d} \right) \quad (7.1)$$

$$\frac{\partial y_k}{\partial t} \phi_j + \phi_j \mathbf{U} \cdot \nabla y_k = \phi_j D \nabla^2 y_k + K_L a \left(x_k - \frac{y_k}{K_d} \right) \quad (7.2)$$

where ϕ_i is hold up of the i^{th} phase, D is the effective diffusivity (comprising of both eddy and molecular diffusion), $K_L a$ is overall volumetric mass transfer coefficient, K_d is the distribution constant. Value of $K_L a$ and K_d are obtained from literature ([Gonda and Matsuda, 1986](#)) for the phase system considered. To ensure mass continuity the form of the source term is consistent in either phase. Thus it is seen mass exchange term is calculated based on the difference in concentration of the solute in each phase

and overall volumetric mass transfer coefficient. The two species transport equations are coupled with each other through the source term. As the problem involves partitioning of one solute in two different phases, solute concentration in organic and aqueous phase are related through the following equation.

$$y_k = K_d x_k \quad (7.3)$$

The pulsing action was introduced into the computational model using an user defined function as per Eqn. (3.12) .

As the solute concentration varies across the computational domain the density of either phase also changes. In other words as the solute is partitioned (from organic phase) into aqueous phase density of the organic phase reduces while that of the continuous phase increases. This effect has been incorporated in our model.

7.2.2 Computational domain

For validation of the developed model, reported experimental data on solute end concentrations in a 2 inch PSPC ([Gonda and Matsuda, 1986](#)) are used. Hence, the computational domain is based on the reported geometry. A standard sieve plate cartridge (23% opening area, 3 mm hole diameter, 5 cm inter-plate spacing) was used. The column was 2 m in height and had 36 plates. A pulse leg was connected the bottom disengagement section to provide pulsation to the column contents. The phase system used was 30% TBP in dodecane and 0.1 N Nitric acid.

As before a reduced number of plates (5 plates) has been considered in this chapter so as to limit the size of the computational domain and the resulting computational time. Unsteady state simulations are carried out with a time step of 0.01 sec which corresponds to Courant numbers less than 0.5 in all cases. The computational domain, boundary conditions and grid density used in this chapter are the same as mentioned in section 5.2.3 in chapter 5 and have been omitted here for brevity.

7.3 RESULTS AND DISCUSSION

7.3.1 Validation

The mass transfer prediction of the developed CFD-PBE approach is first validated against reported experimental results. Gonda and Matsuda (Gonda and Matsuda, 1986) reported back extraction (stripping) of heavy metal solute from organic (dispersed phase) to aqueous (continuous phase) in a 2 inch diameter PSPC. Solute concentration in the organic phase fed to the column bottom was 97 gpl while the aqueous phase did not contain any solute. Solute concentration in each phase was reported at various locations along the column height leading to a solute concentration profile of each phase.

The computational model used in this work comprises of only 5 plates to ensure that computational time remains within reasonable limits. Solute concentration in organic phase entering the column and solute concentration in aqueous phase at the location of 5th plate from bottom goes into the model as inputs while the model predicts solute concentration in the aqueous phase exiting the column and in the organic phase exiting 5th plate from the bottom. Table 7.1 below shows the comparison of the predicted and reported values of solute concentration in organic phase at location of the 5th plate from bottom and that in aqueous phase at the column bottom. It is seen that the absolute average relative error in prediction of our model is 2.8 %. Hence, the 2D CFD-PBE approach can directly predict mass transfer from one phase to another with good accuracy.

Table 7.1: Comparison of CFD PBM predicted values against experimental data

	CFD (gpl)	Experi mental (gpl)	Absolute Average Relative Error (%)
Solute concentration at 5 th plate (from bottom) in organic phase	87.21	91.38	2.78
Solute concentration at 1 st plate (from bottom) in aqueous phase	48.504	49	

7.3.2 Local hydrodynamic and mass transfer aspects

In this section we use the validated numerical model to understand the complex hydrodynamics in PSPC and its resultant effect on transport of species from one phase to another. [Fig. 7.1](#) below shows the contour of dispersed phase hold up and Sauter mean drop diameter in a typical interplate zone. As the flow field is time varying due to pulsation the contours are shown at positive peak of the pulse.

Accumulation of the dispersed phase is clearly seen at the base of the sieve plates. The contour plot of Sauter mean drop diameter reveals that drop of smaller size are formed at the location of the sieve holes and drop diameter increases below the next sieve plate. This is due to the fact that turbulence dissipation rates are higher at the location of the holes (as evident from [Fig. 7.2](#)) which leads to increased breakage rates leading to the smaller drops at location of the sieve holes. As the dispersion moves up and reaches the next plate they tend to coalesce and drop size increases. [Fig. 7.2](#) shows the contour plot of the turbulence dissipation rates, axial continuous phase velocity and axial dispersed phase velocity for the positive peak of the pulsing cycle.

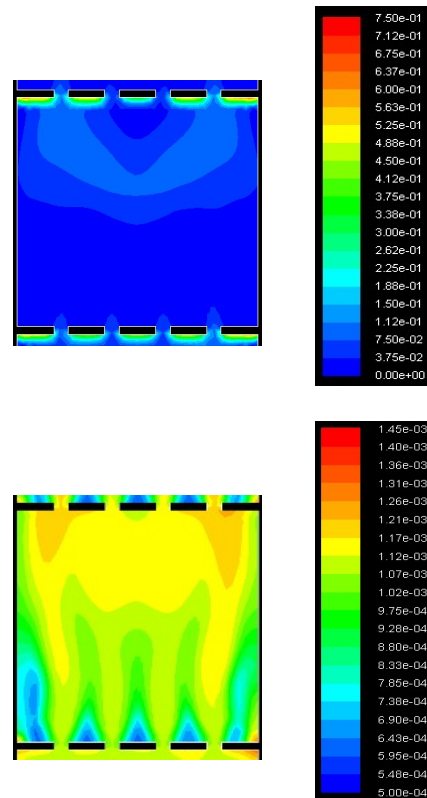


Figure 7.1: Contour plot of dispersed phase hold up (-) (top) and Sauter mean drop diameter (m) (bottom)

Fig. 7.2 also shows the axial velocity contour plot of continuous phase and dispersed phase. It is seen that during the upstroke (i.e. positive peak of the pulse) the continuous phase is also being pushed up along with dispersed phase even though the general direction of flow of the continuous phase is downwards. Presence of small recirculations in the continuous phase are also visible near the wall (as evidenced by negative values of axial continuous phase velocity near the wall). However no circulations are observed for the dispersed phase.

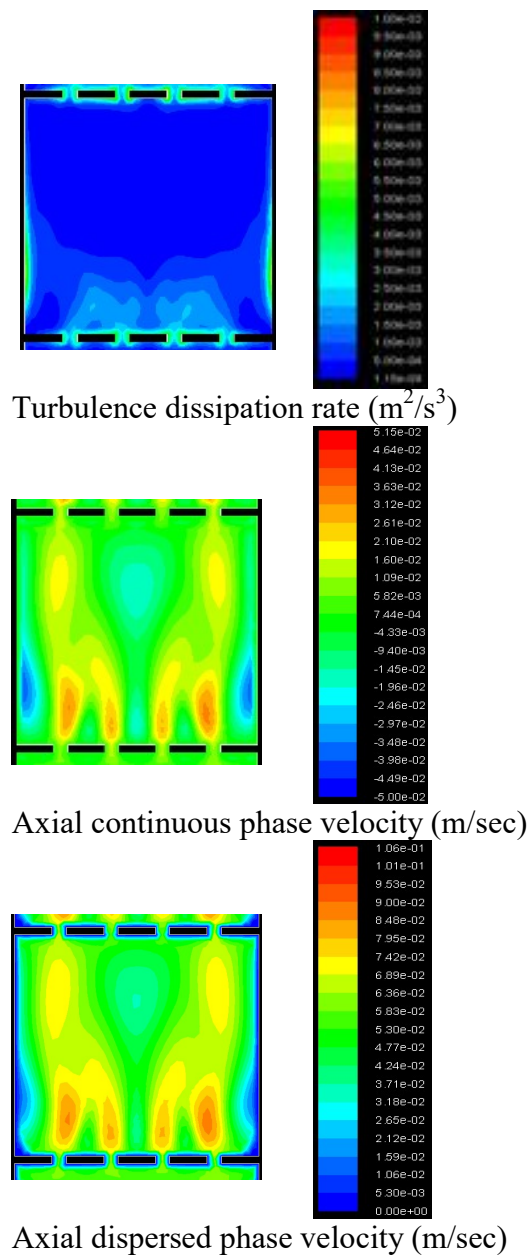


Figure 7.2: Contour plot of turbulence dissipation rate, axial continuous phase velocity, and axial dispersed phase velocity

Fig. 7.3 shows the solute concentration (in terms of solute mass fraction) in the organic (dispersed) phase and that in the aqueous (continuous) phase.

A gradual decrease in concentration of the solute as the dispersed phase moves up is clearly observed. At the same time whatever solute leaves the dispersed (organic)

phase is transferred to the continuous (aqueous) phase and is reflected as an increase in the solute concentration in the continuous phase as it flows downward.

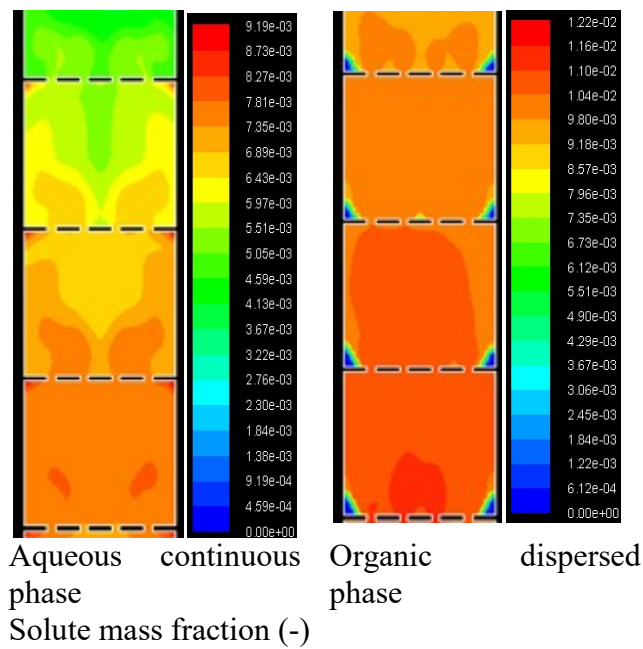


Figure 7.3: Contour plot of solute mass fraction in continuous and dispersed phase.

Fig. 7.4 shows the density of the organic phase across the entire computational domain. It is seen that density of the dispersed phase decreases as it flows upward along the column. Density of either phase is linked to the composition of that phase. Thus the density of the dispersed phase (organic) is seen to reduce as solute is transferred from organic to aqueous phase.

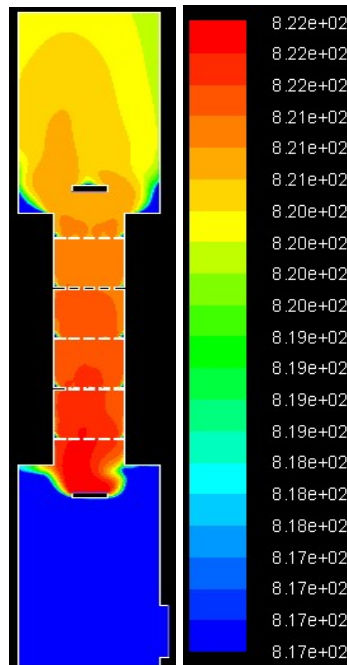


Figure 7.4: Density of the dispersed phase (kg/m^3)

7.4 CONCLUSION

The following conclusion could be drawn from the above work

- 1) A 2D CFD-PBE numerical technique was developed which could predict space and time varying hydrodynamics and resultant interphase mass transfer characteristics in a pulsed sieve plate extraction column for the first time in reported literature.
- 2) The developed model was validated against reported experimental data on solute concentration in organic and aqueous phases in a 2 inch PSPC. The model prediction was very close to reported results, the absolute average relative error being 2.78%.
- 3) The validated model was then used to understand the local variation of different hydrodynamics parameters like dispersed phase hold up, Sauter mean drop diameter, turbulence dissipation rates and continuous and dispersed phase axial velocity. Transfer of mass from organic phase to aqueous was also clearly revealed along the computational domain.
- 4) Finally the work provides a way to directly calculate the mass transfer performance of a pulsed sieve plate extraction column from first principles without need of much empirical inputs.

CHAPTER 8

CONCLUSION AND FUTURE WORK

8.1 CONCLUSION

CFD simulations of single-phase flow in a pulsed sieve plate column were carried initially out. This constituted the first step to tackle the problem of numerical modeling of pulsed sieve plate extraction columns (PSPC). Different possibilities to make computations faster were evaluated. It was found that 2D simulations of pulsed sieve plate column can be carried out to get a reasonably good estimate of axial dispersion in single-phase flow. This formed the basis of using 2D model for further studies on two phase counter-current flow as well. For 2D representation of the actual geometry, hole diameter should be kept same as in the actual geometry. Pitch should be varied to keep the percent free area same. A geometry with reduced number of plate could be used to carry out CFD simulations. Four plates were found to be sufficient. Once again this formed the basis for selecting a reduced geometry for two phase simulations. One novelty that was proposed in single-phase CFD modeling of PSPC was that of a snapshot approach to predict single-phase axial dispersion coefficient. Instead of the direct approach (which involved coupled solution of RANS and the scalar transport equation), a snapshot approach was Shown to significantly save the computational time. The snapshot approach involved solution of scalar transport equation alone for four flow fields corresponding to four different points of the sinusoidal pulsing velocity. The computational approach embedding the above recommendation for quick estimate of axial dispersion coefficient in single-phase flow in a pulsed sieve plate column was validated using the experimental data. A good agreement between the predicted and reported axial dispersion coefficients was observed. The validated computational approach was also found to give physically

realistic prediction of effect of hole diameter and percent free area on axial dispersion coefficients.

The study thus provided useful tips to simulate single-phase flow in large scale sieve plate columns so that computational efforts can be reduced significantly while not sacrificing too much on the accuracy of the predictions.

In the second step, two-phase flow of 30% TBP in dodecane – 3 N nitric acid system in a pulsed sieve plate column (PSPC) was simulated using a 2D model. This represented the first attempt to model counter-current two phase flow in PSPC. Dispersed phase was assumed to be monodispersed. Quantitative accuracy of the model was studied by comparing the predicted hold up with experimentally reported values of hold up. Representative drop diameter was obtained from experimentally reported values. Different drag models reported in literature were compared and drag models accounting for the effect of hold up on drag coefficient were found to be better than the drag models which do not account for the effect of hold up on drag coefficient. In particular Kumar-Hartland drag law was found to be the most suitable with the absolute average relative error between the predicted and reported values of hold up being around 15%. In an approach which basically means lumping all uncertainties in two-phase model in the model constant of the drag model, the model of Kumar-Hartland was modified to reduce the absolute average relative error between the hold up predicted by two-phase CFD model and experimental hold up. It was found that a single drag model cannot represent the entire range of pulsing velocity. For lower pulsing velocities, a drag model that predicts lower drag coefficient was required. For higher pulsing velocities (≥ 2.5 cm/s), a drag model predicting higher drag coefficient was needed. The modified drag model was implemented in the two-phase CFD simulations and the absolute average relative error between predicted and reported hold up was found to be about 6%. Hold up values predicted by CFD simulations were compared with the hold up values obtained

from the empirical correlations reported in literature. CFD simulations were found to be distinctly better than the empirical correlations. However one disadvantage in this model was that the user had to provide the experimental value of representative drop diameter separately. This was a serious problem as it is difficult to obtain values of representative drop diameter for different conditions experimentally. Hence, the next attempt was to test an approach where the representative drop diameter that went as input to the CFD model could be estimated from a suitable correlation for Sauter mean (representative) drop diameter. This correlation which was identified after screening several empirical correlations reported to estimate the drop diameter in pulsed sieve plate columns. Quantitative accuracy of the computational approach was tested by comparing its predictions of dispersed phase hold up with the reported experimental values of hold up and the absolute average relative error in prediction of hold up was found to be somewhat higher (about 17%). Similar to the approach followed earlier the model of Kumar-Hartland was modified to bring the hold up predicted by two-phase CFD model closer to the experimentally measured values. A piecewise model was used. For lower pulse intensities, a drag model that predicts lower drag coefficient was used. For higher pulsing intensities (≥ 2.5 cm/s), a drag model predicting higher drag coefficient was used. After incorporating the modified drag law in the two-phase CFD model and the absolute average relative error was found to be about 5.8 %. The versatility of the CFD model embedding the modified drag model was tested by comparing its performance against experimental results of dispersed phase hold up in another pulsed column having a different geometry and employing a different phase system. The absolute average relative error between the predicted and experimental results on hold up was about 15%. This result was significantly better than that obtained using standard Kumar-Hartland drag model which was seen to severely under-predict dispersed phase hold up. It was also found to be better than the reported empirical correlations to predict dispersed phase hold up in

pulsed sieve plate columns reported in literature. The computational approach embedding a modified version of Kumar-Hartland drag model thus offers a simplified way of predicting dispersed phase hold up in a pulsed sieve plate columns and thus can be useful for design and optimization calculations. The next logical step was to develop a completely predictive 2D coupled CFD-PBE based model of PSPCs. In this development the representative drop size that goes into the CFD model is obtained from first principles and not from an empirical correlation. This reduces the empiricism involved in the modeling. Moreover as PB equations are solved (in conjunction with the flow field equations) an entire spatial temporal evolution of the Sauter mean drop diameter could be obtained. Hence, using this approach the assumption of monodispersed drops (same drop used to represent the hydrodynamics in the column) used in previous work was also negated. Thus the CFD-PBE based model provides a complete picture of drop size and hold up variation over space and time across the entire computational domain of PSPC. The model was extensively validated against in house experimental data which were obtained by varying both operating (continuous and dispersed phase velocity) and geometrical (different interplate spacing and column diameter) conditions. Absolute average relative errors in prediction of dispersed hold up and Sauter mean drop diameter were about 12% and 16 % respectively. The validated model was used to understand the spatial and temporal variation of the local hydrodynamics parameters. Spatial variations of various hydrodynamic variables in an inter-plate zone were analyzed at the positive and negative peaks of the pulse. At the positive pulse peak of the pulse the dispersed phase was observed to be ejecting out of the sieve holes while during the negative peak of the pulse large accumulation of the dispersed phase below the plates was also observed. Drops were observed to be smaller at the location of sieve holes while their size increases as they approached the next plate above. Turbulence dissipation rates were also observed to be high at the location of the holes. Higher values of turbulence

dissipation rates and smaller drops were observed during the positive peak of the pulsing cycle. Thus the model was able to predict the complex hydrodynamics in a PSPC both qualitatively as well as quantitatively. Re-circulations were observed to be more prominent in the continuous phase than in the dispersed phases. The model could be used as a tool to get useful insights into two-phase hydrodynamics prevalent in PSPCs. Such insights would be helpful for optimum design of the PSPCs.

The next step was to determine axial dispersion coefficient in PSPC under two phase counter-current operation. This is an essential hydrodynamic parameter necessary for estimating mass transfer performance of the column. Continuous phase axial dispersion in two-phase flow of 30% TBP in dodecane – water system in a pulsed sieve plate column was simulated using a 2D two-fluid CFD-PBE approach. Experiments were also carried out in a 3 inch pulsed sieve plate extraction column to obtain axial dispersion coefficient in continuous phase for different values of continuous and dispersed phase velocity. The model could simultaneously predict spatial and temporal variations of dispersed phase hold up and Sauter mean drop diameter in the column. The model was then used to carry out a virtual tracer study to predict axial dispersion coefficient. Method of classes was used to solve the PB equations. Standard breakage and coalescence kernels reported in literature were used. Quantitative accuracy of the computational approach to predict axial mixing (in continuous phase) was tested by comparing its predictions of axial dispersion coefficient with the experimentally measured values of the same. The absolute average relative error in prediction of axial dispersion coefficient was found to be 3.83%, respectively..

The validated CFD-PB model was used to gain insights into the fundamental flow patterns inside the column. Smaller drops were seen to form in regions near the sieve holes which are characterised by higher values of turbulence dissipation rates. At low dispersed phase velocities sustained re-circulations in the continuous phase were

observed while the dispersed phase was seen to preferentially move through the center of the column. However as the dispersed phase velocity was raised the re-circulations in the continuous phase decreased in span as well as strength and the dispersed phase was also seen to move more uniformly across the column cross section. This observation explained the reason for the decrease in axial dispersion coefficient with increase in dispersed phase velocity as was seen in experimentals as well as in numerical predictions. Even though validation was done for continuous phase axial dispersion coefficient only the model could be used to obtain axial dispersion coefficient in dispersed phase.

Finally having developed a comprehensive model that can predict all the relevant hydrodynamics parameters in a PSPC with reasonable accuracy an attempt was made to directly predict mass transfer of a solute from one phase to another using CFD-PBE approach. A 2D CFD-PBE numerical technique was developed which could predict space and time varying hydrodynamics and resultant interphase mass transfer characteristics in a pulsed sieve plate extraction column for the first time in reported literature. The developed model was validated against reported experimental data on solute concentration in organic and aqueous phases in a 2 inch PSPC. The model prediction was very close to reported results, the absolute average relative error being 2.78%. Having validated the model it was then used to understand the local variation of different hydrodynamics parameters like dispersed phase hold up, Sauter mean drop diameter, turbulence dissipation rates and continuous and dispersed phase axial velocity. Transfer of mass from organic phase to aqueous was also clearly revealed along the computational domain. Thus the work provides a way to directly calculate the mass transfer performance of a pulsed sieve plate extraction column from first principles without need of much empirical inputs.

8.2 FUTURE WORK

Based on the work carried out in this research work the following activities can be considered so as to further the fundamental knowledge with regard to two phase pulsatile flow in pulsed column.

The drag law used in final CFD-PBE approach reported in this research work was based on rising/settling of a drop in non pulsatile flow field. The concentrated drag laws reported for monodispersed CFD model are also empirical in nature and are based on experiments in a non pulsatile flow. The drag acting on a liquid drop in presence of other liquid drops in a pulsatile flow field can be estimated using CFD. Thus from first principles it is possible to estimate a drag law (for concentrated dispersions) that is applicable under pulsed flow conditions.

Moreover the breakage and coalescence kernels used in the present work were semi empirical in nature and the constant there in have been derived based on experiments conducted in stirred tanks. Similar fundamental experimental on drop breakage and coalescence under pulsatile flow field can be carried out and kernels for drop breakage and coalescence under pulsatile flow conditions may be proposed.

Finally CFD-PBE based approach to predict hydrodynamics and mass transfer in pulsed columns with different type of internals like disc and doughnut columns can be considered. These types of internals are less prone to choking during operation and may be able to handle solid laden streams without frequent back washes.

One more important parameter was experimental determination of axial dispersion coefficient (in either phase) in large diameter columns under two phase conditions. Radiotracer technique can be employed to estimate axial dispersion in both continuous and dispersed phase in pulsed columns (both sieve plate columns and disc

and doughnut columns). Some preliminary attempts were made in this regard but the further work needs to be carried out in this field.

NOMENCLATURE

A_D	Empirical constant used in Kumar-Hartland model [-]
A	Pulse amplitude [L]
a_1, a_2, a_3	Empirical constant used in Morsi Alexander model [-]
B	Empirical constant used in Kumar-Hartland model[-]
$C_{1\varepsilon}, C_{2\varepsilon}, C_\mu$	Constants in standard k- ε model [-]
C_D	Drag coefficient [-]
C	Tracer concentration [M/ L ³]
d_h	Sieve plate hole diameter [L]
d_p	Drop diameter [L]
d_{32}	Sauter mean drop diameter [L]
D	Effective tracer diffusivity [L ² /T]
D_a	Axial dispersion coefficient [L ² /T]
f	Pulse frequency [1/T]
$F(\theta)$	Ratio of concentration at dimensionless time θ to maximum concentration [-]
\bar{F}_2	External force acting on secondary (dispersed phase) [M/ L ² T ²]
$\bar{F}_{lift,j}$	Lift force acting on secondary phase [M/L ² T ²]
$\bar{F}_{vm,j}$	Virtual mass force acting on secondary phase [M/L ² T ²]
$G_{k,m}$	Kinetic energy generation term for the mixed phase [1/LT ³]
k	Turbulent kinetic energy [L ² / T ²]
δk	Incremental change in turbulent kinetic energy [L ² / T ²]
K_{ij}	Interphase momentum exchange coefficient [-]
K	Empirical constant used in modified Schiller Naumann drag model[-]
K_d	Distribution coefficient, [-].
$K_L a$	Overall volumetric mass transfer coefficient, [1/s].

m_{ij}	Mass transfer rate from 1st phase to 2nd phase [M/ L ³ T]
\overline{R}_{ij}	Interphase exchange force [M L/ T ²]
Re	Reynolds number [-]
p	Static pressure term used in Navier-Stokes equation [M/ LT ²]
\overline{U}_i	Velocity vector of i th phase as used in Navier-Stokes equation [L/T]
\overline{U}_{ij}	Velocity vector of interphase momentum transfer (from phase 1 to phase 2) [L/T]
\overline{U}_m	Mixture velocity vector as used in the closure equations [L/T]
U_p	Pulsing velocity [L/T]
V_d	Dispersed phase superficial flow velocity [L/T]
V_c	Continuous phase superficial flow velocity [L/T]
X	Ratio of tracer effective diffusivity to domain average turbulent viscosity [-]
x	Concentration of solute in aqueous phase [-]
y	Concentration of solute in organic phase [-]

Greek letters

α_2	Phase fraction of phase 2 (dispersed phase) [-]
ε	Turbulent kinetic energy dissipation rate [L/ T ³]
$\delta \varepsilon$	Incremental change in turbulent kinetic energy dissipation rate [L/ T ³]
μ	Viscosity [M/LT]
ϕ	Dispersed phase hold up [-]
ρ	Density [M/ L ³]
σ^2	Second moment of the F curve [T ²]

θ Dimensionless time [-]

Subscripts

i i^{th} phase.

j j^{th} phase.

k k^{th} species.

Abbreviations

PSPC Pulsed sieve plate column

PDDC Pulsed disc and doughnut column

CFD Computational fluid dynamics

PBE Population balance equation

CFD-PBE Computational fluid dynamics- -population balance equation

PIV Particle image velocimetry

LDV Laser dopler velocimetry

REFERENCE

- Amokrane, A.; Charton, S.; Sheibat; Othman, N.; Becker, J.; Klein, J.P.; Puel, F. (2014a). Development of a CFD–PBE coupled model for the simulation of the drops behavior in a pulsed column. *The Canadian Journal of Chemical Engineering*, 92(2): 220-233.
- Amokrane, A.; Charton, S.; Lamadie, F.; Paisant, J.F.; Puel, F. (2014b) Single-phase flow in a pulsed column: Particle Image Velocimetry Validation of a CFD based model. *Chemical Engineering Science.*, 114: 40-50.
- Amokrane, A.; Maass, S.; Lamadie, F.; Puel, F.; Charton, S. (2016). On droplets size distribution in a pulsed column. Part I: In-situ measurements and corresponding CFD–PBE simulations. *Chemical Engineering Journal*, 296: 366-376.
- Alopaeus, V.; Jukka K.; Kari I. K. (1999) Simulation of the population balances for liquid–liquid systems in a non ideal stirred tank. Part 1 Description and qualitative validation of the model. *Chemical Engineering Science* 54(24): 5887-5899.
- Alopaeus, V.; Koskinen, J.; Keskinen, K. I.; Majander, J. (2002) Simulation of the population balances for liquid–liquid systems in a non ideal stirred tank. Part 2—parameter fitting and the use of the multi block model for dense dispersions. *Chemical Engineering Science*, 57(10): 1815- 1825.
- Angelov, G.; Gourdon, C. (2007) Flow pattern in a pulsed-flow extraction column during the pulsation cycle. *Bulgarian Chemical Communications*, 39(1): 65.
- Attarakih, M.; Hlawitschka, M.W.; Abu-Khader, M.; Al-Zyod, S.; Bart, H.J. (2015) CFD-population balance modeling and simulation of coupled hydrodynamics and mass transfer in liquid extraction columns. *Applied Mathematical Modeling*, 39(17): 5105-5120.

Augier, F.; Masbernat, O. (2003) Slip velocity and drag law in a liquid-liquid homogeneous dispersed flow. *AIChE Journal*, 49(9): 2300-2316.

Aubin, J.; Fletcher, D.F.; Xuereb, C. (2004) Modeling turbulent flow in stirred tanks with CFD : the influence of the modeling approach, turbulence model and numerical scheme. *Experimental Thermal and Fluid Science*, 28(5): 431-445.

Baird, M. H. I, 1974. Axial dispersion in a pulsed plate column. *Canadian Journal of Chemical Engineering*, 52: 750–755.

Bardin-Monnier, N.; Guiraud, P.; Gourdon, C. (2003a) Lagrangian simulations contribution to the knowledge of discs and doughnuts pulsed solvent extraction columns hydrodynamics. *Chemical Engineering and Processing: Process Intensification*, 42(7): 503-516.

Bardin-Monnier, N.; Guiraud, P.; Gourdon, C. (2003b) Residence time distribution of droplets within discs and doughnuts pulsed extraction columns via Lagrangian experiments and simulations. *Chemical Engineering Journal*, 94(3): 241-254.

Barnea, E.; Mizrahi, J. (1975) A generalized approach to the fluid dynamics of particulate systems part 2: Sedimentation and fluidization of clouds of spherical liquid drops. *Canadian Journal of Chemical Engineering*, 53(5): 461-468.

Besagni, G.; Guédon, G.; Inzoli, F. (2014) Experimental and Numerical Study of Counter-Current Flow in a Vertical Pipe. *ASME 12th Biennial Conference on Engineering Systems Design and Analysis*.

Boyadzhiev, L.; Spassov, M. (1982) On the size of drops in pulsed and vibrating plate extraction columns. *Chemical Engineering Science*, 37: 337–340.

Bujalski, J.M.; Yang, W.; Nikolov, J.; Solnordal, C.B.; Schwarz, M.P.(2006). Measurement and CFD simulation of single-phase flow in solvent extraction pulsed column. *Chemical Engineering Science*, 61: 2930-2938.

Bhole, M.R.; Joshi, J.B.; Ramkrishna, D. (2008) CFD simulation of bubble columns incorporating population balance modeling. *Chemical Engineering Science*, 63 (8): 2267-82.

Calabrese, R. V.; Chang, T. P. K.; Dang, P. T. (1986) Drop breakup in turbulent stirred tank contactors, Part-I: Effect of dispersed phase viscosity. *AIChE Journal*, 32: 657–666.

Cheng, X.; Chen, X. (2011) Applying Improved Eulerian Model for Simulation of Air-Water Flow in a Hydraulic Jump. *World Environmental and Water Resources Congress*, 3882-3896.

Coulaloglou, C. A.; Tavlarides, L. L. (1977) Description of interaction processes in agitated liquid-liquid dispersions. *Chemical Engineering Science*, 32: 1289–1297.

Chaturabul, S.; Wannachod, P.; Rojanasiraprapa, B.; Summakasipong, S.; Lothongkum, A.W.; Pancharoen, U. (2012) Arsenic removal from natural gas condensate using a pulsed sieve plate column and mass transfer efficiency. *Separation Science and Technology* 47(3): 432-439.

Din, G.U.; Chughtai, I.R.; Inayat, M.H.; Khan, I.H. (2010) Modeling of a two-phase counter-current pulsed sieve plate extraction column - A hybrid CFD and radiotracer RTD analysis approach. *Separation and Purification Technology*, 73 (2): 302-309.

Drumm, C.; Attarakih, M.M.; Bart, H.J. (2009) Coupling of CFD with DPBM for an RDC extractor. *Chemical Engineering Science*, 64 (4): 721-732.

Drumm, C.; Bart, H. J. (2006) Hydrodynamics in a RDC Extractor: Single and Two-Phase PIV Measurements and CFD Simulations. *Chemical engineering & technology* 29(11):1297-1302.

Ellison, C.V.(1952) Continuous solvent recovery process using pulse contacting column. *Report of Oak Ridge National Lab, USA, ORNL-1224.*

Ferreira, A.E.; Agarwal, S.; Machado, R.; Gameiro, M.L.F.; Santos, M.; Reis, T.A.; Ismael, M.R.C.; Correia, J.N.; Carvatho, J.M.R.(2010) Extraction of copper from acidic leach solution with Acorga M5640 using a pulsed sieve plate column. *Hydrometallurgy* 104(1): 66-75.

Forney, L.J.; Skelland, A.H.P.; Morris, J.F.; Holl, R.A. (2002) Taylor vortex column: large shear for liquid-liquid extraction. *Separation Science and Technology*, 37(13): 2967-2986.

Fogler, H.S. (1986) Elements of chemical reaction engineering. Prentice Hall India.

Gabler, A.; Wegener, M.; Paschedag, A. R.; Kraume, M. (2006) The effect of pH on the experimental and simulation results of transient drop size distributions in stirred liquid-liquid dispersions. *Chemical Engineering Science*, 61: 3018–3024.

Gandhir, A.; Wardle, K.E. (2012) Analysis of fluid flow above the upper wear of an annular centrifugal contactor. *Separation Science and Technology*, 47(1): 1-10.

Gameiro, M.L.F.; Machado, R.M.; Ismael, M.R.C.; Reis, T.A.; Carvatho, J.M.R. (2010) Copper extraction from ammoniacal medium in a pulsed sieve-plate column with LIX 84-I. *Journal of Hazardous Materials*, 183(1-3): 165-175.

Gimbun, J.; Chris D.R.; Zoltan K. N. (2009) Modeling of mass transfer in gas–liquid stirred tanks agitated by Rushton turbine and CD-6 impeller: a scale-up study. *Chemical Engineering Research and Design*, 87(4): 437-451.

Grinbaum, B.(2006) Review Article: The existing models for simulation of pulsed and reciprocating columns – how well do they work in the real world. *Solvent Extraction and Ion Exchange* 24: 795-822.

Gonda, K.; Matsuda, T. (1986) Solvent extraction calculation model for PUREX process in pulsed sieve plate column. *Journal of Nuclear Science and Technology*, 23(10): 883-895.

Grafschafter, A.; Siebenhofer, M. (2017) Design Rules for the Taylor-Couette Disc Contactor. *Chemie Ingenieur Technik*, 89(4): 409-415.

Hsia, M. A.; Tavlarides, L. L. (1980) A simulation model for homogeneous dispersion in stirred tank. *Chemical Engineering Journal*, 20: 225–236.

Howarth, W. J. (1964) Coalescence of drops in a turbulent flow field. *Chemical Engineering Science*, 19: 33–38.

Kagan, S.; Aerov, M.; Lonik, V.; Volkova, T. (1965) Some hydrodynamic and mass transfer problems in pulsed sieve-plate extractors. *International Chemical Engineering*, 5 (4): 656–661.

Kagan, S.Z.; Veisbein, B.A.; Trukhanov, V.G.; Muzychenko, L.A. (1973) Longitudinal mixing and its effects on mass transfer in pulsed-screen extractors, *International Chemical Engineering*, 13 (2): 217–220

Kashid, M.N.; Agar, D.W.; Turek, S. (2007) CFD modeling of mass transfer with and without chemical reaction in the liquid–liquid slug flow microreactor. *Chemical Engineering Science*, 62(18-20): 5102-5109.

Kerdouss, F.; Bannari, A.; Proulx, P.; Bannari, R.; Skrga, M.; Labrecque, Y. (2008) Two-phase mass transfer coefficient prediction in stirred vessel with a CFD model. *Computers & chemical engineering*, 32(8): 1943-1955.

Khopkar, A.R.; Kasat, G.R.; Pandit, A.B.; Ranade, V.V. (2006a) Computational Fluid Dynamics Simulation of the Solid Suspension in a Stirred Slurry Reactor. *Industrial and Engineering Chemistry Research*, 45: 4416-4428.

Khopkar, A.R.; Ranade, V.V. (2006b) CFD simulation of gas–liquid stirred vessel: VC, S33, and L3 flow regimes. *AIChE Journal*, 52(5): 1654-1672.

Kolhe, N.S.; Mirage, Y.H.; Patwardhan, A.V.; Rathod, V.K.; Pandey, N.K.; Mudali, U.K.; Natarajan, R. (2011) CFD and experimental studies of single-phase axial dispersion coefficient in pulsed sieve plate column. *Chemical Engineering Research and Design*, 89(10): 1909-1918.

Kumar, S.; Srinivasulu, N.; Khanna, A. (2011) CFD Simulations to Validate Two & Three Phase Up-flow in Bubble Columns. *World Academy of Science, Engineering and Technology*, 5: 11-20.

Kumar, A.; Hartland, S. (1983) Correlations for dispersed phase hold up in pulsed sieve-plate liquid-liquid extraction columns. *Chemical Engineering Research and Design*, 61: 248-252.

Kumar, A.; Hartland, S. (1985) Gravity settling in liquid/liquid dispersions. *Canadian Journal of Chemical Engineering*, 63(3): 368-376.

Kumar, A.; Hartland, S. (1994) *Empirical prediction of operating variables in pulsed column, Handbook of Solvent Extraction*; John Wiley and Sons: New York, US.

Kumar, A.; Hartland, S. (1996) Unified correlation for the prediction of drop size in liquid-liquid extraction columns. *Industrial and Engineering Chemistry Research*, 35: 2682-2695.

Kumar, A.; Hartland, S. (1986) Prediction of drop size in pulsed perforated-plate extraction columns. *Chemical Engineering Communication*, 44: 163-182

Kumar, A.; Hartland, S. (1988) Prediction of dispersed phase hold up in pulsed perforated-plate extraction columns. *Chemical Engineering and Processing: Process Intensification*, 23(1): 41-59.

Kumar, A.; Hartland, S. (1989) Prediction of continuous-phase axial mixing coefficients in pulsed perforated-plate extraction columns. *Industrial & engineering chemistry research*, 28 (10): 1507-1513.

Kumar, A.; Hartland, S. (1999) Correlations for prediction of mass transfer coefficients in single drop systems and liquid–liquid extraction columns. *Chemical Engineering Research and Design*, 77 (5): 372–384.

Lade, V.; Rathod, V.; Bhattacharyya, S.; Manohar, M.; Wattal, P. (2013) Comparison of normal phase operation and phase reversal studies in a pulsed sieve plate extraction column. *Chemical Engineering Research and Design*, 91(6): 1133–1144.

Laso, M.; Steiner, L.; Hartland, S. (1987) Dynamic simulation of liquid-liquid agitated dispersions. Derivation of a simplified model. *Chemical Engineering Science*, 42 (10): 2429–2436.

Lorenz, M.; Haverland, H.; Vogelpohl, A. (1990) Fluid dynamics of pulsed sieve plate extraction columns. *Chemical Engineering and Technology*, 13(1): 411–422.

Liu, J. Q.; Li, S. W.; Jing, S. (2015) Hydraulic Performance of an Annular Pulsed Disc- and Doughnut Column. *Solvent Extraction and Ion Exchange*, 33(4): 385-406.

Liebermann, E.; Jealous, A.C. (1953) Application of the pulse column for uranium recovery from K-25 wastes. *Report of Oak Ridge National Lab, USA* ORNL-1543.

Mate, A.; Masbernat, O; Gourdon, C. (2000) Detachment of a drop from an internal wall in a pulsed liquid-liquid column. *Chemical Engineering Science*, 55(11): 2073-2088.

Marchisio, D. L.; Vigil, R. D.; Fox, R. O. (2003). Implementation of the quadrature method of moments in CFD codes for aggregation–breakage problems. *Chemical Engineering Science*, 58(15): 3337-3351.

Misek, T. (1964) The hydrodynamic behavior of pulsed liquid–liquid extractors. *Collection of Czechoslovak Chemical Communication*, 29: 1755–1766.

Miyauchi, T.; Oya, H. (1965) Longitudinal dispersion in pulsed perforated-plate columns. *AIChE Journal*, 11(3): 395–402.

Modes, G.; Bart, H. J. (2001) CFD simulation of non ideal dispersed phase flow in stirred extraction columns. *Chemical engineering and technology* 24(12): 1242-1245.

Morsi, S.A.; Alexander, A.J. (1972) An investigation of particle trajectories in two-phase flow systems. *Journal of Fluid Mechanics*, 55(2): 193-208.

Nabli, M.S.A.; Guiraud, P.; Gourdon, C. (1997) Numerical experiment: a tool to calculate axial dispersion coefficient in disc and doughnut pulsed extraction column. *Chemical Engineering Science*, 52 (14): 2353–2368.

Narsimhan, G.; Gupta, G.; Ramkrishna, D. (1979) A model for transitional breakage probability of droplets in agitated lean liquid-liquid dispersions. *Chemical Engineering Science*, 34: 257.

Nabli, M.A.; Guiraud, P; Gourdon, C. (1998) CFD contribution to a design procedure for discs and doughnuts extraction columns. *Chemical Engineering Research and Design*, 76(8): 951-960.

Niebuhr, D., Vogelpohl, A., (1980) Axial mixing in pulsed sieve-plate extraction columns, *German Chemical Engineering*, 3: 264–268

Noroozi, S.; Hashemabadi, S.H. (2009) CFD Simulation of Inlet Design Effect on Deoiling Hydro cyclone Separation Efficiency. *Chemical Engineering and Technology*, 32 (12): 1885–93.

Noh, J.S., Kim, S.D., (1980) Axial dispersion in a pulsed extraction column, *J. Korean Institute of Chemical Engineers*, 18 (3): 141–152

Pilhofer, T.; Mewes, D. (1979) Siebbodenextraktionskolonnen, VCH-Verlag, Weinheim

Rao, K.V.K., Jeelani, S.A.K., Balsubramanian, G.R. (1978) Back mixing in pulsed perforated plate columns, *Canadian Journal of Chemical Engineering*, 56: 120–123

Ranade; V.V.; Tayalia, Y.; Krishnan, H.(2002) CFD predictions of flow near impeller blades in baffled stirred vessels: Assessment of computational snapshot approach. *Chemical Engineering Communications*, 189(7): 895-922.

Rusche, H. (2002) Computational fluid dynamics of dispersed two phase flows at high phase fractions. Thesis submitted for the degree of Doctor of Philosophy of the University of London and Diploma of Imperial College.

Retieb, S.; Guiraud, P.; Angelov, G.; Gourdon, C. (2007) Hold up within two-phase countercurrent pulsed columns via Eulerian simulations. *Chemical Engineering Science*, 62(17): 4558-4572.

Sato, T.; Sugihara, K.; Taniyama, I. (1963) Performance characteristics of pulsed perforated plate columns. *Kogaku Kogaku*, 27: 583–586.

Sathe, M.J.; Deshmukh, S.S.; Joshi, J.B.; Koganti, S.B. (2010) Computational Fluid Dynamics Simulation and Experimental Investigation: Study of Two-Phase Liquid–Liquid Flow in a Vertical Taylor–Couette Contactor. *Industrial and Engineering Chemistry Research*, 49: 14–28.

Sarkar, S.; Sen, N.; Singh, K.K.; Mukhopadhyay, S; Shenoy, K.T. (2017) Effect of operating and geometric parameters on dispersed phase hold up in Pulsed Disc and Doughnut and Pulsed Sieve Plate Columns: A comparative study. *Chemical Engineering and Processing: Process Intensification*, 118: 131-142.

Schön, J.;Schmieder, H.;Kanellakopulos, B. (1990) Operating experience with Minka: U-Pu separation in the presence of technetium with an organic continuous pulsed column. *Separation Science and Technology* 25(13-15): 1737-1750.

Schiller, L.; Naumann, Z. (1935) *Ver. Deutsch Ing.*

Sehmel, G.A.; Babb, A.L. (1963) Hold up studies in a pulsed sieve-plate solvent extraction column. *Industrial & Engineering Chemistry Process Design and Development*, 2(1): 38-42.

Singh, K. K.; Mahajani, S. M.; Shenoy, K. T.; Ghosh, S. K. (2009). Population balance modeling of liquid–liquid dispersions in homogeneous continuous-flow stirred tank. *Industrial and Engineering Chemistry Research*, 48(17): 8121-8133.

Singh, K.K.; Mahajani, S.M.; Shenoy, K.T.; Ghosh, S.K. (2007) Computational fluid dynamics modeling of a bench-scale pump-mixer: Head, power and residence time distribution. *Industrial and Engineering Chemistry Research*, 46(7): 2180-2190.

Singh, K.K.; Mahajani, S.M.; Shenoy, K.T.; Ghosh, S.K. (2008) CFD modeling of pump-mix action in continuous flow stirred tank. *AIChE Journal*, 54(1): 42-55.

Srinivasulu, K.; Venkatnarsaiah, D.; Varma, Y.B.G. (1997) Drop size distribution in liquid pulsed columns. *Bioprocess Engineering*, 17 (3): 189–195.

Srinikethan, G.; Prabhakar, M. A.; Varma, Y. B. (1987) Axial dispersion in plate-pulsed columns. *Bioprocess Engineering*, 2(4): 161-168.

Smoot, L.D.; Mar, B.W.; Babb, A.L. (1959) Flooding characteristics and separation efficiencies of pulsed sieve-plate extraction columns. *Industrial and Engineering Chemistry Research*, 51 (9): 1005–1010.

Sovova, H. (1981) Breakage and coalescence of drops in a batch stirred vessel-II Comparison of model and experiments. *Chemical Engineering Science*, 36 (9), 1567–1573.

Szafran, R.G.; Kmiec, A. (2004) CFD modeling of heat and mass transfer in a spouted bed dryer. *Industrial and engineering chemistry research*, 43(4): 1113-1124.

Thronton, J.D. (1957) Liquid–liquid extraction part III: the effect of pulse waveform and plate geometry on the performance and throughput of a pulsed column. *Trans. I Chem E*, 35; 316–330.

Torab-Mostaedi, M.; Safdari, J. (2009) Prediction of mass transfer coefficients in a pulsed packed extraction column using effective diffusivity. *Braz. J. Chem. Eng.*, 26(4): 685-694.

Tung, L.S.; Luecke, R.H. Mass transfer and drop size in pulsed-plate extraction columns. *Ind. Eng. Chem. Process Des. Dev.* 1986, 25, 664-673

Usman, M.R.; Sattar, H.; Hussain, S.N.; Muhammad, H.; Asghar, A.; Afzal, W. (2009) Drop size in a liquid pulsed sieve plate extraction column. *Braz. J. Chem. Engg.*, 26(4): 677-683.

Venkatnarsaiah, D.; Verma, Y.B.G. (1998) Dispersed phase hold up and mass transfer in liquid pulsed column. *Bioprocess Engineering*, 18: 119–126.

Vikhansky, A.; Markus K. (2004) Modeling of a RDC using a combined CFD-population balance approach. *Chemical Engineering Science* 59(13): 2597-2606.

Wang, H.; Jia, X.; Wang, X.; Zhou, Z.; Wen, J.; Zhang, J, (2014) CFD modeling of hydrodynamic characteristics of a gas-liquid two-phase stirred tank. *Applied Mathematical Modeling*, 38(1): 63-92.

Wang, F.; Mao, Z.S. (2005) Numerical and experimental investigation of liquid–liquid two-phase flow in stirred tanks. *Industrial and Engineering Chemistry Research*, 44: 5776–5787.

Walvekar, R.G.; Choong, T.S.Y.; Hussain, S.A.; Khalid, M.; Chuah, T.G. (2009) Numerical study of dispersed oil–water turbulent flow in horizontal tube. *Journal of Petroleum Science and Engineering*, 65(3-4): 123-128.

Wardle K. E.; Allen, T. R.; Anderson, M. H.; Swaney, R. E. (2008) Free surface flow in the mixing zone of an annular centrifugal contactor. *AIChE Journal*, 54(1):74–85.

Wardle, K.E.; Allen, T.R.; Swaney, R.(2009) CFD simulation of separation zone of an annular centrifugal contactor. *Separation Science and Technology* 44(3): 517-542.

Wardle, K.E. (2011). Open-source CFD simulations of liquid-liquid flow in the annular centrifugal contactor. *Separation Science and Technology* 46(15): 2409-2417.

Yadav, R.L.; Patwardhan, A.W. (2008) Design aspects of pulsed sieve plate columns. *Chemical Engineering Journal*, 138(1-3): 389-415.

Yadav, R.L.; Patwardhan, A.W. (2009) CFD modeling of sieve and pulsed-sieve plate extraction columns. *Chemical Engineering Research and Design*, 87(1): 25–35

Yu, Y.H., Kim, S.D. (1987) Axial dispersion hold up and flooding characteristics in pulsed column. *Can. J. Chem. Eng.*, 65: 752–758

Xiaojin, T.; Guangsheng, L. (2011) CFD simulations of flow characteristics in pulsed-sieve-plate extraction columns. *Industrial and Engineering Chemistry Research*, 50(2): 1110-1114.
